LBNL-40816
CONF-9609353-
UC-404

ERNEST ORLANDO LAWRENCE
BERKELEY NATIONAL LABORATORY

Proceedings of a Workshop on Methods for Neutron Scattering Instrumentation Design

Ernest Orlando Lawrence Berkeley National Laboratory September 23–25, 1996

Rex P. Hjelm, Editor

September 1997

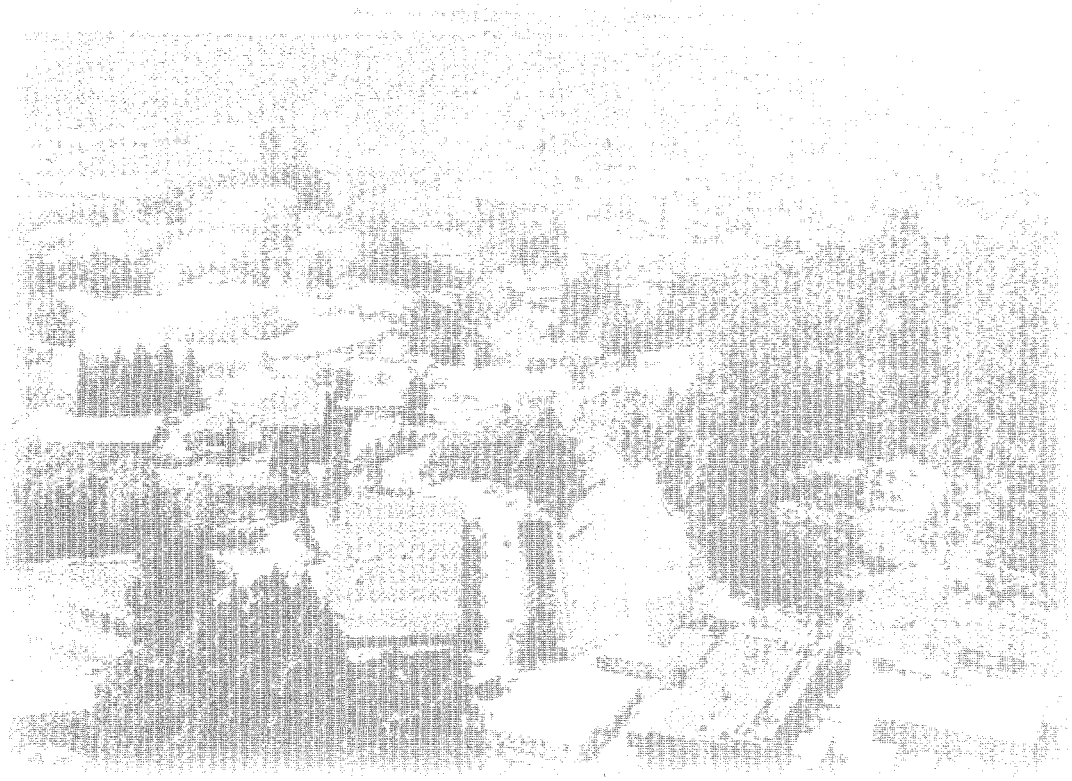

LBNL-40816
CONF-9609353
UC-404

Proceedings of a Workshop on Methods for Neutron Scattering Instrumentation Design*

Ernest Orlando Lawrence Berkeley National Laboratory
September 23-25, 1996

Edited by

Rex P. Hjelm
Manuel Lujan Jr. Neutron Scattering Center
Los Alamos Neutron Science Center
Los Alamos National Laboratory
Los Alamos, New Mexico

* This work was supported by the U.S. Department of Energy, Office of Energy Research, Office of Basic Energy Sciences, in part at the Lawrence Berkeley National Laboratory under Contract No. DE-AC03-76SF00098, and in part at the Los Alamos National Laboratory under Contract No. W-7405-ENG-36.

DISCLAIMER

Table of Contents

Meeting Goals:

In view of the current level of activity worldwide associated with the design and construction of new, next-generation neutron sources, it appears highly desirable to review the design tools and techniques available to the neutron scattering community for the design of new instruments suites for these sources. More precisely, this meeting aims at addressing the following questions:

1. Review the present situation regarding approaches to neutron scattering instrument design and the tools available for this purpose.

2. Determine the present and future needs of the neutron scattering community regarding techniques and design tools for neutron scattering instrument design.

3. Given that these tools can be used in a variety of ways for:

- Analysis of existing instruments,
- Design of new instruments,
- Optimization of existing or new instruments,
- Planning of experiments,
- Teaching,

how do we best address the needs of the community in these various categories? Where do we focus future efforts? How do we share information and codes between different institutions?

4. How can we validate our design tools? How do we implement proposal mechanisms that would allow beam time to be devoted to instrument development and code benchmarking? Should we create dedicated beamlines to test neutron optical elements, measure their performance, and help develop better models?

5. How do we measure instrument performance? Should we define "standard" test to measure instrument performance? What are meaningful figures of merit?

Meeting Organization

Organizing Committee:

I. Anderson (Institut Laue-Langevin)
J. Copley (National Institute of Standards and Technology)
K. Crawford (Argonne National Laboratory)
L.L. Daemen (Los Alamos National Laboratory)
W. Hamilton (Oak Ridge National Laboratory)
R.P. Hjelm (Los Alamos National Laboratory)
M. Johnson (Rutherford-Appleton Laboratory)
G. Kearley (Institut Laue-Langevin)

Funded in part by the Los Alamos National Laboratory

Los Alamos National Laboratory is operated by the University of California under contract W-7405-ENG-36 from the United Stated Department of Energy

Meeting Agenda

Welcome and meeting goals

9:00 - 9:10: Welcome and Meeting Goals- W. Oosterhuis (DOE)
9:10 - 9:30: Scope and goals of the workshop– R. P. Hjelm

Session 1: Design Tools for X-ray Scattering Instruments

Topics - Overview of design tools currently available
- How are these tools being used and by whom ?
- What was the general approach/philosophy followed in the development of these tools ? What was the history of the developments of these design tools ?
- How is the development of these tools supported ?
- What are future directions for the development of these tools ?

Chairman:: J.R.D. Copley

9:30 - 10:10: **G.E. Ice** (ORNL) - Modeling of x-ray beamlines and devices.

10:10 - 10:30: Break

10:30 - 11:10: **J. Authur** (SSRL) - Modern Synchrotron X-ray Optics.

11:10-11:50 **M. Khan** (U. Wisconsin) - SHADOW

11:50 - 12:30 Open discussion: Lessons learned from the x-ray scattering community.

12:30 - 14:00: Lunch: Posters and demonstrations

Session 2: Design Tools for Neutron Scattering Instruments

Topics - Overview of existing tools
- Approaches to neutron scattering instrument design
- Examples of successful designs
- Examples of mistakes and lessons learned

Chairman:: R.P. Hjelm

14:00-14:40: **L. Passell** (BNL) - Historical Overview of Neutron Instrument Design.

14:40 - 15:20: **K. Crawford** (ANL) - Approaches to instrument design at pulsed spallation sources.

15:20 - 15:40: Break

15:40 - 16:20: **T. Brun** (LANL) - Matching instruments and sources.

16:20 - 17:00: Discussion: Lessons learned on neutron instrument design.

Session 3: Instrument Design - Analytical & Numerical Techniques

Topics - Examples of successful instrument design
- Phase space transformation methods
- Ray tracing
- Optimization methods
- Examples of successful instrument design.
- Figures of merit for measuring performance and optimizing instruments.
- Benchmarking: comparison of calculated and measured performance.
- Monte Carlo and other numerical techniques.
- Treatment of background and noise.

Chairman:: W. Hamilton

9:00 - 9:30: **M. Johnson** (RAL) - Figures of merit.

9:30 - 10:00: **D. Sivia** (RAL) - Bayesian experimental design.

10:00 - 10:30: **B. David** (RAL) - Figures of merit: the view from the experimental perspective.

10:30 - 11:00: Break

11:00 - 11:40: **R. Robinson** (LANL) - Matrix methods.

11:40 - 12:30: Discussion– The role of analytical techniques. Figures of merit. Optimization

12:30 - 14:00: Lunch: Posters and demonstrations

Session 4: Instrument Design - Analytical & Numerical Techniques

Chairman:: K. Crawford

14:00-14:35: **R. Gaehler** (TU Muenchen) - Coherence properties of neutron beams for scattering instrumentation

14:40 - 15:15: **P. Seeger** (LANL) - MCLIB, a general Monte Carlo library for simulation of neutron scattering instruments.

15:15 - 15: 35: Break

15:35 - 16:00: **F. Trouw** (ANL) - Visualizing Simulation Results

16:00 - 17:00 Discussion: The codes: What can be done to improve code sharing and collaboration? Other computational aspects.

19:00 Conference Diner: UC Faculty Club

Session 5: Modeling of Neutron Optical Components

Topics - Overview of existing models.
- Generation of scattering kernels for simulating samples.
- Identify model deficiencies and need for new/improved models.
- Validation of models.

Chairman: L. Daemen

9:00 - 9:40: **J.R.D. Copley** (NIST) - The design of a reactor-based time-of-flight spectrometer

9:40 - 10:00: **C. Hayes** (ILL) - Toroidal mirrors.

10:00 - 10:30: Break

10:30 - 10:50: **M. Popovici** (U. Missouri) - Modeling triple-axis spectrometers optics.

10:50 - 11:20: **C. Zeyen** (ILL) - Modeling of Spin Echo Three Axis Spectrometer (classical TAS and magnetic optics.

11:20 - 11:40: **N. Rosov** (NIST) - Modeling components of an neutron spin echo spectrometer.

11:40 - 12:30: Discussion— Benchmarking and testing models. Modeling imperfections in optical elements. Models for sources and samples.

12:30 - 14:00: Lunch: Posters and demonstrations

Discussion: Present and Future Needs of the Community

Goals: - Open discussion

Chairman: M. Johnson

14:00 - 14:40 Presentations on the present and future needs for instrumentation design:

R. Pynn
K. Crawford
W. Wagner
F. Mezei

14:40 - 16:00 Discussion–Present and future needs of neutron scattering instrument design.

A Workshop on
Methods for Neutron Scattering Instrument Design
Introduction and Summary

Rex P. Hjelm
Manuel Lujan Jr. Neutron Scattering Center
Los Alamos Neutron Science Center
Los Alamos National Laboratory

The future of neutron and x-ray scattering instrument development and international cooperation was the focus of the workshop on "Methods for Neutron Scattering Instrument Design" September 23-25 at the E.O. Lawrence Berkeley National Laboratory. These proceedings are a collection of a portion of the invited and contributed presentations.

The international gathering of about 50 participants representing 15 national facilities, universities and corporations featured oral presentations, posters, discussions and demonstrations. Participants looked at a number of issues concerning neutron scattering instruments and the tools used in instrument design. Objectives included: (1) determining the needs of the neutron scattering community in instrument design computer code and information sharing to aid future instrument development, (2) providing for a means of training scientists in neutron scattering and neutron instrument techniques, and (3) facilitating the involvement of other scientists in determining the characteristics of new instruments that meet future scientific objectives, and (4) fostering international cooperation in meeting these needs. The scope of the meeting included: (1) a review of x-ray scatteinrg intrument design tools, (2) the a look at the present staus of neutron scattering instrument design tools and models of neutron optical elelments, and (3) discussions of the present and future needs of the neutron scattering community.

Why are these objectives are important? As Larry Passell (BNL) pointed out in a review of the history of neutron scattering through 1960, early neutron scientists had the luxury of experimenting with the instruments to arrive at a design that worked. The importance of prototyping was reiterated by Kent Crawford (IPNS) in his review of the concepts of instrument design and optimization for pulsed sources. However, because of the complexity of modern instruments, it is difficult to do this with built instruments. Analysis and simulation becomes a must.

The general theme of instrument design set by Crawford's talk and reiterated many times in subsequent presentation was a "stepwise" approach involving careful consideration of the objectives for the instrument followed by back of the envelope calculations. To produce optimal instrument configurations, analytical calculations give a first cut for the instrument geometry, followed by detailed analysis and simulations using methods that are most appropriate for the detailed problems at hand to incorporate more subtle features such as non-Gaussian pulse shapes. An important advantage of analysis and simulation techniques is that they allow inexperienced instrument designers to "prototype" cheaply and obtain a feeling for the importance of various instrument parameters.

Several discussions covered general principles of analytical and computational tools for the analysis of neutron scattering instruments. These included matrix methods (Rob Robinson, MLNSC), coherence volume analysis (Roland Gaeller, TU München), and Monte Carlo methods (Phil Seeger, MLNSC). Matrix methods provide a means for determining instrument resolution and estimates of the total intensity from the resolution volume. There are codes based on these methods for double and triple axis spectrometers, reviewed by Mihai Popovici (MURR). Coherence volume analysis demonstrated that one can think about neutron scattering either in terms of traditional resolution calculations (Frauenhoffer diffraction) or in terms of beam coherence (Fresnel diffraction) and get the same answer. The detailed wave analysis brings to light some interesting new possibilities for instrument design. Monte Carlo methods allow for detailed predictions of instrument performance that are not available from other methods.

Presentations on the details of recent instrument designs and on moderator performance covered these and other methods of neutron instrument design. John Copley led us through the development of a cold neutron chopper spectrometer at NIST, which, like IN5 at the ILL, has four disc choppers. Unlike IN5, however, the NIST instrument uses three counter-rotating choppers to improve resolution. The bandwidth-defining choppers have different size slots cut in the wheels. John used acceptance diagrams, ray tracing, phase space arguments, Monte Carlo and ray tracing methods to determine chopper configurations, chopper slot numbers and sizes and the effects of guide geometry.

The combination of analytical calculations and simulation methods have lead to innovative designs for neutron spin echo (NSE) instruments at the ILL and the NIST. Carmel Hayes (ILL) described the implementation of a torroid mirror for the high intensity small-angle spin echo instrument, IN15. The copper mirrors provide signal to background in the 10^{-4} to 10^{-5} range for wavelengths between 17 and 25 Å, and provide intensity gains of up to 30, allowing the instrument minimum Q to be about 0.001 $Å^{-1}$ with a short instrument. Ray tracing calculations by John Copley were used in the development of the mirrors. Claude Zeyen (ILL) described work on magnetic field shaping needed to realize a high resolution triple axis spectrometer NSE, IN20. In these designs, analysis showed what was best to do, whereas simulations allowed optimization of a complex design. Nick Rosov described work on polarization analysis using a two-dimensional detector for the NIST NSE. The key to this technique is the use of small mirrors on the detector that have to be positioned so that any scattered neutron must be reflected by a mirror surface before entering the detector active volume.

Some interesting new instrument developments were presented in the discussions. Tom Rieker (U. New Mexico) explored the possibilities of using Soller slits as collimators and analyzers for a time-of-flight ultra small-angle neutron scattering instrument. Holgar Tieze-Jaensch (ISIS) described the performance and new ideas of improvement of the rotating-analyzer spectrometer. Experimental results showing a more efficient means of neutron beam polarization using a polarizing beam splitter were presented by M. Takeda and his colleagues (Tohoku University). Addressing a critical needed for the measurement of neutron scattering Bart Czirr (Photogenics, Inc) discussed the performance of ^{10}B solid state neutron detectors.

Torben Brun (MLNSC) illustrated the uses of MCNP in understanding the output of neutron moderators. Water moderation simulations by MCNP are in excellent agreement with measurement. The situation with liquid hydrogen is different, where there are discrepancies between measurement and calculation at low energy, probably due to a lack of understanding the para-orthohydrogen mix.

The interrelated questions of matching instrument configurations with the measurement, and how we measure instrument performance was discussed in three presentations. Mike Johnson (ISIS) considered how one defines a figure of merit that is consistent with Shannon information theory, taking into account count rate, measurement time, Q and E resolution of the various data channels, the number of data channels and the background. Devinder Sivia (ISIS), using Baysian analysis, dealt with the general question of experimental design and the quality of information that can be extracted from the data in the presence of noise and background and the Q and E resolution of each data channels. Sivia pointed out that the quality of a measurement, hence the figure of merit is inexorably coupled to what we want to learn. Bill David (ISIS), continued with this point, showing through a model approach to least squares fitting of crystallographic data, that the data quality really concerns how much we can learn from a measurement. These analyses highlighted the need for flexibility in instrument configuration, as well as the need to devise methods for planning measurements to match the capabilities of the instrument with the question being asked, in order to maximize what is learned.

The development of a tool for neutron instrument design clearly is a difficult task requiring cooperation within the neutron scattering community. Such an effort has been made before in the area of modern x-ray synchrotron instruments, which are also complicated and expensive,

and where there was also a need for confidence that the instrument is optimized *before construction.* Unlike what tends to be the case for neutron instrumentation, the design and fabrication of synchrotron instruments is usually in the hands of groups external to the facility. A generalized ray tracing program optimized for synchrotron x-ray optics, SHADOW, has been developed to allow users to model instrument optics. This program was reviewed by Mumit Khan of the University of Wisconsin and is used at 120 sites in 20 countries. It is widely used for synchrotron radiation work, x-ray lithography and even astronomy. The program allows the user to select from different x-ray sources and optical devices to construct an optical system. Output gives information on image quality size and shape, resolution phase, divergence and so-on. The code has been validated by experiment.

The availability of SHADOW has had a major impact on the design of x-ray instrument optics. Gene Ice of Oak Ridge pointed out that SHADOW provides a simple way to experiment with ideas and concepts, which can then be verified in the laboratory. The success of the predictions leads to confidence in the code, fostering further applications and code development. The results lead to rules of thumb that are used as a starting point for more sophisticated designs.

Clearly, a generalized modeling tool like SHADOW would benefit the neutron scattering community. What should the features of such a tool be? In his summary of the needs of the community, Crawford made the case that there should be improved Monte Carlo simulation codes, which should include tools for easily defining instrument geometry, using three-dimensional visualization of instruments including solid geometry visualization using CAD tools. The code should be a library of modules, each corresponding to an instrument's elements. There is a need for faster, more efficient codes. Crawford pointed out that the implementation details could best be serviced by seeking the services of professional software engineers. Finally, there is the need to benchmark the codes—a necessity if the results from simulating complex instruments are to be trusted.

Mike Lampton of Stellar Software stated that most of the effort in developing a commercial product goes into the development of a user interface, owing to the importance of the interface for the program to be an effective tool. The power of being able to visualize an instrument, see the rays that are passed through the instrument, and visualize the results of the simulation were very well illustrated in Mike's demonstration of the optical ray tracing design and analysis package, "Beam Four". Franz Trowe supported the importance of visualization in simulations. Using Geomview, a package of three dimensional display tools from the University of Wisconsin, Trowe showed how the display of the complex geometry of an instrument facilitates its design. These sorts of tools can be used as an aid in teaching the fundamentals of neutron scattering instrument design.

The Los Alamos instrument simulations package presented by Phil Seeger, has many of the desired features in that it allows the assembly of optical elements, such as sources, collimators, choppers, detectors and various scattering kernels for samples. A graphics based user interface is under development that will allow the user to set up the instrument, define elements parameters, sources and samples, visualize the resulting instrument set up, and run the program. A more complete tool kit would mix methods for modeling the neutron optics, plus provide for neutron transport codes for calculating backgrounds.

However, the neutron scattering community needs more than simulation tools. Summing up his recommendations, Roger Pynn (LANSCE) stressed the need to share tested tools that can be trusted, share information, pay attention to careful thinking about instrument designs, preserve and increase our knowledge base. Crawford's recommendations were for a complete bibliography of neutron instrumentation papers, as well as for beamlines for testing optical components and for instrument prototyping. Werner Wagner (PSI) pointed out that another challenge is to develop detailed simulation techniques based on Monte Carlo and analytical methods, in order to test novel ideas and produce good designs. As an example, Wagner and his co-authors, describe the design of Fourier Chopper Time-of-Flight Diffractometer for strain measurements. Feri Mezei gave some examples from HMI where thinking about and optimizing instruments paid off. HEAT and FLEX

demonstrated substantial gains in efficiency over the ILL counterparts, the result of a number of small gains. Other issues that need to be explored, in Feri's view, are optimal and novel uses of guides and optimization of sources. In the paper included the proceedings Mezei stressed the need in the design for accelerator-based facilities for a departure from past practice. He point out the need for total optimization of facilities from the accelerator through to the instrument suite. Doing this clearly requires new design tools.

How can the neutron scattering community address some of these needs? Mike Johnson suggested that a repository of neutron instrument designs and concepts be set up as a web site. Ideas about instrument design, computer codes, design concepts results all should be included. We also need to set up standards for the development of code that can be placed in a common package and foster cooperation in the development of new codes.

ACKNOWLEDGMENTS:

I would like to thank the organizing committee for organizing this meeting. Particular thanks goes to Molley Field and Henry Rutkowski of LBNL, for local organization. Thanks is also due to Bill England and Garth Tietjen for editorial help. The hard work of presenters and authors is also gratefully acknowledged. Finally, This meeting would not have been possible without the support and funding provided by the Los Alamos National Laboratory. Los Alamos National Laboratory is operated by the University of California under contract W-7405-ENG-36 from the United Stated Department of Energy

MODELING OF X-RAY BEAMLINES AND DEVICES

Gene E. Ice
Oak Ridge National Laboratory

ABSTRACT

X-ray beamlines on synchrotron sources are similar in size and complexity to beamlines at state-of-the-art neutron sources. The design principles, tools, and optimization strategies for synchrotron beamlines are also similar to those of neutron beamlines. We describe existing design tools for modeling synchrotron radiation beamlines and describe how these tools have evolved over the last two decades. The development of increasingly powerful modeling tools has been driven by the escalating cost and sophistication of state-of-the-art beamlines and by a world-wide race to exploit advanced synchrotron radiation sources.

INTRODUCTION

X-ray beamlines on synchrotron sources are expensive and complicated instruments. First generation (parasitic operations) and second generation (dedicated small emittance) beamlines are ~20 m long with ~1/4 inch of steel shielding and cost ~$1-2 M [1]. Third generation (undulator) sources require beamlines ~60 m long with ~1" of lead shielding and cost ~$4-7M [2]. Typical beamline layouts are illustrated in Fig. 1. As shown in Fig. 2, new beamlines often contain expensive and complicated first-of-their-kind components. These new components demand careful modeling before fabrication. In addition, as the cost of beamlines has risen, beamline developers have increasingly relied on modeling to develop confidence that each beamline will be optimized for its mission.

1st/2nd Generation ~1/4" steel/ (20 m long)/ $1-2M

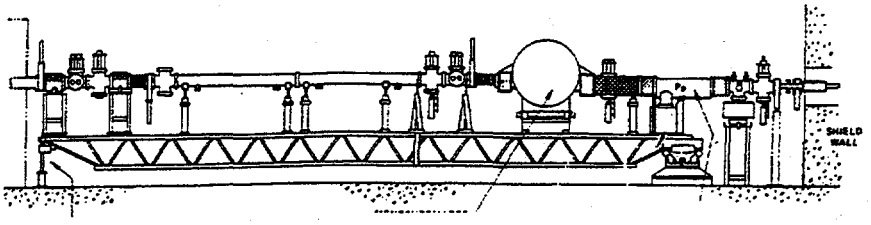

3rd Generation ~1" lead/ (60 m) long $4-7M

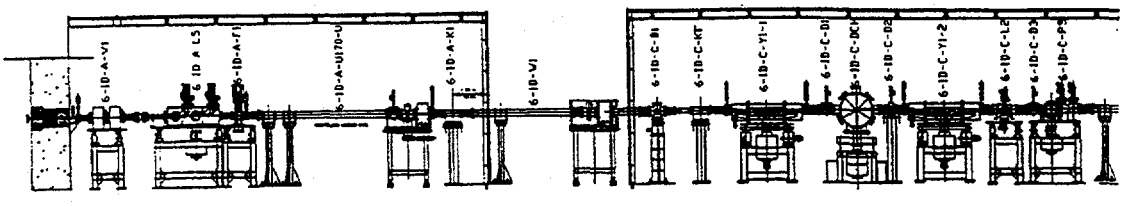

Fig. 1 Typical beamlines on synchrotron sources.

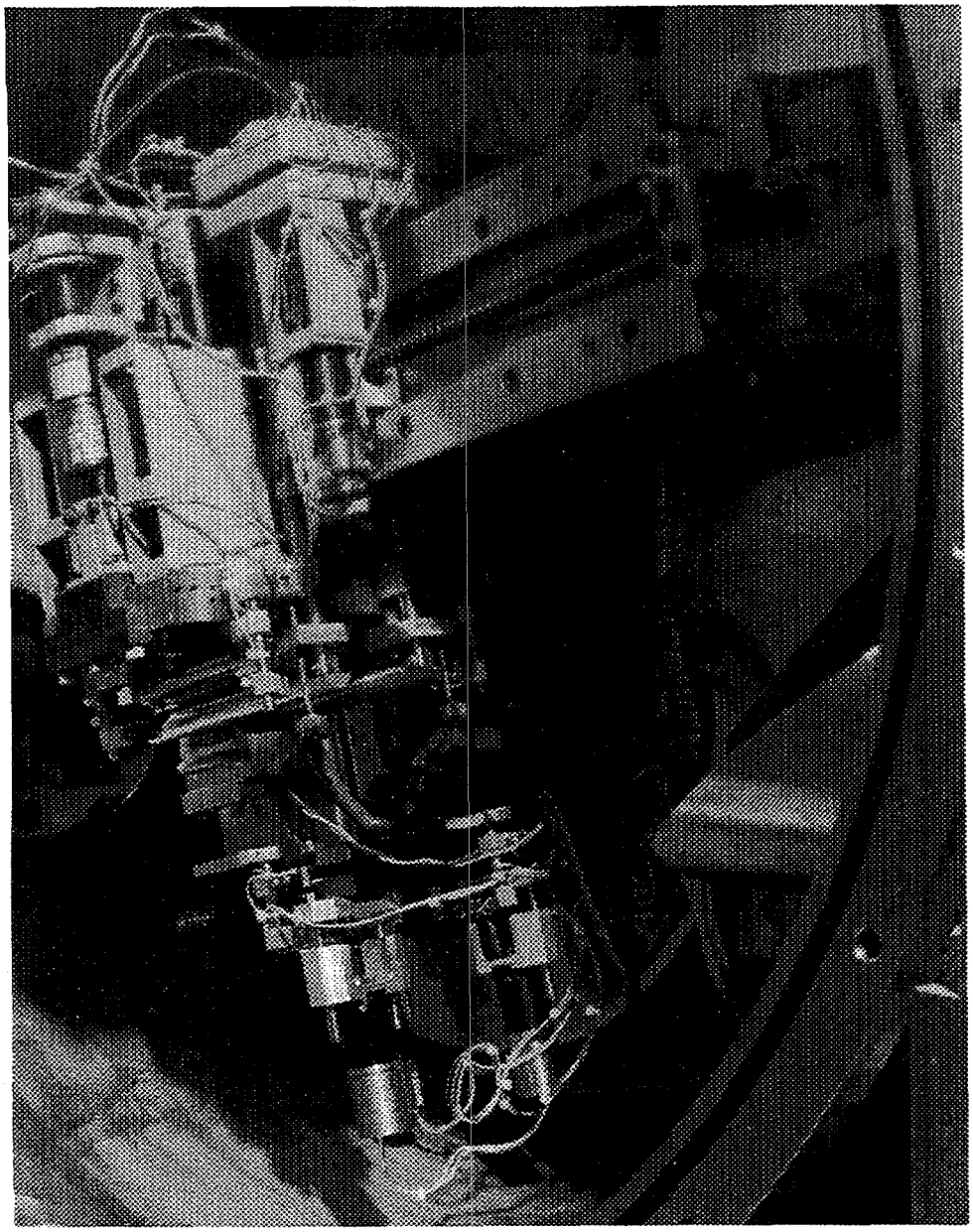

Fig. 2 Sagittal focusing double crystal monochromator on beamline X14 at the NSLS. The photograph shows some of the 12 in-vacuum motors used to align the two crystals and dynamically bend the second crystal to a cone. This device was the first of its kind.

In general, beamline modeling is an iterative process. As shown in Fig. 3, modeling begins by defining a beamline mission. Beamline mission sets the beamline requirements: energy resolution, momentum transfer resolution, flux, tunability, harmonic rejection, and sample volume. Other factors also guide (restrict) synchrotron beamline design such as shielding requirements for personnel protection, background considerations, vacuum for beam transport, and thermal considerations.

Modeling is an iterative process

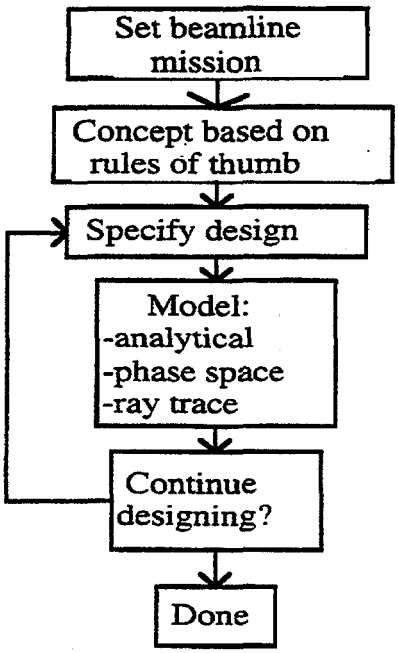

Fig. 3 Flow diagram for beamline design.

After defining the beamline mission and required characteristics, the next step in beamline modeling is to conceptualize the beamline based on simple "rules of thumb." For example, sagittal focusing (Fig. 4) can collect more radiation than meridional focusing, but the aberrations are more difficult to control. Similarly, the 20 times larger scattering angles of crystals relative to total-external-reflection mirrors means that crystal optics can be about 20 times shorter than mirrors.

Since synchrotron optics are dominated by a small number of optical elements, it is possible to rule out certain designs quickly and rapidly narrow-in on the most likely optical components. Figure 5 shows the designs of seven beamlines at the Advanced Photon Source as conceived in late 1994. As can be seen in Fig. 5, the beamlines designs are dominated by a small number of components.

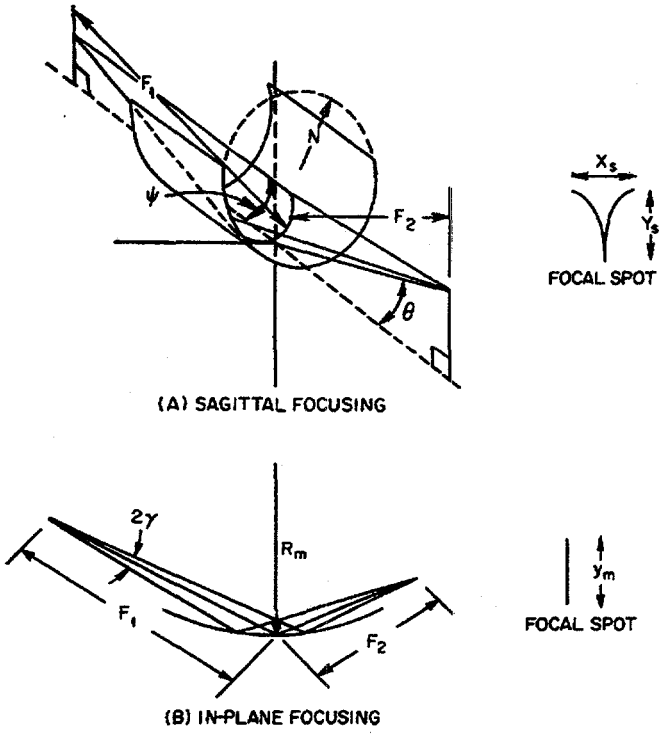

Fig. 4 Sagittal (out-of-plane) and meridional (in-plane) focusing.

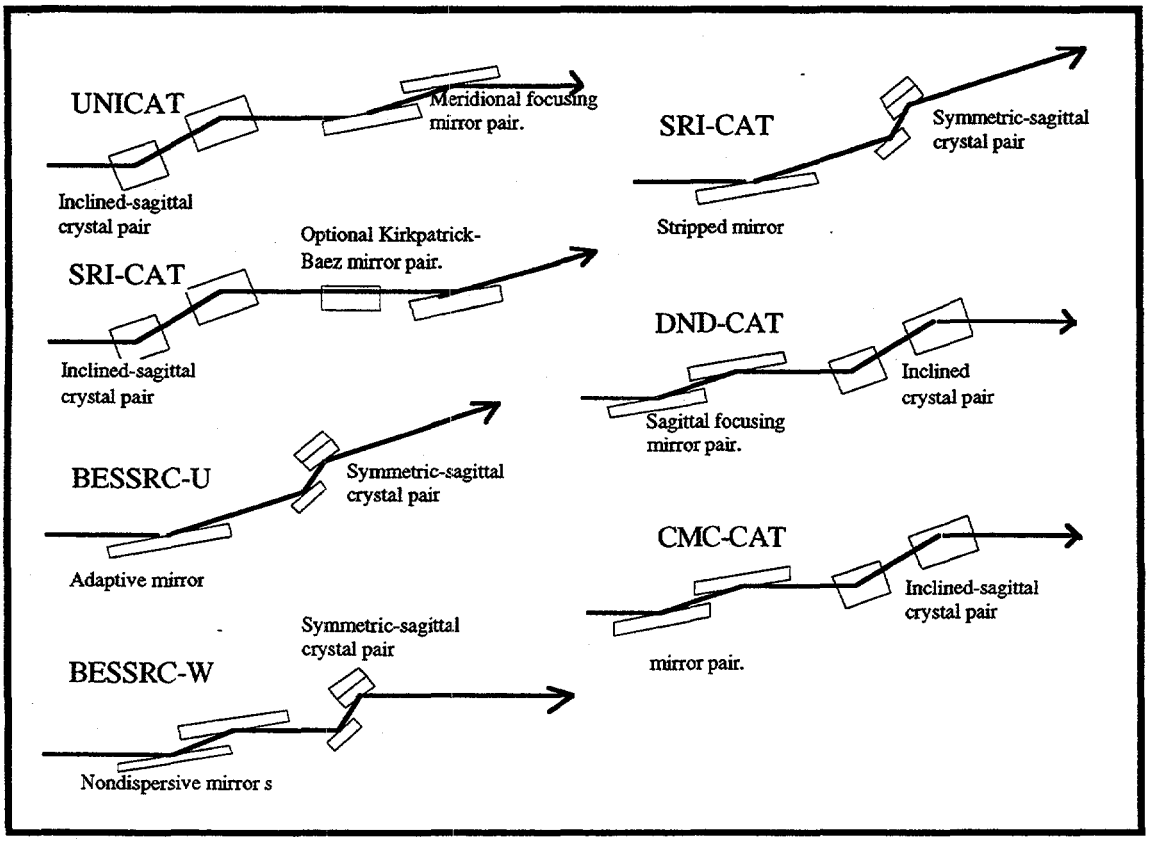

Fig. 5. Conceptual beamline designs at the APS.

The next step in beamline modeling involves specifying beamline parameters for modeling. This is followed by detailed modeling of component performance, and modeling of the overall beamline with analytical, phase space or ray trace models. The estimated beamline performance is then compared to alternative designs and the process is iterated until the designer is satisfied as illustrated in Fig. 3.

FOUNDATIONS OF X-RAY OPTICS

Early modeling of x-ray instrumentation built on x-ray optical principles developed for conventional x-ray sources and on x-ray astronomy. For example, the basic theory of x-ray focusing with mirrors [3,4] and x-ray focusing with crystals, [5-7] has a long history of use with conventional sources and Kirkpatrick and Baez [3] demonstrated the principles of an x-ray microscope/microprobe with crossed meridional mirrors (Fig. 6) long before the discovery of synchrotron radiation. The introduction of x-ray synchrotron sources in the 70s however, led to synchrotron specific instrumentation papers and to whole conferences devoted to synchrotron radiation instrumentation [8,9]. These conferences and papers began addressing the new challenge of utilizing tunable and extremely intense x-ray sources.

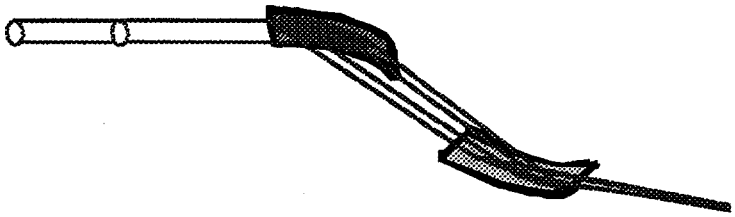

Fig. 6 Kirkpatrick-Baez mirror pair.

The First International Conference on Synchrotron Instrumentation and Developments was held in Orsay France in 1977 [8]. This conference attracted over 170 participants and was extended to a three day meeting with over 65 papers. In 1978 a Workshop on X-ray Instrumentation for Synchrotron Radiation Research at the Stanford attracted over 150 participants and again more than 65 papers. These early conferences introduced scientists to many new concepts including mosaic crystal focusing monochromators, synthetic multilayers, phase space optics, and x-ray induced mirror damage. Conference proceedings and refereed journal articles were augmented with synchrotron facility reports. For example, thermal analysis of components [10] (Be windows, etc.), software and experimental design [11], source properties[12], and a host of other topics of great interest to beamline designers were treated through facility reports. In addition synchrotron radiation books began to be published which included detailed considerations on instrumentation design [1].

ANALYTIC MODELING

For individual beamline components it is often possible to study their behavior through analytical techniques. These techniques are fast and can be integrated into ray-tracing programs which combine multiple components. Mirror reflectivity (Fig. 7) can be calculated from fairly simple programs to estimate the dependence on surface coating, x-ray energy and glancing angle [13]. Surface roughness, its spectral density function and contamination can also be treated by analytical models to estimate their effect on mirror performance [14-16]. Analytical models are also used to estimate the aberrations associated with various focusing schemes [3,17]. With a Kirkpatrick-Baez mirror system, a simple analytical formula estimates the divergence which can be collected before aberrations dominate the demagnified image size. Analytical models have also been used to study the Bragg angle matching between x-ray crystals with a flat-crystal sagittal-crystal pair. Sparks, et

al. [18] were able to show that a cylindrically curved crystal set for M~1/3 intercepts a fan of radiation at a nearly constant Bragg angle. A nondispersive flat-crystal sagittal-crystal pair were also found to match Bragg angles for a wide range of magnifications when the focusing crystal was bent to a conical (Fig. 8) shape [19].

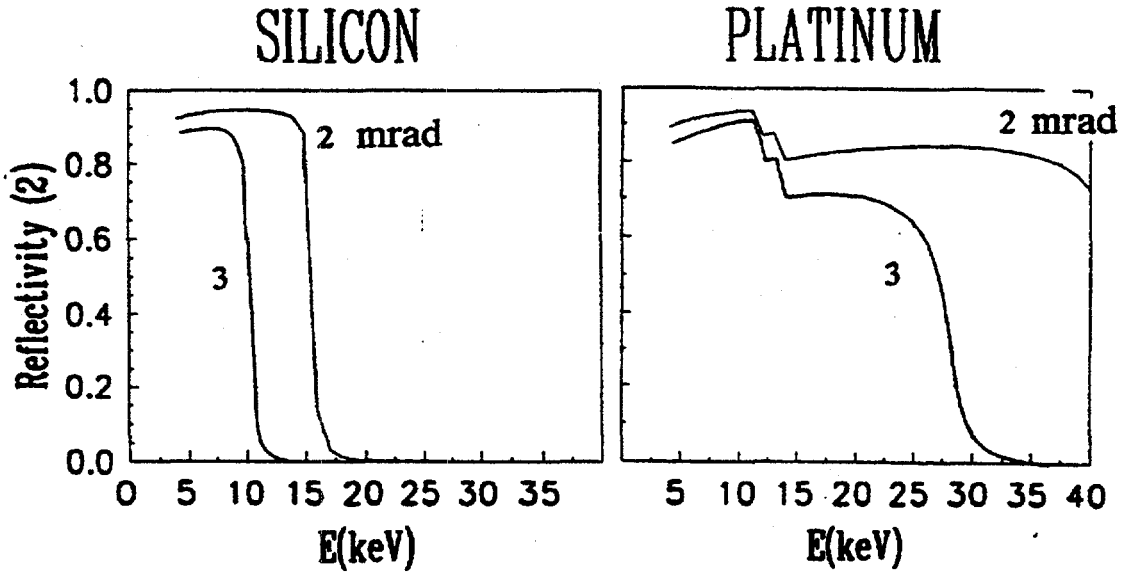

Fig. 7 Mirror x-ray reflectivity through a pair of non-dispersive mirrors as a function of x-ray energy, coating, and glancing angle.

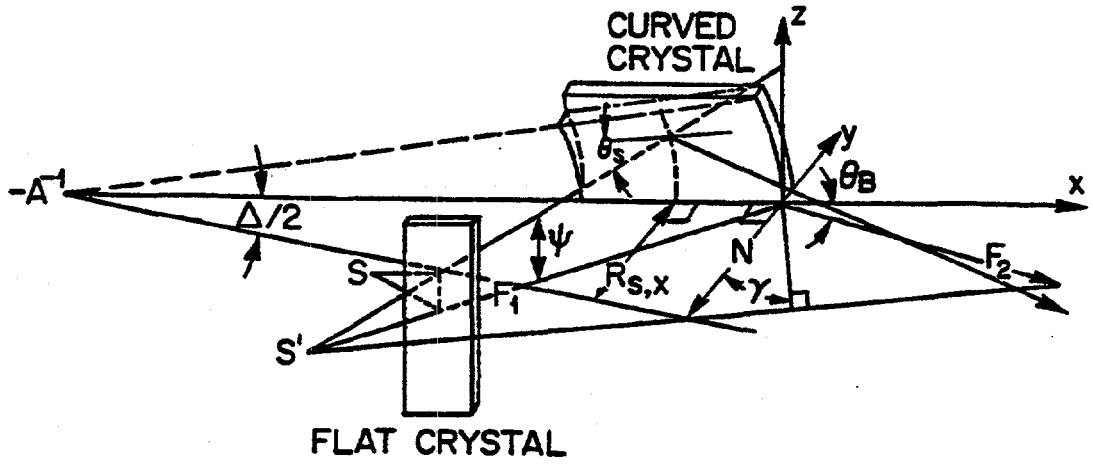

Fig. 8

Conical crystal geometry.

PHASE SPACE OPTICS

Powerful phase space modeling techniques are also often used to study the behavior of synchrotron beamlines and components. Phase space optical approaches originated with charged particle optics of the accelerator based sources. Within the phase space description, it is possible to follow the beam from the source through optics and then map the fraction of the source which is transported to the experiment. The key advantage of phase space optics is the ability to predict performance limits of various optical schemes. In addition, phase space optics can be used to

estimate the deleterious effects of apertures and surface roughness. With phase space optics, it is fairly easy to estimate the surface roughness required to preserve x-ray brilliance (Fig. 9). Although the general techniques are very powerful, they are difficult to use with complicated optics. The best publication is somewhat difficult to find [20].

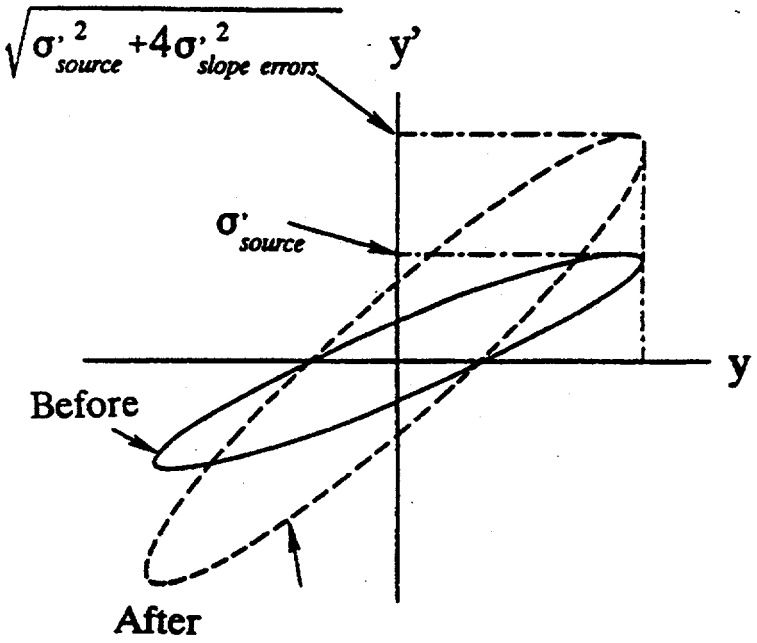

Fig. 9 Surface roughness effect on x-ray brilliance.

RAY TRACING

Modeling of complicated x-ray components and beamlines is most often done using ray tracing techniques. An early suite of ray tracing programs was introduced by Darsbury around 1982. These were soon followed by the program SHADOW [21] around 1985. SHADOW has become the x-ray standard because it accurately handles many different optical elements. In particular SHADOW, unlike some other programs, handles asymmetric crystals and rough surfaces.

One problem with SHADOW is its cumbersome interface. Early versions of SHADOW also suffered from a limited number of rays, and a limited number of computer platforms. These problems have restricted routine use of SHADOW. Most often SHADOW is used to *verify* beamline designs. Beamline designers tend to use faster and more use-friendly ray-trace programs to develop beamline concepts.

Specialized ray-tracing programs are often fast and flexible but are not as well tested and hence not as convincing as SHADOW. For example, a suite of programs have been coded at ORNL to help in the design of x-ray microbeam and x-ray diffraction beamlines. These programs are very fast, can handle 10^6 rays easily and can be configured for simple optimization of beamline design. However these programs cannot easily handle diffraction limited conditions, are only accessible to expert programmers, and are not stable (i.e. the code changes at the users whim). Nevertheless, even simpler ray tracing programs have been used to discover these and new ray optical designs.

The discovery of the cylindrical crystal focusing geometry is a good example of an application of a simple x-ray ray-tracing program. Sparks, et.al. [18] studied the Bragg angles of rays reflected through a flat-crystal cylindrical-crystal nondispersive pair (Fig. 8). To their surprise, at a magnification near 1/3, the Bragg angles matched for a large divergence out of the diffracting

plane. This discovery led to the development of dynamical sagittal crystal focusing optics which have been widely adapted for focusing synchrotron radiation. (Fig. 10).

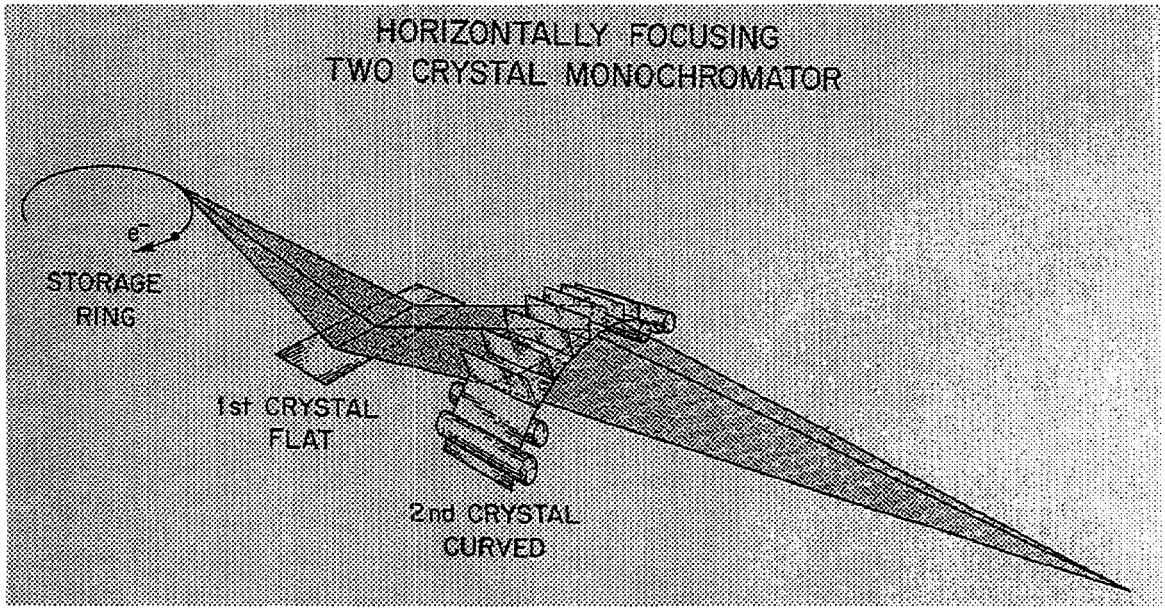

Fig. 10. Beamline optics for beamline X14 at the NSLS. The double crystal monochromator focuses the horizontal beam divergence with a dynamically-bent sagittal-focusing Si crystal.

A simple ray-tracing program was also used to discover that sagittal crystal focusing could be improved by going to a conically bent crystal [19]. This program was designed to search for an optimum cone angle at various magnifications. The program found that near M=1 the aberrations resulting from sagittal crystal focusing were minimized. This discovery led to the development of beamline X14 at the National Synchrotron Light Source (NSLS) which was the first beamline designed to use a dynamically bent two-crystal monochromator [22].

A simple ray-tracing program also found that a so called "inclined crystal" could be used to focus the out-of-plane synchrotron radiation divergence from an undulator. The inclined geometry[23] is designed to distribute the thermal load from a small high-intensity x-ray beam. The crystal surface is cut at an angle relative to the reflecting Bragg planes, but unlike an asymmetric geometry, the cut is perpendicular to the diffracting plane (Fig. 11). A ray tracing program was used much like an experiment to test the focusing properties of a sagittally focusing inclined crystal pair [24]. It came as a complete surprise that for an inclined crystal, the radius of curvature increases inversely with the cosine of the cut angle. This property greatly extends the tunable range of an inclined crystal of a given thickness compared to a sagittal focusing symmetric crystal. The program also mapped out the range over which aberrations were small (Fig. 12).

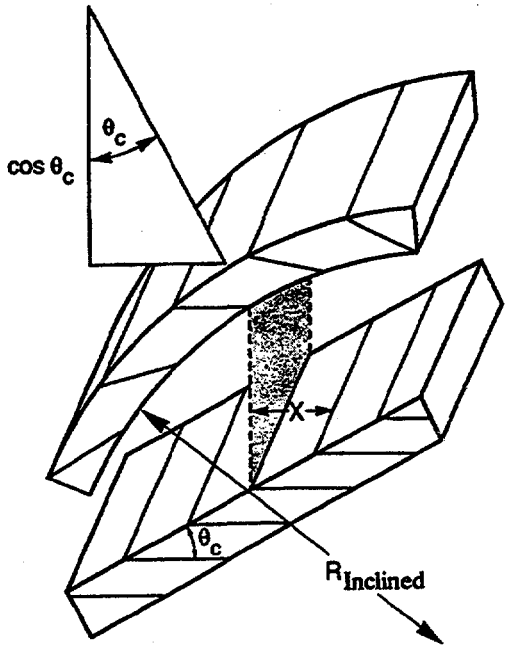

Fig. 11. Inclined crystal geometry showing the diffraction plane, Bragg planes and crystal surfaces. The second crystal is cylindrically curved to focus the beam horizontal divergence.

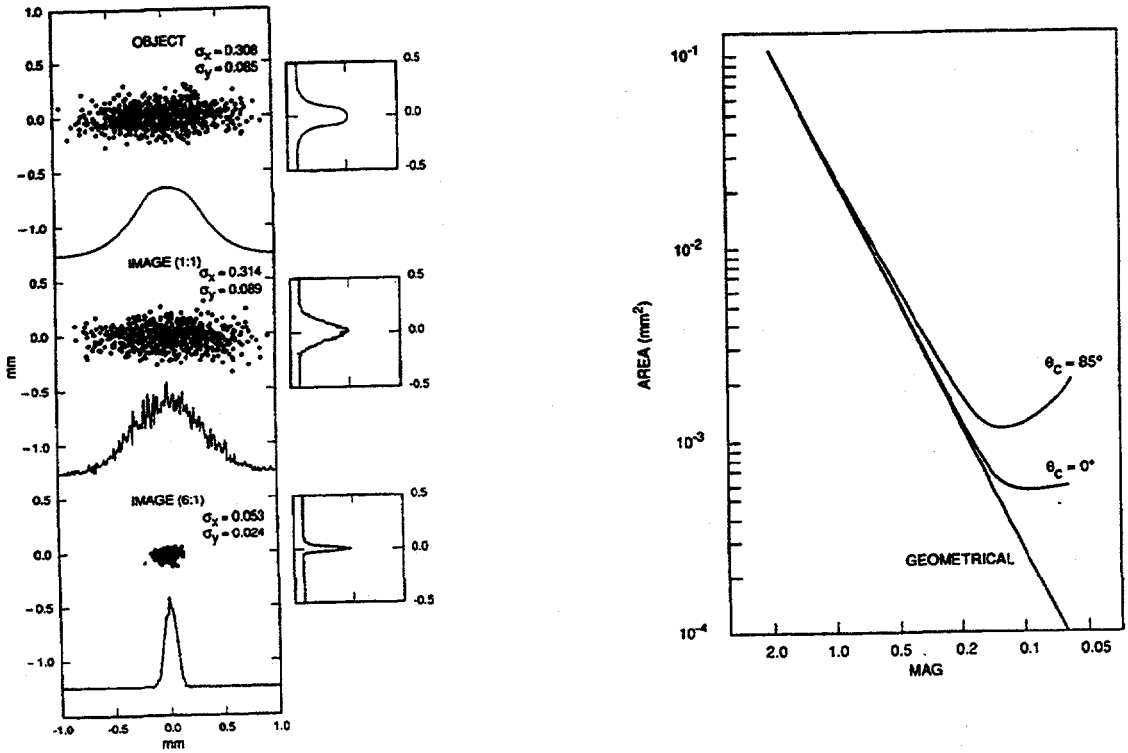

Fig. 12. Aberrations as a function of magnification for an undulator source and with a sagittal focusing inclined monochromator.

OTHER BEAMLINE MODELING RESOURCES

Source properties are critical to synchrotron beamline design. Analytical calculations and numerical recipes have evolved to accurately predict the source properties of bend magnet, wiggler and undulator synchrotron sources. Undulator source properties are particularly complicated and the program URGENT has provided the community with a fast, well documented program to predict the source properties of most undulator devices [23].

Shielding also presents a very important aspect of beamline design for high energy synchrotron sources. Although analytical models exist for shielding design, these are complicated to apply. Numerical codes based on the analytic models allow rapid verification that the analytic model predicts adequate shielding under all possible conditions [26,27].

CONCLUSION

There are many design tools available for modeling the performance of synchrotron radiation beamlines. These tools have evolved rapidly over the last two decades and allow beamline designers to predict the performance of new beamline concepts. Because of a vigorous and growing community interested in the design of synchrotron radiation instrumentation, design tools are constantly being tested and improved. The availability of several standard tools has simplified the task of verifying beamline designs.

ACKNOWLEDGEMENT

Research sponsored by the Division of Materials Sciences, U.S. Department of Energy under contract DE-AC05-96OR22464 with Lockheed Martin Energy Research Corporation.

REFERENCES

1. See for example Herman Winick, in *Synchrotron Radiation Research* , H. Winick and S. Doniach Editors, Plenum Press, New York and London, pp. 27-59 (1980).

2. N. Ipe, D.R. Haeffner, E.E. Alp, S.C. Davey, R.J. Dejus, U. Hahn, B. Lai, K.J. Randall, and D. Shu, *Guide to Beamline Radiation Shielding Design at the Advanced Photon Source* **ANL/APS/TB-7**, Argonne Il (1993).

3. P. Kirkpatrick and A.V. Baez, "Formation of Optical Images by X-rays", *J. Opt. Soc. Am.* **38** 766 (1948).

4. A. Franks, "X-ray Optics", *Sci. Prog. Oxf.* **64**, 371 (1977).

5. H. H. Johann, *Z. Phys.* **69** 185 (1931).

6. T. Johansson, *Z. Phys.* **82** 507 (1933).

7. V. L. Hamos, *Annalen der Physik,* **5** 716 (1933).

8. F. Wuilleumier and Y. Farge eds., *Nucl. Inst. and Methods* **15**, "Proceedings of the International Conference on Synchrotron Radiation Instrumenation and Methods", Orsay France, (1977).

9. H. Winick and G. Brown eds., SSRL Report **78/04**, "Workshop on X-ray Instrumentation for Synchrotron Radiation Research", (1978).

10. N. Hower and C. Jako, SSRL Technical Report **78/02**, "Thermal Test of A Synchrotron Radiation Beam Port Model (1978) and W. Thomlinson and K. Ludwig, BNL Informal Report 26420, "Analysis of Thermal Problems of X-ray Beam Lines", (1979).

11. B. M. Kincaid, SSRP Report **75/03**, "Synchrotron Radiation Studies of K-Edge X-ray Absorption Spectra; Theory and Experiment" (1975).

12. G.K. Green, "Spectra and Optics of Synchrotron Radiation", in BNL 50595 Vol. II, proposal for a National Synchrotron Light Source, (1977).

13. J. J. LePage, "Grazing Incidence Reflection Measuremtns on Beryllium", Workshop on X-ray Instrumentation for Synchrotron Radiation Research, H. Winick and G. Brown eds., SSRL Report **78/04**, (1978); D. H. Bilderback "Reflectance of X-ray Mirrors From 3.8 to 50 keV" CHESS Technical Memorandum No. 16 (1981).

14. E.L. Church and P.Z. Takacs, "Prediction of mirror performances from laboratory measurements", in *X-ray/EUV Optics for Astronomy and Microscopy,* Proc. SPIE **1160** 323 (1989).

15. E.L. Church and P.Z. Takacs, "The interpretation of glancing incidence scattering measurements", in *Grazing Incidence Optics* Proc. SPIE **640** (1986).

16. A.K. Freund, F. deBergevin, G. Marot, C. Riekel, J. Susini, L. Zhang, and E. Ziegler, "X-ray mirrors for the European Synchrotron Radiation Facility", *Opt. Eng.* **29** 928 (1990).

17. G.E. Ice and C.J. Sparks," Focusing Optics for a Synchrotron X-Radiation Microprobe", *Nucl. Inst and Methods* **222** 121 (1984).

18. C.J. Sparks, B.S. Borie and J.B. Hastings,"X-ray monochromator for focusing synchrotron radiation above 10 keV", *Nucl. Inst. and Meth.* **172** 237 (1980).

19. G.E. Ice and C.J. Sparks, 'Conical geometry for sagittal focusing as applied to x-rays from synchrotrons", *J. Opt. Soc. Am.* **11** 1265 (1994).

20. E. Johnsom, H. Hulbert and L. Berman, *AIP Proceedings* **249** AIP New York 1 859 (1992).

21. F.Cerrina, SPIE **503** 68 (1984); B.Lai and F. Cerrina, SPIE **563** 174 (1985).

22. A. Habenschuss, G.E. Ice, C.J. Sparks and R.A. Neiser, "The ORNL Beamline at the National Synchrotron Light Source", *Nucl. Inst and Meth.* **A266** 215 (1988).

23. A.T. Macrander, W.K. Lee, R.K. Smither, D.M. Mills, C.S. Rogers, and A.M. Khounsary, Nucl. Instrum. Meth. **A319** 188 (1992).

24. G.E. Ice and C.J. Sparks, "Sagittal crystal focusing of undulator radiation with high heat load inclined crystals", *SPIE* **1740** 11 (1992).

25. R.P.Walker andB. Diviacco, "Urgent: A program for calculating Undulator Radiation properties," Proc. 4th Int. Conf. Synchrotron Radiation Instrumentation, Chester, July 1991.

26. G.E. Ice, "Preliminary and Final Design Reports for the UNI-CAT ID Beamline," (1994 and 1995).

27. G. Rosenbaum, SBC CAT PDR and private communication.

NEUTRON SPECTROSCOPY: HOW IT ALL BEGAN

Laurence Passell

Brookhaven National Laboratory, Upton, NY, USA

Abstract

Abstract:The early history of neutron specroscopy is briefly presented

1932-1945

Most of James Chadwick's scientific contemporaries saw his discovery of the neutron in 1932 as the end of a long and exceedingly difficult search for the identity of the basic building blocks of the atomic nucleus. But to Enrico Fermi and his collaborators at the University of Rome - newly involved in a study of artificial radioactivity - it was both an end and a beginning: an end in that the elusive neutral particle had at last been found and a beginning in that the neutron appeared to offer expanded possibilities for the production of radioactive nuclei. Before the year was out the University of Rome Group was deeply immersed in a systematic study of neutron-induced radioactivity.

Some two years later, in 1934, while attempting - unsuccessfully - to reproduce an earlier-reported neutron activation investigation, the Rome Group found, to their considerable astonishment, that the level of induced activity seemed to depend on where in their laboratory the measurement was made. Searching for the origin of this curious effect, they began interposing various materials into the space between the target and the Ra-Be source that provided the neutrons. One material they tried, paraffin wax, produced a dramatic increase in the level of activation. Fermi, a theorist who had only recently turned his hand to experimental nuclear physics, was initially puzzled by this unexpected result. But it led him to what he afterwards referred to as "the most important discovery I ever made". After pondering the matter he came to the conclusion that the Ra-Be neutrons were losing energy by colliding with protons in the paraffin and that this "moderating effect" was what had increased the capture probability.

The following year, at Columbia University, Dunning, Pegram, Fink, Mitchell and Segre[1], using the device shown in Figure 1, demonstrated that paraffin wax was indeed an effective neutron moderator, exactly as Fermi had surmised. As the forerunner of a long line of spectrometers operating on the time-of-flight principle, the device they built to put Fermi's idea to the test is worth looking at in detail. Basically, it consisted of a pair of identical aluminum disks mounted 54 cm apart on a common shaft, each with alternating cadmium-covered and open sectors. As the speed of rotation was increased, the downstream disk absorbed neutrons with progressively greater velocities. Dunning et al found that the greatest drop in intensity occurred at rotation speeds of 2900 to 3000 rpm from which they inferred that the most probable velocities in the moderated part of the incident neutron spectrum were in the range of 2250 to 2700 m/sec.

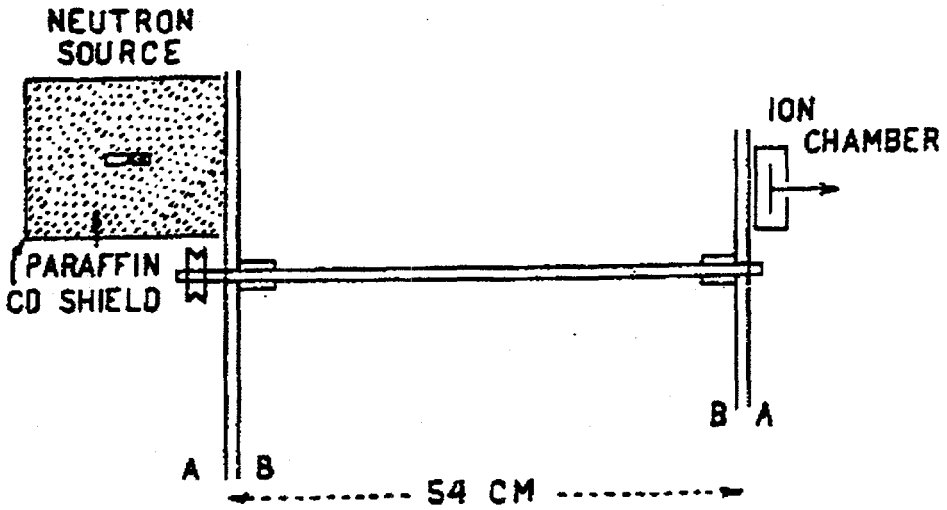

Schematic drawing of mechanical velocity selector for slow neutrons. *A*, rotating disk with Cd sectors; *B*, fixed disk with Cd sectors.

J.R. Dunning, G.B. Pegram, G.A. Fink
D.P. Mitchell and E. Segre
Phys. Rev. 48, 704 (1935)

Fig. 1 Schematic of the mechanical velocity selector built by Dunning, Pegram, Fink, Mitchell and Segre in 1935.

The discovery that neutrons could be slowed down to energies in the thermal range had profound ramifications. One was that it inspired Leo Szilard to consider the possibility of a self-sustaining, neutron-producing chain reaction. Another was that it led to speculation that thermal neutrons might some day be useful spectroscopically since they were known to be not only charge-neutral but also to have energies and de Broglie wavelengths comparable to the collective excitation energies and interatomic spacings in condensed matter. Lacking at the time, of course, were sources that could provide thermal beams of adequate intensity. Nonetheless, soon after Fermi's epic discovery attempts were made to establish that neutrons did, indeed, have a spectroscopic potential, remote though it then appeared to be.

In 1936 Mitchell and Powers [(2)], following up on the earlier neutron studies at Columbia, built the device shown in Figure 2 to explore the possibility that thermal neutrons, like x-rays, could be diffracted by ordered crystalline materials.. To compensate for the extremely low thermal beam intensities produced by their paraffin-moderated Ra-Be source, Mitchell and Powers mounted an array of MgO single crystals around a central, cylindrical shield designed to screen the detector from direct, line-of-sight source neutrons. When the crystals were oriented to Bragg reflect neutrons with wavelengths in the neighborhood of 1.6 A (2475 m/sec) - which had earlier been observed to be the most probable wavelength in the thermal part of the spectrum - count rates were found to be six to eight times higher. It thus became evident that coherent reflection could, at least in principle, be employed both as a monochromating method and for atomic-scale structural determinations.

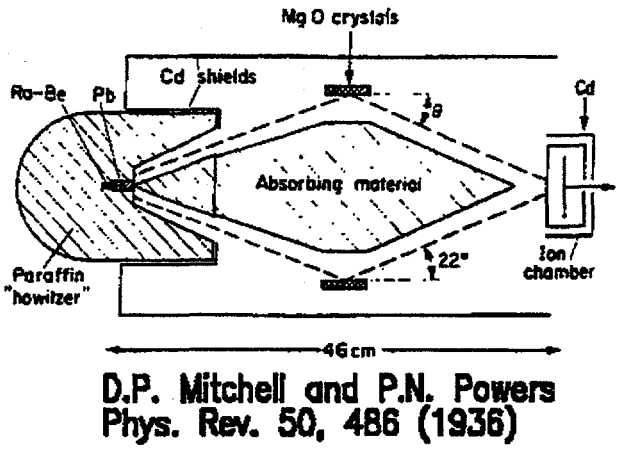

Fig. 2 Schematic of the apparatus built by Mitchell and Powers in 1936 for their investigation of neutron diffraction.

By this time investigations of the hyperfine splitting of spectral lines had established that neutrons (like protons and electrons) had an intrinsic spin and (like their charged counterparts) must therefore possess a magnetic moment. In 1939 Louis Alvarez and Felix Bloch - uitilizing the more intense accelerator-produced neutron beams then available - were able to demonstrate that neutron scattering in ferromagnets was a spin-dependent process and that partially polarized beams could be produced by simply passing them through blocks of magnetized iron. Once a way had been found to polarize neutrons, it was then possible to employ the magnetic resonance methods pioneered by Isidore Rabi and his collaborators at Columbia University to measure the magnetic moment of the neutron. The spectrometer built by Alvarez and Bloch [3] in 1940 to make the original measurement is shown in Figure 3. It was the first of many neutron instruments to utilize polarized neutrons and it was also the first in which resonance techniques were employed.

While these initial evaluations of the properties and possible uses of thermal neurons were being made in the United States, Fermi and his collaborators were pressing ahead with their exploration of neutron-induced radioactivity. Progressing slowly through the periodic table, they ultimately began to concentrate their attention on neutron capture in uranium, the heaviest known element, in the belief it would lead them to even heavier elements (transuranics) not present in nature. They were soon joined in the search for transuranics by Irene Curie and her collaborators in Paris and by Otto Hahn, Lise Meitner and Fritz Strassmann in Berlin. Initially, the efforts of all three groups were fruitless: no evidence of radioactive atoms with the expected chemical properties could be found.. Finally, in 1939, Hahn and Strassmann made an exhaustive chemical analysis of the products of thermal neutron capture by uranium and established that intermediate-mass radioactive nuclei, not transuranics, were being produced. They were thus led to the startling conclusion that neutron capture in uranium led to a totally new process, neutron-induced-fission. Soon thereafter it was determined that both neutrons and intermediate-mass nuclei were produced in the fission process. Hahn and Strassmann's astonishing discovery had thus moved Szilard's idea of a self-sustaining neutron-generating chain reaction an important step closer to reality.

VII. 3. Neutron magnetic moment

The earliest resonance measurement of the neutron magnetic moment was that of Alvarez and Bloch (ALV 40). A schematic diagram of their apparatus is shown in Fig. VII. 2. Their neutrons were produced by deuteron bombardment of Be; they were polarized and analysed by passing them through magnetized pieces of Swedish iron about 4 cm thick. With these pieces of iron the neutron transmission increased about 6 per cent. on application of the magnetic field. A Rabi type

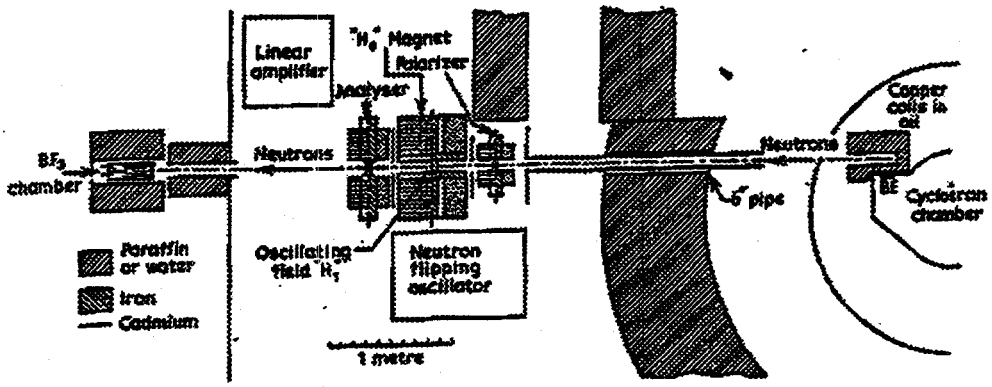

FIG. VII. 2. Plan of apparatus for Alvarez and Bloch neutron magnetic moment measurement (ALV 40).

single-oscillating field was used to induce the transitions. A typical neutron resonance curve is shown in Fig. VII. 3. The magnetic field was calibrated in terms of the magnetic field and frequency inside a cyclotron tuned to accelerate protons. The result of this experiment was $\mu_n = 1{\cdot}93 \pm 0{\cdot}02$ nuclear magnetons.

L.W. Alvarez and F. Bloch, Phys. Rev. 57, 111 (1940)

Fig. 3 Schematic of the apparatus built by Alvarez and Bloch in 1940 for the original measurement of the magnetic moment of the neutron.

These crucial experiments were carried out in a political atmosphere that ultimately became so hostile that it forced many of Europe's most prominent scientists, among them Fermi and Szilard, to relocate in the United States. By September of 1939, when World War II engulfed Europe, the European emigre scientists and their American counterparts had moved the United States to the forefront in nuclear research. At some time between September, 1939 and December, 1941 (when the United States entered the War), Szilard, who had settled in New York City, succeeded in his quest to persuade an initially skeptical Fermi (then a member of the Columbia University faculty) that a neutron-generating chain reaction based on the fission process was a practical possibility.

Late in 1942, a group under Fermi's direction completed construction of what would come to be known as the CP-1 reactor and demonstrated the first self-sustaining fission chain reaction.. In the excitement of the moment it is doubtful that anyone present thought to consider that the fission process - apart from its potential to produce weapons of unparalleled destructive power - could also produce thermal neutron beams of unprecedented intensity. Be that as it may, once the

practicality of generating and controlling fission chain reactions had been demonstrated, the nuclear weapons development program escalated rapidly. Reactor construction, as part of this program, was given the highest possible priority. A little more than two years later reactors capable of producing beams of thermal neutrons were in operation at both the Argonne and Clinton Laboratories. Not surprisingly, the needs of the weapons program pre-empted the possible use of reactors as neutron sources for basic science investigations.

1945-1960

It was only after World War II came to an end in August 1945 that reactor-produced thermal neutron beams finally became available to the scientific community. Once given the opportunity, the select few at the Argonne and Clinton Laboratories who had access to these beams immediately set to work to determine what role (if any) neutrons might be able to play in exploring the atomic-scale properties of crystalline solids and other forms of condensed matter. Characteristically, Fermi led the way in this new endeavor.

From the beginning it was recognized that improvements in reactor design as well as a realistic evaluation of possible spectroscopic applications required, first and foremost, a more complete understanding of the neutron scattering and absorptive properties of nuclei. Thus in the immediate post-war years the primary focus was on two kinds of instruments: those intended to measure scattering and absorption cross sections and those designed to determine - for spectroscopic purposes - the signs and magnitudes of scattering amplitudes.

As would be expected, the first reactor-based neutron instruments employed the same operating principles as their earlier, pre-war counterparts. They were of two basic types, those utilizing diffraction from single crystals and those employing time-of-flight to define neutron energies. In the "single crystal" category were instruments developed in early 1946 by Lyle Borst and his coworkers [4] at the Clinton Laboratory (now known as the Oak Ridge National Laboratory) and by Walter Zinn [5] - probably in collaboration with Fermi - at the Argonne Laboratory. A schematic of Zinn's spectrometer is shown in Figure 4. Consisting of a pair of cadmium-slits to define the incident polychromatic beam, a monochromating (calcite) single crystal and a shielded, BF_3 neutron detector, it would be classified today as a "single-axis" spectrometer. Energy scanning required a combined (1:2) rotation of the crystal and the arm supporting the detector. Cross sections were determined by measuring the energy dependence of transmission through a sample of the material of interest placed in the monochromatic beam between the crystal and the detector.

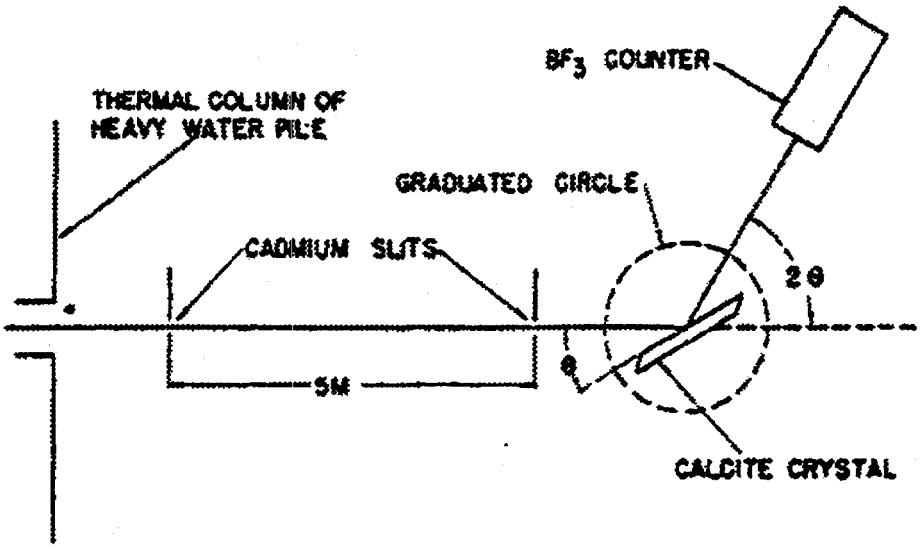

First experimental arrangement.

W.H. Zinn
Phys. Rev. 71, 752 (1947)

Fig. 4 Schematic of Zinn's 1947 single-axis spectrometer.

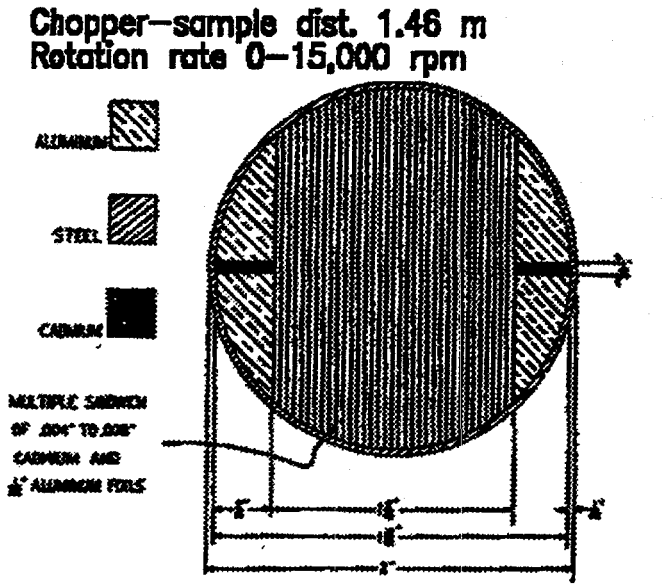

Cross section of the shutter of the velocity selector.

E. Fermi, J. Marshall and L. Marshall
Phys. Rev. 72, 193 (1947)

Fig. 5 Schematic of the rotor of the original Fermi chopper built in 1947.

During the war years the time-of-flight approach had been extensively used for accelerator-based neutron cross section measurements. Aware of this, Fermi and his collaborators [6] decided it would be useful to adapt these well-established time-of-flight techniques to reactor-based cross section studies. Figure 5 shows the original "Fermi chopper" built at the Argonne Laboratory reactor and called (somewhat misleadingly) by its creators "a velocity selector". Small by current standards, it had a rotor only two inches in diameter and was driven (at speeds as high as 15000 rpm) by a belt attached to the motor of a shop grinder. A stack of aluminum plates separated by cadmium foil spacers in the center of the rotor introduced the requisite pulsed structure into the transmitted polychromatic beam. Neutron energies were determined by measuring their time-of-flight from the rotor to a bank of four shielded BF_3 detectors 1.46 meters away. The corresponding time dependence of the transmission through a sample placed between the rotor and the bank of detectors determined the energy dependence of the cross section.

Fermi and his coworkers were also the inventors of the polycrystalline neutron filter. The original test of the concept [7] was made at the Argonne reactor early in 1946 using a 23 cm long block of crystalline graphite. Subsequently the group demonstrated that blocks of poycrystalline beryllium and beryllium oxide were also excellent filter materials.

From the viewpoint of condensed matter studies, there was at least as much need to measure scattering amplitudes as cross sections. This led to the next step forward in instrument development. Both the Argonne and Oak Ridge Groups were aware that only in the case of mono-isotopic (or nearly so), spin-zero nuclei, such as helium, carbon, oxygen, etc, was it possible to derive scattering amplitudes directly from the measured scattering cross sections. Most scattering amplitudes, it was recognized, would have to be determined either from studies of diffraction from two-element crystalline materials or from measurements of critical angles for total reflection. The construction of what we would now call two-axis diffractometers was thus undertaken as one part of this two-pronged attack on the scattering amplitude problem.

Fermi's Group at the Argonne reactor built the first two-axis instrument. Adapted from Zinn's original single-axis spectrometer, it had a CaF_2 monochromating crystal on the first axis and, on the second axis, a goniometer designed to support and align a single crystal sample. An arm carrying a shielded detector rotated around the second axis. Today we would describe the upgraded Zinn spectrometer as a single crystal neutron diffractometer. With it Fermi and Leona Marshall [8] measured the intensities of low-index Bragg reflections from a number of two-element single crystals. By selecting crystals of known structure containing one element whose scattering amplitude had already been determined, they were able to derive from the observed diffracted intensities both the relative sign and magnitude of the unknown scattering amplitude.

Ernest Wollan and Clifford .Shull [9] chose to attack the scattering amplitude problem in a slightly different way. The two-axis instrument shown in Figure 6 was built for them at Oak Ridge not long after the Argonne diffractometer became operational. Of the same basic design as the Argonne instrument, the Oak Ridge diffractometer had one important advantage: it was motor-driven and had an automated data collection system and thus could operate unattended in a continuous-scanning mode. Where the Wollan and Shull approach differed from Fermi and Marshall's was that they chose to work with powder samples. Even though the diffracted intensities were lower, using powders eliminated the need to make extinction corrections to the diffracted intensities, a source of significant systematic error in the single crystalmeasurements. With today's perspective, we see the Wollan-Shull two-axis instrument as the first in a long line of automated neutron powder diffractometers.

Diffraction measurements determined only the relative signs of the scattering amplitudes. Casting about for a way to put the determinations of sign on an absolute basis, the Argonne Group turned to reflection techniques: the existence (absence) of finite-angle total reflection being identified, with, repectively, positive (negative) scattering amplitudes. Reflectometry also had another attractive feature: in cases where finite-angle total reflection was observed, the scattering amplitude could be directly derived from the measured critical angle. The first neutron reflection measurements were made by Fermi and Marshall [8] using mirrors of selected metals mounted on the sample axis of the Argonne diffractometer. It is interesting to note that these measurements and others that followed were made solely to determine the signs and (in some cases) the magnitudes of scattering amplitudes. Almost three decades would pass before neutron reflection would be reintroduced as a microscopic-scale probe of surfaces and interfaces.

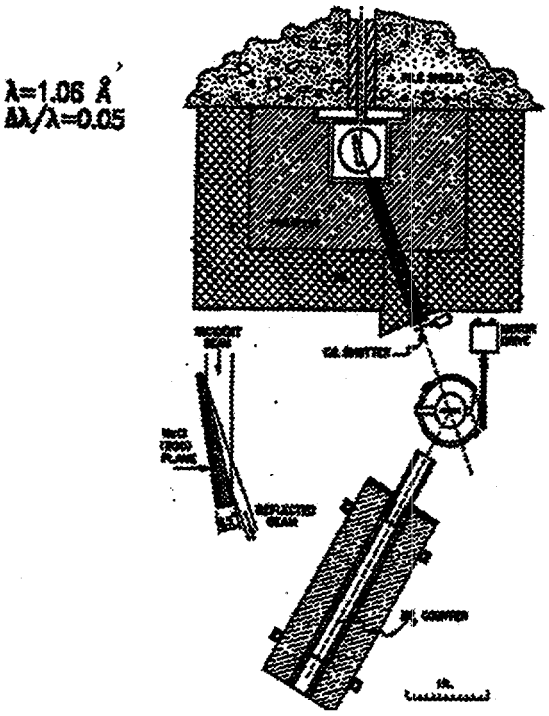

Arrangement of apparatus, showing the monochromating crystal (detailed in left center) collimating slits, shielding, second spectrometer with location of powder specimen and counter.

E.O. Wollan and C.G. Shull
Phys. Rev. 73, 830 (1948)

Fig. 6 Schematic of Wollan and Shull's 1948 powder diffractometer.

Another major step forward in neutron spectroscopy, although it wasn't apparent at the time, was P.R. O'Connor and G.T. Seaborg's [10] 1948 investigation of the neutron-producing spallation reaction. More than two decades would elapse before spallation would be seen as a practical alternative to fission as a means of generating copious neutron beams for research.

Although the beams produced by the first reactors were considerably more intense than those provided by either Ra-Be sources or, for that matter, the accelerators of the day, they were still only marginally adequate for diffraction measurements. Aware that neutron diffraction was unlikely to be competitive for the kinds of structural studies that traditionally fell within the domain of x-ray crystallography, the early neutron spectroscopists chose, instead, to take advantage of the magnetic moment of the neutron and concentrate on an area that was not then accessible with x-rays and about which little was known; i.e. magnetism and magnetically ordered structures. It was, in fact, an early attempt to explore magnetic ordering in iron with neutrons that led Donald Hughes and his collaborators [11] to the realization that small angle neutron scattering was a potentially valuable source of information concerning structures of intermediate scale (in this case magnetic domains). Figure 7 shows the facility they built in 1949 for small-angle studies at the Argonne reactor. Utilizing a polychromatic beam defined by cadmium slits, their instrument can be seen today as the first step towards the creation of the small-angle-neutron-scattering spectrometers that are used today to explore the microscopic-scale configurations of polymers and biological systems.

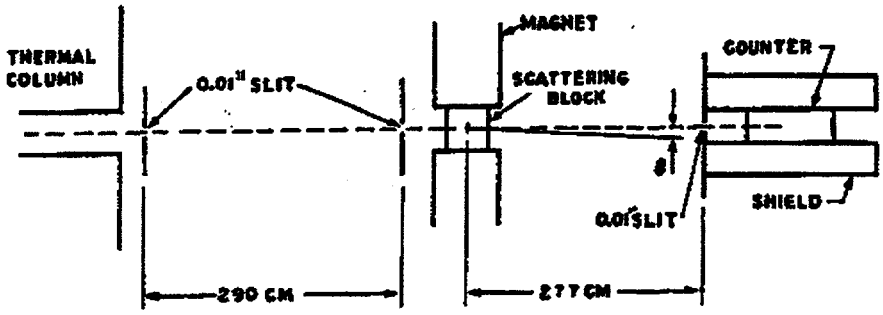

Equipment for study of small-angle scattering; the neutron intensity as a function of θ is measured by moving the counter and slit in the plane of the figure (horizontal plane).

D.J. Hughes, M.T. Burgy, R.B. Heller and J.W. Wallace, Phys. Rev. 75, 565 (1949)

Fig. 7 Schematic of the Hughes, Burgy, Heller and Wallace apparatus built in 1949 for small angle investigations.

As a unique source of information relating to magnetic structures and magnetic ordering transitions, neutron diffraction investigations soon began to attract the attention of the scientific community. This rapid rise of interest in magnetic systems was the inspiration for the next step forward in instrumentation: a polarization-analysis capability, it was recognized,would increase the sensitivity and selectivity of magnetic measurements. Thus a search began for better ways to polarize neutrons,

Up to the end of 1949, neutron instruments and instrument components were basically copies of their x-ray and accelerator physics counterparts. But in attacking the polarization problem, a purely neutron approach emerged. Both the Argonne and Oak Ridge groups decided to try exploiting a concept that derived from Otto Halpern and M.H. Johnson's [12] theoretical analysis of neutron interactions with magnetic atoms; namely that the nuclear and magnetic parts of the scattering were coherent and would therefore interfere. Looking through tables of the commonly available ferromagnetic materials, Morton Hamermesh at Argonne found one, cobalt, in which the magnetic scattering amplitude was larger than the nuclear amplitude. He suggested that one of the two spin states of the neutron would have a positive scattering amplitude and therefore be totally reflected at finite angles, while the other , having a negative scattering amplitude, would only totally reflect at zero angle. Capitalizing on Argonne's earlier experience with mirrors, Hughes and Merle Burgy [13] constructed a pair of identical cobalt mirrors bonded to copper substrates, one to serve as polarizer and the other as polarization analyzer. Although they were not able to align the cobalt magnetic moments completely with the available field, Hughes and Burgy nevertheless found they could produce substantially better broad-band polarizations by reflection than could be achieved by the earlier method of transmitting the beams through magnetized iron. Theirs was the first demonstration of neutron polarization by reflection.

Charateristically, the Oak Ridge Group chose to apply the interference concept somewhat differently. Based on their familiarity with diffraction techniques, Shull, Wollan and Walter Koehler [14] made a search for ferro or ferri-magnetic single crystals with low-index Bragg reflections in which the nuclear and magnetic parts of the scattering were so closely matched that only one of the two spin states of the neutron would scatter coherently. Using transmission through magnetically saturated iron to analyze the polarization of the Bragg-reflected beam, they were able to show that the monochromatic beam produced by the (220) Bragg reflection from a magnetically saturated single crystal of magnetite (a ferrimagnet) was essentially 100 percent

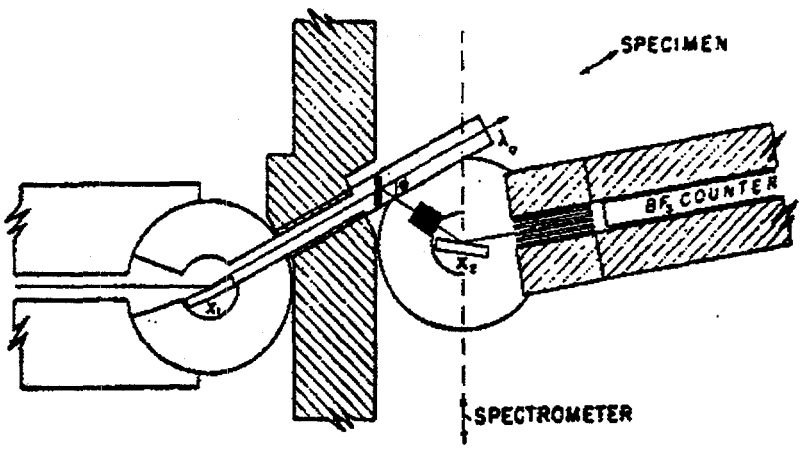

Schematic diagram of the apparatus. The angle of scattering ϕ can be changed by moving the specimen and the spectrometer as indicated.

B.N. Brockhouse, Phys. Rev. 99, 601 (1955)

Fig. 8 Schematic of Brockhouse's original triple-axis spectrometer built in 1954..

polarized. This striking result inspired the subsequent building of a number of crystal diffractometers with a polarization analysis capability.

Another instrument introduced during these early years was the helical-groove, slow-neutron velocity selector. By replacing the slotted-disk rotor of Dunning et al with a rotor containing spiral grooves, J.G. Dash and H.S. Sommers, Jr [15] were able to produce continuous, monochromatic, slow neutron beams by mechanical means alone. Although the helical-groove velocity selector subsequently fell into disfavor because its resolution and spectral range were limited, it is now coming back into its own both as a higher-order filter and as a monochromator for special applications (such as small angle scattering) where lower energy neutrons are preferred and high intensity is more important to the over-all performance of the instrument than energy resolution.

Because Argonne and Oak Ridge were the only places where facilities for neutron spectroscopy were available, almost all neutron instrument development work up to this point was concentrated at these two laboratories. But within a few years of the end of World War II new laboratories for nuclear and condensed matter research were under construction, not only in the United States but in Canada, western Europe and the Soviet Union, and as fast as these these new institutions were completed they began to build their own reactors and organize neutron scattering programs. With facilities for neutron research becoming more generally accessible, the focus of instrument development then began to shift from Argonne and Oak Ridge to the newer institutions.

In the early post-war years, reactor-produced beam intensities were barely sufficient for elastic studies and inelastic scattering investigations weren't given any serious consideration. But by the early 1950's a second generation of reactors producing more intense beams had come on-line and Bertram N. Brockhouse decided that the time had come to try adding a third axis (for an energy analyzing crystal) to the two-axis spectrometer. The first triple-axis spectrometer, which he built and installed at the NRX reactor at Canada's Chalk River Laboratory [16], is shown in Figure 8. With it Brockhouse made the first direct observations of propagating and diffusive modes in condensed matter systems launching thereby the new field of inelastic neutron spectroscopy.

It is interesting to note that in cases where instruments based on either crystal diffraction or time-of-flight could serve experimental needs equally well, both types tended to be developed at about the same time and were, for the most part, equally convenient and effective. Thus while plans to build a triple-axis spectrometer were moving forward at Chalk River, a variety of time-of-flight and combined crystal diffraction and time-of-flight approaches to inelastic spectroscopy were also under active consideration. at other laboratories. At Harwell, for example, Peter Egelstaff was thinking in terms of building a phased, two-rotor system to produce bursts of monochromatic neutrons [17]. But the technical problems of operating such systems and handling the large amounts of data they produced were not then easily resolved, and it would be well into the next decade before instruments based on time-of-flight became available for inelastic scattering investigations.

With increasing emphasis on inelastic neutron spectroscopy, a demand arose for spectrally tailored beams, particularly beams of sub-thermal energy. Interestingly, attempts to down-shift the spectrum of Ra-Be neutrons with cryogenically cooling hydrogenous moderators had actually been made in pre-war days, but the results had been inconclusive [18]. But by the 1950's numerous advances had been made in neutron technolgy and Egelstaff and his collaborators at Harwell decided to have another look at the problem. Coming ultimately to the conclusion that liquid hydrogen and deuterium offered the best prospects for success, they designed and constructed a liquid hydrogen moderator that was installed in Harwell's BEPPO reactor [19]. It performed so well that another was soon made for their DIDO reactor. Building on this early experience, liquid hydrogen (deuterium) moderators were subsequently installed in a number of other research reactors.

Retrospective

Looking back, 1960 appears as a watershed year for neutron spectroscopy. At that point, most of the basic instrumental concepts were in-place and neutron-based experiments were beginning to have a considerable impact on condensed matter physics. But it was a field still plagued by many problems. Certainly the major one was that it was very much source-constrained: beam intensities were marginal even at the best reactors and collecting statistically reliable data was a time-consuming and not always successful process. And because the vacuum tube electronics of the day were prone to drift and malfunction, even in the rare instances when sufficient beam time was available, reproducing data tended to be difficult, particularly when small cross section processes were the major focus of the investigation. Beyond that, the performance of the instruments themselves left much to be desired. Those employng crystal diffraction for monochromation were handicapped by the inadequate reflectivity of the available crystals; those based on time-of-flight had problems relating to support bearings and speed and phase control systems and were,. in addition, adversely affected by the limitations of their vacuum-tube-based data collection and data analysis systems.

In the decades that followed, high flux research reactors would be designed and built, stable transistorized electronics and digital computers would become commonly available, neutron guides would make their appearance, much better monochromating and polarizing crystals would be found and the development of magnetic suspension bearings and computerized instrument control, data collection and data analysis systems would bring time-of-flight-based spectrometers to full parity with their crystal-based counterparts. But even with these many technological advances, it is still easy to discern in today's state-of-the-art instruments the pervasive influence of instruments built by the first neutron spectroscopists long ago.

REFERENCES

(1) J.R. Dunning, G.B. Pegram, G.A. Fink, D.P. Mitchell and E. Segre - Phys. Rev. 48, 704 (1935)

(2) D.P. Mitchell and P.N. Powers - Phys. Rev. 50, 486 (1936)

(3) L.W. Alvarez and F. Bloch - Phys. Rev. 57, 111 (1940)
(4) L.B. Borst, A.J. Ulrich, C.L. Osborne and B. Hasbrouck - Phys. Rev. 70, 108A (1946)
(5) W.H. Zinn - Phys. Rev. - 71, 752 (1947)
(6) E. Fermi, J. Marshall and L. Marshall - Phys. Rev. 72, 193 (1947)
(7) H.L. Anderson, E. Fermi and L. Marshall - Phys. Rev. 70, 815 (1946)
(8) E. Fermi and L. Marshall - Phys. Rev. 71, 666 (1947)
(9) E.O. Wollan and C.G. Shull - Phys. Rev. 73, 830 (1948)
(10) P.R. O'Connor and G.T. Seaborg - Phys. Rev. 74, 1189 (1948)
(11) D.J. Hughes, M.T. Burgy, R.B. Heller and J.W. Wallace - Phys. Rev. 75, 565 (1949)
(12) O. Halpern and M. H. Johnson - Phys. Rev. 55, 898 ((1939)
(13) D,J, Hughes and M.T. Burgy - Phys. Rev. 81, 498 (1951)
(14) C.G. Shull, E.O. Wollan and W.C. Koehler - Phys. Rev. 84, 912 (1951)
(15) J.G. Dash and H.S. Sommers, Jr. - Rev. Sci. Inst. 24, 91 (1953)
(16) B.N. Brockhouse - Phys. Rev. 99, 601 (1955)
(17) P.A. Egelstaff - Proceedings of the First International Conference on the Peaceful Uses of Atomic Energy vol 4, pg 70 United Nations, N.Y 1956
(18) W.F. Libby and E.A. Long - 52, 592 (1937)
(19) J. Butterworth, P.A. Egelstaff, H. London and F.J. Webb - Phil. Mag. 2, 917 (1957)

APPROACHES TO INSTRUMENT DESIGN AT PULSED NEUTRON SOURCES

R. K. Crawford*
IPNS
Argonne National Laboratory
Argonne, IL 60439

Abstract

A number of tools are used in the design of scattering instruments for pulsed neutron sources. Initial design is based largely on simple analytical calculations. More complicated analytical calculations and Monte Carlo simulations come into play as the design is optimized to maximize the data rate and to improve the data quality. Examples are used to illustrate the relative roles of these different computational tools. Areas are also identified where appropriate computational tools are currently lacking.

DESIGN ISSUES

An instrument is designed to do a certain kind of science. Before beginning the design, one must be clear about what is to be measured.

- Is this a diffractometer or an inelastic instrument (how many wavelength analyses are required)?
- What are the desired energy and momentum transfer ranges?
- What are the desired resolutions?
- Is polarization to be used?

Once these questions have been answered, the next step is to form a concept of an instrument that can perform these measurements to the desired specifications. One must decide how to perform the necessary wavelength analyses. A totally new idea of how to make these measurements is always welcome, but this is exceedingly rare. Most methods currently used for wavelength analyses are just extensions of the basic techniques developed in the 1940s, namely time–of–flight (TOF), velocity selector, Bragg reflection, or transmission through a filter. Once the method is selected, it remains to define the geometry of the instrument and to specify the components in detail. The design then needs to be evaluated and optimized, and perhaps compared with alternative designs meeting the same specifications. External constraints, including spatial conflicts with neighboring instruments, conflicting requirements for shared moderators, etc., must be considered in selecting and optimizing the design.

In assessing instrument performance, one needs to look at actual resolutions and data rates, and possible trade–offs between these. Data quality is also extremely important. This can include statistical errors (related to data rate), calibration procedures to minimize systematic errors, instrument background, sample–dependent background, container scattering, multiple scattering

* Work supported by U.S. department of Energy, BES, contract No. W-31-109-ENG-38.
in the sample or sample and surroundings, etc. One needs appropriate tools to assess each of these quantities, in order to fully evaluate a particular design.

Ideally, some of these tools may also prove useful once the instrument is built. Possible uses include the design and planning of experiments and the analysis of the data and evaluation of

sources of problems in the data. Finally, many of these tools also have potential as training devices for the non–expert.

For pulsed sources the instrument designers must also consider questions relating to the target–moderator–reflector system, including the width and shape of the pulse from the moderator, the intensity spectrum, the source repetition rate, and the background between pulses. The background from high energy neutrons is a major concern in the design of instruments for pulsed sources. Frame overlap (related to the source repetition rate) needs to be considered in determining the instrument geometry. Finally, at least one of the wavelength analyses must be made using TOF in order to make effective use of the pulsed nature of the source.

The design tools available include simple analytical calculations, more sophisticated analytical calculations, Monte Carlo simulations, and measurements using a prototype.

SIMPLE ANALYTICAL CALCULATIONS

Simple analytical formulas are used to fix the geometry and scale of the instrument. Use of such formulas has frequently been referred to as "back–of–the–envelope" calculations. However, anyone who has ever dined with a group of scientists knows that a table napkin is really the preferred medium for such calculations. Thus we will refer to these as "napkin" calculations.

To indicate the process and the level of accuracy that can be expected, we will work through such calculations for one particular example - a crystal–analyzer quasielastic spectrometer similar to the QENS instrument at IPNS. The crystal–analyzer geometry is shown schematically in Fig. 1. This instrument is to use the 002 planes of a graphite analyzer (002 d–spacing = 3.348 Å) to select a particular scattered energy $E_{sc} \approx 3.6$ meV, chosen to allow use of a beryllium filter to remove the higher order reflections from the graphite. The analyzer crystals select the wavelength λ_{sc} given by

$$\lambda_{sc} = 2 d_{Bragg} \sin\theta_{Bragg} \tag{1}$$

and the scattered energy is related by

$$E_{sc} = \frac{m}{2}\left(\frac{h}{2m\, d_{Bragg} \sin\theta_{Bragg}}\right)^2 = \frac{20.45}{\left(d_{Bragg} \sin\theta_{Bragg}\right)^2} \tag{2}$$

for d_{Bragg} in Å and E_{sc} in meV. For this 3.6 meV final energy, $\theta_{Bragg} \approx 45.4°$.

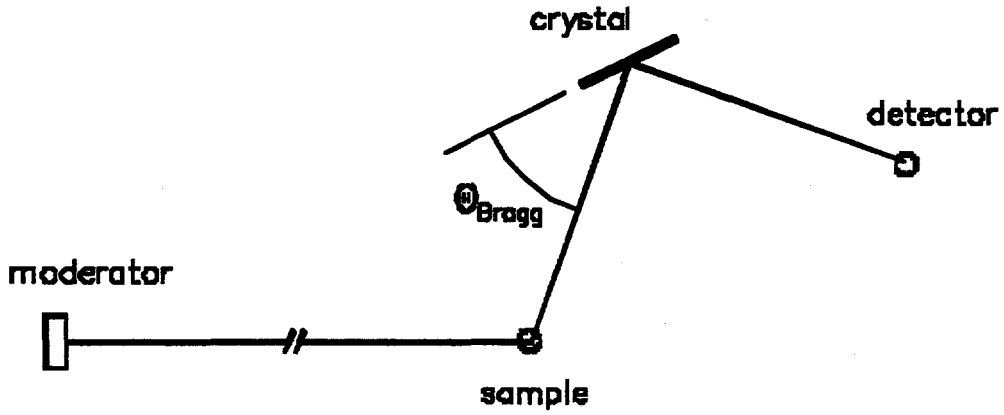

Figure 1. Basic geometry for a crystal–analyzer spectrometer.

The sample–analyzer–detector flight time t_{sc} is given by

$$t_{sc} = \frac{m}{h}\lambda_{sc} L_{sc} = \frac{\lambda_{sc} L_{sc}}{3955.4} \tag{3}$$

and the incident energy is determined by TOF time t according to

$$E_{inc} = \frac{m}{2}\left(\frac{L_{inc}}{t - t_{sc}}\right)^2 = 5.23\times 10^{-6}\left(\frac{L_{inc}}{t - t_{sc}}\right)^2 \tag{4}$$

for E_{inc} in meV, L_{sc} and L_{inc} in m, and t and t_{sc} in s. The variable of interest is the energy transfer, given by

$$E = E_{inc} - E_{sc} \tag{5}$$

The scattered flight path sample–analyzer–detector is short, say $L_{sc} \approx 1$ m, to maximize the solid angle sampled by the analyzers while minimizing the required crystal and detector area. The instrument views a 10 cm × 10 cm poisoned solid methane moderator at a 30 Hz source. We want to design the instrument to have a quasielastic resolution $\delta E \leq 70$ μeV.

The resolution requirements determine the instrument geometry. The energy resolution is determined from the variation in the energy transfer E, given by

$$\delta E = \frac{\partial E}{\partial t}\delta t_p + \frac{\partial E}{\partial L_{inc}}\delta L_{inc} + \frac{\partial E}{\partial L_{sc}}\delta L_{sc} + \frac{\partial E}{\partial \theta_{Bragg}}\delta\theta_{Bragg} \tag{6}$$

Assuming δL_{sc} and $\delta\theta_{sc}$ are uncorrelated so the resolution contributions can be added in quadrature gives

$$\frac{\delta E}{E_{inc}} \approx \left\{ \left(\frac{2\delta t_p}{t - t_{sc}} \right)^2 + \left(\frac{2\delta L_{inc}}{L_{inc}} \right)^2 + \left(\frac{2t_{sc}}{t - t_{sc}} \frac{\delta L_{sc}}{L_{sc}} \right)^2 + \left(2\left[\frac{t_{sc}}{t - t_{sc}} + \frac{E_{sc}}{E_{inc}} \right] \cot\theta_{Bragg}\, \delta\theta_{Bragg} \right)^2 \right\}^{1/2} \tag{7}$$

For quasielastic scattering, $\lambda_{inc} \approx \lambda_{sc}$. The measured fwhm source pulse width for a poisoned solid methane moderator at $\lambda_{inc} = \lambda_{sc} = 4.77$ Å is $\delta t_p \approx 50$ μs.

For a fwhm resolution $\delta E = 70$ μeV with equal L, θ, and t resolution contributions we need

$$\frac{2\delta t_p}{t - t_{sc}} = \frac{1}{\sqrt{3}} \frac{\delta E}{E_{inc}} \leq 0.011 \tag{8}$$

which requires

$$L_{inc} = \frac{3955.4\,(t - t_{sc})}{\lambda_{sc}} \geq 7.5 \text{ m} \tag{9}$$

For equal L, θ, and t resolution contributions we also need

$$2\left(1 + \frac{L_{sc}}{L_{inc}}\right) \cot\theta_{Bragg}\, \delta\theta_{Bragg} \approx \frac{1}{\sqrt{3}} \frac{\delta E}{E_{inc}} \approx 0.011 \tag{10}$$

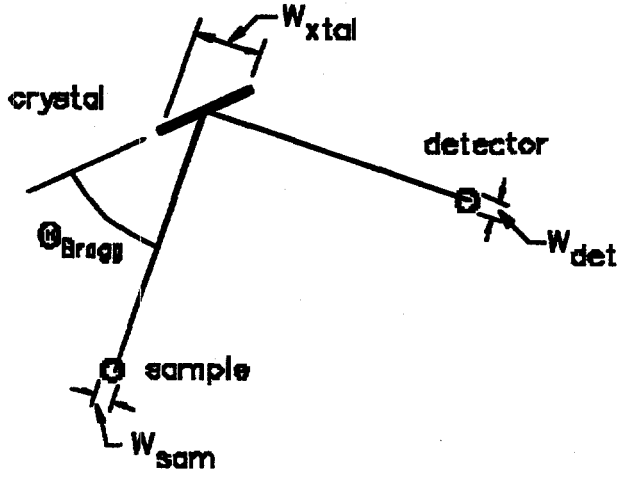

Figure 2. Sample-analyzer-detector geometry showing the natural collimation for a single analyzer crystal.

Using the natural collimation provided by the geometry shown in Fig. 2, we can show that the fwhm variation in the Bragg angle is

$$\delta\theta_{Bragg} \approx \frac{0.7\left(W_{sam}^2 + W_{det}^2\right)^{1/2}}{L_{sc}} \tag{11}$$

which requires

$$W_{sam} \approx W_{det} \leq 0.5\,\text{cm} \tag{12}$$

For equal L, θ, and t resolution contributions we also must have

$$\frac{2}{L_{inc}}\left\{\left(\delta L_{inc}\right)^2 + \left(\delta L_{sc}\right)^2\right\}^{1/2} \approx \frac{1}{\sqrt{3}}\frac{\delta E}{E_{inc}} \approx 0.011 \tag{13}$$

which is satisfied for

$$\delta L_{inc} \approx \delta L_{sc} \leq 2.9\,\text{cm} \tag{14}$$

This is rather large, so this resolution condition does not impose an immediate constraint.

The quasielastic spectrometer QENS at IPNS is an instrument of this type, having $L_{inc} = 8$ m and $L_{sc} = 1.1$ m. QENS uses the 002 planes of graphite analyzers with $\theta_{Bragg} = 45°$, has 0.625 cm diameter sample and detectors, and views a $10\,\text{cm} \times 10\,\text{cm}$ poisoned solid methane. The measured quasielastic resolution of this instrument is $\delta E = 70\,\mu\text{eV}$. Thus this exercise essentially reproduces the parameters for the quasielastic spectrometer QENS using only very simple resolution calculations. This is a typical result, that a simple analytical resolution estimate is adequate to fix the instrument scale and geometry.

MORE SOPHISTICATED ANALYTICAL CALCULATIONS

Neutrons are very expensive to produce, so we want to design the instrument to make maximum use of them. Thus a major part of the effort in designing neutron scattering instruments is involved with optimizing the geometry to increase the data rate without spoiling the resolution. Typically, this is done after the basic instrument parameters are defined by simple calculations as indicated above.

The data rate in a given TOF channel for a detector at a given scattering angle 2θ and energy transfer E on a crystal–analyzer spectrometer is given by

$$I(E,\theta) \approx \varphi\left(E_{inc}\right)\left\{N\frac{d^2\sigma}{d\Omega\,dE}\right\}_{sample} \varepsilon_{det}\left(E_{sc}\right)\Delta\Omega\,\Delta E_{sc}\,\Delta E_{inc} \tag{15}$$

where $\varphi(E_{inc})$ is the flux on sample per unit energy, N is the number of scattering centers in the sample, $(d^2\sigma/d\Omega dE)$ is the differential scattering cross–section of the sample, $\varepsilon(E_{sc})$ is the detector efficiency, $\Delta\Omega$ is the scattering solid angle used, ΔE_{sc} is the range of scattered energies accepted by the analyzer system, and ΔE_{inc} is the energy width of the incident energy TOF bin. Inspection of this formula indicates several potential methods for increasing the data rate:

- Increase the flux on sample
- Increase the sample size
- Improve the detector efficiency
- Increase the scattering solid angle sampled
- Increase the range of accepted scattered energies

Which of these can we do without compromising the desired resolution?

We return to the quasielastic spectrometer example considered above, and consider as an example the effects of increasing the scattering angle sampled. For a flat crystal, increasing the crystal horizontal dimension increases $\delta\theta_{Bragg}$, which is not allowed by resolution constraints. Can we increase the crystal horizontal dimension without increasing $\delta\theta_{Bragg}$?

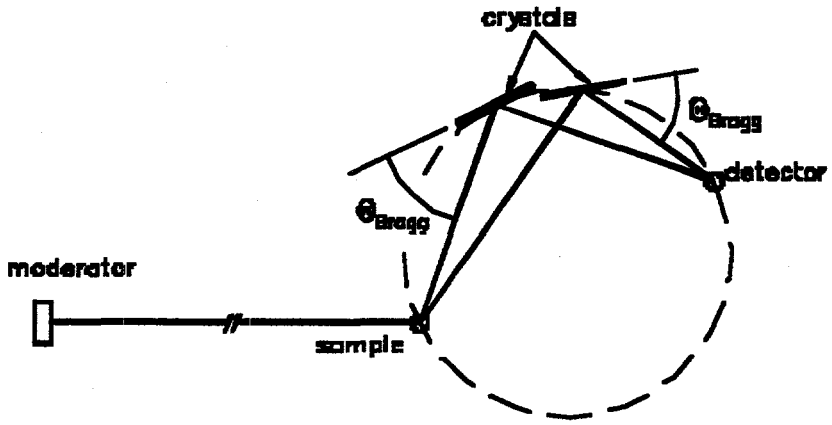

Figure 3. Constant θ_{Bragg} focusing of a crystal–analyzer array.

A "tablecloth" analytical calculation (more extensive than a napkin calculation) leads us to the concept of constant θ_{Bragg} focusing, shown schematically in Fig. 3. To achieve such focusing, the centers of the analyzer crystals must lie on a circle passing through the sample and detector, while the reflecting planes must be inclined by varying amounts relative to the circle tangent, as shown in the figure. With this geometry, different paths will have different L_{sc}, and this will constrain the size of the crystal array.

MONTE CARLO SIMULATIONS

The spectra measured in a neutron scattering instrument result from a probability–weighted integration over the various possible neutron paths from moderator to sample to detector. The Monte Carlo technique uses a suitable set of randomly–selected neutron paths to simulate these integrals. Quantities to integrate over include the source spectrum, the surface of moderator, the volume of the sample, the volume of the crystal array and the volume of the detector.

To perform these integrals we can use probability–weighted paths, where at each interaction point the various possible paths of interest are assigned an appropriate probability and these weighted paths of interest are then followed on through the instrument. An extreme version of this is the use of "forcing techniques", where only paths with vertices in the necessary volumes are considered. Alternatively, we can use probability–terminated paths, where probabilities are used to select only one possible outcome at each interaction point, and the resulting path is followed through the instrument. The former approach is usually computationally more efficient. Furthermore, we can choose to treat general case, or we can include only the interactions of interest. We will refer to the latter approach as "ad hoc Monte Carlo".

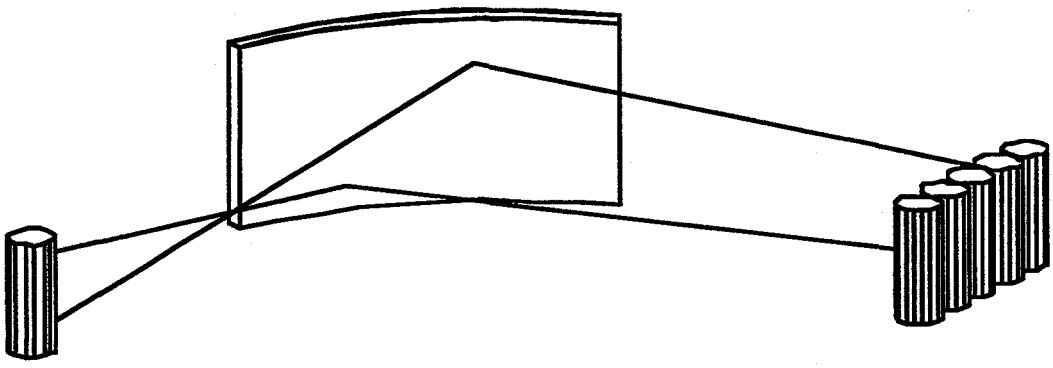

Figure 4. Geometry for an ad hoc Monte Carlo simulation of the performance of a crystal–analyzer array. Two of the many alternate neutron paths from sample to analyzer array to detectors are shown.

As an example of an ad hoc Monte Carlo simulation, suppose we want to calculate the resolution contribution from the scattering flight path in the quasielastic spectrometer considered above, this time including 3–dimensional effects. The geometry is shown in Fig. 4. Monte Carlo will allow us to explore the effects of increasing the crystal or detector vertical dimension and the effects of vertical curvature of the crystal array. These are conditions that are difficult to explore with analytical calculations. For these simulations the incident beam is irrelevant, so we can consider only the effects of the scattering paths. We use random positions within the sample, random positions on the surface of the crystal array (assuming the crystals are thin) weighted to scale to random directions from sample, and random positions within the volume of the detector array, weighted according to detection probability and crystal mosaic distribution. The calculated distribution of θ_{Bragg} for this weighted distribution of paths then gives E_{sc} and δE_{sc}.

The use of a general Monte Carlo program to simulate the full 3-dimensional performance of the complete instrument is most useful after the instrument design is complete or nearly complete. This general Monte Carlo simulation tracks neutron paths through the entire instrument, and can indicate whether the instrument is performing as you believe it should and whether there are any "surprises" that need to be accounted for in the design. If this simulation provides a sufficiently accurate representation of the instrument, it can also be useful in designing experiments and in analyzing data once the instrument is built.

THE USE OF PROTOTYPES

Despite the extensive array of calculational tools available, there are still a number of questions that these tools are inadequate to answer. Foremost among these are the questions relating to data quality, including effects of imperfections in the beam optics and the magnitude of the background for various choices of beam geometry. If answers to these questions are essential to the instrument design, there is no choice but to make measurements on a prototype of the instrument or instrument component. Prototype measurements also serve as useful benchmarks against which to test the calculational tools.

DISCUSSION OF DESIGN TOOLS

In this paper we have tried to indicate the relative roles played by simple analytical calculations, more sophisticated analytical calculations, ad hoc Monte Carlo simulations, general Monte Carlo simulations, and prototype measurements. All of these have their uses, but there are still some problems that cannot be handled adequately by any of the calculational tools, and it frequently is not practical to use prototypes. Thus there are still some areas in which improvement is needed.

Most of these problem areas are related to low–probability events, to complex geometries, or to inadequate modeling of physical processes. Among these are problems associated with tailoring the incident beam. Questions here include the geometry and choice of materials for collimators and apertures. These can involve issues such as the correct modeling of surface scattering and the treatment of the stopping or scattering and thermalization of fast neutrons in some of the more massive collimator elements. In all cases, very low probability events must be considered in order to assure that the beam definition meets the requirements for sharpness at the edges.

Another large class of problems that are not well treated by any calculational techniques are those associated with instrument and sample–dependent background. Issues include treatment of multiple scattering in the sample and other components, and thermalization of fast neutrons in the instrument components and in various parts of the shielding must be considered in many cases. Proper modeling of scattering from the interior surfaces of the instrument can also be an issue. The shielding geometries are usually very complicated and a composite of different types of materials are used to thermalize and then stop the neutrons in the shielding. Also, it is usually difficult to determine appropriate source terms to use in such a calculation.

Finally, it would be desirable to extend the use of some of these computational techniques, particularly the general Monte Carlo simulations, into other areas, such as the diagnosis and analysis of experimental design and/or problems in data, and to instrument simulations that could be used as teaching aids. Such applications will require detailed modeling of most of the instrument components, some detailed cross–section information for the samples, and a user–friendly, fast, reliable general Monte Carlo code.

CONCLUSION

In this paper we have attempted to indicate a typical path through the instrument design process, and to show where the available tools are or are not adequate for the job. The simple analytical calculations are the natural starting point to define the overall instrument geometry. More sophisticated analytical calculations can then lend considerable insight to the optimization of instrument performance, including the recognition of potential focusing geometries. Ad hoc Monte Carlo simulations are extremely useful for analyzing particular instrument components and optimizing their performance. Finally, general Monte Carlo simulations of entire instruments serve as a useful check for processes that may have been overlooked in the design.

One of the most important tools, however, is not strictly calculational. Probably the most important of the design tools is the thought process of the instrument designer. Clearly some thinking is required in the beginning, in order to define the instrument requirements and a general concept for the instrument. However, all too often thinking stops when computing starts, and it is important to avoid this trap. The designer should stop and think at every stage of the process, asking such questions as "Do these results make sense?" or "Are the results indicating that a different design concept might be appropriate?". Frequent use of simple analytical calculations to check the results of more complicated analytical calculations or Monte Carlo simulations can eliminate many problems.

The stages in a typical instrument design process are summarized here.

- THINK - define concept and requirements
- Simple analytical calculations
- THINK - what do these calculations imply
- More complicated analytical calculations
- THINK - is a better way to do the measurement indicated by the analysis
- Ad hoc Monte Carlo for various components
- THINK - has an optimum condition been found and do the results make sense
- Prototype ?
- THINK - what are the implications of the measurements
- Detailed conceptual design
- General Monte Carlo for design verification ?
- THINK - are there any surprises

Improvements in any of the available tools can help this process

ANALYTICAL TECHNIQUES FOR INSTRUMENT DESIGN - MATRIX METHODS

R. A. Robinson
Los Alamos National Laboratory, Los Alamos, NM 87545, USA

Abstract

We take the traditional Cooper-Nathans approach, as has been applied for many years for steady-state triple-axis spectrometers, and consider its generalisation to other inelastic scattering spectrometers. This involves a number of simple manipulations of exponentials of quadratic forms. In particular, we discuss a toolbox of matrix manipulations that can be performed on the 6-dimensional Cooper-Nathans matrix: diagonalisation (Møller-Nielsen method), coordinate changes (e.g. from $\{\Delta\mathbf{k}_I,\Delta\mathbf{k}_F\}$ to $\{\Delta E, \Delta Q$ & 2 dummy variables$\}$, integration of one or more variables (e.g. over such dummy variables), integration subject to linear constraints (e.g. Bragg's Law for analysers), inversion to give the variance-covariance matrix, and so on. We show how these tools can be combined to solve a number of important problems, within the narrow-band limit and the gaussian approximation. We will argue that a generalised program that can handle multiple different spectrometers could (and should) be written in parallel to the Monte-Carlo packages that are becoming available. We will also discuss the complementarity between detailed Monte-Carlo calculations and the approach presented here. In particular, Monte-Carlo methods traditionally simulate the real experiment as perfomed in practice, given a model scattering law, while the Cooper-Nathans method asks the inverse question: given that a neutron turns up in a particular spectrometer configuration (e.g. angle and time of flight), what is the probability distribution of possible scattering events at the sample? The Monte-Carlo approach could be applied in the same spirit to this question.

1. INTRODUCTION

In any measurement of inelastic neutron scattering from dispersive collective excitations (sound or spin waves, for instance), it is essential to know both the energy and Q resolution of the experiment. It may also be useful to know the correlations between them, as these correlations may be exploited to "focus" the scattering and improve the resolution of the experiment at no cost in intensity. While well-established methods[1-4] exist for the triple-axis spectrometer, the same treatment is not usually applied to time-of-flight spectrometers, even though they have been used to measure dispersive excitations in the past[5]. However, with the recent advent of high-intensity spallation sources, there is more interest in studying dispersive excitations on time-of-flight spectrometers. To date, there have been successful studies of high-energy spin waves in itinerant ferromagnets [6,7] and low-dimensional magnetic systems[8-10]. Serious consideration is being given to neutron Brillouin scattering [11-15], where relatively high energies and good resolution are required. Furthermore, a number of different time-of-flight crystal-analyser spectrometer concepts have been proposed and tested [16-23], with the specific intention of measuring collective excitations. Although there are resolution calculations for pulsed-souce crystal analyser spectrometers [16,18], they are somewhat cumbersome. There is clearly a need for an approach which is less dependent on the specifics of the spectrometer configuration. In this article, we present such an approach, which exploits well known matrix algebra and properties of exponentials of quadratic forms. In practice, rather than ploughing through the whole problem algebraically, one can then use standard numerical matrix subroutines [24] to do the arithmetic.

It is not our intention here to model every minute detail of the spectrometer resolution function as one can in a Monte-Carlo simulation, or as has been done analytically for chopper spectrometers [25]. Rather, we present an approach which is easily applied to any inelastic scattering spectrometer, which is computationally fast and which readily gives the essential features of the

resolution function in (**Q**,E) space. This is achieved by working in the gaussian approximation, which will be reasonable if the individual components of the resolution are symmetric and lacking in long tails. For the case of time distributions from pulsed moderators, this is not the case [26-28] and the detailed lineshape will be incorrect. However, even in this case, the means and standard deviations will be reliable and the essential features of focussing will be readily apparent.

The approach presented here is a generalisation of the methods [1,2] widely used for triple-axis spectrometers, on which phonon and magnon dispersion curves have been measured routinely for at least 30 years. For this type of spectrometer, the primary and secondary spectrometer resolutions are uncoupled, a fact that greatly simplifies the description of the spectrometer resolution. In both the Cooper-Nathans [1] and Nielsen-Møller [2] methods one starts out with a gaussian description of the resolution function in a 6-dimensional space, 3 components for errors in the incident wave-vector $\mathbf{k_I}$ and 3 for the final wave-vector $\mathbf{k_F}$ Thus, the probability of a neutron making it through the spectrometer is

$$P = P_0 \exp -\frac{1}{2}\left\{ \underline{x}^T \cdot \underline{M} \cdot \underline{x} \right\} \qquad (1),$$

where $\underline{x}$ is a 6-dimensional vector representing errors in $\mathbf{k_I}$ and $\mathbf{k_F}$ and $\underline{M}$ is a 6x6 symmetric matrix containing all of the resolution information:

$$\underline{x} = \left(\Delta k_{I\,\parallel}, \Delta k_{I\,\perp}, \Delta k_{I\,Z}, \Delta k_{F\,\parallel}, \Delta k_{F\,\perp}, \Delta k_{F\,Z} \right) \qquad (2).$$

In the Nielsen-Møller method, one diagonalises this matrix and then convolves the 6 resultant independent distributions with the sample scattering law to obtain the observed resolution. In the Cooper-Nathans method, one performs a change of coordinate system, in order to describe the resolution in terms of errors in the energy transfer E and 3 components of wave-vector transfer **Q**. For instance, one may want to work in terms of $(\Delta E,\Delta Q_{\parallel},\Delta Q_{\perp},\Delta Q_z)$ where $\Delta Q_{\parallel}$ and $\Delta Q_{\perp}$ are components of the error in **Q** within the scattering plane and parallel and perpendicular to **Q** and ΔQ_z is the error in **Q** perpendicular to the scattering plane, or one may want to work in terms of $(\Delta E,\Delta Q_x,\Delta Q_y,\Delta Q_z)$ where ΔQ_x and ΔQ_y are components of the error in **Q** within the scattering plane and parallel and perpendicular to some other axis (like a reciprocal lattice vector of the sample). So if

$$\underline{x}' = (\Delta E, \Delta Q_1, \Delta Q_2, \Delta Q_3, \chi_1, \chi_2) \qquad (3)$$

where χ_1 and χ_2 are dummy variables (for instance, one might choose $\chi_1 = \Delta k_{F\perp}$ and $\chi_2 = \Delta k_{Fz}$).

2. CHANGING COORDINATES

The new coordinates are related to the old ones by a matrix $\underline{A}$:

$$\underline{x}' = \underline{A} \cdot \underline{x} \quad ; \quad \underline{x} = \underline{A}^{-1} \cdot \underline{x}' \qquad (4).$$

Within a linear approximation, the elements of $\underline{A}$, a_{ij}, are the partial derivatives for the transformation:

$$a_{ij} = \frac{\partial x'_i}{\partial x_j} \; ; \; a^{-1}_{ij} = \frac{\partial x_i}{\partial x'_j} \qquad (5),$$

and therefore the determinants of $\underline{\mathbf{A}}$ and $\underline{\mathbf{A}}^{-1}$ are the Jacobians for the transformation and the inverse transformation respectively:

$$|A| = \frac{\partial(x'_1, x'_2, \ldots, x'_n)}{\partial(x_1, x_2, \ldots, x_n)} \; ; \; |A^{-1}| = \frac{\partial(x_1, x_2, \ldots, x_n)}{\partial(x'_1, x'_2, \ldots, x'_n)} \qquad (6).$$

Then

$$P = \frac{P_0}{|A|} \exp -\frac{1}{2}\left\{ \underline{x}'^{T} \cdot \underline{A}^{-1\,T} \cdot \underline{M} \cdot \underline{A}^{-1} \cdot \underline{x}' \right\} \qquad (7).$$

We have couched the above in the elegant language of matrix algebra, following Refs. 3 and 4. This allows us to use many standard mathematical identities and to deal with cases where algebraic diagonalisation is difficult.

3. INTEGRATION OVER EXPONENTIALS OF QUADRATIC FORMS

If

$$P = P_0 \exp -\frac{1}{2}\left\{ \underline{x}^{T} \cdot \underline{A} \cdot \underline{x} \right\} \qquad (8),$$

where **x** is a vector in n dimensions, then

$$\int P \, dx^n = P_0 \frac{\left(\sqrt{2\pi}\right)^n}{\sqrt{|A|}} \qquad (9).$$

The most obvious application of this formula is to give the *resolution volume* of the spectrometer directly.

4. INTEGRATION OVER ONE DIMENSION OF A QUADRATIC FORM

If

$$P = P_0 \exp -\frac{1}{2}\left\{ \underline{x}^{T} \cdot \underline{A} \cdot \underline{x} \right\} \qquad (10),$$

then the integral over the kth component of **x**, x_k, is

$$\int P \, dx_k = \sqrt{\frac{2\pi}{a_{kk}}} \exp -\frac{1}{2}\left\{ \underline{x}''^{T} \cdot \underline{A}'' \cdot \underline{x}'' \right\} \qquad (11),$$

where **x''** is the same as **x** but with the kth component removed

$$\underline{x}'' = x''_i = x_i \quad \text{for } i \neq k \tag{12},$$

and

$$\underline{A}'' = a''_{ij} = a_{ij} - \frac{a_{ik}\, a_{jk}}{a_{kk}^2} \quad \text{for } i \neq k\,,\ j \neq k \tag{13}$$

An alternative method is to work with the inverse matrices as follows:

(a) Invert the matrix $\underline{A}$ to give $\underline{A}^{-1}$
(b) Cross out the row and column corresponding to the integrable variable.
(c) Invert this reduced matrix back into the original space to give $\underline{A''}$. The corresponding prefactor P" is then given by:

$$P'' = P_0 \sqrt{2\pi} \sqrt{\frac{|A''|}{|A|}} \tag{14}$$

Either of these methods can be used to integrate either over a dummy variable or a physically uninteresting variable.

5. INTEGRATION OVER ONE DIMENSION SUBJECT TO A CONSTRAINT

If

$$P = P_0 \exp -\frac{1}{2}\left\{ \underline{x}^T \cdot \underline{A} \cdot \underline{x} \right\} \tag{15}$$

and we want to integrate over the kth dimension subject to the constraint that x_k is equal to a linear combination of the other components of **x**:

$$x_k = \sum_{i \neq k} b_i\, x_i = \underline{b} \cdot \underline{x}'' \tag{16}$$

where **x"** is the same as **x** but with the kth component removed, as in Eq. (12), then

$$\int P \delta(x_k - \underline{b}.\underline{x}'') dx_k = P_0 \exp -\frac{1}{2}\left\{ \underline{x}''^T . \underline{A}''' . \underline{x}'' \right\} \tag{17},$$

where

$$\underline{A}''' = a'''_{ij} = a_{ij} + b_i a_{kj} + b_j a_{ik} + b_i b_j a_{kk} \tag{18}.$$

There are two obvious applications for this tool: either to reduce the number of variables, or to integrate over a plane (for instance a dispersion surface).

6. INTEGRAL OVER A PLANAR DISPERSION SURFACE

If one is in a coordinate system $\mathbf{x} = (\Delta E, Q_1, Q_2, Q_3)$, and the dispersion surface of an excitation branch can be defined in those coordinates such that the unit vector normal to the plane is $\hat{\underline{n}}$, then we simply need to rotate coordinates such that $\hat{n}$ is along one of the new coordinate axes (say the ith axis), using Eq. (7) in which A is now a unitary matrix. The new matrix will be $\underline{\mathbf{A}}^{-1\mathrm{T}}.\underline{\mathbf{M}}.\underline{\mathbf{A}}^{-1}$. Its inverse $\underline{\mathbf{A}}.\underline{\mathbf{M}}^{-1}.\underline{\mathbf{A}}^{\mathrm{T}}$ will contain as its ith diagonal element the variance of the distribution along $\hat{n}$: σ_n^2. Now, experiment scans are not normally made along normals to dispersion surfaces. In the case of time-of-flight spectrometers, they are made along the time-of-flight locus for that particular detector, and for triple-axis spectrometers, constant-**Q** scans or constant-E scans along symmetry direction are common practice. In any case, the scan direction can always be defined by a unit vector $\hat{\underline{c}}$ along the scan direction. The width along the scan direction is then simply

$$\sigma_c = \sigma_n / | \hat{\underline{n}} \cdot \hat{\underline{c}} | \qquad (19),$$

where $| \hat{\underline{n}} \cdot \hat{\underline{c}} |$ is simply the cosine of the angle between $\hat{n}$ and $\hat{c}$. This argument follows that given by Nielsen and Møller[2]. We discuss what their method amounts to in Section 9 below. Note however that we do not have to diagonalise M to obtain this result.

7. DEFINING THE AXES OF AN ELLIPSE IN 2 DIMENSIONS

If

$$P = P_0 \exp -\frac{1}{2}\left\{ \underline{x}^{\mathrm{T}} \cdot \underline{A} \cdot \underline{x} \right\} \qquad (20)$$

where **x** is a 2-dimensional vector, the lines of equal probability are ellipses, which can be described by an angle of inclination θ, semi-major and semi-minor axes a and b. For the one standard deviation contour, θ, a and b are given by:

$$\tan 2\theta = \frac{a_{12}}{2(a_{11} - a_{22})} \qquad (21),$$

$$a^2 = a_{11} \cos^2\theta + a_{22} \sin^2\theta + \frac{a_{12}}{2} \sin\theta \cos\theta \qquad (22)$$

and

$$b^2 = a_{11} \sin^2\theta + a_{22} \cos^2\theta - \frac{a_{12}}{2} \sin\theta \cos\theta \qquad (23)$$

Note, however, that these values are dependent on the units used for x_1 and x_2. If one uses these values to plot out ellipses, the values of a, b and θ are dependent on the scales used for x_1 and x_2. This is very useful if one wants to plot out the projected resolution function on top of a two-dimensional map of intensity, or on top of a calculated dispersion curve (see Fig. 4 of Ref. 9).

8. QUADRATIC FORMS AND THE VARIANCE-COVARIANCE MATRIX

If

$$P = P_0 \exp -\frac{1}{2}\left\{ \underline{x}^T \cdot \underline{A} \cdot \underline{x} \right\} \tag{24}$$

then inverse matrix $\underline{A}^{-1}$ is simply the variance-covariance or error matrix in which

$$a_{ii}^{-1} = \langle x_i^2 \rangle \quad ; \quad a_{ij}^{-1} = \langle x_i x_j \rangle \tag{25}$$

where the "-1" refers to the inverse of $\underline{A}$. Note that this relation can be used both ways: (a) it can be used to set a problem up in terms of the parent distributions, where the matrices are diagonal and one only needs to know the standard deviations of those distributions, and (b) at any time in the analysis, the matrix $\underline{A}$ can be inverted to provide the variances in each of the coordinates, without performing any explicit integrals. By comparison with Eq. (7), then

$$\underline{A}.\underline{M}^{-1}.\underline{A}^T = \langle x_i x_j \rangle \tag{26}$$

and the prefactor is simply defined as before.

9. THE NIELSEN-MØLLER METHOD[2] IN THE MATRIX APPROACH

Once one has the 6-dimensional matrix $\underline{M}$, one need not immediately project on to the 4 dimensions ($\Delta E, Q_1, Q_2, Q_3$), but one can always diagonalise it straight away in six dimensions. This has been done algebraically for the triple-axis spectrometer by Nielsen and Møller [2], and we could clearly do this step numerically for any spectrometer: one merely needs to rotate by a matrix made up of the eigenvectors of $\underline{M}$ to end with a diagonal matrix, whose diagonal elements are the eigenvalues of $\underline{M}$. The eigenvalues correspond to inverse widths of independent distributions and the eigenvectors are the axes defining those distributions. In the triple-axis case the eigenvectors have some physical significance, because the primary and secondary spectrometers are uncoupled. But in general this is not the case. The particular merit of the Nielsen-Møller method is that one can calculate separately the incident- and final-resolution contributions to the scan width of Eq. (19) including the effects of the dispersion surface, and then try to optimise the instrumental parameters by matching them. In the general case, diagonalisation does not yield such a separation and the method does not have the same utility. Indeed the dispersion surface (or its normal to be more precise) must be transformed into the independent coordinates. This is actually fairly straightforward: one simply projects the independent axes onto the 4 dimensions ($\Delta E, Q_1, Q_2, Q_3$) and adds the contributions to the total width in quadrature there.

10. WAYS TO PREPARE THE COOPER NATHANS MATRIX

There are three different ways to prepare $\underline{M}$ (and thereby its inverse $\underline{M}^{-1} = \langle x_i x_j \rangle$):

(a) Do an analytic calculation of the traditional type[1,22,23] and calculate all the terms algebraically.

(b) Use the matrix method right from the beginning:
   (i) Start out with the variances of all the parent distributions (for instance, angles to define particle trajectories, coordinates to describe point and time of origin in source and likewise to describe scattering point in sample and, orientation of mosaic block in

a crystal analyser, angle of particle relative to a slot in a chopper, and so on). This will give a diagonal matrix in those coordinates, as many as are necessary. In a full 3-dimensional calculation, there must be at least six such coordinates.

(ii) If there are more than six coordinates, they will be related by constraints, which must be written down in the form given in 5. One can then integrate over the extra variables using Eqs. (17) and (18) sequentially, if necessary, to get down to six dimensions.

(iii) Transform from these coordinates to the errors in $\mathbf{k}_I$ and $\mathbf{k}_F$ given in Eq. (2). Use Eq. (7) to do this.

(c) Via the Monte-Carlo method:

(i) Do a Monte-Carlo calculation, in which the scattering process at the sample is unconstrained but that the neutron arrives in the nominal detector element at the nominal time. Within the calculation, calculate the error matrix for the 3 components of $\mathbf{k}_I$ and the 3 components of $\mathbf{k}_F$, to get $\langle x_i x_j \rangle$.

(ii) Invert $\langle x_i x_j \rangle$ to get $\underline{M}$.

11. COMPARISON WITH MONTE-CARLO SIMULATION

Because it is so easy to make algebraic or programming errors in calculations of this nature, it is this author's belief that it should be checked against a Monte-Carlo simulation. There are two types of calculation that are useful. The first mimics the present analytic calculation in that it explores all possible neutron trajectories through the spectrometer which end up in the correct detector element at the correct time. For each history, we can determine any of the variables described above and calculate their variances and covariances. Thus, any of the matrices can be calculated, including M in six dimensions. By this means, the analytic calculation can be checked at every stage. This is not the way Monte-Carlo simulations of spectrometers are normally done, however.

The alternative approach, which is independent of any matrix manipulation is to mimic an experiment with a delta-function scatterer (like Bragg scattering, though in this case we can also calculate for non-zero energy transfers). So for each neutron trajectory arriving at the sample, we we assume that

$$d^2\sigma/d\Omega dE = \delta(\mathbf{Q} - \mathbf{Q}_0, E - E_0) \qquad (27)$$

Then the neutrons are spread out in both time and angle from the nominal values and one determines $\mathbf{Q}$ and E, in exactly the same ways as in an experiment. Then the distribution of neutrons $I(\mathbf{Q},E)$ is actually the inverse of the resolution function described above[2], in the sense that:

$$I(\mathbf{Q},E) = R(-\mathbf{Q},-E) \qquad (28)$$

But one cannot determine the distributions of $\mathbf{k}_I$ and $\mathbf{k}_F$ independently, for exactly the same reason that one cannot in a real experiment. So, while one can map out the resolution matrix in terms of $(\Delta E, Q_1, Q_2, Q_3)$, one cannot obtain it in the full six dimensions. This can be a handicap in diagnosing errors, by comparison with the analytic calculation.

Of course Monte-Carlo calculation has far greater potential when it comes to modelling real spectrometers. One need not assume gaussian distributions: realistic moderator pulse shapes [26-28] can be included, as can realistic crystal reflectivity profiles[29,30] or the real geometries of moderators, samples and detectors. On the other hand the analytic approach given here is much

much faster and readily lends itself to studies of spectrometer optimisation in which many different configurations are explored and evaluated.

12. DISCUSSION

In Sections 2 - 8 we have simply provided a toolkit for manipulating the resolution matrix and its inverse, the error matrix. The tools can be used in a many different ways to get different results from the matrix M. For instance, we have described how to get resolution volumes (Section 3), widths of observed scans (Section 6), elliptical projections that represent the resolution function in useful coordinates (Section 7) and the projected energy- and Q-resolutions (section 8). In the last case, it is trivial to calculate the Q-resolution, something which is rarely done for chopper spectrometers. But much more is possible.

Suppose we wish to know the incident-energy and final-energy resolution: then we take $\underline{\mathbf{M}}$ and transform it into coordinates including E_I and E_F, along with 4 dummy variables. Then invert the transformed matrix and two of the diagonal elements will contain the variances for E_I and E_F. Indeed, the corresponding off-diagonal term will be their covariance.

On crystal-monochromator instruments (like the triple-axis spectrometer), it is normal to think of resolution in terms of angular distributions defined by Soller collimators, whereas on time-of-flight machines, the divergences are defined by apertures. If small samples are used on triple-axis spectrometers, one should also include the effect of sample size on the allowed neutron trajectories. And, likewise, when Soller collimators are installed on time-of-flight instruments, one should consider the effect of limiting the allowed divergence as well as limiting translational coordinates by means of apertures. In the latter case, this effect has been considered by Carpenter and Mildner[31], but it is easy to do this in the present formalism. All one needs to do is prepare a new Cooper-Nathans matrix $\underline{\mathbf{M}}$, using the method of Section 10(b), but adding the distribution of angles allowed by the Soller collimator and using the constraint that the difference in positional deviations on source and sample define the angular deviation.

Or suppose we wish to compare the resolution characteristics of two different types of spectrometer (e.g. the triple-axis and chopper spectrometer) for the same measurement. All one needs to do is calculate $\underline{\mathbf{M}}$ for each spectrometer and then perform the same manipulations from there on, at least if the scattering triangles are the same. If they are not, one needs to account for different sample orientations and the fact that the dispersion surface may be oriented differently. Or if we think of a new type of spectrometer, the same program can be used to analyse its resolution characteristics - one just has to calculate $\underline{\mathbf{M}}$ for it, using one or more of the methods in Section 3. For instance it would be easy to apply these ideas to a time-of-flight crystal-monochromator spectrometer like IN4 in Grenoble [32] or as has been proposed for the pulsed spallation sources.

Another area of application would be that of spectrometer optimisation. We give here a fast general method of calculating the full resolution function for any spectrometer, and if the prefactors are included the intensity too. Clearly, one can try to optimise the spectrometer within this framework. This is already done routinely, within certain limits, for triple-axis spectrometers. But one can go further: the idea of "total performance"[33] has been gaining ground. By this, one means considering the whole spectrometer from source to detector, including optical components, monochromators and choppers, as a complete system to be optimised. While there are good descriptions[29,30] of mosaic crystals and their reflectivity profiles as a function of angle and neutron energy, these are not usually included in an integral way in the optimisation of reactor instruments. Likewise, for pulsed sources, it is only recently that a parametric description[28] of the moderator flux and time distributions has been given. If such descriptions are included in the method given in this article, then one can really try to optimise "total performance." Indeed, the

final component of such an optimisation should perhaps be one of the new figures of merit proposed, on the basis of information theory, by Silver et al.[34].

ACKNOWLEDGEMENTS

This work was supported by the U.S. Department of Energy, Office of Basic Energy Sciences, and other Department of Energy programs under Contract W-7405-ENG-32 to the University of California. I am glad to acknowledge a number of useful discussions with Stuart Trugman, Toby Perring and Roger Pynn.

REFERENCES

1. M. J. Cooper and R. Nathans, *Acta Cryst.* **23**, 357 (1967)
2. M. Nielsen and H. B. Møller, *Acta Cryst.* **A25**, 547 (1969)
3. M. Popovici, *Acta Cryst.* **A31**, 507 (1975) and references therein.
4. H. Grimm, *Nucl. Instrum. Meth.* **219**, 553 (1984).
5. see for instance R. Pynn and G. L. Squires, *Proc. Roy. Soc. Lond* **A326**, 347 (1972).
6. C. -K. Loong, J. M. Carpenter, J. W. Lynn, R. A. Robinson and H. A. Mook, *J. Appl. Phys.* **55**, 1895 (1984).
7. T. G. Perring, A. T. Boothroyd, D. McK. Paul, A. D. Taylor, R. Osborn, R. J. Newport, J. A. Blackman, and H. A. Mook, *J. Appl. Phys.* **69**, 6219 (1991).
8. K. Yamada, M. Arai, Y. Endoh, S. Hosoya, K. Nakajima, T. G. Perring and A. D. Taylor, *J. Phys. Soc. Japan* **60**, 1197 (1991).
9. S. E. Nagler, D. A. Tennant, R. A. Cowley, T. G. Perring and S. K. Satija, *Phys. Rev.* **B44**, 12361 (1991).
10. S. M. Hayden, G. Aeppli, R. Osborn, A. D. Taylor, T. G. Perring, S. -W. Cheong and Z. Fisk, *Phys. Rev. Lett.* **67**, 3622 (1991).
11. W. Reichardt, in *Proceedings of the Workshop on Neutron Scattering Instrumentation for SNQ*, Maria Laach 3-5th September 1984, ed. R. Scherm and H. Stiller, Jü lich Report Jü l-1954, p.312.
12. P. A. Egelstaff, in *Proceedings of the VIIIth meeting of ICANS*, Oxford 8 -12th July 1985, Rutherford Appleton Laboratory Report RAL-85-110 Vol II p.546.
13. R. A. Robinson, *Physica* B **156&157**, 557 (1989).
14. R. A. Robinson, in *Proceedings of Xth meeting of ICANS*, Los Alamos 3-7 October 1988, *Inst. of Physics Conf. Ser.* **97**, 311 (1989).
15. J. -B. Suck, P. A. Egelstaff, R. A. Robinson, D. S. Sivia and A. D. Taylor, *Europhys. Lett.* **19**, 207 (1992).
16. C. G. Windsor, R. K. Heenan, B. C. Boland and D. F. R. Mildner, *Nucl. Instrum. Meth.* **151**, 477 (1978).
17. K. Tajima, Y. Ishikawa, K. Kanai, C. G. Windsor and S. Tomiyoshi, *Nucl. Instrum. Meth.* **201**, 491 (1982).
18. R. A. Robinson, R. Pynn and J. Eckert, *Nucl. Instrum. Meth.* **A241**, 312 (1985).
19. C. Andreani, C. J. Carlile, F. Cilloco, C. Petrillo, F. Sachetti, G. C. Stirling and C. G. Windsor, *Nucl. Instrum. Meth.* **A254**, 333 (1987).
20. U. Steigenberger, M. Hagen, R. Caciuffo, C. Petrillo, F. Cilloco and F. Sachetti, *Nucl. Instrum. Methods* **B53**, 87 (1991).
21. R. Geick and H. Tietze, *Nucl. Instrum. Meth.* **A249**, 325 (1986).
22. Y. Todate, K. Tajima, H. Ikeda and S. Tomiyoshi, *Jap. J. Appl. Phys.* **29**, 1220 (1990).
23. M. Hagen and U. Steigenberger, *Nucl. Instrum. Meth.* **B72**, 239 (1992).
24. see for instance W. H. Press, B. P. Flannery, S. A. Teukolsky and W. T. Vetterling, *Numerical Recipes* (Cambridge University Press, Cambridge, 1986)
25. C. -K. Loong, S. Ikeda and J. M. Carpenter, *Nucl. Instrum. Meth.* **A260**, 381 (1987).
26. J. M. Carpenter, R. A. Robinson, A. D. Taylor and D. J. Picton, *Nucl. Instrum. Meth.* **A234**, 542 (1985).

27. S. Ikeda and J. M. Carpenter, *Nucl. Instrum. Meth.* **A239**, 536 (1985).
28. R. A. Robinson and J. M. Carpenter, *Nucl. Instrum. Methods* **A307**, 359 (1991).
29. A. K. Freund, in: *Proc. Conf. on Neutron Scattering*, Gatlinburg, Tennessee, June 6-10 (1976) Oak Ridge National Laboratory Report CONF-7606061-P2 (1976) p.1143.
30. R. A. Robinson and A. K. Freund, Institut Laue Langevin Report 85FR13T (1985).
31. J. M. Carpenter and D. F. R. Mildner, in *Proc. XIth Meeting of ICANS*, Tsukuba 22-26th October 1990, KEK Report 90-25, Vol. II p.655 (1991).
32. *Guide to Neutron Research Facilities at the ILL*, eds. H. Blank and B. Meier, (Institut Laue Langevin, Grenoble), 1988.
33. N. Watanabe, in *Proc. XIth Meeting of ICANS*, Tsukuba 22-26th October 1990, KEK Report 90-25, Vol. II p.637 (1991).
34. R. N. Silver, D. S. Sivia and R. Pynn, in *Advanced Neutron Sources 1988*, Inst. of Physics Conf. Ser. **97**, 673 (1989).

BRAGG OPTICS COMPUTER CODES FOR NEUTRON SCATTERING INSTRUMENT DESIGN

Mihai Popovici, William B. Yelon, Ronald R. Berliner
Missouri University Research Reactor, Columbia, USA
Alexandru D. Stoica
Institute of Physics and Technology of Materials, Bucharest, Romania

Abstract:

Computer codes for neutron crystal spectrometer design, optimization and experiment planning are described. Phase space distributions, linewidths and absolute intensities are calculated by matrix methods in an extension of the Cooper-Nathans resolution function formalism. For modeling the Bragg reflection on bent crystals the lamellar approximation is used. Optimization is done by satisfying conditions of focusing in scattering and in real space, and by numerically maximizing figures of merit. Examples for three-axis and two-axis spectrometers are given.

1. Introduction

In the early 1970's, after the resolution function formalism was invented [1], curved monochromators and related focusing techniques also emerged [2]. The question arose of how to express spatial focusing effects in the resolution function language.

A paper by Dorner [3] highlighted the physical meaning of the resolution matrix **M** as the inverse of the covariance matrix of the scattering space **X**-variables, and that of the normalization factor as the product of the **k**-space volumes of the monochromator and analyzer units. A general procedure of computing resolution functions was soon advanced [4]. By differentiating the wavevector transfer $\mathbf{Q}=\mathbf{k}_i-\mathbf{k}_f$ and energy transfer $\hbar\omega=(k_i^2-k_f^2)\hbar^2/(2m)$ one obtains $\mathbf{X}=\mathbf{BY}$, where $\mathbf{Y}=(\Delta\mathbf{k}_i,\Delta\mathbf{k}_f)$ is a vector (or column matrix) having 6 or 5 components and **B** is a 4x6 or 3x5 matrix (for inelastic and elastic scattering cases, respectively). Then one gets $\mathbf{M}^{-1}$ standardly as $\mathbf{M}^{-1}=\mathbf{B}\mathbf{N}^{-1}\mathbf{B}^T$, $\mathbf{N}^{-1}$ being the covariance matrix of **Y**-variables - the matrix of second-order moments $\mathbf{N}^{-1}=\{\langle Y_iY_j\rangle\}$. The integral of the distribution function $p(\mathbf{Y})$ gives the normalization factor, proportional to $\sqrt{\det(\mathbf{N}^{-1})}$ in the Gaussian approximation. For going beyond the Gaussian approximation, expansions in Hermite polynomials were proposed [4], with first Gaussian terms corresponding to matrices of second-order moments, and further terms corresponding to tensors of higher-order moments of the distributions.

This procedure is applied to the case of curved crystals by extending **Y** to a vector **Z** that includes the spatial variables $\Delta\mathbf{r}$ of the sample, $\mathbf{Z}=(\Delta\mathbf{k}_i,\Delta\mathbf{r},\Delta\mathbf{k}_f)$ [5]. This is similar to the phase space treatment of the synchrotron radiation (SR) optics [6], but goes up to the detector by including the scattering process. The covariance matrix $\mathbf{G}^{-1}=\{\langle Z_iZ_j\rangle\}$ is computed from the instrument geometry, Bragg law constraints (and Soller collimators, if any) accounted for. The normalization factor is proportional now to $\sqrt{\det(\mathbf{G}^{-1})}$. $p(\mathbf{Y})$ is the integral of the distribution function $p(\mathbf{Z})$ over $\Delta\mathbf{r}$, so one obtains $\mathbf{N}^{-1}$ by simply eliminating from $\mathbf{G}^{-1}$ the rows and columns corresponding to $\Delta\mathbf{r}$. In the case of flat crystals and Soller collimators one gets the Cooper-Nathans results with the sizes of the source, crystals, sample and detector accounted for.

The matrix technique was first applied in a program for neutron time-of-flight (TOF) diffraction [7] used for the optical design of a diffractometer at the Dubna IBR-2 reactor [8]. The program went beyond the Gaussian approximation by accounting for higher-order moments of some of the variables. An early program for curved-crystal three-axis spectrometers followed [9].

A series of computer programs have been written in 1984-1990 in Romania under a project supported in part by IAEA Vienna. Programs for computing neutron intensities at sample already existed [10]. Codes considering both resolution and intensity were developed under the project, for design and optimization of scattering instruments, as well as for planning experiments. The three-axis and two-axis spectrometer programs have been extensively used for the design of focusing configurations, especially after having been upgraded at the Missouri University Research Reactor (MURR). They have already been presented [5,11] and will only briefly be described.

2. Modeling the Bragg reflection

For neutron optics computations, simple modeling of the Bragg reflection on bent crystals is needed. In our matrix programs, the Bragg law is assumed to hold at every point in the crystal for the local value of the reciprocal lattice vector τ. The variation of τ is computed by the theory of elasticity [12], leading to an improved version of the old lamellar model for perfect crystals [13].1

The Bragg law $\mathbf{k}_i$-$\mathbf{k}=\tau$, written in projections, gives three relations. One of them just defines Δk_i, the other two act as constraints on the distribution of spatial variables at source, monochromator and sample. Mathematically, spatial focusing occurs when these constraints are accounted for. The effective sample size becomes finite even for an infinitely extended sample and depends on the radii of curvature that enter the elements of the matrix of constraints. With flat crystals and Sollers, the constraints modify the effective collimation of the reflected beam, making it finite even if no collimator is in place (see [5,14] for the procedure of introducing constraints).

The contribution to the reflectivity width due to bending is added in quadrature to the flat crystal reflectivity width by the matrix procedure itself. Reflectivity curves of bent perfect crystals are obtained as trapezoids with widths [12] and peaks [17] in agreement with the dynamical theory for homogeneously curved plates [15]. Mosaic crystal reflectivities are approximated by Gaussians of width given by the standard theory (plus the contribution from bending, usually small).

The conservation of phase volumes, as required by the Liouville theorem, is checked (the determinants of covariance matrices of phase space variables must be equal before and after reflection). For perfect crystals it is automatically satisfied. For mosaic crystals a factor has to be inserted [10,5] as at asymmetric reflection the mosaic model conserves **k**-volumes only.

A library of crystal planes of interest for neutron monochromators is built in the programs. The phase space distribution of neutrons at sample, beam size included, is given as an intermediate result (in the Gaussian approximation; for shape details, Monte Carlo programs would be needed). A technique of measuring phase space distributions with powder samples and position sensitive detection (PSD) is planned to be developed on a test bench for neutron monochromators to be installed at MURR within a project awarded recently by DOE under the "Facilities Initiative".

3. The figure of merit

The neutron state is "marked" differently in conventional and bent crystal spectrometers. With flat crystals, the Bragg angle "marker" is the angular deviation from the beam axis, which is controlled by collimation. With bent crystals the Bragg angle depends on where the neutron strikes the crystal, so the role of the marker is played by the positions where the diffraction in the crystal and the scattering in the sample occur. Collimation can be relaxed. Accurate marking for high resolution is achieved with thin crystals of narrow reflectivity width and thin plate samples.

Experiment optimization involves trading intensity for resolution. In our codes this is done by maximizing a figure of merit defined as the ratio of the peak intensity at detector I_{peak} to the square of the linewidth w at given scattering law. The maximal figure of merit depends on k_i and the type of instrument (conventional or bent-crystal). The relation $I_{peak}=F_m(k_i)w^2$ expresses the well-known rule that to improve resolution n times one has to sacrifice intensity n^2 times.

To go to the maximal figure of merit at given configuration, in conventional instruments one balances the collimator divergences. In bent-crystal instruments one balances the contributions

---

1 The components of τ in the reference frame directed with axis 1 along the nominal τ_0 of the unbent crystal, axis 3 out of the diffraction plane, are obtained as [5,12,14]: $\tau_1=\tau_0(1+b\xi_e-Ax\ \mathrm{sgn}(\theta+\chi)/R_e)$; $\tau_2=\tau_0[c\xi_e+(y+Bx)\mathrm{sgn}(\theta+\chi)/R_e]$; $\tau_3=\tau_0(c'\xi_a-z\ \cos\chi/R_a)$, (1) where ξ_e,ξ_a are the flat crystal reflectivity curve variables in the diffraction (equatorial, subscript e) and out-of diffraction (axial, subscript a) planes, R_e,R_a are the radii of curvature in the same planes, x,y,z are the spatial coordinates in the crystal plate (corresponding to thickness, lateral extension and height, respectively), θ is the Bragg angle and χ the crystal cutting angle (zero for symmetric reflection), b=0 and $b=\cos\theta\cos\chi/\sin(\theta-\chi)$ for mosaic and perfect crystals, respectively, c=c'=1 for mosaic crystals, $c=\cos\theta\sin\chi/\sin(\theta-\chi)$, c'=0 for perfect crystals, $A=1-(1+\kappa)\cos^2\chi$, $B=(1+\kappa)\sin\chi\cos\chi$, $\kappa=-u_{xx}/u_{yy}$ with u_{xx} and u_{yy} the deformation tensor components normal and parallel to the surface (can be computed through elastic constants and curvatures [12,15]). For plastically bent perfect crystals the situation is not clear and equations for modeling the Bragg reflection have yet to be worked out. For lack of a better solution, in this case the programs put $u_{xx}=0$, an approximation accepted with SR [16]. Second order terms in (1) have also been derived [14].

to linewidths coming from the thickness and reflectivity width of crystals, and from the sample size (diameter or thickness). With PSD, the spatial resolution must also match the sample size.

The figure of merit $F_m(k_i)$ can be increased by shifting the spectrum or by changing the instrument type (or by a combination of both). The ILL Grenoble success story is an illustration of the former approach. However, shifting the neutron spectrum with cold sources comes at the price of a restricted access range in the $(\mathbf{Q},\omega)$ space. Changing the instrument from conventional to focusing has a price too: for the resolution to be high, the sample size (or thickness) must be small.

Our experience with early codes showed that computing resolutions and intensities through matrix (or Monte Carlo) methods is not sufficient. Guidance is needed as to the arrangements to be considered and to the expected results. To get it, the conditions of focusing in scattering and the residual linewidths (when these conditions are satisfied) have been investigated [18,5,11,19]. The results were incorporated in the codes, which can go automatically to optimal configurations. The figure of merit is then further maximized by balancing the various contributions to linewidths.

4. Three-axis spectrometer code

After analytical conditions for focusing in scattering were derived [18], the early three-axis program [9] was written anew, overhauled into the design and optimization code TRAX [5]. Agreement with experiment was found for linewidths as well as intensities [5]. Projections of the resolution ellipsoid were measured by a novel technique with powder samples [5]. The program has been used occasionally in Berlin and Saclay. It was upgraded and put in user-friendly form in 1992-93 at MURR [11]. It was recently "married" at ILL with the RESCAL program [20] into the RESTRAX resolution program [21]. Linewidths and peak intensities are computed for vanadium and for "standard" phonon and diffraction cross sections. Computed absolute intensities have to be corrected separately for absorption in air and sample, neutron guide losses, opacity of Soller collimators and detector efficiency.

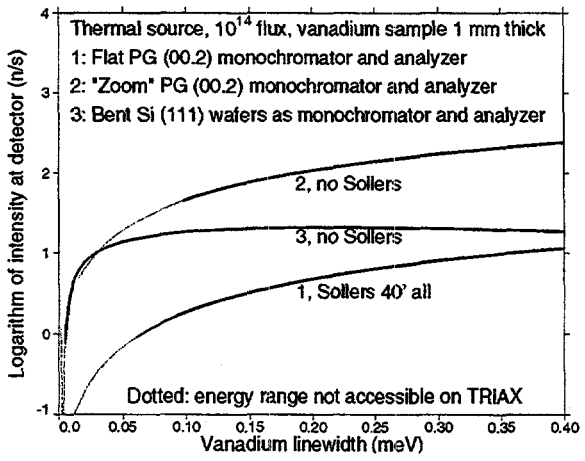

Fig. 1. Peak intensities as function of linewidths, vanadium sample, focusing (2,3) vs conventional (1) arrangements.

Figure 1 shows computed peak intensities (uncorrected, logarithmic scale) for vanadium thin plate samples on a spectrometer that was installed recently at MURR, with quite typical geometry [22]. The linewidths on the abscissa were obtained by varying the incident neutron energy. Curve 1 is for a conventional arrangement with 40' Sollers, horizontally flat and vertically focusing pyrolytic graphite (PG) monochromator, flat PG analyzer, sample in symmetric transmission. With no Sollers, "zoom" monochromator (doubly focusing), sample at optimal orientation and analyzer horizontally curved, the peak intensities are computed to be more than 20 times higher (curve 2). Curve 3 is for commercial thin Si (111) wafers instead of PG, with spherical curvature (pneumatic bending), sample at optimal orientation. Bent perfect silicon

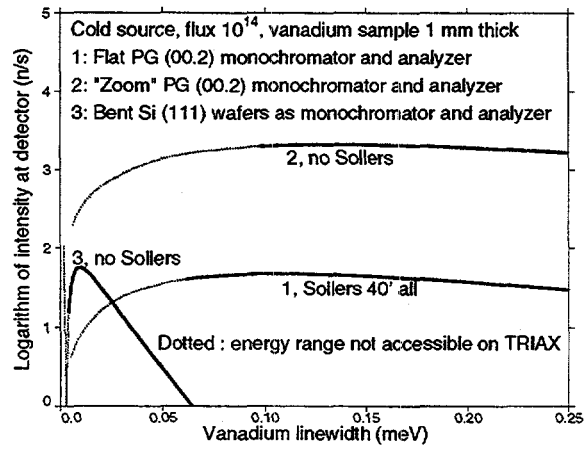

Fig. 2. Same as figure 1, cold source (20 K) instead of thermal

appears to allow going to extremely high resolutions, at intensities comparable to those that would be obtained with PG "zoom" crystals at actually inaccessible Bragg angles.

The data in figure 2 were computed under the same conditions as in figure 1, except for the neutron spectrum (20 K assumed instead of 340 K). A cold source is seen to increase the figures of merit by an order of magnitude, but also to double the gain from focusing (curve 2 over 1). With commercial thin Si wafers, resolutions of 10 mev would correspond to the peak of the spectrum (curve 3). Twice thicker silicon plates would shift the curve 3 by doubling the linewidths and quadrupling the intensities, but bending them without breaking would become a problem. The problem could be circumvented with packets of thin wafers [23], but to put together the reflectivity curves of individual wafers, these must be tilted one relative to another.

Variable curvature devices for bending silicon wafers of 6" diameter, by controlled sub-pressure (vacuum method) as well as by the 4-point mechanical method, have been fabricated at MURR (for two-bent-crystal SANS arrangements [24]). A problem with the pneumatic bending is the curvature non-uniformity. Wafers of still larger diameter will probably be needed to ensure the uniformity required for very high resolutions.

5. Two-axis spectrometer code

The first version of the two-axis spectrometer code DAX was written ten years ago. It has also been upgraded at MURR [11], but has yet to be put in user-friendly form. It has the option of double reflection monochromators, with curvatures automatically set at phase space matching [25]. Absorption in sample can be accounted for. The figure of merit that is maximized numerically refers to powder diffraction. Separate versions were adapted to small angle neutron scattering (SANS) with the two-crystal (flat or bent) technique, to multilayer monochromators (single or double) for pinhole SANS arrangements, and to double crystal SR monochromators (with Si or Ge crystal planes only). The programs have been used in the design of monochromator units for neutron powder diffraction, SANS and SR (see [11,19] for reviews).

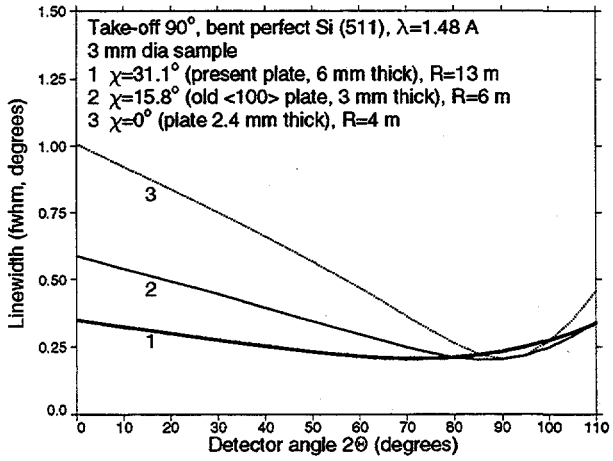

Fig. 3. Profile functions for different reflection asymmetries

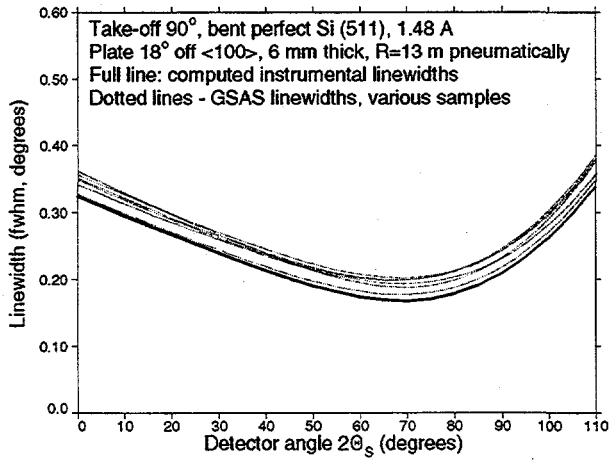

Fig. 4. Computed and measured (GSAS) profile functions

Figure 3 refers to bent silicon (511) monochromators on the high-resolution powder diffractometer with PSD at MURR [26]. It shows the effect of the asymmetry of reflection on the profile function for Rietveld analysis (dependence of powder diffraction linewidths on the detector angle, having the same functional form in focusing and conventional instruments). The plate thickness is close to the breaking limit in each case. Curve 3 is for symmetric reflection (χ=0). Curve 2 corresponds to a <100> plate with a natural χ of 15.8° (vacuum bent) that was used temporarily. The present monochromator (curve 1) was cut from a large diameter ingot for increased reflection asymmetry (χ=31°, thickness 6 mm, bent pneumatically with compressed air). The flattening of the profile function on passing from 3 to 1 gives an intensity gain in excess of 1.5, whereas in conventional instruments such a flattening involves heavy losses.

Figure 4 shows GSAS [27] profile functions (dotted lines) for various samples measured at MURR with bent Si (511) monochromator. They are slightly above the instrumental profile (thick line, same as curve 1 of figure 3), as expected for materials having some intrinsic line broadening.

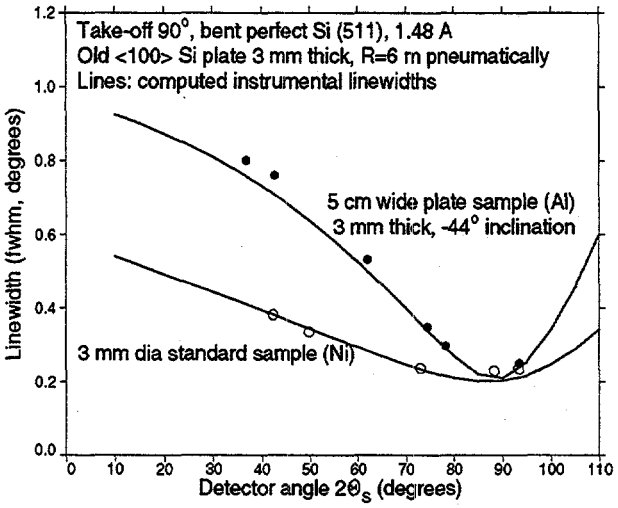

Fig. 5. Computed and measured linewidths, standard 3 mm dia and extended plate samples on the MURR PSD diffractometer

Figure 5 shows the computed and observed linewidths for a standard sample of small diameter and a plate sample with fixed orientation, optimized for 90° detector angle. The minimal linewidth for the plate sample corresponds to its thickness (3 mm), the contribution of the lateral extension (5 cm) having been canceled by the focusing in scattering. The <100> plate monochromator was used in these measurements, so the lower curve in figure 5 is the same as curve 2 in figure 3. The profile function for plates will coincide with that for small-diameter samples, if the PSD range is narrow enough and the plate orientation is varied during the detector scan.

For the planned upgrade of the MURR PSD diffractometer, a perfect Si monochromator, curved both horizontally (mechanical 4-point method) and vertically (by segmentation) was fabricated and bench-tested [28]. It has a multiple choice of wavelengths with the (511), (331), (311) or (533) reflections. The plate was obliquely cut from an 8" diameter <100> ingot so as to have all these planes in the same zone and ideally the same asymmetry of reflection (same optimal curvature) for two of them, (511) and (331).

Such units, optimized for particular geometries, can be designed and fabricated at MURR, at reasonable cost. They go to the practical limit of what elastically bent silicon can give for high resolution powder diffraction. Further progress is possible with plastic bending methods.

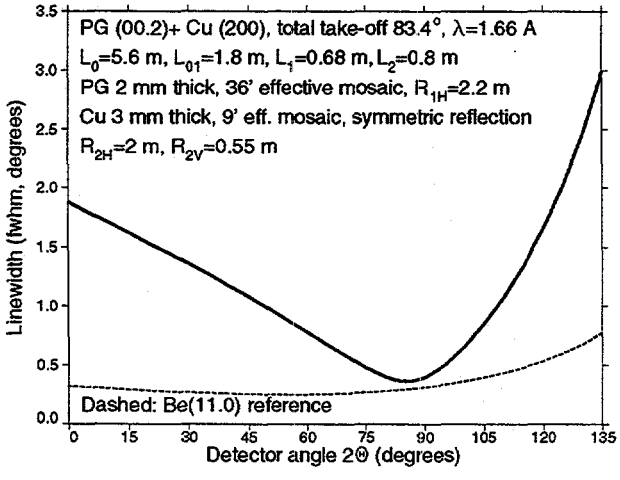

Fig. 6. Profile function for a microfocus monochromator unit

Neutron microfocusing is achievable with double reflection by bent crystals in (+,+) setting. With flat crystals, such a setting is dispersive and gives low intensity, but the beam is self-collimated. With bent crystals one can get high intensity at phase space matching, and the beam can be focused into small spots [19]. Mosaic crystals and symmetric reflection can be used, as the angular divergence of the doubly reflected beam is very large anyway. Bench tests have confirmed expectations [19,29].

Microfocus double monochromators for diffraction stress profiling have been designed for MURR and ORNL. One of them is presented in figure 6. The profile function is shown for PG (00.2) + Cu (200), 2x2x5 mm sample, PSD of 2 mm spatial resolution. At a computed beam size at sample of 4x5 mm, the linewidths around 90° detector angle are seen to be still narrow enough. For the Fe (211) line an intensity gain of about 90 is expected over the ORNL HB-2 configuration with flat mosaic Be (11.0) that was taken as reference.

A microfocus monochromator with two Cu (200) crystals is being fabricated for the stress profiling instrument under installation at MURR [19,30]. A technology of two-dimensional plastic bending of thin copper plates, with minimal induced mosaic spread, needs to be developed.

6. Problems and perspectives

A possible development is a modular code for arrangements with any sequence of units, similar to SR codes [31], but with matrices all the way instead of Monte Carlo. Going beyond the Gaussian approximation is needed for hybrid TOF + crystal configurations. A more realistic model of the Bragg reflection on mosaic crystals is needed, that would automatically conserve phase space volumes. The reflectivity of plastically bent crystals needs to be modeled.

Theoretical analysis and bench-testing of bent packets of thin wafers, relative tilts included, could revive a good old idea [23].

Second-order aberrations might come into play on going to very high resolutions with open beams. This has to be checked. Second-order terms in the neutron optics have been derived for powder diffraction [14], but a comprehensive computational technique has yet to be developed.

There are difficulties with the alignment of bent crystal instruments, related to the strong correlation between real space and wavevector space variables. It is precisely these correlations that make focusing possible, so such difficulties are unavoidable. A theory of misalignments is needed.

This work was supported in part by the grant DOE-DE-FG02-96ER45599.

References

1. M.J. Cooper and R. Nathans, *Acta Cryst.* **23**(1967)357.
2. H. Maier-Leibnitz, *Some Lectures in Neutron Physics*, Dubna: JINR, 1970, p.183; Proc Symp. *Neutron Inelastic Scattering*, Vienna: IAEA, 1972, p.681.
3. B. Dorner, *Acta Cryst.* **A28**(1972)319.
4. A.D. Stoica, *Acta Cryst.* **A31**(1975)189.
5. M. Popovici, A.D. Stoica and I. Ionita, *J. Appl. Cryst.* **20**(1987)90.
6. T. Matsushita and H. Hashizume, *Handbook on Synchrotron Radiation*, Vol. **1**, ed. E.E. Koch, North-Holland: Amsterdam, 1982, p.261; P. Suortti and A.K. Freund, *Rev. Sci. Instrum.* **60**(1989)2579.
7. A.D. Stoica, *Acta Cryst.* **A31**(1975)193; M. Popovici, A.D. Stoica, A. Bajorek, *Acta Cryst.* **A31**(1975)197.
8. A.M. Balagurov, D. Bally, V. Chirtoc, Z. Gheorghiu, M. Popovici, A.D. Stoica and E. Tarina, *Report JINR-P10*, Dubna, 1976, and *Report IFA-FN-48*, Bucharest, 1976.
9. M. Popovici, *Acta Cryst.* **A31**(1975)507.
10. H. A. Graf, *Report HMI-B-403*, Hahn-Meitner Institut: Berlin, 1983; R.A. Robinson and A.K. Freund, *Report ILL-85-FR-13T*: Grenoble, 1985.
11. M. Popovici, W.B. Yelon, R. Berliner, A.D. Stoica, I. Ionita and R. Law, *Nucl. Instr. Meth.* **A338**(1994)99.
12. A.D. Stoica and M. Popovici, *J. Appl. Cryst.* **22**(1989)448.
13. G. Egert and J. Dachs, *J. Appl. Cryst.* **3**(1970)214.
14. M. Popovici and A.D. Stoica, *J. Appl. Cryst.* **25**(1992)331.
15. F.N. Chukhovskii, K.T. Gabrielyan and P.V. Petrashen, *Acta Cryst.* **A34**(1978)610; V.I. Kushnir and A.T. Macrander, *Nucl. Instr. and Meth.* **A347**(1994)331.
16. E. Erola, V. Eteläniemi, P. Suortti, P. Pattison and W. Thomlinson, *J. Appl. Cryst.* **23**(1990)35.
17. J. Kulda, *Acta Cryst.* **A40**(1984)120.
18. M. Popovici and A.D. Stoica, *J. Phys.* **E16**(1983)662.
19. M. Popovici and W.B. Yelon, *J. Neutron Research* **3**,1(1995)1.
20. M. Hargreave and P.H.C. Hullah, PCL London, 1979; F. Frings, ILL Grenoble, 1986.
21. J. Kulda and J. Saroun, *ILL Report 95KU5082*, 1995; *Nucl. Instr. and Meth.* **A379**(1996)155.
22. K.W. Herwig, S.A. Werner and J.J. Rhyne, *MURR Annual Report*, 1992, p.84.
23. F. Frey, *Nucl. Instr. and Meth.* **115**(1974)277 and **125**(1975)9; J. Kalus, *J. Appl. Cryst.* **8**(1975)361.
24. M. Popovici, W.B. Yelon, R. Berliner and B.J. Heuser, *J. Phys. Chem. Solids* **56**(1995)1425.
25. M. Popovici, A.D. Stoica, B. Chalupa and P. Mikula, *J. Appl. Cryst.* **21**(1988)258.
26. C. Tompson, D. Mildner, M. Mehregany, J. Sudol, R. Berliner and W.B. Yelon. *J. Appl. Cryst.* **17**(1984)385.
27. A.C. Larson and R.B. Von Dreele, *LANL Report LAUR 89-748*, Los Alamos, 1994.
28. M. Popovici and W.B. Yelon, *J. Neutron Research* **5**(1997), in press.

29. M. Popovici and W.B. Yelon, *Zeitschrift für Kristallographie* **209**(1994)640.
30. D.A. Witte, A.D. Krawitz, R.A. Winholtz, R.R. Berliner and M. Popovici. *J. Neutron Res.* **5**(1997), in press.
31. B. Lai and F. Cerrina, *Nucl. Instr. and Meth.* **A246**(1986)337; B. Lai, K. Chapman and F. Cerrina, *Nucl. Instr. and Meth.* **A266**(1988)544.

THE MCLIB LIBRARY: NEW FEATURES

Philip A. Seeger
Manuel Lujan Jr. Neutron Scattering Center and Sumner Associates
Los Alamos National Laboratory
Los Alamos, NM 87545 USA

Abstract

This report describes the philosophy and structure of MCLIB, a Fortran library of Monte Carlo subroutines that has been developed to test designs of neutron scattering instruments. Emphasis is placed on new features added to the library since the previous presentation of MCLIB at ICANS-XIII in October, 1995 [1]. These new features include toroidal mirrors, writing and reading source files, splitting and banking of histories, and a Maxwellian probability distribution. The only change of a program structure has been to include charge and polarization vector in the description of a particle. The latest release of the source code and documentation may be obtained by anonymous ftp from *ftp://azoth.lansce.lanl.gov/pub/mclib/*. Work is also continuing on a more friendly web-based user interface, and user input is requested for additional features to be added to the library.

INTRODUCTION

Monte Carlo is a method to integrate over a large number of variables. Random numbers or samples from random distributions are used to select a value for each variable, and the integrand is then evaluated. The process is repeated a large number of times and the resulting values of the integrand are averaged. For a neutron transport problem, we first select a neutron from the source distribution, and project it through the instrument using either deterministic or probabilistic algorithms to describe its interaction whenever it hits something, and then (if it hits the detector) tally it in a histogram representing where and when it was detected. This is intended to simulate the process of running an actual experiment (but it is *much* slower). Monte Carlo is a useful supplement to analytical treatment of an instrument, in particular to check and demonstrate "non-intuitive" focusing arrangements, but should never be used as a substitute for thinking.

The process is carried out in two stages. First a program must be generated to describe the geometry of the specific instrument being simulated; for example, the program LQDGEOM may be used to define a small-angle scattering instrument with pinhole collimation, up to three choppers, and an on-axis 2-dimensional position sensitive detector. Essentially all of the user interaction occurs in this stage. To simplify this step, a web page is being developed [2], linked to the home page of the Manuel Lujan Jr. Neutron Scattering Center, *http://www.lansce.lanl.gov/mlnsc/*. This will eventually allow users to design instruments by defining the locations and properties of a variety of beam elements. Whether from a stand-alone program or from this web page, the output is a geometry file containing the complete problem definition.

The geometry file is then passed to a second-stage program, for example MC_RUN (which can be downloaded from *ftp://azoth.lansce.lanl.gov/pub/mclib/* along with the Monte Carlo library and documentation). This will be executed at the user's facility to transport neutrons and tally the results in histograms. Principal outputs are a file with a statistical summary, and a data file with histograms of the spectrum and detector. A third stage, which is not part of the Monte Carlo process, is to perform whatever data reduction is appropriate to the experiment being simulated. Some measure of the information content (or a "figure of merit") is then used to evaluate the design of the instrument.

GEOMETRY DESCRIPTION

The geometry of a system is described by surfaces and regions. A *surface* is defined by a general 3-dimensional quadratic equation of the form

$$A\,x^2 + B\,x + C\,y^2 + D\,y + E\,z^2 + F\,z + G + P\,xy + Q\,yz + R\,zx = 0 \qquad 1$$

with 10 coefficients, plus a roughness parameter (*BETA*). The surface divides 3-dimensional space into two parts, which are called the + and − sides of the surface depending on whether the left-hand side of Eq. 1 evaluates to a positive or a negative value. For example, a plane perpendicular to the z-axis at z = 1 can be expressed by the equation z⊇−⊇1⊇= 0, *i.e.*, $F = 1$ and $G = -1$ (all other coefficients zero). Then all points with $z < 1$ are on the − side and all points with $z > 1$ are on the + side of the surface. Higher-order surfaces such as toroids that can not be described by Eq. 1 must instead be defined as parameters of a special region (*e.g.*, toroidal mirror, type 14). The scaling of Eq. 1 is arbitrary, but we tend to evaluate non-quadratic surfaces as m (coefficients *B*, *D*, and *F* dimensionless and *G* in m) and quadratic surfaces as m^2 (coefficients *A*, *C*, *E*, *P*, *Q*, and *R* dimensionless, coefficients *B*, *D*, and *F* in m, and *G* in m^2). The parameter *BETA* is the length of a randomly oriented 3-dimensional vector that is added to the unit vector normal to the mathematical surface to determine the surface orientation when a particle interacts. For a perfect smooth surface, *BETA* = 0; for 0 < *BETA* < 1, *BETA* is the sine of the maximum angular deviation of the surface normal from smooth. If *BETA* < 0 (or *BETA* >> 1), the surface is completely random.

The geometric shape of each *region* is defined by its relationship to all of the defined surfaces. A positive or negative integer is placed in the region definition if every point in the region is on the + or − side of the corresponding surface, and surfaces that do not bound the region are set to zero. Special characteristics of the boundary are given by the value of the integer: ±1 for an ordinary surface with roughness *BETA* and the possibility of refraction or critical reflection; ±2 for total reflection; ±3 for diffuse scattering (independent of *BETA*); ±4 for total absorption; ±5 for cases requiring special action (such as a coordinate transformation) whenever a particle enters or leaves the region; and ±6 if the neutron history is to be split after crossing the surface. Care must be taken to avoid reentrant regions, but provision is made for having a "scattering chamber" region type that may contain embedded regions (*e.g.*, samples and detectors). Surfaces of embedded regions are marked by adding 10 to the surface type number, and are *not* tested as part of the definition of being inside the region. When the trajectory of a particle inside the region intersects the surface, it will exit if a valid region exists on the other side, but will otherwise remain in the enclosing region. This method must also be used with care, since particles within the embedded regions also pass the test for being within the enclosing region.

Regions have names and have associated types. Defined type numbers are listed here, and the definitions of parameters are given in Appendix A. Types that have been added since the ICANS 13 proceedings [1] are marked "*".

Simple material types:

type 0 = total absorber; no parameters
type 1 = amorphous unpolarized material; 4 parameters
type 2 = aluminum, including Bragg edges; no parameters
type 3 = hydrogenous, including multiple scattering
type 4 = supermirror represented by trapezoidal reflectivity; 4 parameters
type 5 = beryllium at 100K, including Bragg edges; no parameters
type 6 = single-crystal filter, Freund formalism; 3 parameters

Complex regions:
type 10 = multi-aperture collimator
type 11 = multi-slit collimator, vertical blades; 3 or 5 parameters
type 12 = multi-slit collimator, horizontal blades; 3 or 5 parameters
type 13.0 = crystal monochrometer; 10 parameters
* 13.1 = monochromator without beam axis bend (analyzer); 10 parameters
*type 14 = toroidal mirror; 10 parameters

Time-dependent regions:
types 20.n = chopper (disk or blade); 6 parameters
20.0 or 20.2 for motion in x-direction, 20.1 or 20.3 for y-direction
20.2 or 20.3 is counter-rotating (fully closed when edges at 0)
type 21 = Fermi chopper (not yet implemented)
type 22 = gravity focuser; 5 parameters
type 23 = removable beamstop; no parameters

Scattering samples:
type 30 = sample that scatters at constant Q; 2 parameters
type 31 = scattering sample of hard spheres; 2 parameters
type 32 = isotropic scatterer with fixed energy change; 2 parameters
type 34 = inelastic scattering kernel; no parameters; *NAME* is '[path]filename' of $S(\alpha,\beta)$ file in MCNP Type I format
type 35 = scattering from layered reflectometry sample; $1 + 4N$ parameters
type 36 = scattering from isotropic polycrystalline powder; 6 parameters + 2 × table length

Detectors (zero- and one-dimensional):
type 40 = detector; 9 parameters
type 41 = vertical linear detector; 14 parameters
type 42 = horizontal linear detector; 14 parameters
type 44 = longitudinal linear detector; 14 parameters

Detectors (two-dimensional):
type 43.nm = 2-D detector; 19 or 22 parameters
43.00, 43.10, 43.20, rectilinear coordinates, respectively (X,Y), (Z,Y), (X,Z)
43.01, 43.11, 43.21, plane polar coordinates (ρ, ϕ), axes respectively Z, X, and Y
* 43.02, 43.12, 43.22, cylindrical coordinates, respectively (Z, ϕ), (X, ϕ), (Y, ϕ)
* 43.03, 43.13, 43.23, spherical coordinates (θ, ϕ), axes respectively Z, X, and Y

Scattering chamber:
type 50 = scattering chamber, void-filled. No parameters, but other regions may be embedded, indicated by surface types with 10s digit on.

Sources:
types 90.n = source size and phase space to be sampled; 14-18 parameters
90.1 or 90.2 with rectangular aperture(s)
90.4 with vertical offests of apertures (option numbers may be added)
type 91 = source energy distribution table and line shape parameters; 12 parameters plus length of table
*type 95 = source file, direct-access binary; no parameters, but NAME must be '[path]filename' for the file. The file must be opened with logical unit number 95.

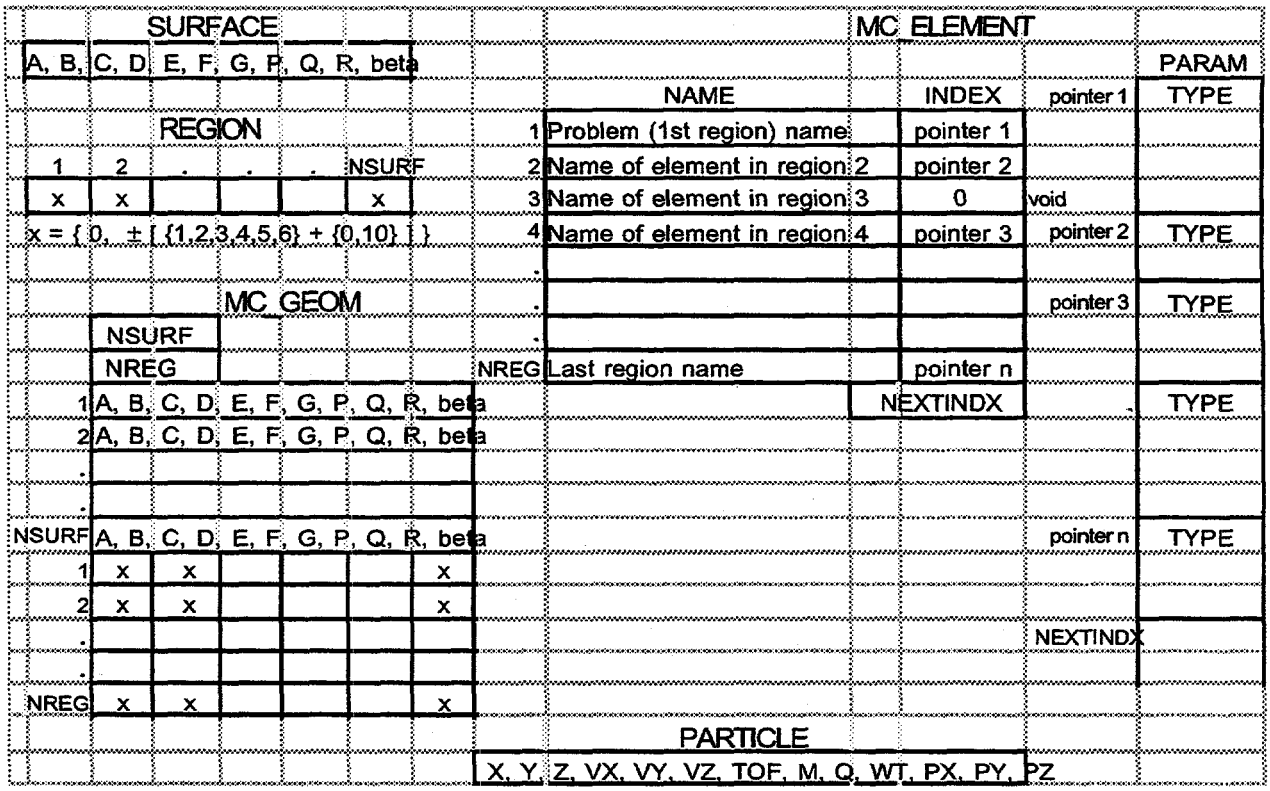

Figure 1. Structures used in MCLIB.

PROGRAM STRUCTURES

The relationships of the structures used by MCLIB are shown schematically in Fig. 1. Each surface is a record of type /SURFACE/, and elements are referenced as *(e.g.)* SURFACE.G. Similarly, a geometric region is a record of type /REGION/, which is a vector *IGEOM* of 2-byte integers, of length equal to the maximum allowed number of surfaces. An additional structure, MC_GEOM, contains the numbers of surfaces and regions in the problem, *NSURF* and *NREG*, and arrays of surface and region records. Information about types within the regions is contained in a structure called MC_ELEMENT that includes *NAME* and *INDEX* arrays, the parameter block *PARAM*, and the pointer *NEXTINDX* to the next available location in *PARAM*. Structures MC_GEOM and MC_ELEMENT represent the complete description of the instrument being simulated.

The final structure, PARTICLE, is the object that is acted upon by the beam element subroutines in the library. It includes position, velocity, time of flight, mass (1 for a neutron), charge (0 for a neutron), statistical weight, and vector polarization (not yet implemented in the code). A purely "analog" Monte Carlo traces each individual neutron until it is either lost or detected. MCLIB uses "weighted" neutrons, and in many of the processes the statistical weight is multiplied by the probability of survival instead of using a random number to decide whether to terminate the history ("Russian Roulette"). This is especially beneficial when scattering probability is small, as in subcritical reflection. To track more long-wavelength neutrons (which in general have larger scattering probability), the source distribution usually used is $\lambda^2 I(\lambda)$ instead of $I(\lambda)$ and the initial weight is proportional to $1/\lambda^2$. The tallied results are then the sum of detected neutron weights. The relative error in each bin, however, depends on the number of histories recorded.

NEW AND REVISED SUBROUTINES

The following routines have been added or modified. The most up-to-date listing of the subroutine abstracts and of the source codes may be found at *ftp://azoth.lansce.lanl.gov/mclib/.*

ANGTORUS04 Aug 96	computes the cosine of the angle of incidence with respect to a toroidal surface (including wobble)
DISTORUS08 Dec 96	finds distance along a trajectory to a horizontal or vertical toroidal shell (including gravity)
GET_SPACE25 Jan 96	added source brightness to calling sequence
N_SOURCE25 Jan 96	get source neutron: added Q and polarization vector; may read from direct-access binary file (type 95)
OPERATE27 Aug 96	find what happens to particle within region: small-angle scattering ~λ^2; additional region for chopper blade material; add toroidal mirrors (type 14)
PLMXWLN25 Mar 96	probability from Maxwellian
PLNORM 23 Jul 96	probability from normal distribution (faster algorithm)
POWDER 07 Dec 95	scatter from polycrystalline powder sample, was always isotropic if $\lambda >$ 2nd edge
SRC_PROB11 Jul 96	probability density /meV/μs from type 91 table (new)
TESTIN 04 Apr 96	find if within region, now computes in double precision

The program MC_RUN has also had several modifications, most notably:

- prepare direct-access .MON output file for subsequent use as a source, and open and initialize the source file if type=95
- periodic output of data (.DAT) file for protection against computer crashes during long runs
- fix error in refraction into void, including type=50
- bank 20 levels of saved neutrons instead of 1; split by 2 after surface type ±6
- test for "trapped" neutrons that could cause a job to freeze

CREATING A NEW TYPE

The process of adding toroidal mirrors to MCLIB will be used as a case study. There were four steps:

1. Define a new region type (14) and assign parameters and names.
2. Develop needed algorithms and procedures (DISTORUS and ANGTORUS).
3. Insert the "methods" for the new type in subroutine OPERATE.
4. Test, debug, and refine the previous three steps.

1. There is renewed interest in the use of focusing mirrors in neutron instruments, for example the proposal of Benno Schoenborn for a Laue protein-crystallography instrument [3], and a recent paper by John Copley [4]. Although an ellipsoid would be the optically preferred shape, a toroid may be more practical to manufacture. Since a toroid can not be defined as a *surface* by Eq. 1, it was necessary to define it as a *region.* The nature of the region is that it is divided into two subregions by the toroidal surface. The ten parameters can be seen in Appendix A at type 14. The torus is defined by its major radius R, the radius r of the generating circle, the offset of the center of the generating circle from the beam axis, and the longitudinal position of the center of revolution. Also, the sign of the major radius shows which side of the beam axis the center is on, and the sign of the minor radius is used as a flag for orientation: + for horizontal and − for vertical. (The choice of parameter three as a small offset instead of distance from the center of the

torus was crucial to maintaining precision.) The fifth parameter is surface roughness, and then three parameters are provided to define a rotation of the instrument beam axis after reflection. Finally, there are two pointers to define the materials inside and outside the torus. The "inside" material is in front of the mirror surface, and is usually void, indicated by a pointer of zero. The "outside" is the mirror surface/substrate, and the pointer is the offset of its definition in the *PARAM* block relative to the torus parameters; *e.g.*, if the material type immediately follows this block, then the pointer value is 12 (or 1 + *NUMBER_14*, the number of cells in *PARAM* used by type 14).

2. Finding the intersections of a line with a torus (a quartic surface) is not a trivial problem. Previous codes [4,5] have solved the problem very generally with sophisticated methods to retain precision. My approach was to begin with three limiting assumptions and one complication:

- only the near half of the toroid is relevant
- only the outer (concave) half-shell of the toroid is relevant
- only real solutions for the intersections are relevant
- the particle trajectory is a gravitational parabola instead of a straight line.

At this stage I had the assistance of Mike Fitzsimmons and Tom Klugel (MLNSC) to study methods of setting up and solving the fourth-order equation. The first method we used to set up the equation was copied from [5], using analytic derivatives of the trajectory in the coordinate system of the torus. This ran into serious difficulties when gravity was included (see §4 below), and the eventual solution was first to bracket the nearest and furthest intersections (if any!) of the parabola with bounding cylinders and planes of the relevant portion of the torus, and to solve for the distance from the surface parametrically *vs.* time of flight at five equally spaced points. Since the spacing of the points is uniform, multiplication by a predetermined constant matrix solves for the coefficients of the fourth-order equation of nearest distance as a function of time. One or two real roots (if any) are then found by the "safe" Newton-Raphson method discussed in *Numerical Recipes* [6], which uses bisection to keep the roots bracketed whenever the iteration step would move outside the current bracket. For further details, see the source code for DISTORUS in file MCLIB.SRC at *ftp://azoth.lansce.lanl.gov/pub/mclib/*.

Finding the angle of incidence, subroutine ANGTORUS, is far simpler. It is essentially a copy of WOBBLE with derivatives of the torus equation instead of Eq. 1. As in DISTORUS, precision is enhanced by accounting for the fact that the major radius of the torus is large compared to any other distance.

3. Inclusion of type-specific code in subroutine OPERATE requires adherence to the overall structure of the routine, and will probably be the most difficult (or dangerous) aspect for a user to add a function to MCLIB. Here is the scenario:

- When a particle enters a region, OPERATE is called with the following references:
  - *PART* = record containing description of particle (input/output)
  - *EXDIST* = distance to exit surface particle is aimed at (m) (input/output)
  - *PARAMS* = array with description of what is in this region (input)
  - *GEOM* = structure with all surface and region definitions (input)
  - *IREG* = region number of device, or subregion within device (input/output)
  - *JSURF* = surface number, if particle is initially on surface (input)
  - *KSURF* = surface number that particle is pointed toward (input/output)
  - *NAME* = name of region, used as file name for type 34 (input)
  - *TRANSMIT* = flag to compute transmission of sample types 30-39 (input)
  - *FLAG* = flag set to .FALSE. if (*e.g.*) chopper in wrong frame (output)
  - *PART_2* = description of particle created by operation (output)
  - *DET_WT* = statistical weight of detected particle (output)
  - *IX, IY* = position bin numbers of detected particle (output)

ISEED = random-number generator seed (input/output)

- OPERATE determines the region type from *PARAMS*(1) and transfers to the appropriate block of code in an IF-THEN-ELSE IF structure (this will become a CASE structure when F90 is more widespread).
- The code may use any variables marked "input" and may change any variables marked "output" in the above list. Local variables will have to be declared, and any variables to be retained across entries must have distinctive names and be placed in a SAVE statement.
- Valid operations include: moving the particle to the exit from the region with possible reeducation of statistical weight to account for absorption (set *EXDIST* to 0); selection of a subregion without moving; reflection (set *KSURF* negative); rotate the coordinate system; statistically split the particle or create a new one (in *PART_2*); scatter either elastically or inelastically; multiple scattering, keeping control through several motions of the particle till it reaches the region exit; detect the particle and find encoded position in detector. Examples of all these possibilities can be found in OPERATE.FOR.
- For compatibility with older Fortran compilers without recursive subroutines, the code should not make any calls to OPERATE for processing subregions. Use no numbered statements. Style should be similar to the existing OPERATE.FOR code.

In the case of the toroidal mirror, the actions are to determine the distance to the torus and which side the particle is on using DISTORUS, and to move either to that surface or the region exit (whichever is closer) through the appropriate material, compute reflection probability using ANGTORUS and the ratio of scattering length densities across the surface, and repeat all of these actions till the region is exited. Note that *only* material types 0 (void), 1 (amorphous non-magnetic), or 4 (supermirror layer) are allowed, due to the restriction that all code for the type must be inline. In fact, the code for type 1 and type 4 regions has been copied into this block.

4. The debugging of this module is an example of cooperation with outside users. The code had been tested by reproducing the results in [4], but in a different coordinate system. When John Copley tried to use the code, there were subtle errors. It took one more test to show that my code was at fault, rather than John's interpretation of it, two more rounds of modification and testing to uncover a serious philosophical flaw in the algorithm, and two more rounds to "perfect" the code. This version passes all tests, and is twenty times faster [7] than the program used previously.

SMALL-ANGLE SCATTERING

The original paper on curved-mirror neutron optics [8] suggested small-angle scattering as an application. The authors considered a bent mirror forming a cylinder with axis transverse to the

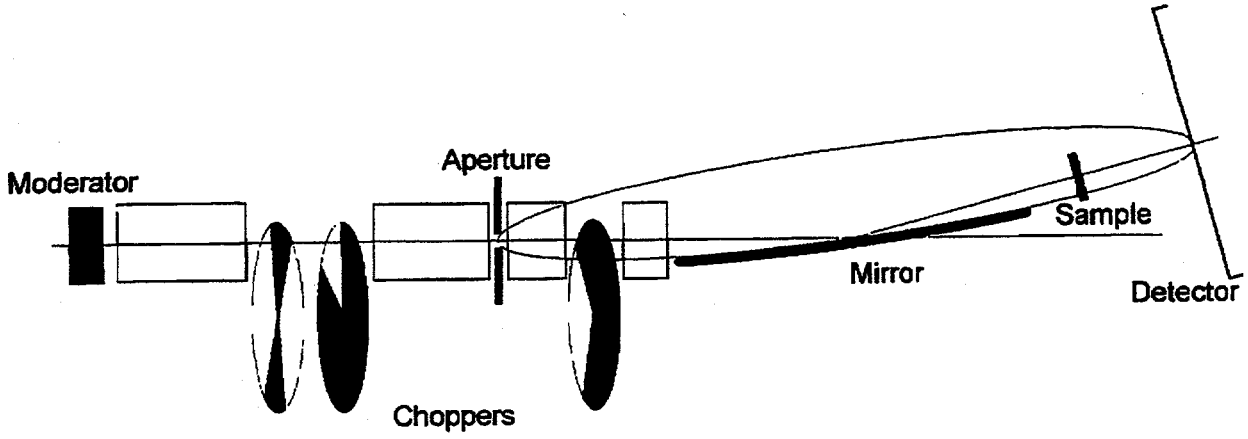

Figure 2. Small-Angle Scattering instrument using a focusing mirror for increased intensity.

beam, and a narrow slit aperture with the solid angle of the mirror matched to the solid angle of the neutron source. The same geometrical matching can be applied to illuminate a mirror that focuses in two dimensions, as illustrated in Fig. 2. (Note that the transverse dimensions in Fig. 2 are exaggerated by a factor of 10 relative to the longitudinal dimensions.) The MCLIB code allows us to compare mirror shapes in this geometry: the ideal ellipsoid, the tangent toroid, cylindrical segments (with longitudinal cylinder axes), or toroidal segments (bent cylinders with varying curvatures). Compared to a two-aperture collimation system with the same resolution, a factor of 10 increase in intensity is possible because the full illuminated surface of the moderator may be viewed. The tradeoff between intensity and resolution depends on the single aperture.

The mirror considered as an example was 3.0 m long and 75 mm wide, with a major axis of 9 m and transverse (minor) axes of 157 mm. The glancing is 1° at the center (beam axis bent by 2°). The radius-of-curvature parameters of the tangent toroid are $R = 257.77$ m and $r = 78.54$ mm. The source aperture had a diameter of 2.0 mm, located at one focus of the ellipsoid; at this eccentricity, the focus is less than 1 mm from the vertex. Also, the transverse diameter of the ellipsoid at the focus is only 2.7 mm, so the source is "large" in terms of optical properties, and Monte Carlo is a useful tool a estimating resolution at the detector placed at the other focus. The detector pixel size was made small (0.25 mm) and the encoding uncertainty was zero so as not to affect the computed resolution when compared to the source aperture size, which contributes 0.50 mm to the standard deviation in each detector coordinate. Since the effect of gravity is always included in the algorithms of MCLIB (for any particles with rest mass), it is necessary to place the source aperture (and the detector center) below the instrument axis *if the reflection plane is horizontal* by a distance that is proportional to wavelength, such that the nominal trajectory at the mirror center is horizontal. However, *if the reflection is upwards* (mirror horizontal and concave up), then no correction is necessary because the excess downward velocity acquired before striking the mirror is reflected and then canceled by downward acceleration after reflection (this cancellation is exact only for neutrons reflected at the center of the mirror, but is independent of wavelength). For a white source (*i.e.*, spallation) the vertical reflection plane is much to be preferred.

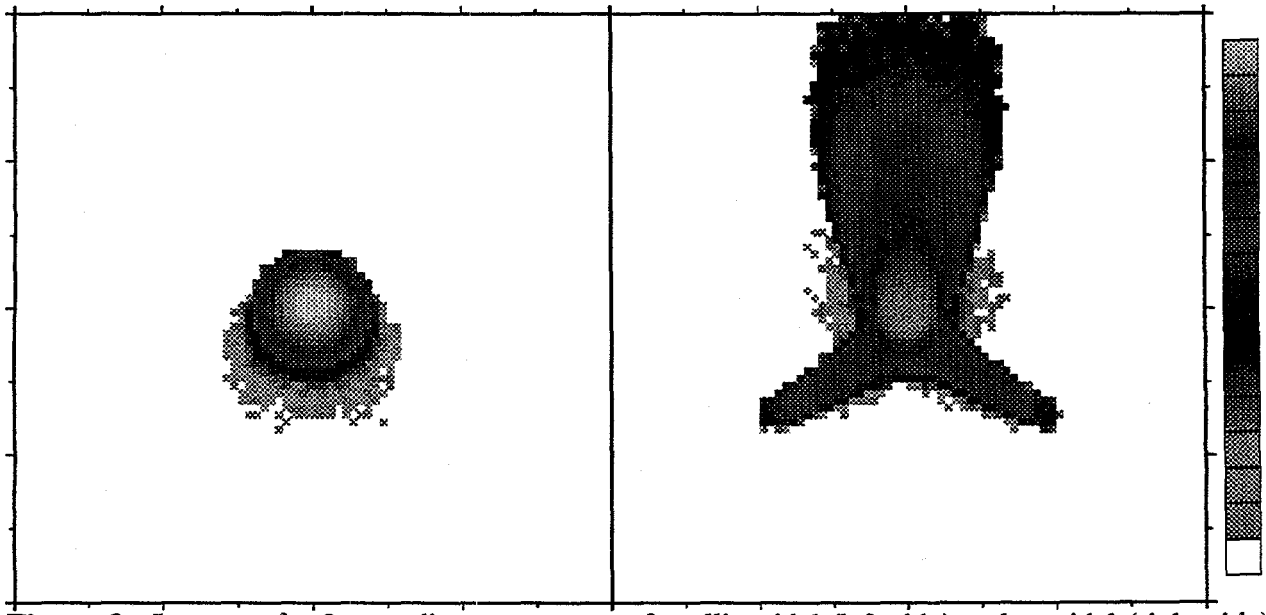

Figure 3. Images of a 2-mm diameter aperture for ellipsoidal (left side) and toroidal (right side) focusing mirrors. The reflection plane is vertical (upward) to correct for gravity. Each pattern is a histogram for 250000 detected neutrons with wavelength distribution from 2–20 Å, from a coupled liquid-hydrogen moderator. Each figure is 20 mm square on the detector (printed at four times size), and the intensity scale is logarithmic from 1 to 93250 counts per pixel.

A comparison of the beam spots for the ellipsoid and toroid is shown in Fig. 3, for vertical reflection of a cold-moderator spectrum from 2–20 Å. (A supermirror reflecting layer was assumed, and reflectivity is good above 3 Å.) The standard deviations for the ellipsoid are 0.64 mm in both the horizontal and vertical directions, and those for the toroid are 1.05 mm horizontal and 2.29 mm vertical. A minimum Q-value less than 0.001 $Å^{-1}$ could be achieved with this geometry in an instrument of total length 13 m (with the ellipsoidal mirror). Further details of this simulation will be presented later.

REQUESTS FOR ADDITIONAL ELEMENT TYPES

It is hoped that the MCLIB code will be generally useful to designers of neutron instruments. For this goal to be realized, two sets of improvements are being pursued. First, the general user interface is being moved to a web page so that geometry files may be constructed more easily than is now possible. Second, we are soliciting input of algorithms from interested or potential users, so that the code will do what *you* want. Please communicate with the author by e-mail to *PASeeger@aol.com* if you have any questions or suggestions.

ACKNOWLEDGEMENT

This work was supported by the U. S. Department of Energy, Office of Basic Energy Sciences and other Department of Energy programs under Contract W-7405-ENG-32 to the University of California.

REFERENCES

1. P. A. Seeger, "The MCLIB Library: Monte Carlo simulation of neutron scattering instruments," 13th Meeting of the International Collaboration on Advanced Neutron Sources, October 11–14, 1995, Paul Scherrer Institut, Villigen, Switzerland, *PSI Proceedings* **95-02**, pp. 194–212.
2. T. G. Thelliez, L. L. Daemen, P. A. Seeger, and R. P. Hjelm, Jr., "A user-friendly geometry interface for the Monte Carlo neutron optics code MCLIB," 13th Meeting of the International Collaboration on Advanced Neutron Sources, October 11–14, 1995, Paul Scherrer Institut, Villigen, Switzerland, *PSI Proceedings* **95-02**, pp. 307–311.
3. B. P. Schoenborn and E. Pitcher, in *Neutrons in Biology*, B. P. Schoenborn and R. B. Knott, eds., Plenum Press, New York, pp. 433–444 (1996).
4. J. R. D. Copley, *Rev. Sci. Instrum.* **67** (1996) 188–194.
5. G. Hummer, subroutine TORUS, Feb. 28, 1995.
6. W. H. Press, S. A. Teukolsky, W. T. Vettering, and B. P. Flannery, *Numerical Recipes in Fortran, Second Ed.*, Cambridge University Press, New York, §9.4 (1992).
7. C. Lartigue, private communication.
8. H. Maier-Leibnitz and T. Springer, *J. Nucl. Energy Parts A/B* **17** (1963) 217–225.

APPENDIX A. MC_ELMNT.INC

```
C Definitions of beam elements which may occur in regions, and their parameters
C
C P. A. Seeger, April 20, 1994
C  04 Jan 1995: define offsets of parameters within blocks, rather than
C            structure with UNIONs [PAS]
C  10 Jan 1995: modified source type 90; added type 91 for source spectrum
C            and lineshape description [PAS]
C  01 Feb 1995: added types 5 (Be), 13 (crystal monochromator), and 35
C            (reflectrometry) [PAS]
C  15 Feb 1995: modified type 91; moved structure definition to MC_GEOM.INC
C            [PAS]
C  04 Mar 1995: types 90.n for rectangular and/or offset phase space [PAS]
C  09 Mar 1995: type 44 (longitudinal detector); all detectors need surface
C            number [PAS]
C  06 Jun 1995: 2 more parameters in monochromator type 13 [PAS]
C  13 Jul 1995: type 36, general powder [PAS,Uli Wildgruber,Luke Daemon]
C  04 Aug 1995: type 6, single-crystal filter [PAS]
C  26 Aug 1995: type 32, isotropic scatterer [PAS]
C  05 Sep 1995: revised parameters for pulse shape (type 91) [PAS]
C  16 Oct 1995: changed parametrization of supermirror (type 4) [PAS]
C  11 Nov 1995: add NUMBER_nn to all types [PAS]
C  22 Nov 1995: add subtypes and coordinate origin to type 43 [PAS]
C  24 Jan 1996: type 95, source from direct-access binary file [PAS]
C  05 Aug 1996: type 14, toroidal mirror [PAS]
C  01 Jul 1997: type 13.1; revised Ikeda-Carpenter form for type 91 [PAS]
C  03 Jul 1997: changed subtypes of type 43 (2 digits) [LLD,PAS]
C
C The first entry in PARAM for each element identifies the
C  type, followed by a varying number of parameters.
C
      INTEGER ELMNT_TYPE
      PARAMETER (ELMNT_TYPE=0)
C type 0 = total absorber; no additional parameters
        INTEGER NUMBER_00
        PARAMETER (NUMBER_00=1)
C type 1 = amorphous unpolarized material; 4 parameters
C       Real and Imaginary scattering-length density (10**10/cm**2)
C       macroscopic scattering cross section (1/m)
C       velocity-dependent cross section, at 1 m/us (1/us)
        INTEGER REAL_RHO, IMAG_RHO, NSIGMA0, NSIGMAV, NUMBER_01
        PARAMETER (REAL_RHO=1,IMAG_RHO=2,NSIGMA0=3,NSIGMAV=4,
     1           NUMBER_01=5)
C type 2 = aluminum, including Bragg edges; no additional parameters
        INTEGER NUMBER_02
        PARAMETER (NUMBER_02=1)
C type 3 = hydrogenous, including multiple scattering; 1 parameter
C       Relative hydrogen density compared to water
        INTEGER H_DENSITY, NUMBER_03
        PARAMETER (H_DENSITY=1,NUMBER_03=2)
C type 4 = supermirror represented by trapezoidal reflectivity; 4 parameters
C       Real & Imaginary scattering-length density (10**10/cm**2) (see type 1)
C       Supermirror multiplier
```

```
C      Refectivity at maximum supermirror limit
       INTEGER SUPER_MULT, SUPER_REFL, NUMBER_04
       PARAMETER (SUPER_MULT=3,SUPER_REFL=4,NUMBER_04=5)
C  type 5 = beryllium at 100K, including Bragg edges; no additional parameters
       INTEGER NUMBER_05
       PARAMETER (NUMBER_05=1)
C  type 6 = single-crystal filter, Freund formalism; 3 parameters
C         xsec = sigfree*(1-exp(-C2/lambda**2)) + sigabs*lambda
C      Limiting (short wavelength) free-atom macroscopic cross section (1/cm)
C      -ln(1 - (sig(1A)-sigabs)/(sigfree-sigabs)) (A**2)
C      sum of 1/v macroscopic cross sections at 1A (1/cm/A)
       INTEGER XSIGFREE, X_C2, XSIGABS, NUMBER_06
       PARAMETER (XSIGFREE=1,X_C2=2,XSIGABS=3,NUMBER_06=4)
C
C  type 10 = multi-aperture collimator
C  type 11 = multi-slit collimator, vertical blades; 3 or 5 parameters
C      Spacing of slits, centerline-to-centerline (m)
C      Rate of convergence (>0) or divergence (<0) of one slit
C      Z at entrance of the region, where spacing is measured (m)
       INTEGER C_DELTA, C_TAPER, C_ZENTER
       PARAMETER (C_DELTA=1,C_TAPER=2,C_ZENTER=3)
C      For a curved system (bender),
C        sine of half the angle of bend
C        cosine of half the angle of bend
       INTEGER B_SIN_PHI, B_COS_PHI, NUMBER_11
       PARAMETER (B_SIN_PHI=4,B_COS_PHI=5,NUMBER_11=6)
C  type 12 = multi-slit collimator, horizontal blades; 5 parameters
C         Same parameters as type 11
       INTEGER NUMBER_12
       PARAMETER (NUMBER_12=6)
C  type 13.n = crystal monochromator; 10 parameters
C      Twice the crystal plane spacing (A)
C      following 3 parameters are ignored if type=13.1:
C        Nominal Z position for rotation of instrument axis (m)
C        Sine and cosine of take-off angle
C      X-, Y-, and Z-components of mosaic spread, rms of sines of angles
C      rms spread of plane spacing, (delta d)/d
C      max number of loops (or microcrystal orientations) to try
C      probability normalization factor per try, derived from reflection
C        probability at peak wavelength: 1 - (1-max_prob)**(1/trys)
       INTEGER M_2D_SPACE, M_Z0, M_SIN_2TH, M_COS_2TH, M_ROTX,
     1         M_ROTY, M_ROTZ, M_D_SPREAD, M_TRY, M_PROB, NUMBER_13
       PARAMETER (M_2D_SPACE=1,M_Z0=2,M_SIN_2TH=3,M_COS_2TH=4,
     1           M_ROTX=5,M_ROTY=6,M_ROTZ=7,M_D_SPREAD=8,
     2           M_TRY=9,M_PROB=10,NUMBER_13=11)
C  type 14 = toroidal mirror; 10 parameters
C      Radius of rotation of torus, from axis to center of generating
C        circle; positive if torus axis right of or above beam axis (m)
C      Radius of cross section of torus; negative if torus vertical (m)
C      Offset of center of generating circle from beam axis (m)
C      Z-coordinate of torus axis (m)
C      Surface roughness parameter
       INTEGER TORUS_A, TORUS_B, TORUS_D, TORUS_Z, TOR_BETA
C      sin, cos, and Z-center for beam axis rotation (if any)
```

```
      INTEGER TOR_SIN_TH, TOR_COS_TH, TOR_Z_ROT
C      Offsets to parameter blocks for interior and exterior regions,
C        zero if void; types 1 and 4 are supported
      INTEGER INSIDE_OFFSET, OUTSIDE_OFFSET, NUMBER_14
      PARAMETER (TORUS_A=1, TORUS_B=2, TORUS_D=3, TORUS_Z=4,
     1           TOR_BETA=5, TOR_SIN_TH=6, TOR_COS_TH=7, TOR_Z_ROT=8,
     2           INSIDE_OFFSET=9, OUTSIDE_OFFSET=10, NUMBER_14=11)
C
C  types 20.n = chopper (disk or blade); 6 parameters
C        .0 or .2 for motion in x-direction, .1 or .3 for vertical
C        .2 or .3 is counter-rotating (fully closed when edges at 0)
C      Linear velocity of opening crossing beam centerline (m/us)
C      Time to cover or uncover half the width of the moderator (us)
C      Nominal time at which opening chopper edge crosses zero (us)
C      Nominal time at which closing chopper edge crosses zero (us)
C      Phase jitter of chopper, rms (us)
C      Period of chopper (us)
      INTEGER CHP_VEL, CHP_HALF, CHP_OPEN, CHP_CLOSE,
     1        CHP_JITTER, CHP_PERIOD, NUMBER_20
      PARAMETER (CHP_VEL=1,CHP_HALF=2,CHP_OPEN=3,CHP_CLOSE=4,
     1           CHP_JITTER=5,CHP_PERIOD=6,NUMBER_20=7)
C  type 21 = Fermi chopper
C  type 22 = gravity focuser; 5 parameters
C      acceleration (m/us**2), and rms phase jitter (us)
C      nominal times for start and top of upward stroke (us)
C      time between pulses (us)
      INTEGER G_ACCEL, G_JITTER, G_START, G_TOP, G_PERIOD, NUMBER_22
      PARAMETER (G_ACCEL=1,G_JITTER=2,G_START=3,G_TOP=4,G_PERIOD=5,
     1           NUMBER_22=6)
C  type 23 = removable beamstop; no additional parameters
      INTEGER NUMBER_23
      PARAMETER (NUMBER_23=1)
C
C      first parameter of many samples is -ln(transmission at 1 A)
      INTEGER SIGMA_1A
      PARAMETER (SIGMA_1A=1)
C  type 30 = sample which scatters at constant Q; 1 additional parameter
C        value of Q for scatter (1/A)
        INTEGER Q_SCATTER, NUMBER_30
        PARAMETER (Q_SCATTER=2,NUMBER_30=3)
C  type 31 = scattering sample of hard spheres; 1 additional parameter
C         hard-sphere radius for scatter (A)
        INTEGER R_SPHERE, NUMBER_31
        PARAMETER (R_SPHERE=2,NUMBER_31=3)
C  type 32 = isotropic scatterer with constant energy change; 1 additional
C         inelastic energy change (0 if elastic) (eV)
        INTEGER DELTA_E, NUMBER_32
        PARAMETER (DELTA_E=2,NUMBER_32=3)
C  type 34 = inelastic scattering using MCNP file; no parameters, but NAME
C      must be '[path]filename' for the file
      INTEGER NUMBER_34
      PARAMETER (NUMBER_34=1)
C  type 35 = scattering from layered reflectrometry sample; 1 + 4*N parameters
C      number of layers, including substrate
```

```
C       parameters for each layer, starting with substrate:
C         4pi*Real and Imaginary scattering-length density (1/A**2)
C         Thickness of layer (zero for substrate) (A)
C         Roughness, 2*sigma**2 of outer surface of this layer (A**2)
        INTEGER NLAYERS, REAL4PINB, IMAG4PINB, THK_LAYER, ROUGHNESS,
     1          NUMBER_35
        PARAMETER (NLAYERS=1, REAL4PINB=2, IMAG4PINB=3,
     1             THK_LAYER=4, ROUGHNESS=5, NUMBER_35=2)
C   type 36 = scattering from isotropic polycrystalline powder; 6+2*N parameters
C       number of Bragg edges included
C       limiting (short wavelength) macroscopic total xsection (1/cm)
C       macroscopic incoherent scattering xsection (1/cm)
C       macroscopic 1/v scattering xsection at 1 A (1/cm/A)
C       macroscopic 1/v absorption xsection at 1 A (1/cm/A)
C       table of d-spacings of Bragg edges (A), followed by explicit 0 and
C         table of cumulative macroscopic xsections at 1 A (1/cm/A**2)
        INTEGER N_BRAGG, PSIGMAT, PSIGMAI, PSIGMAS, PSIGMAA, D_BRAGG,
     1          NUMBER_36
        PARAMETER (N_BRAGG=1,PSIGMAT=2,PSIGMAI=3,PSIGMAS=4,PSIGMAA=5,
     1             D_BRAGG=6,NUMBER_36=7)
C
C   type 40 = detector; 9 additional parameters
C       first parameter of all detectors is surface number
C       second parameter of all detectors is -ln(1 - efficiency at 1 A)
        INTEGER DET_SURF, D_ALPHA_1A
        PARAMETER (DET_SURF=1,D_ALPHA_1A=2)
C       time-of-flight clock parameters:
C         minimum and maximum times (us)
C         number of time channels
C         if logarithmic, dt/t (otherwise dt/t = 0)
C         minimum clock tick in determining log scale (us)
C         electronic delay of detector events (us)
C         repeat period of data-acquisition electronics (us)
C       Note: if t-o-f is logarithmic, TMAX is overriden
        INTEGER D_TMIN, D_TMAX, D_TCHANS, D_DT_OVER_T, D_TICK, D_DELAY,
     1          D_T_PERIOD, NUMBER_40
        PARAMETER (D_TMIN=3,D_TMAX=4,D_TCHANS=5,D_DT_OVER_T=6,
     1             D_TICK=7,D_DELAY=8,D_T_PERIOD=9,NUMBER_40=10)
C   type 41 = vertical linear detector; 14 additional parameters
C         locations of bottom and top of detector (m)
C         number of detector elements
C         size of detector element (m)
C         root-mean-square encoding error of detector (m)
        INTEGER DET_YMIN, DET_YMAX, DET_NY, DET_DELY, DET_RMSY,
     1          NUMBER_41
        PARAMETER (DET_YMIN=10,DET_YMAX=11,DET_NY=12,DET_DELY=13,
     1             DET_RMSY=14,NUMBER_41=15)
C   type 42 = horizontal linear detector; 14 additional parameters
C         locations of left and right ends of detector (m)
C         number of detector elements
C         size of detector element (m)
C         root-mean-square encoding error of detector (m)
        INTEGER DET_XMIN, DET_XMAX, DET_NX, DET_DELX, DET_RMSX,
     1          NUMBER_42
```

```
      PARAMETER (DET_XMIN=10,DET_XMAX=11,DET_NX=12,DET_DELX=13,
     1           DET_RMSX=14,NUMBER_42=15)
C  type 43.nm = 2-D detector; 19 or 22 additional parameters
C       n = axis orientation digit: .0 = Z,  .1 = X,  .2 = Y
C       m = coordinate type digit: .00 = rectilinear, .01 = plane polar,
C                                  .02 = cylindrical, .03 = spherical
C       ------------------------------------------------------------------
C     m  n|      .0        |      .1        |      .2
C     ----+----------------+----------------+----------------
C     .00 |    (X, Y)      |    (Z, Y)      |    (X, Z)
C         |                |                |
C     .01 | (rhoXY, phiXY) | (rhoZY, phiZY) | (rhoXZ, phiXZ)
C         |                |                |
C     .02 |  (Z-Z0, phiXY) |  (X-X0, phiZY) |  (Y-Y0, phiXZ)
C         |                |                |
C     .03 | (thetaZ, phiXY) | (thetaX, phiZY) | (thetaY, phiXZ)
C     ------------------------------------------------------------------
C     where:  rhoXY = sqrt[(X-X0)^2 + (Y-Y0)^2)] = distance from Z-axis (m),
C           phiXY = arctan[(Y-Y0)/(X-X0)] = angle from +X toward +Y (rad),
C           thetaZ = arctan[rhoXY/(Z-Z0)] = angle away from Z-axis (rad)
C     Parameters:
C        locations of min and max X (abscissa) edges of detector (m or rad)
C        number of detector elements in the abscissa direction
C        width of detector abscissa element (m or rad)
C        root-mean-square abscissa encoding error of detector (m or rad)
C        locations of min and max Y (ordinate) edges of detector (m or rad)
C        number of detector elements in the ordinate direction
C        height of detector ordinate element (m or rad)
C        root-mean-square ordinate encoding error of detector (m or rad)
C        origin of coordinates (m)
      INTEGER DET2_XMIN, DET2_XMAX, DET2_NX, DET2_DELX, DET2_RMSX
      INTEGER DET2_YMIN, DET2_YMAX, DET2_NY, DET2_DELY, DET2_RMSY
      INTEGER DET2_X0, DET2_Y0, DET2_Z0, NUMBER_43
      PARAMETER (DET2_XMIN=10,DET2_XMAX=11,DET2_NX=12,
     1           DET2_DELX=13,DET2_RMSX=14,DET2_YMIN=15,
     2           DET2_YMAX=16,DET2_NY=17,DET2_DELY=18,
     3           DET2_RMSY=19,DET2_X0=20,DET2_Y0=21,
     4           DET2_Z0=22,NUMBER_43=23)
C  type 44 = longitudinal linear detector; 14 additional parameters
C       locations of upstream and downstream ends of detector (m)
C       number of detector elements
C       size of detector element (m)
C       root-mean-square encoding error of detector (m)
      INTEGER DET_ZMIN, DET_ZMAX, DET_NZ, DET_DELZ, DET_RMSZ,
     1        NUMBER_44
      PARAMETER (DET_ZMIN=10,DET_ZMAX=11,DET_NZ=12,DET_DELZ=13,
     1           DET_RMSZ=14,NUMBER_44=15)
C
C  type 50 = scattering chamber, void-filled.  No parameters, but other regions
C     may be embedded, indicated by surface types with 10s digit on.
      INTEGER NUMBER_50
      PARAMETER (NUMBER_50=1)
C
C  types 90.n = source size and phase space to be sampled; 14-18 parameters
```

```
C      edges of rectangular moderator face (m)
       INTEGER MOD_XMIN, MOD_XMAX, MOD_YMIN, MOD_YMAX
       PARAMETER (MOD_XMIN=1,MOD_XMAX=2,MOD_YMIN=3,MOD_YMAX=4)
C      location and radius (half-width) of apertures which define beam (m)
       INTEGER APTR1_Z, APTR1_R, APTR2_Z, APTR2_R
       PARAMETER (APTR1_Z=5,APTR1_R=6,APTR2_Z=7,APTR2_R=8)
C      additional vertical space to sample for gravity focus (m)
       INTEGER G_DELY2
       PARAMETER (G_DELY2=9)
C      min and max neutron energy to be sampled (eV)
C      time between beam pulses and square pulse width (us)
       INTEGER S_EMIN, S_EMAX, S_PERIOD, S_WIDTH
       PARAMETER (S_EMIN=10,S_EMAX=11,S_PERIOD=12,S_WIDTH=13)
C      offset to parameter block with spectrum and lineshape parameters
       INTEGER E_OFFSET
       PARAMETER (E_OFFSET=14)
C      (optional) half-heights of apertures, type 90.1 or 90.2 (m)
       INTEGER APTR1_Y, APTR2_Y
       PARAMETER (APTR1_Y=15,APTR2_Y=16)
C      (optional) vertical offsets of apertures, type 90.4 (m)
       INTEGER APTR1_Y_OFFSET, APTR2_Y_OFFSET, NUMBER_90
       PARAMETER (APTR1_Y_OFFSET=17,APTR2_Y_OFFSET=18,NUMBER_90=19)
C  type 91 = source energy distribution table and lineshape parameters; 12
C    parameters plus length of table
C      number of entries in energy table (1 is special case)
C      location in table of center of normal distribution (index units)
C        or value of nominal neutron velocity (m/us) (if # entries = 1)
C      standard deviation of normal distribution (table index units)
C        or relative fwhm of velocity selector (if # entries = 1)
C      source brightness, summed over limits of E_TABLE (n/ster/m**2/MW/s)
       INTEGER N_E_TABLE, CENT_TABLE, SIGMA_TABLE, S_BRIGHT
       PARAMETER (N_E_TABLE=1,CENT_TABLE=2,SIGMA_TABLE=3,S_BRIGHT=4)
C      ------------------------------------------------------------------
C      Parameter |    Gaussian/exponential   | Ikeda-Carpenter/exponential
C        Name    |      (T_WIDTH >= 0)       |    (-1 <= T_WIDTH < 0)
C      ----------+---------------------------+---------------------------
C      TAU_TH1   |Late-time exponential (us) |Late-time exponential (us)
C      TAU_TH2   |Intermediate exponential (us)|Intermediate exponential (us)
C      TAU2_RATIO|Fraction of TAU_TH2        |Fraction of TAU_TH2
C      TAU_EPI   |Epithermal time const. (us/A)|Mean (t/lambda) (us/A)
C      T_DELAY   |Gaussian midpoint (us/A)    |Early exponential (us/A)
C      T_WIDTH   |Gaussian width (us/A)       |- fraction in early exp., or
C                |                           |  -1 if no early exp.
C      ------------------------------------------------------------------
       INTEGER TAU_TH1, TAU_TH2, TAU2_RATIO
       PARAMETER (TAU_TH1=5,TAU_TH2=6,TAU2_RATIO=7)
C      epithermal (high energy) time constant proportional to lambda (us/A)
C        or mean (t/lambda) parameter of Ikeda-Carpenter (us/A) (if width<0)
C      Gaussian delay and width, /lambda (us/A) (width < 0 is special case)
       INTEGER TAU_EPI, T_DELAY, T_WIDTH
       PARAMETER (TAU_EPI=8,T_DELAY=9,T_WIDTH=10)
C      switching function 1/e point (A) and power (slope)
       INTEGER SWITCH_LAMBDA, SWITCH_POWER
       PARAMETER (SWITCH_LAMBDA=11,SWITCH_POWER=12)
```

```
C      origin of table of cumulative energy distribution (weighted by
C        lambda**2) of source spectrum on equally spaced normal-curve values
C        of log(energy/1meV)
       INTEGER E_TABLE, NUMBER_91
       PARAMETER (E_TABLE=13,NUMBER_91=13)
C type 95 = source file, direct-access binary; no parameters, but NAME must
C      be '[path]filename' for the file.  File format is
C      1st record: 16 bytes of coding information and 17-character ID
C      2nd record: 40-character TITLE of job that created the file
C      3rd record: source surface definition
C      4th record: # of histories (integer*4), sum of weights, source MW-s,
C                  modified source brightness, phase space, lethargy
C      records 5-(# of histories+4): source neutrons
       INTEGER NUMBER_95
       PARAMETER (NUMBER_95=1)
C
```

Quantifying the Information Measured by Neutron Scattering Instruments

M W Johnson

Rutherford Appleton Laboratory,
Chilton, Didcot, Oxon OQ11 0QX, UK

Abstract

The concept of the *information content* of a scientific measurement is introduced, and a theory is presented which enables the information that may be obtained by a neutron scattering instrument to be calculated. When combined with the time taken to perform the measurement the *bandwidth* of the instrument is obtained. This bandwidth is effectively a *figure of merit* which is of use in three respects: in the design of neutron instrumentation, the optimisation of measurements, and in the comparison of one instrument with another.

1 Introduction

The purpose of this paper is to offer a new tool for assessing the 'usefulness' of instruments. We will do this by quantifying the rate at which information may be obtained using a neutron diffractometer or spectrometer. The techniques used may be straightforwardly extended to any other counting instruments.

What is information? A theory of information transmission was first developed by Shannon [1] and its application to science has been explored by Bruillouin [2] , and Jaynes [3] , among others. This theory disentangles the qualitative aspects of information content (which are nonetheless important) from the quantitative aspects. In this paper we apply this theory to instrumental measurements.

Consider a system, S, which, as far as an observer is concerned, can be in Λ_0 equally probable states. If further information is given to the observer, which reduces the number states that S can be in to Λ_1, then the content (I) of this information is defined as:

$$I = K \ln(\Lambda_0 / \Lambda_1) \tag{1}$$

This definition of information results in an additive rule for independent information. Thus if information is received in two stages, our knowledge about a system changing from Λ_0 to Λ_1 to Λ_2 , the total information received is equal to the sum of the information received:

$$I_T = K \ln\left[\frac{\Lambda_0}{\Lambda_2}\right] = K \ln\left[\frac{\Lambda_0}{\Lambda_1}\frac{\Lambda_1}{\Lambda_2}\right] = K \ln\left[\frac{\Lambda_0}{\Lambda_1}\right] + K \ln\left[\frac{\Lambda_1}{\Lambda_2}\right] = I_1 + I_2 \tag{2}$$

In a similar way a message may be said to contain information I_M :

$$I_M = K \ln(M_0 / M_1) \tag{3}$$

where M_0 and M_1 are the number of possible messages before and after the message was received. If the message is unambiguous then M_1 will equal unity and the information content of the message simply equal to $K\ln(M_0)$. Thus, if a signalling system can transmit a binary digit of length n bits, the number of possible messages will be 2^n , and the information content will be given by:

$$I_M = K\ln(2^n) \tag{4}$$

The coefficient K in the above expressions is arbitrary, but if chosen to be equal to 1/ ln(2) then the information is expressed in units of 'bits' . Thus substituting this value for K into equation 4 gives a value for I_M of n bits, in agreement with the binary message length.

In a similar way, the use of an instrument to perform a measurement may be considered a transmission of information. We may calculate the quantity of information in a similar way, by considering the number of outcomes that were possible before the measurement, and compare it to the number possible after the measurement.

2 The scalar counter

All neutron scattering instruments are essentially counting devices. We must therefore begin by establishing the information contained in an experiment involving a single scalar counter. The number of possibilities before the measurement is clearly related to the maximum count that can be measured by the scalar in the time chosen. With a maximum count of M, it could be argued that the information contained in the measurement is:

$$I = K\ln(M+1) \tag{5}$$

since one possible count has been determined (Λ_1) from the M+1 (including zero) possible before the measurement occurred (Λ_0). This is too superficial since it ignores the effect of statistical noise. The number of possibilities after the measurement is related to the probability distribution of the 'true count' θ that may be derived from the actual count k. When this is taken into account the result is:

$$I = K\ln\sqrt{M/2\pi} \tag{6}$$

The details of this derivation, together with other results given below are to be found in reference [5]. Having obtained the information content of a single scalar counter it is necessary to consider the effects of backgrounds. Such backgrounds may be broadly of two sorts, those that are independent of the actual count, k, but may be regarded as a constant fraction of the maximum possible count (b = f.M), and those that are linearly related to the actual count k (b = f.k). Of course the background could be a mixture of these two types, or related in a more complex way to both.
Here we will consider the first type of background. Using the result C4 - appendix of reference [5] we may, quite generally write the information content of a pair of counts (k,l) from foreground and background measurements:

$$I_{sample} = K\sum_k\sum_l p_{kl}\ln(\Lambda_0/\Lambda_{kl}) \tag{7}$$

where p_{kl} is the probability of the pair of measurements, and Λ_0, Λ_{kl} the possibilities before and after the measurements. The details of the calculation are given in the appendix section E of reference [5] and give the result:

$$I_s = K \ln \sqrt{\frac{M}{2\pi}} + K \ln \left[\frac{(1-f)}{(1+f)^{1/2}} \left(\frac{2f}{1+f} \right)^{f/(1-f)} \right] \tag{8}$$

where the background, b = f M .

The equation (8) may be written

$$I_s = K \ln \sqrt{\frac{cM}{2\pi}} \tag{9}$$

where the maximum count, *M*, is now modified by the factor, c, which is given by

$$c = \left[\frac{(1-f)}{(1+f)^{1/2}} \left(\frac{2f}{1+f} \right)^{f/(1-f)} \right]^2 \tag{10}$$

Thus *c(f)* is a measure of the effective reduction in the maximum count M due to the presence of a background , $b = fM$. It will be seen that 10% background equivalent to a 50% reduction in intensity, and 50% background equivalent to reducing the intensity by more than 90%.

3 A spectrum of scalar counts

We are now in a position to evaluate the information content of measurement on an instrument that consists of a series of scalar counters. From the additive rule for independent measurements (2) the information contained in a spectrum of n_c independent scalar counters will be :

$$I = \frac{K}{2} \ln \prod_{i=1,n_c} \frac{c_i M_i}{2\pi} \tag{11}$$

where c_i and M_i are the background correction and maximum count for the i^{th} scalar. If we can make the simplifying assumption that these are the same for all scalars then equation (11) reduces to:

$$I_s = K n_c \ln \sqrt{\frac{cM}{2\pi}} \tag{12}$$

where n_c is the number of channels in the spectrum of scalar counters.

Care must be taken in calculating n_c, since it is the number of *independent* channels in a spectrum. Thus, in a time-of-flight spectrum with n_t time channels n_c is generally less than n_t since the data recorded in adjacent time channels is not independent. To calculate the effective number of

independent time channels we may use the equation (B4) to determine the effective width, Δ, of a peak in a spectrum.

It is interesting to note that the effective width (Δ_e) of an exponential peak with a shape $y = \exp\{-t/\tau\}$ is $\Delta_e = e\tau$ which, when expressed in terms of the standard deviation σ_e or full-width at half height (w_e) is $\Delta_e = e\sigma_e = ew_e / \ln 2 = 3.9w$. For a Gaussian $\Delta_g = \sigma\sqrt{2\pi e}$, and hence $\Delta_g = 4.13\sigma_g = 1.76w_g$. Thus it will be seen that a Gaussian has an effective width that is greater than an exponential peak of similar standard deviation. In fact it has been shown [4] that, for a given standard deviation, the Gaussian is the widest (least informative) peak shape of all.

Knowing the effective peak width in a time spectrum (Δ_t) we may calculate the number of independent time channels by dividing the time axis into channels with these widths. For example a time-of-flight pattern in which the exponential peak shape varies such that $w = rt$ (where r = 5.10^{-4}) the number of independent time channels is given by

$$n_t = \int_{t_1}^{t_2} \frac{dt}{\Delta_t} = \int_{t_1}^{t_2} \frac{dt}{3.9rt} = \frac{1}{3.9r}\ln(t_2/t_1) \qquad (13)$$

which for the HRPD instrument at ISIS operating between 1 and 5Å gives a value for n_t of 822. It is also straightforward to show that, if instead of choosing to describe the powder diffraction pattern as a time spectrum, we had worked in units of neutron momentum ($Q \propto 1/t$), the number of momentum channels n_Q is the same. We may therefore rewrite equation (13) in terms of the momentum channels n_q , or , for an inelastic spectrometer in terms of the energy channels n_e , so long as each is calculated using the effective width parameter in the appropriate units, and is calculated from the resolution function using equation (14).

$$\Delta = \exp\left\{-\int dx\ p(x)\ln p(x)\right\} \qquad (14)$$

For instruments which measure both momentum and energy changes, for which the resolution in energy and momentum are independent, and in which all channels have equal c and M :

$$I = Kn_Q n_E \ln\sqrt{\frac{cM}{2\pi}} \qquad (15)$$

In situation where Δ_q and Δ_w are not independent, the product $n_q n_w$ must be replaced by n_C channels, representing the number of independent areas into which the q-w plane may be divided, using a 2-d version of equation (14).

4 Different sample states

By altering the conditions of the sample, changing its temperature for example, we are given new information about a, potentially, different sample. An instrument that is capable of changing

sample temperature from 200 to 1000 C in steps of 2C can provide 400 independent measurements. Thus we may combine the results outlined above to arrive at the complete equation for the information that may be obtained from a single sample:

$$I = Kn_s n_c \ln\sqrt{\frac{cM}{2\pi}} \tag{16}$$

The above equation combines our knowledge about the count-rate, background, resolution and range of the instrument together with the sample environment ranges of an instrument to produce a figure for the information content of a measurement or series of measurements on a single sample.

5 The bandwidth of an instrument

So far we have left out of this analysis the time taken to do experiments. Clearly an instrument that takes a long time to set up and make a measurement is inferior to one that is quick to operate. For this reason we wish to express the total effectiveness of an instrument as a bandwidth - and calculate the rate at which instruments can acquire information. Introducing the term R for the maximum rate that the i^{th} channel can count, gives for a single sample state:

$$I = Kn_c \ln\sqrt{\frac{cR(t-t_s)}{2\pi}} \tag{17}$$

Where t_s is the set-up time of the experiment.

To understand the variation of this information measure as a function of time it is shown in Figure 1. For a certain length of time the information gained is zero (O to A in Figure 1). This time is comprised two parts: the set-up time and the time taken for the expected maximum effective count (i.e. $cR(t-t_s)$) to exceed 2π (since a scalar that has a maximum count below this value is providing no new information). From point A onwards the information content increases - but only logarithmically.

Fig 1

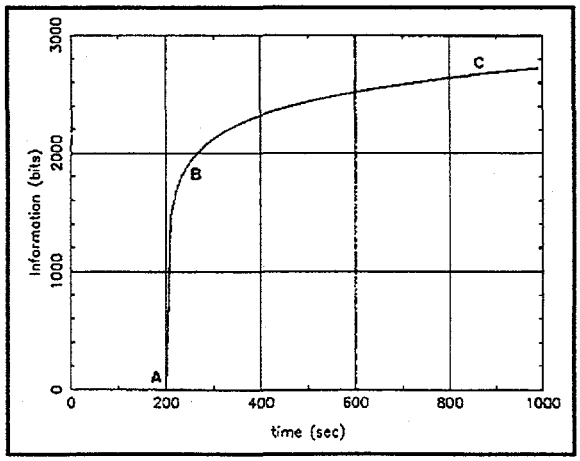

The bandwidth (B) of the instrument may be defined by the rate, in ' bits / sec ', that information is obtained. The expression for this quantity is therefore given by:

$$B = \frac{K n_s n_c}{t} \ln \sqrt{\frac{cR(t - t_s)}{2\pi}} \tag{18}$$

This measure is not constant and varies with the length of the measurement ,t. It reaches a maximum at point B in Figure 1 and then declines. For later times , at C for example, the information gained will be greater , but the rate at which it has been acquired will be slower. It is interesting to note that the time at which the bandwidth is at its highest is when (if $c \approx 1.0$)

$$Rt = 2\pi e \tag{19}$$

which means after there are approximately 17 counts in the highest scalar. This is clearly at a point in the data collection at which there is too little information for the run to be complete but it does provide some explanation for the 'first neutrons are best' phenomenon. They certainly provide the most information *per neutron* of the whole run.

If we now consider a set of runs, each lasting a time t_r the total information gained over a time t will be:

$$I = \frac{K n_c t}{t_r} \ln \sqrt{\frac{cR(t_r - t_s)}{2\pi}} \tag{20}$$

Such an equation is relevant for a series of different sample environment settings on the same sample, or in the case of a 3-AXIS instrument where data is recorded at a series of different orientations of the same sample. The above equation now allows us to compare the rate at which information can be collected, taking into account, intensity, backgrounds, resolution, temperature ranges and set up time.

To compare instruments with one another is known to be difficult, and since their bandwidths vary with time it is not possible to simply place instruments on a single real axis for comparison. It must also be remembered that in setting the values for R and n_c in equation 19 the values may be calculated for an ideal sample, to give the highest bandwidth possible for that instrument; or may be modified to account for the effects of measuring samples which will lower these ideal values. The instrument and sample must often be considered as a system if useful results are to be obtained.

One way to proceed is to list the information that may be gathered, in certain lengths of time from a single, ideal sample. A simple instrument, a low resolution liquids diffractometer for example, will acquire information rapidly, but never achieve a very high value in reasonable length of time

due to the logarithmic nature of the information gain. A very complex instrument, such as a triple-axis spectrometer, may have a lower data collection rate, but a much higher eventual information gain since the information is dominated in this case by the number of crystal settings that may be employed (thus affecting n_c) and not the count rate of the instrument.

Thus a useful way to proceed is to enumerate the information gain, from a single sample, that may be obtained from an instrument over certain lengths of time. This has been done for a range of time periods, and for a set of 'typical' instruments - the results being shown graphically in Fig. 2.

6 Discussion

The information content of a measurement, and the bandwidth of an instrument may provide measures of their usefulness, but how do these measures relate to the quality or quantity of 'science' that might be done using them? At the highest level the purpose of the measurement might be to provide evidence for the mechanism of high temperature superconductivity - but the connection between such high-level goals and the raw data is not straightforward.

Fig.2

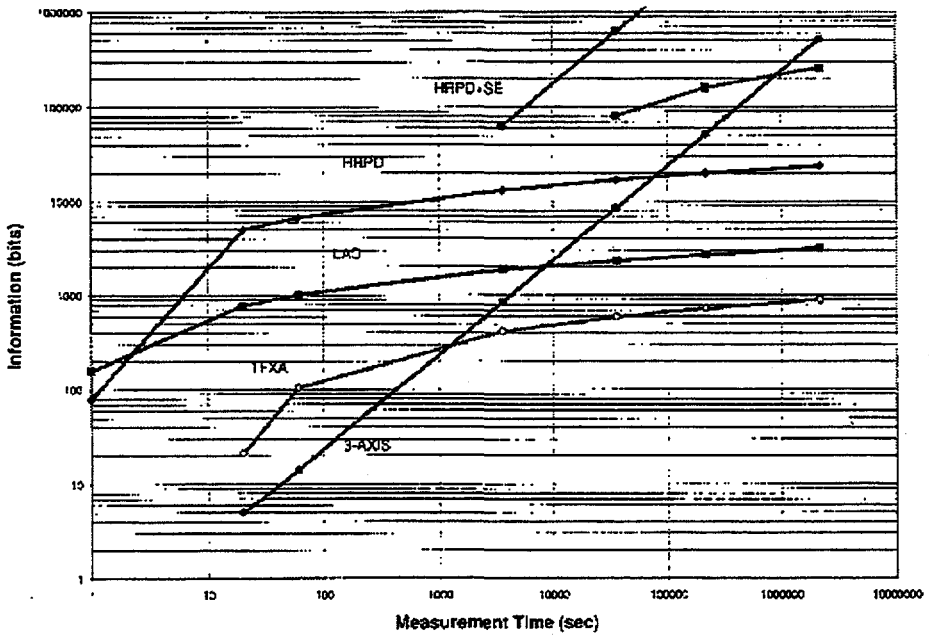

What we have done, in determining the information content of a measurement made using a particular instrument, is to determine the *discriminating* power of the instrument. Thus we have effectively determined the total number of *'distinguishable data states'* that a particular measurement can identify. We can call this the total number of states in d-space. However, raw data is not the object of interest. The end product of all data analysis is a parameterised model of the system under study. We may call this the p-space.
In crystallography, for example, the p-space consists of lists of atom types, positions and thermal amplitudes. In spectroscopic studies the p-space might consists of modes, frequencies and amplitudes. What does our knowledge of the maximum number of distinguishable d-states (n_d) tell us about the number of distinguishable p-states (n_p) ? The answer is that :

$$n_p \leq n_d \qquad (21)$$

since in the mapping from d-space to p-space:

i) one-to-many mappings are not allowed since they imply a single data state could give rise to more than one *distinguishable* p-space state, and ii) many-to-one mappings reduce n_p.

The information content of the p-space data (I_p) is related to that in the d-space (I_d) through a similar relationship

$$I_p \leq I_d \tag{22}$$

This result derives from equation (21) above together with the fact that the probability of each of the d-space states was considered equally probable. Introducing non-equal probabilities into either n_d or n_p reduces the information content. It is interesting to compare the information content of a measurement on the High Resolution Powder Diffractometer (HRPD) at ISIS with one of its results in p-space. The results of a powder diffraction measurement on a sample of benzene produced a crystallographic description of the crystal lattice that involved a total of 27 parameters which were described using approximately 120 decimal digits. The length of this p-space message is therefore around 400 bits , significantly less than the d-space information content of approximately 20 kbits.

7 Acknowledgements

My thanks to Bill David, Devinder Sivia, and Andrew Taylor who commented on the paper, and to Ruth Johnson who has helped to clarify many tortuous sentences.

8 References

1. C E Shannon & W Weaver, *The Mathematical Theory of Communication*, (University of Illinois Press, Urbana & Chicago, 1949) , Illini Books ed. 1963.
2. L Brillouin, *Science and Information Theory*, (Academic Press, New York, 1962)
3. E T Jaynes, *Papers on Probability, Statistics and Statistical Physics*, (D Reidel Publishing Co., Dordrecht , 1983) Ed. R D Rosenkrantz, Synthese Library, vol. 158.
4. A A Sveshnikov, *Problems in Probability Theory, Mathematical Statistics and Theory of Random Functions*, (Dover Publications, New York, 1978)

Elements of Bayesian Experimental Design

D. S. Sivia
Rutherford Appelton Laboratory
Chilton, Oxon, OX11 0QX, United Kingdom

We consider some elements of the Bayesian approach that are important for optimal experimental design. While the underlying principles used are very general, and are explained in detail in a recent tutorial text (Sivia 1996), they are applied here to the specific case of characterising the inferential value of different resolution peakshapes. This particular issue was considered earlier by Silver, Sivia and Pynn (1989, 1990a, 1990b), and the following presentation confirms and extends the conclusions of their analysis.

1. Introduction

Fig. 1. is a schematic representation of the idealised design process for the construction of a new neutron scattering instrument or facility. Long before the hardware is ever built, the proposed spectrometer is simulated in software, perhaps through the use of appropriate ray-tracing Monte Carlo programs. In essence, the instrumental parameters, such as the lengths of the flight-paths, collimation angles, moderator poison-depth, and so on, are varied to obtain the best data from a typical input signal or scattering law. The crux of the problem is, of course, what do we mean by the "best" data?

Well, the easiest response is to simply look at the resulting simulated measurements and decide which appears to be better. Such visual considerations usually lead to:

(i) a preference for symmetric-looking data;

(ii) the use of a figure-of-merit of the type "$\mathit{Total\ number\ of\ neutrons}/(\mathit{FWHM})^2$", where FWHM is the full-width-half-maximum of the resolution, or point-spread, function.

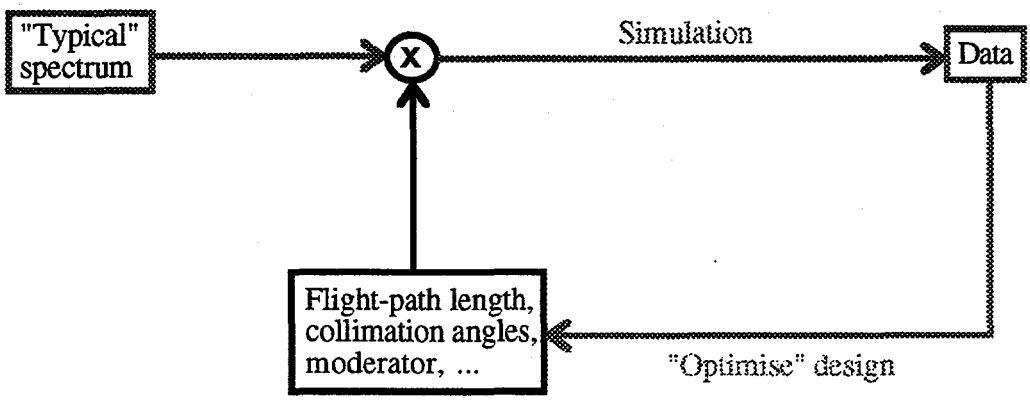

Fig. 1: A schematic illustration of the process of instrument design; the central issue is what we mean by "optimise".

To improve on these naive conclusions, we must take a step back and ask ourselves: why do we do experiments? Clearly, because we want to learn something! Therefore, the more we learn about our object of interest (per unit time, or money, or whatever) the better the experimental design. While this basic criterion is eminently reasonable, its implementation tends to be awkward as it often raises as many questions as it answers. Despite the difficulties, however, it's well worth thinking about optimal experimental design: even if we can only manage a rather crude analysis, the insight it provides can be of enormous benefit in guiding us in the right direction. We illustrate some the issues involved with a few simple examples in Section 2, generalise the analysis is Section 3 and conclude with Section 4.

2. Simple examples

In order to see the sort of difficulties that arise when we consider optimal instrument design, let's begin with some fairly easy problems; although elementary in nature, they are highly instructive because the situations are simple enough to be understood in detail.

Amplitude and position of a peak

Suppose we have a sharp isolated peak (δ-function) which is blurred by a Gaussian resolution function of width w to yield a noisy signal of scattered neutrons. Then, with some suitable approximations, it can be shown (Sivia 1996) that the uncertainty in the inferred amplitude A and position μ of the peak allowed by the data is roughly given by:

$$\langle \delta A^2 \rangle \propto \frac{T + B\sqrt{2}}{T^2 w} \quad , \quad \langle \delta \mu^2 \rangle \propto \frac{w\left(T + B\sqrt{8}\right)}{T^2} \quad \text{and} \quad \langle \delta A \delta \mu \rangle \approx 0 \quad , \qquad (1)$$

where T is the amount of time for which the measurements are made and B is the magnitude of a slowly-varying background (which might also be proportional to T). If the background signal is negligible, then we find that the reciprocal of the location-uncertainty yields the conventional figure-of-merit:

$$\langle \delta \mu^2 \rangle \propto \frac{w^2}{Tw} \propto \frac{(\text{FWHM})^2}{\text{Total number of neutrons}} \quad . \qquad (2)$$

This is not the complete answer, of course, as Eq. (1) also tells us that the uncertainty in A is inversely proportional to w. Thus, we are faced with a typical experimental design dilemma: for a given amount of data collection time, the accuracy in our estimate of the peak position is improved by making the resolution function as narrow as possible while a broader point-spread function is needed to obtain a reliable measure of the amplitude! Such conflicting requirements can only be settled through a deeper soul-searching about exactly what is most important to us, but the analysis has helped to focus our attention on the relevant issues. Two other conclusions that can be drawn from Eq. (1) are that (i) the errors in our estimates of the amplitude and position of an isolated peak are essentially uncorrelated, and (ii) the uncertainty in our inference of both parameters is inversely proportion to $\sqrt{T}$ for Poisson data.

Relative amplitudes of two closely-spaced peaks

Now let's move on to a problem that resembles the analysis of powder diffraction data, albeit in its most embryonic form: the extraction of Bragg peak intensities from two reflections of known, but closely-spaced, locations. We will assume that both peaks are inherently narrow, so that the signal of scattered neutrons is dominated by the resolution function, and consider the effect of the four alternative lineshapes shown in Fig. 2(a): a Gaussian, a triangle, a rectangular box and a sharp-edged exponential. While these idealised point-spread functions may be somewhat removed from reality, they will still help us to gain an appreciation of the main points. They have been scaled to have the same area and FWHM, although our general conclusions would be very similar had we equalised their variance instead.

Fig. 2(b) shows a plot of the relative uncertainty in the ratio of the intensities of the two Bragg peaks, $\sigma(z)/z$ where $z=I_1/I_2$, as a function of the separation ΔX between them. The curves are for the case when the true ratio is unity, and for a certain level of counting statistics; if data were collected for ten times longer, then all the lines would be shifted down by a factor of $\sqrt{10}$. We see that the error-bars converge to the same (small) value in the well-separated limit $\Delta X >>$ FWHM. This is as expected because it is simply the total number of scattered neutrons, or the integrated area under the resolution function, that controls the reliability of the intensity estimates for isolated peaks. The shape of the point-spread function becomes important, however, when the reflections start to overlap significantly. Indeed, Fig. 2(b) shows that, for a given $\Delta X <<$ FWHM, the ratio uncertainty ($\delta z/z$) satisfies the relationship:

$$\text{Total number of neutrons} \times \left\langle \left(\frac{\delta z}{z} \right)^2 \right\rangle \propto \begin{cases} (\text{FWHM})^2 & \text{Gaussian / triangle} \\ \text{FWHM} & \text{top - hat / exponential} \end{cases} . \qquad (3)$$

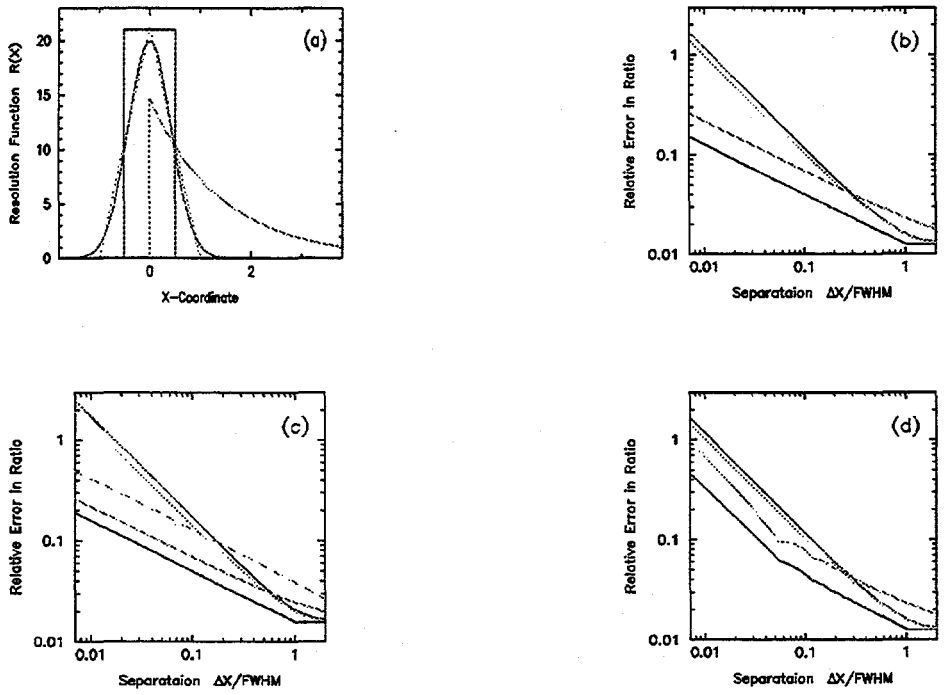

Fig. 2: The relative uncertainties in the inferred ratio of the intensities of two closely-spaced Bragg peaks for the four different resolution functions shown in (a). In (b) and (d) the true ratio is unity, while it is four in (c); (d) is for data that were binned 16 times more coarsely than those for (b) and (c).

Therefore, while a four-fold increase in the experimental time is required to compensate for a doubling in the width of a Gaussian resolution function (or a halving in the separation between the peaks), only a two-fold increase is needed in the case of a sharp-edged exponential point-spread function.

The curves in Fig. 2(c) are for an identical set-up to the one in Fig. 2(b), except that the true ratio of the Bragg intensities is four instead of unity. The main difference that results is that the reliability of the inferred ratio from the asymmetric, decaying, resolution function depends on the order in which the smaller and larger peaks appear. Thus we meet another dilemma that often confronts us in optimal experimental design problems: what's best can depend on the answer! This difficulty can be resolved here by weighing it against the versatility afforded by having a sharp-edged point-spread function: the reliability from even the adverse orientation is better than that for the Gaussian case, for example, when $\Delta X \ll$ FWHM, and also Eq. (3) tells that any misfortune is more easily compensated for by increased counting time in that instance. The only real drawback in having a peak-shape with a sharp edge is that we need to have good resolution in our X measurement space (spatial and/or temporal) in order to make the most of it. This is illustrated in Fig. 2(d), which is for the same set-up as in Fig. 2(b) except that the data where collected in bins that were 16 times more coarse; for very close Bragg peak spacing, the uncertainty behaviour of the ratio from the top-hat and exponential point-spread functions starts to mimic that from the Gaussian and triangle.

3. A more general analysis

Rather than working through more elaborate specific examples, let's extend the analysis by considering a generic data analysis problem. In essence, our central task usually boils down to one of making inferences about an object of interest, defined by a set of parameters $\{a_j\}=\mathbf{a}$, given a set of data **D**, from experimental set-up E, and the relevant background information I. As such, our state of knowledge (or ignorance) is encapsulated in the conditional probability distribution function (pdf) $\text{prob}(\mathbf{a}|\mathbf{D},\text{E},\text{I})$. The position of the maximum can be regarded as our best estimate of **a**, while the spread of the posterior pdf about this point indicates our degree of uncertainty; the sharper the posterior pdf, the more reliable the inference.

The criterion for optimal experimental design is then simply one of trying to make the posterior pdf for **a** as narrow as possible. To see how the data enter into this equation, we need to use Bayes' theorem:

$$\text{prob}(\mathbf{a}|\mathbf{D},\text{E},I) \propto \text{prob}(\mathbf{D}|\mathbf{a},\text{E},I) \times \text{prob}(\mathbf{a}|I) \quad , \tag{4}$$

where we have dropped an unnecessary conditioning on E in the term on the far right-hand-side. Thus, the measurements influence our inference of **a** through the likelihood function and so we must look at the way in which the set-up E affects the spread of $\text{prob}(\mathbf{D}|\mathbf{a},\text{E},\text{I})$: the sharper this pdf, the greater the constraints imposed by the data and the more we learn from the experiment.

Singular Value Decomposition

In order to summarise the essential breadth-characteristics of the likelihood function, it is convenient to make a multivariate Gaussian approximation to it. This is most easily done by expanding its logarithm as a quadratic Taylor series about the maximum at $\mathbf{a}_0$:

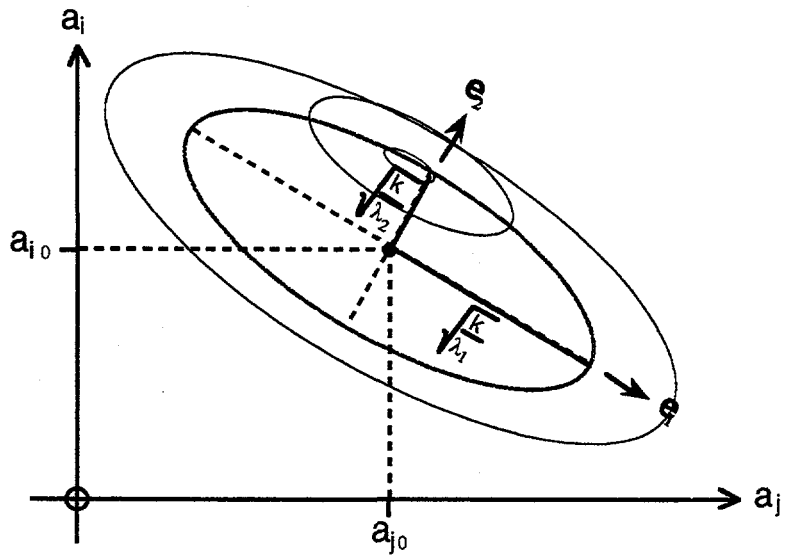

Fig. 3: The Gaussian, or quadratic, approximation to the likelihood function, where its width and orientation is given by the eigen-properties of the second-derivative **H** matrix.

$$\text{prob}(\mathbf{D}|\mathbf{a},\mathrm{E},I) \propto exp\left[-\frac{1}{2}(\mathbf{a}-\mathbf{a}_0)^T\mathbf{H}(\mathbf{a}-\mathbf{a}_0)\right] , \tag{5}$$

where the elements of the (real) symmetric matrix **H** are given by minus the second-derivatives $\partial^2 L/\partial a_i \partial a_j$, evaluated at $\mathbf{a}_0$, and $L = \log_e[\text{prob}(\mathbf{D}|\mathbf{a},E,I)]$. The situation is illustrated in Fig. 3, which represents a 2-dimensional slice through the pdf of Eq. (5). Within this approximation, the width and orientation of the likelihood function is determined by the eigen-properties of **H**:

$$\mathbf{H}\boldsymbol{e}_i = \lambda_i \boldsymbol{e}_i \ . \tag{6}$$

The eigenvectors $\{\mathbf{e}_i\}$, which are the principle directions of the ellipsoid in Fig. 3, yield the linear combinations of the parameters $\{a_j\}$ that can be estimated independently of each other; the square-roots of the reciprocal of the eigenvalues $\{\lambda_i\}$ give the corresponding reliabilities.

Large eigenvalues ($\lambda \to \infty$), therefore, indicate the features of the object of interest that are determined well by the data, where as small ones ($\lambda \to 0$) warn of great uncertainty. As such, the effective "number of good measurements" N_{good} is equivalent to the number of directions in which the likelihood function is narrower than some desired value. One suitable measure of this quantity is:

$$N_{good} = \sum_{i=1}^{M} \frac{\lambda_i}{\lambda_0 + \lambda_i} , \tag{7}$$

where unity is contributed to the sum when $\lambda_i >> \lambda_0$, and nothing is added when $\lambda_i << \lambda_0$. We cannot claim anything particularly fundamental about the choice of the formula in Eq. (7), other than it being analogous to a statistic that appears in classic MaxEnt data analysis (Gull 1989) which has a similar interpretation. The important point is that the information content of a set of data, with regard to the M parameters $\{a_j\}$ defining the object in which we are interested, is contained in the eigenvalue spectrum of the log-likelihood function; Eq. (7) simply represents a single-value

measure which captures an essential characteristic of it, and lies in a continuum between zero and M.

Resolution functions

Since experimental measurements are usually regarded as being subject to independent, additive, Gaussian noise, the likelihood function is given by the exponential of the χ^2 misfit statistic (the sum of the squares of the "data minus fit over the error-bar" residuals):

$$L = log_e\left[\text{prob}(\mathbf{D}|\mathbf{a},E,I)\right] = \text{Constant} - \frac{\chi^2}{2} \quad . \tag{8}$$

While Eq. (8) may be highly idealised, it's a good approximation to the Poisson model when there are more than a few counts per channel. The components of the important **H** matrix are then related to the second (partial) derivatives of χ^2:

$$H_{ij} = \frac{1}{2}\frac{\partial^2\chi^2}{\partial a_i \partial a_j} \quad . \tag{9}$$

If the problem is linear, so that the object-to-data transform can be written as:

$$D_k = \sum_{j=1}^{M} O_{kj}\, a_j + C_k \pm \sigma_k \ , \tag{10}$$

where k = 1,2, 3, ..., N, and the elements of the matrix **O** (whose ijth element would be like $\exp[-(x_k-x_j)^2/2w^2]$ for a Gaussian blur) and vector **C** (which might equal to a constant for a slowly-varying background) are independent of **a**, then Eq. (9) becomes:

$$H_{ij} = \sum_{k=1}^{N} \frac{O_{ki}\, O_{kj}}{\sigma_k^2} \quad . \tag{11}$$

For the specific case of a convolution with a invariant resolution function r(x), it can be shown (Sivia 1996) that the eigenvalue spectrum of **H** is roughly given by its Fourier transform R(ω). That is to say, the eigen-functions are:

$$e_i(x) \propto \sin(\omega_i x) \quad \text{and} \quad \cos(\omega_i x) \ , \tag{12}$$

and the corresponding eigenvalues are:

$$\lambda_i \propto \frac{T\left|R(\omega_i)\right|^2}{(1+B_f)R(0)} \ , \tag{13}$$

where T is the amount of time for which the data are collected, B_f is the fraction of the neutron counts emanating from the background signal, as compared to those from the spectrum of interest, and R(0) is the integral of r(x). While the sines and cosines of Eq. (12) only hold exactly under simple ideal conditions, being replaced by wavelet-like functions in practice, a Rayleigh-Ritz type argument (e.g. Arfken 1970) suggests that Eq. (13) should provide a good approximation to the eigenvalue spectrum more generally.

The eigenfunctions of Eq. (12) tell us that, for a convolution problem, it is natural to think about the object of interest, a spectrum f(x) say, as being constructed from the sum of sines and cosines; the eigenvalues of Eq. (13) indicate how well the related coefficients in the series

expansion can be estimated from the data. In particular, the uncertainty in the structure on length-scales of $1/\omega$ is given by the reciprocal of $|R(\omega)|$. Since the magnitude of the Fourier transform of r(x) systematically becomes smaller for large ω's, as illustrated in Fig. 4, higher frequency features become increasingly unreliable. This confirms our intuition that information about fine detail is lost in a blurring process. The degree of the loss is not uniform, of course, and depends strongly on the shape of the point-spread function. This is readily seen from Fig. 4, which shows the Fourier transforms of a Gaussian and a sharp-edged exponential resolution function (both having the same FWHM and area); the eigenvalue spectrum from the former nose-dives rapidly towards zero, where as it decays away only slowly for the latter. One consequence of this behaviour is that we cannot differentiate between two closely-spaced narrow peaks and one of a moderate width when the data are subject to a broad Gaussian blur, but we can do so when the resolution function has a sharp edge. Figure 4 also indicates that to compensate for a doubling in the FWHM of a Gaussian r(x), at the finest level of detail, would

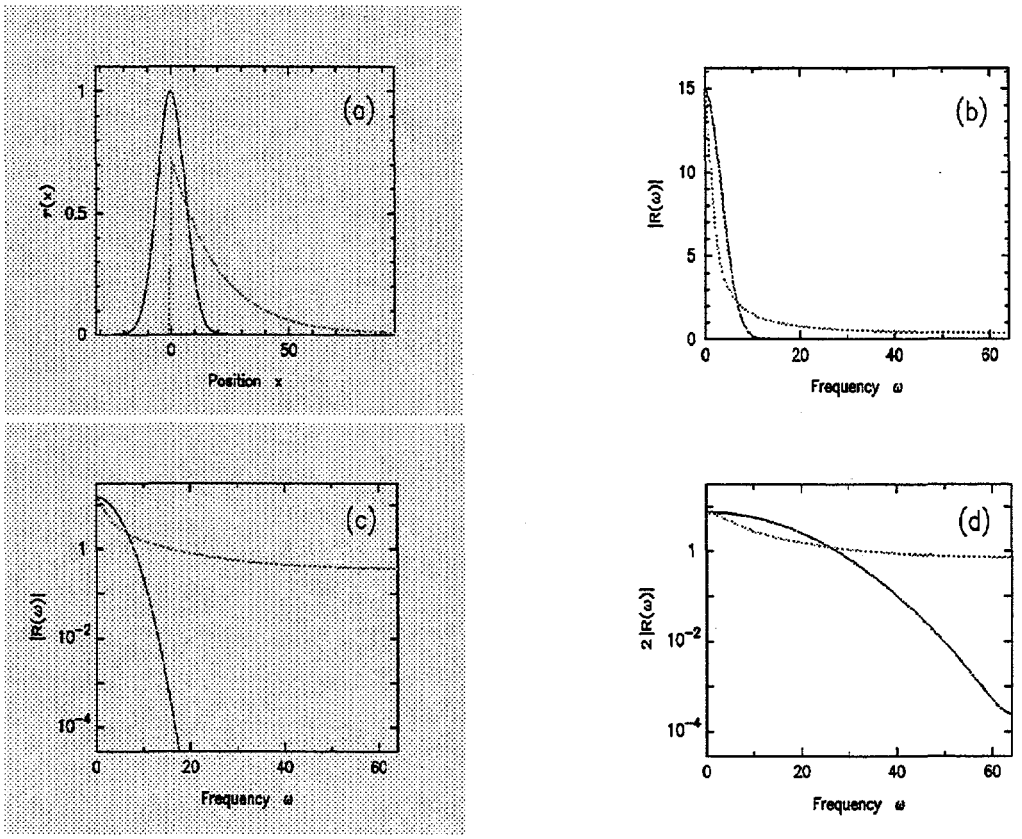

Fig. 4: **(a)** A Gaussian and exponential resolution function having the same FWHM and integrated area. **(b)** The modulus of their Fourier transforms. **(c)** The same as (b), but plotted on a logarithmic scale. **(d)** The equivalent of (c), but for a Gaussian and exponential having only a quarter of the width in (a).

entail an increase in the count time by many orders of magnitude! As mentioned earlier, the only proviso to the numerous advantages of having a sharp edge in our response function is that the data must be collected in bins of sufficiently high resolution.

4. Conclusions

The topic of optimal experimental, or instrument, design is both important and messy. The essence, of course, is very easy: we need to make the data as sensitive as possible to the object of interest. Its implementation, however, is usually not so straightforward! There are two main reasons for this: (i) what's best depends on the precise question being asked; and even worse, (ii) what's best can depend on the answer we're seeking. Despite these, and many other, difficulties, it's always well worth thinking about the question of optimal experimental design in a Bayesian manner; at the very least, it might stop us from doing anything too silly. For example, we quickly start to appreciate that the shape of a resolution function is often more important than its raw width. In particular, we learn that it is extremely useful to preserve and, if possible, enhance sharp features in a point-spread function if detailed information is required.

References

Arfken, G. (1970), Mathematical Methods for Physicists, Academic Press, New York.

Gull, S.F. (1989), "Developments in maximum entropy data analysis", in Maximum Entropy and Bayesian Methods, Cambridge 1988, ed. J. Skilling, Kluwer, Dordrecht.

Silver, R.N., Sivia, D.S. and Pynn, R. (1989), "Information Content of Lineshapes", in Advanced Neutron Sources 1988, ed. D. K. Hyer, Institute of Physics Conference Series 97, 673-683.

Silver, R.N., Sivia, D.S. and Pynn, R. (1990), "Optimization of Resolution Functions for Neutron Scattering", Nucl. Instr. Meth. A287, 538-550.

Sivia, D.S., Silver, R.N. and Pynn, R. (1990), "The Bayesian approach to optimal instrument design", in Neutron Scattering Data Analysis 1990, ed. M. W. Johnson, Institute of Physics Conference Series 107, 45-55.

Sivia, D.S. (1996), Data Analysis: a Bayesian tutorial, Clarendon Press, Oxford.

THE CONCEPTUAL DESIGN OF A DISK CHOPPER SPECTROMETER

J.R.D. Copley
NIST Center for Neutron Research,
Materials Science and Engineering Laboratory,
National Institute of Standards and Technology,
Gaithersburg, MD 20899, USA

Abstract

We describe methods that we have used for the conceptual design of the Disk Chopper Spectrometer at the Cold Neutron Research Facility, National Institute of Standards and Technology. Most of the discussion concerns the multiple chopper system. No single design method is best in every situation. We believe that an analytical approach is preferable, whenever possible. Graphical methods of expressing problems have been very instructive. We have also found it useful, and occasionally invaluable, to cross-check results obtained using different methods, such as analytical integration and ray-tracing.

INTRODUCTION

One of the new neutron inelastic scattering instruments at the Cold Neutron Research Facility (CNRF), National Institute of Standards and Technology (NIST), is a direct geometry time-of-flight spectrometer known as DCS (Disk Chopper Spectrometer) [1]. The DCS promises to be an exciting addition to the portfolio of instruments at the CNRF. We anticipate that it will be usable over a wide range of incident wavelengths λ_o, from <3 Å [1Å = 0.1 nm] to 10 Å or more, thanks in part to a so-called ``optical filter" [2] and in large measure to the excellent performance of the liquid hydrogen cold source [3]. We also expect that the possibility of operating the instrument in three distinct "resolution modes," to be discussed below, will significantly enhance its range of applications.

The DCS is a direct descendant of the first disk chopper instrument, the IN5 spectrometer at the Institut Laue Langevin (Grenoble, France). Other instruments of this type are MIBEMOL at the Laboratoire Léon Brillouin (Saclay, France), and NEAT at the Hahn-Meitner-Institut (Berlin, Germany) (HMI). Each of these instruments, along with the DCS, uses a number of rotating disk choppers to produce a pulsed monochromatic neutron beam at the sample position. A large array of detectors is placed at a common distance from the sample position, and the energies of the detected neutrons are deduced from their times of arrival [4]. The secondary spectrometer (after the sample) is *conceptually* straightforward to design. In contrast, the conceptual design of the primary spectrometer, especially the multiple chopper system, is far from trivial. Though the designs of the chopper systems of IN5, MIBEMOL and NEAT have been documented [5], relatively little has been written about design *methods*. In the present article we partially redress the situation, describing some of the more important aspects of the approach that was used for the conceptual design of the DCS choppers. We also discuss, albeit briefly, methods that were used to design other components of the DCS.

Since the early stages of planning the CNRF, two time-of-flight (TOF) instruments were envisaged. One was the double monochromator Fermi chopper spectrometer that was already operating in the reactor confinement building. The front end of this instrument was redesigned and the spectrometer was relocated in the neutron guide hall [4]. The second TOF instrument was intended to complement the Fermi chopper spectrometer, with improved energy resolution and a clean elastic line shape. These considerations, with the additional requirement that the instrument

be operable over a broad range of incident wavelengths, led us to conclude that the pulsed monochromatic beam at the sample should be produced using a set of phased disk choppers.

The decision to use phased disks implied that the DCS, in common with IN5, MIBEMOL and NEAT, would have one or more pulsing choppers, monochromating choppers and order removal choppers, plus a frame removal chopper (for a discussion of the functions of these different types of choppers, see Ref. 4). The decision also provoked a number of important questions that were to some extent interdependent. Thus, the process of designing and optimizing the instrument at a conceptual level was iterative. The more basic questions were considered first, and answers were obtained using simplified assumptions about the less important parameters of the instrument. Additional questions were then addressed, and in so doing earlier conclusions were sometimes modified. The process continued over many months, in the course of which several papers were written, describing specific aspects of the overall design [6,7,8]. This exercise was useful in that it helped us to clarify our thoughts during the critical design process.

In the following paragraphs we provide a ``broad brush" description of the approach that was used for the conceptual design of the DCS. The discussion is necessarily brief, and somewhat simplified. What really happened was more complicated and considerably less logical than what is described.

OVERALL PERFORMANCE

As a first step in thinking about the conceptual design of the choppers, we made simple estimates of count rates and resolution widths *for the complete instrument.* We did this in order to develop a quantitative understanding of chopper design constraints imposed by performance requirements for the instrument as a whole. Because of their known advantages (see e.g., Ref. 7) and in common with MIBEMOL and NEAT, we assumed that the DCS would use pairs of counter-rotating choppers to pulse and monochromate the neutrons. To understand the overall performance of the instrument, we assumed that the counter rotating choppers had single slots. We also ignored intermediate order and frame removal choppers and we assumed that the speeds and dimensions of the choppers would be comparable with those of the choppers planned for the NEAT spectrometer, since significantly higher values could not be contemplated due to engineering (*i.e.* safety and material property) considerations. Important quantities that were varied were the chopper slot widths and the distances D_{14} and D_{4S} between the choppers and the sample position (Fig. 1). Reasonable assumptions were made with regard to the wavelength dependence of the cold source intensity, guide dimensions, and the critical angles per unit wavelength of the guide surfaces; some of these parameters were dictated by the design of the cold source itself. We calculated the intensity per pulse at the sample position, and chopper contributions to the elastic energy resolution[9]. Contributions from the sample and detectors were handled using expressions discussed by Windsor [10], treating the size of the sample, along with the dimensions and fill pressure of the assumed gas detectors, as variable quantities. Putting in a value for the sample-detector distance, D_{SD}, we could then compute the overall elastic energy resolution of the instrument. Given a reasonable criterion for the speed of the frame overlap removal chopper, we could also calculate the neutron intensity at the sample position and we could estimate the count rate per detector, assuming that the sample was an isotropic elastic scatterer which scattered, say, 10%

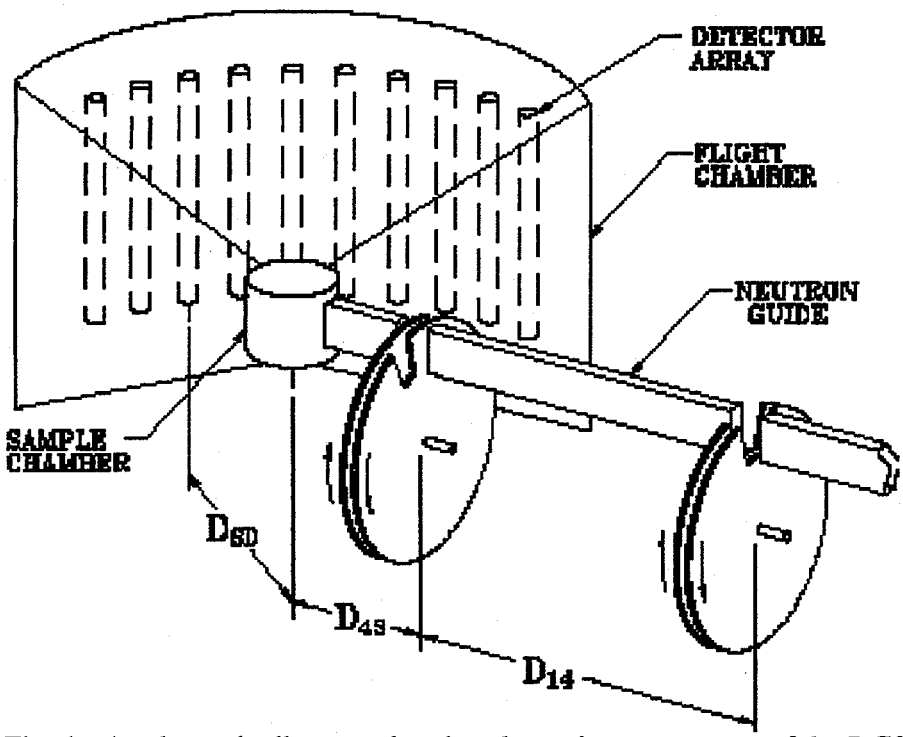

Fig. 1: A schematic diagram showing the main components of the DCS. Two pairs of counter-rotating choppers are shown. Intermediate choppers are omitted. Each chopper is shown with a single slot. Slot widths are $2W_1$ and $2W_4$ for the pulsing and monochromating choppers respectively, and the width of the guide is $2W_G$. of the incident neutrons. It was important to calculate the count rate since the number of detectors required to fill a given solid angle, which strongly influences the total cost of an instrument, depends quadratically on D_{SD}!

These calculations could have been performed using Fortran (or some other programming language), and indeed a few calculations were made in this way, but we found that using a simple spreadsheet program was a more rewarding approach, in the present context and indeed for a number of calculations that the author has performed in the past few years. Such calculations typically require several input parameters which are related by rather simple equations to the output quantities of interest. The input is readily modified, and a number of intermediate quantities can be displayed. The spreadsheet method is good at answering, ``What if?" questions, such as, ``What if I change the incident wavelength from 6 Å to 6.5 Å?," and it is particularly useful when some or all of the implications of a change in an input parameter turn out to be less than obvious. In such situations one can readily work one's way through the spreadsheet in order to understand what is going on. (It is good practice to do cross-check calculations using a conventional programming language, since a disadvantage of the spreadsheet approach is that error discovery is not always straightforward.)

OPTIMIZING THE CHOPPERS AND THE GUIDE

One of the initial design goals for the DCS was to achieve a full width at half maximum (FWHM) energy resolution of ≈10 μeV, with instrument parameters optimized to maximize the intensity in the detectors, using a relatively short wavelength of about 6 Å in order to be able to access a broad range of wave vector transfers. Our spreadsheet calculations told us that this imposed significant constraints on several key parameters, including the distance D_{14}between the chopper pairs, the chopper burst times, the size of the sample, the distance D_{SD}, and the thickness of the detectors. We established that D_{14} and D_{SD} should be roughly 8 m and 4 m respectively, and that the detectors

should be no more than about 12 mm thick. (The actual values of D_{14} and D_{SD} for the DCS are 9 m and 4 m respectively, and the nominal inside thickness of the detectors is 11.5 mm.)

Our treatment of the choppers [9] was still relatively crude, so the next step was to improve our understanding of the transmission properties of two counter-rotating chopper pairs with a guide placed in between. For this purpose, we ignored the small distance between members of a chopper pair, and we ignored the chopper/guide mismatch, *i.e.*, the mismatch between the wedge shape of the chopper slots and the rectangular shape of the guide. With these approximations, we developed [6] analytical expressions for the energy resolution at the detector (elastic and inelastic) and for the intensity at the sample. (The treatment also yielded results for *single* choppers separated by a length of guide [6].) Independent programs were written to confirm the analytical results and to investigate effects due to chopper/guide mismatch.

A key conclusion from these calculations was that optimization imposes conditions on the ratios $2W_1/2W_G$ and $2W_4/2W_G$, where $2W_1$ and $2W_4$ are the widths of the slots in the pulsing and monochromating choppers respectively, and $2W_G$ is the width of the guide. To take a simple example, doubling $2W_1$ and $2W_4$ (in order to improve the count rate at the expense of resolution) implies $2W_G$ should also be doubled. The assumption, and the hope, was that we would be able to design the counter-rotating chopper disks with at least three slots of different widths on each disk, so that we could select from among the same number of resolution/intensity combinations, or ``resolution modes" by changing the relative phases of the disks in each pair. We were therefore faced with the challenge of devising a method to change the width of the guide, since failure to do so would result in considerable intensity loss. The only practical way that we could achieve the effect of changing the guide width, was to design a channeled guide [6, 4], better regarded as a set of nested guides. The analytical treatment was extended to handle such a device and the numerical calculations were similarly modified.

THE TRANSMISSION OF A COUNTER-ROTATING PAIR OF CHOPPERS

In parallel with these developments, we had to determine how many slots we could actually place on a pair of counter-rotating choppers, and where they should be placed, assuming certain slot widths (dictated by the desired burst times of the choppers) and requiring that the chopper pair produce one pulse (and only one pulse) per chopper revolution, in each of its phasing configurations, *i.e.* each of the resolution modes. We initially (and quite unconsciously) assumed that we could neglect the separation between the choppers, which is about 55 mm. The problem could then be succinctly formulated as a (Θ, t) diagram, where t is time and Θ is angular displacement (see Ref. 7, Fig. 2), but a general method of finding acceptable slot locations was not obvious. We concluded that a ``brute force" approach was the most practical way to try to solve a given problem. Using this approach, in combination with the analytical work described in the previous section, we designed slot patterns for the pulsing and monochromating choppers. We also constructed paper models of the disks in order to convince ourselves that our choice of slot locations would work. Our design called for four pairs of diametrically opposed slots on the pulsing chopper disks, and six such pairs on the monochromating chopper disks.

Some weeks after the design had been communicated to the manufacturer, we realized that *the design would not work after all.* We were fortunate that the manufacturer had not started to machine the slots! The problem was that we had failed to appreciate the implications of neglecting the separation between members of a chopper pair. Taking this into account literally added an extra dimension to the problem, since the requirement of only one pulse per revolution had to apply for all conceivable wavelengths in the guide. In the time that a 20 Å neutron takes to travel 55 mm (the approximate distance between two disks of a pair) each disk, turning at 20,000 rpm, rotates more than 33°! Thus, it should not be hard to appreciate that our design for the slots would have been a miserable failure.

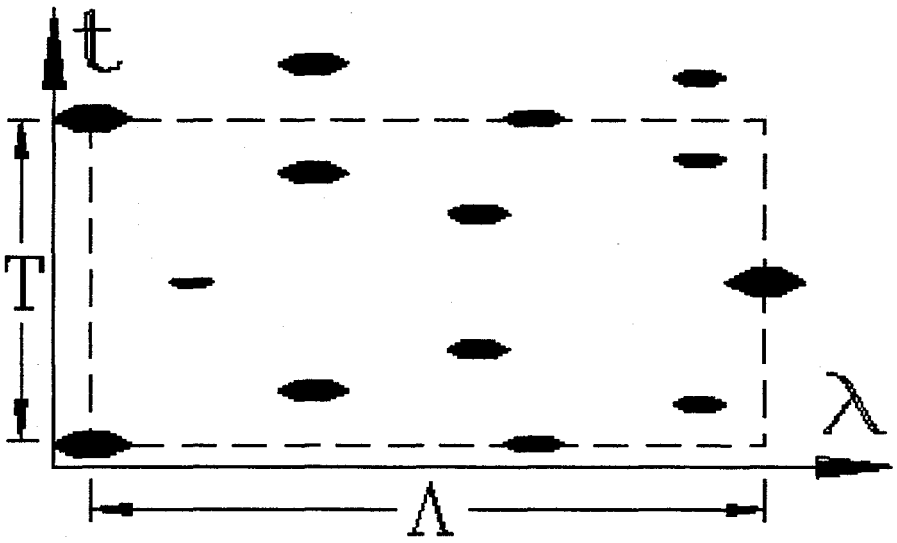

Fig. 2: A typical transmission function $P(\lambda, t)$ for a separated pair of counter-rotating choppers. It is only nonzero within the solid areas. The symmetry of the diagram is centered rectangularly; vectors of the primitive lattice are (0,T) and (Λ, T/2). This particular diagram describes the transmission function for the pulsing choppers of the DCS. For choppers turning at 20,000 rpm with 55 mm separation, T = 3000 μs and $\Lambda \approx 216$ Å..

We accordingly had to develop a method of analyzing the behavior of a *separated* pair of counter-rotating choppers with more than one slot on each disk [7]. The transmission P for such a device is periodic, not only in time with period $T = 2\pi/\omega$, where ω is the rotational speed of the disks, *but also in wavelength* $\lambda$with repeat wavelength $\Lambda = (h/m)(T/2s)$, where h is Planck's constant, m is the neutron mass, and 2s is the chopper separation; $\Lambda$is the wavelength of neutrons that take one complete chopper period to travel the distance between the two disks. For a typical pair of choppers with several slots apiece, $P(\lambda, t)$ is only nonzero within small areas in (λ, t) space (Fig. 2). Neglecting the time dependence of P, the chopper pair is a crude velocity selector which only transmits neutrons whose wavelengths lie within certain bands. The locations of these bands are linearly related to the relative phase of the disks [8].

Combining our previous analytical studies [6]and our desire to have at least three slots of different widths on each disk (and an appropriate channeled guide) corresponding to at least three significantly different resolution modes, we determined the widths of the slots on the disks. For given slot locations it was a simple matter to determine which wavelengths, relative to the desired wavelength λ_o, would be transmitted by a counter-rotating chopper pair, but the challenge was to find acceptable slot locations, *i.e.* slot locations such that the chopper pair produces only one pulse per revolution in each of the resolution modes. Though the task could probably have been automated, we adopted an interactive approach, "manually" adjusting slot locations in order to maximize the smallest of the separations between the lowest unwanted wavelength and the desired wavelength, there being one such quantity for each resolution mode. We also had to take into account the periodicity of the transmission diagram as a function of wavelength, since short wavelength ($\lambda < \lambda_o$)contaminant neutrons will be transmitted if λ_o exceeds a threshold value (which itself is a function of the slot widths and locations and of the resolution mode).

Using this approach, the best slot configurations that we obtained were still not completely satisfactory, because the shortest contaminant wavelength, considering all conceivable operating conditions, was not long enough that we could be entirely sure that it would not cause us problems. On reflection, we realized that we could improve the situation by finding slot configurations that produced different contaminant wavelength spectra for the pulsing choppers and the monochromating choppers. The differences between the spectra were such that the shortest contaminant wavelength *jointly transmitted* by the pulsing and monochromating chopper pairs was considerably longer than the shortest contaminant wavelength transmitted by the chopper pairs considered one at a time [8]. This is how we decided the final slot locations. We also concluded that no more than three slots could be located on each disk (whereas we had previously thought that we could have at least four *pairs of* slots per disk).

ORDER AND FRAME REMOVAL CHOPPERS

At this stage, the conceptual design called for two pairs of counter-rotating choppers, each of which had three slots of different widths, optimized for three distinct resolution modes, such that each pair would transmit one and only one neutron pulse per revolution as long as the desired wavelength λ_O (with the choppers spinning at their maximum speed of 20,000 rpm) was no greater than $\lambda_{max} \approx 15$ Å =, and as long as we could assume that neutrons with wavelengths greater than $\lambda_O + \lambda_C$ = were sufficiently scarce that their presence in the guide could be totally ignored [8]=; the calculated value of the fixed offset λ_C was originally ≈64 Å [8], but a very recent analysis, prompted by the task of writing this paper (!), uncovered an oversight in the earlier calculation; λ_C is in fact ≈ 42 Å. (The values of λ_{max} and λ_C are proportional to the chopper period.)

A single pulsing chopper and a single monochromating chopper, each with single narrow slots, turning with period T, separated by a distance D_{14} , and phased to transmit neutrons of wavelength λ_O , will also transmit neutrons of order k, *i.e.,* neutrons with wavelengths $\lambda_k = \lambda_O + k\Delta\lambda$, where k is a positive or negative integer and $\Delta\lambda = (h/m)(T/D_{14})$ Typically $\Delta\lambda$ is of order 1 Å. For example, $\Delta\lambda \approx 1.32$ Å if T = 3000 μs and $D_{14} = 9$ m. A comparable situation obtains if the single choppers are replaced with counter-rotating chopper pairs, but the range of k is generally more restricted because the chopper pairs act as crude velocity selectors as discussed earlier. To suppress the unwanted orders in a multiple chopper instrument, one (IN5, MIBEMOL) or two (NEAT) intermediate choppers are generally installed. For the DCS we decided to use two order removal choppers. The widths of the single slots in these choppers were chosen to be as small as possible, such that the choppers would not remove neutrons with wavelengths corresponding to k = 0. The positions of the choppers were determined by trial and error, and the final choice of chopper positions was carefully checked using an acceptance diagram procedure [11].

The location of the frame removal chopper is relatively unimportant (though there can be situations where this chopper assists in the task of order removal). For convenience the frame removal chopper is located in the same housing as one of the order removal choppers.

THE REST OF THE INSTRUMENT

A neutron optical filter is installed between the source and the choppers [2]. The device consists of two parallel sections of guide, with a tapered section in between. Angular offsets between the sections are such that there is no line of sight from the source to the choppers. Hence high energy neutrons and γ-rays are strongly attenuated, but long wavelength neutrons are transmitted with high efficiency. The acceptance diagram approach was used for the design of the optical filter, and

ray-tracing calculations were performed to confirm the analytical results and to investigate losses associated with imperfect surface reflectivities. Acceptance diagrams have also been used to estimate the effects of guide cuts at the beam shutter and at the chopper disks, and the intensity loss associated with the inevitable gap between the end of the guide and the sample.

An important component of the DCS is the oscillating radial collimator located within the sample chamber. It is designed to remove much of the scattering from materials surrounding the sample, such as heat shields and vacuum jackets, without significantly reducing the scattering from the sample itself. To quantify our understanding of this type of device, we used analytical and Monte Carlo ray-tracing techniques [12].

FINAL REMARKS

Our experience with the conceptual design of the DCS has taught us several important lessons. We have found that many problems with guide systems and choppers can be usefully formulated, pondered, and sometimes solved, by drawing rather simple two-dimensional straight line diagrams. A good example for guide systems is the (y, β) acceptance diagram, where y and β represent a neutron's transverse spatial and angular coordinates in the horizontal plane [11]. Examples in the context of chopper systems include (y, t) and (Θ, t) plots such as Figs. 1-4 in Ref 13}) and Fig. 2 in Ref.7, (t, x) plots where x represents distance along the direction of travel (e.g., Fig. 19 in Ref.4, Figs. 5 and 7 in Ref. 7), and (λ, t) plots such as those in Ref. 7). A particularly fortunate circumstance is that a single diagram sometimes represents many situations. For example, the (λ, t) diagram shown in Fig. 2 applies for all choices of chopper speed, all choices of incident wavelength, and all three choices of resolution mode, as long as the diagram is correctly located with respect to the t axis and its periodicity in $\lambda$and t is borne in mind.

Certain problems can be formulated by drawing diagrams, analogous to those just discussed, but in three or more dimensions. An example is the (y, β, z,γ)) acceptance diagram, where z and γ represent a neutron's transverse spatial and angular coordinates in the *vertical* plane. Such a diagram is almost impossible to visualize. On the other hand, algorithms almost certainly exist to handle the four-dimensional operations that are required to make manipulations analogous to those used with two-dimensional acceptance diagrams [11], to project the results into a reduced dimensional space so that they can be visualized, and to compute integral properties such as volumes, centroids and widths.

To handle more complicated problems, the author's preference is to see how much progress can be made using analytical techniques, and to use ray-tracing if and when analytical methods are inadequate or cumbersome. Some people prefer to use ray-tracing in all but the simplest situations. This approach has considerable merit but it must be used with care, whenever possible implementing well-known techniques such as importance sampling in order to make the calculation reasonably efficient. Simulations can be very valuable for calculations of intensity and resolution, especially when one wants to incorporate complications such as imperfect guide reflectivities, misalignments, difficult geometries and so on. On the other hand, great caution is required if the object of the exercise is to determine whether the probability of an unlikely event is simply very small or identically zero; a good example is a calculation which seeks to confirm that order removal choppers have been correctly placed. Analytical approaches are not without their own limitations and disadvantages, and mistakes are just as easy to make. There is great merit in using more than one method to solve a problem, since disagreement implies that there is an error in at least one of the approaches. Unfortunately, the fact that there is agreement among the results of different calculations does not necessarily imply that the correct answer has been obtained!

ACKNOWLEDGMENTS

I am particularly indebted to Mike Rowe and Jack Rush (NIST), and to Ruep Lechner (HMI), for their advice and encouragement during (and since) the early stages of design of the DCS. My thanks to Ruep Lechner for sending me one of his computer programs, and to Bernie Olivier for his help with some of the more tedious calculations. I have benefited greatly from numerous discussions with my colleagues at NIST: David Mildner, Terry Udovic, Jeremy Cook, Felix Altorfer and Nick Maliszewskyj.

REFERENCES

[1] F.B. Altorfer, J.C. Cook and J.R.D. Copley, Mat. Res. Soc. Symp. Proc. **376**, 119 (1995).
[2] J.R.D. Copley, J. Neut. Res. **2**, 95 (1994).
[3] J.M. Rowe, P. Kopetka and R.E. Williams, Proceedings
of the Fifth Meeting of the International Group on Research Reactors
(IGORR-V), November 4-6, 1996, Aix-en-Provence, France. Technicatome/CEA.
[4] J.R.D. Copley and T.J. Udovic, J. Res. Natl. Inst. Stand. Technol. **98**, 71 (1993).
[5] Consult "www.ill.fr/in5/IN5.html", "www-llb.cea.fr/menl/spectro/mibemol.html", and "www.hmi.de/grossgeraete/bensc/instrumente/v3.html" for information about IN5, MIBEMOL and NEAT respectively.
[6] J.R.D. Copley, Nucl. Instr. Meth. A **291**, 519 (1990).
[7] .R.D. Copley, Nucl. Instr. Meth. A **303**, 332 (1990).
[8] J.R.D. Copley, Physica B **180 & 181**, 914 (1992).
[9] R.J. Royston, Nucl. Instr. Meth. **30**, 184 (1964).
[10] C.G. Windsor, *Pulsed Neutron Scattering*, Taylor and Francis, London, pp. 217, 237. (1981).
[11] J.R.D. Copley, J. Neut. Res. **1**, 21 (1993).
[12] J.R.D. Copley and J.C. Cook, Nucl. Instr. Meth. A **345**, 313 (1994).
[13] J.R.D. Copley, Nucl. Instr. Meth. A **273**, 67 (1988).

MONTE CARLO

Monte Carlo (MC) cannot be used to prove that something is impossible, e.g., that neutrons cannot get through a device. If MC says that the transmission T>0, we know that T>0; but if MC says T = 0, we do not know whether T = 0 or T>0.

MC is not the best approach in cases where the measured performance only depends on combinations of parameters.

Look at "http://www.ill.fr/in5/IN5.html", "http://www-llb.cea.fr/menl/spectro/mibemol.html", and "http://www.hmi.de/grossgeraete/bensc/instrumente/v3.html" for information about IN5, MIBEMOL and NEAT respectively.

For information about IN5, MIBEMOL and NEAT, look at \newline
"http://www.ill.fr/in5/IN5.html", "http://www-llb.cea.fr/menl/spectro/mibemol.html", and "http://www.hmi.de/grossgeraete/bensc/instrumente\-/v3\-.html" respectively.

Look at "www.hmi.de/grossgeraete/bensc/instrumente\-/v3\-.html", "www-llb.cea.fr/menl/spectro/mibemol.html", and "www.ill.fr/in5/IN5.html", for information about IN5, MIBEMOL and NEAT respectively.

On the use of a toroidal mirror to focus neutrons at the ILL neutron spin echo spectrometer IN15

Carmel Hayes[1*], Berthold Alefeld[2], John R. D. Copley[3], Colette Lartigue[4], F. Mezei[5]

[1] Institut Laue-Langevin, Avenue des Martyrs, B.P. 156, 38042 Grenoble Cedex 9, France

[2] Forschungszentrum Jülich GmbH, Institut für Festkörperforschung, D-52425 Jülich, Germany

[3] National Institute of Standards and Technology, Gaithersburg, MD 20899, USA

[4] Laboratoire de Spectrométrie Physique (associé CNRS), Université Joseph Fourier, B. P. 87, 38402 St. Martin d'Hères Cedex, France

[5] Hahn-Meitner-Institut, Glienicker Str. 100, D-14109 Berlin-Wannsee, Germany

Abstract

The IN15 neutron spin echo spectrometer at the Institut Laue-Langevin (Grenoble) has been designed to accomodate a toroidal focusing mirror. This mirror will be used to increase the intensity at the sample position for measurements at long neutron wavelengths and to perform measurements in the low q-range (10^{-3} Å^{-1}). This paper summarizes the results of ray-tracing simulations for the toroidal mirror system. These calculations were performed in order to assess the effects of the neutron wavelength, gravitational fall, wavelength resolution and spherical aberrations on the quality of the focused beam. The gain in flux that can be expected from the focusing geometry is estimated. The recent installation and characterisation of the mirror is also briefly described.

INTRODUCTION

The IN15 neutron spin echo spectrometer at the Institut Laue-Langevin, Grenoble, has been designed with the aim of (1) increasing the energy resolution and (2) extending the minimum wave vector transfer range (q-range) to the 10^{-3} Å^{-1} range while maintaining a reasonable flux. To achieve these goals, first the precession coils were optimized: the dimensions were increased and larger Fresnel coils were developed to correct the phase inhomogeneities. However, the gain in resolution is mainly obtained by using long wavelength neutrons and IN15 is "fuelled" by neutrons moderated in the ILL cold source. The use of long wavelength neutrons is also a step towards the small q-range. However, in order to perform measurements in the 10^{-3} Å^{-1} range, without building a very long instrument, IN15 was constructed with a focusing option. In this configuration, neutrons are totally reflected by a large toroidal mirror which produces an image of the source aperture in the plane of an area detector. It is thus possible to recover a large solid angle of the diverging incident beam; provided that the image is sufficiently good, this leads to an increase in the intensity at the sample position, compared with the conventional pinhole collimation, without loss of resolution (see refs. [1] and [2] for further discussions).

The aim of this paper is to summarize the results of ray-tracing calculations for the IN15 focusing mirror option. We begin with a short presentation of the ray-tracing programme. The IN15 instrument geometry is then described with details of the chosen toroidal mirror. The results of a number of ray-tracing calculations are then presented with attention paid particularly to the effects of the neutron wavelength, gravitational fall and the wavelength distribution on the quality of the focused neutron beam. Comparisons between an ellipsoidal mirror and the chosen "ellipsoidal-equivalent" toroidal mirror are made. We also estimate the gain in flux that may be expected once the toroidal mirror is used in a spin-echo experiment. Finally, we briefly describe

* Present address: CRC Clinical Magnetic Resonance Research Group, The Royal Marsden NHS Trust,
Downs Road, Sutton, Surrey SM2 5PT, United Kingdom.

the actual (recent) alignment of the 4 m-long mirror, together with the results of preliminary tests of the mirror quality.

RAY-TRACING SIMULATIONS

Programme description

A ray-tracing programme has been written to estimate the imaging properties of doubly-curved mirrors for neutron focusing applications. This programme is described in ref. [3]. Briefly, the programme begins with a definition of the source parameters (neutron wavelength, λ, wavelength resolution, $\Delta\lambda/\lambda$, incident beam divergence, source aperture size and postion), the mirror figure (ellipsoidal, toroidal or cylindrical) and the mirror geometry (size, position, focal length). The paths of a large number of rays are traced to the mirror and the angle of incidence with the mirror surface is determined. If the angle of incidence is less than the critical angle, θc, of the reflecting surface, the path of the reflected ray is traced to the image plane. The number of rays passing through the system at any point after the mirror may be counted. In particular, we have used the programme to count the number of neutrons traversing the sample aperture. An additional programme also exists to simulate a conventional small-angle spectrometer.

The gravitational fall of the neutron, $\Delta(\lambda,L)$, over the flight distance (L) is included in the calculation of the neutron's trajectory. The neutron's gravitational fall depends on its wavelength and on the distance travelled:

$$\Delta(\lambda,L) = \frac{gm^2}{2h^2}\lambda^2 L^2 \qquad 1$$

In Fig. 1 we plot the gravitational fall as a function of the flight distance for 10, 15, 20 and 25 Å neutrons. It is clear that gravitational effects are important at longer neutron wavelengths.

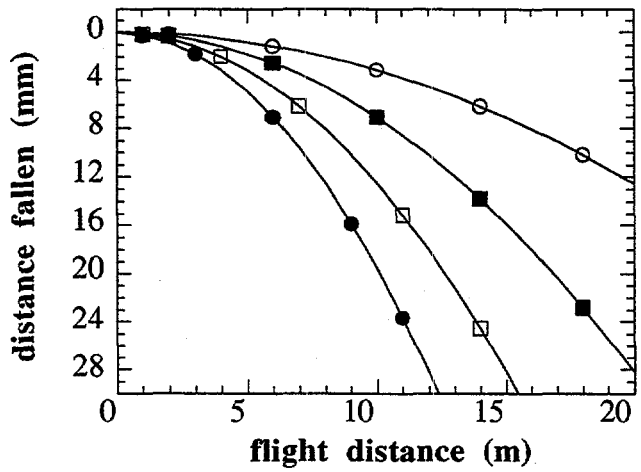

Fig. 1. The distance fallen as a function of the flight distance for a range of neutron wavelengths: 10 Å (-o-), 15 Å (-■-), 20 Å (-□-) and 25 Å (-●-).

IN15 NEUTRON SPIN ECHO SPECTROMETER

A schematic of the IN15 standard spin echo spectrometer geometry is shown in Fig. 2a. The focusing instrument geometry is shown in Fig. 2b: a 4 m-long doubly-curved toroidal mirror is placed half-way between the velocity selector and the position-sensitive detector. The chosen mirror consists of eight identical elements (500 mm x 170 mm). The height of the useful reflecting surface is 150 mm. The reflecting surface is ^{65}Cu, evaporated onto a highly polished

zerodur substrate. The surface microroughness, measured using the Wycko Topo 2D technique, is 3 Å (rms.). The ^{65}Cu layer is protected against oxidation by a thin layer of aluminium. The mirror geometry is fixed so that neutrons with wavelengths greater than 15 Å are reflected.

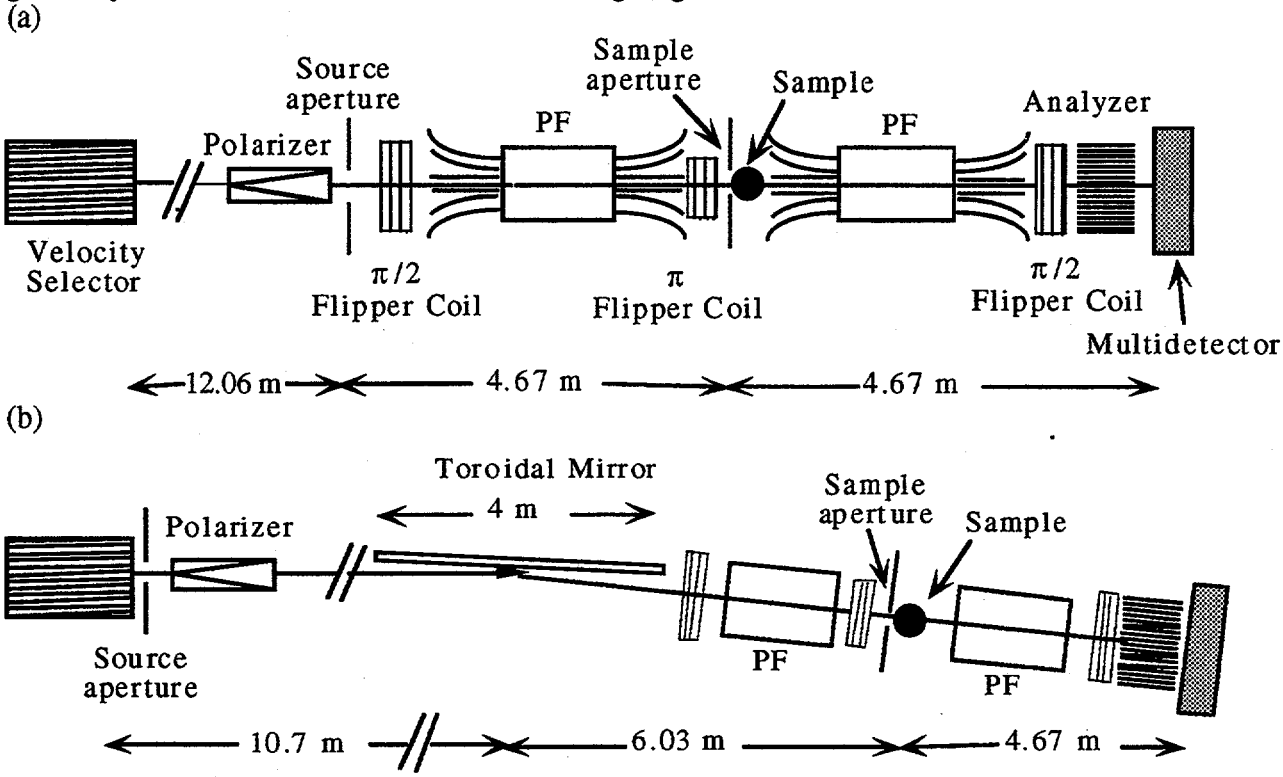

Fig. 2. Schematic of the IN15 neutron spin echo spectrometer: (a) standard configuration, (b) focusing mirror configuration. PF = precession field.

RESULTS OF RAY-TRACING SIMULATIONS

Image quality

In this section, some illustrative examples of ray-tracing calculations for the IN15 focusing instrument geometry are presented. The source aperture size for all calculations is 10 mm and, unless stated otherwise, the wavelength resolution is 15 % (Gaussian distribution). Images are viewed looking towards the detector.

Fig. 3 shows contour plots of the image of a 10 mm-diameter source aperture for three different neutron wavelengths (17, 20 and 23 Å). Figs. 3a and 3b are images formed by a 4 m-long ellipsoidal mirror; Figs. 3c and 3d, are images formed by an "ellipsoidal-equivalent" toroidal mirror (*i.e.* the IN15 mirror). For both mirror types, we also show the effect of the position of the source aperture on the quality of the image. In Figs. 3a and 3c, the source aperture is placed at the focus, in Figs. 3b and 3d, the source aperture is placed a distance $\Delta(\lambda, L)$ (see Eq. 1 above) below the focus, where L = 10.7 m.

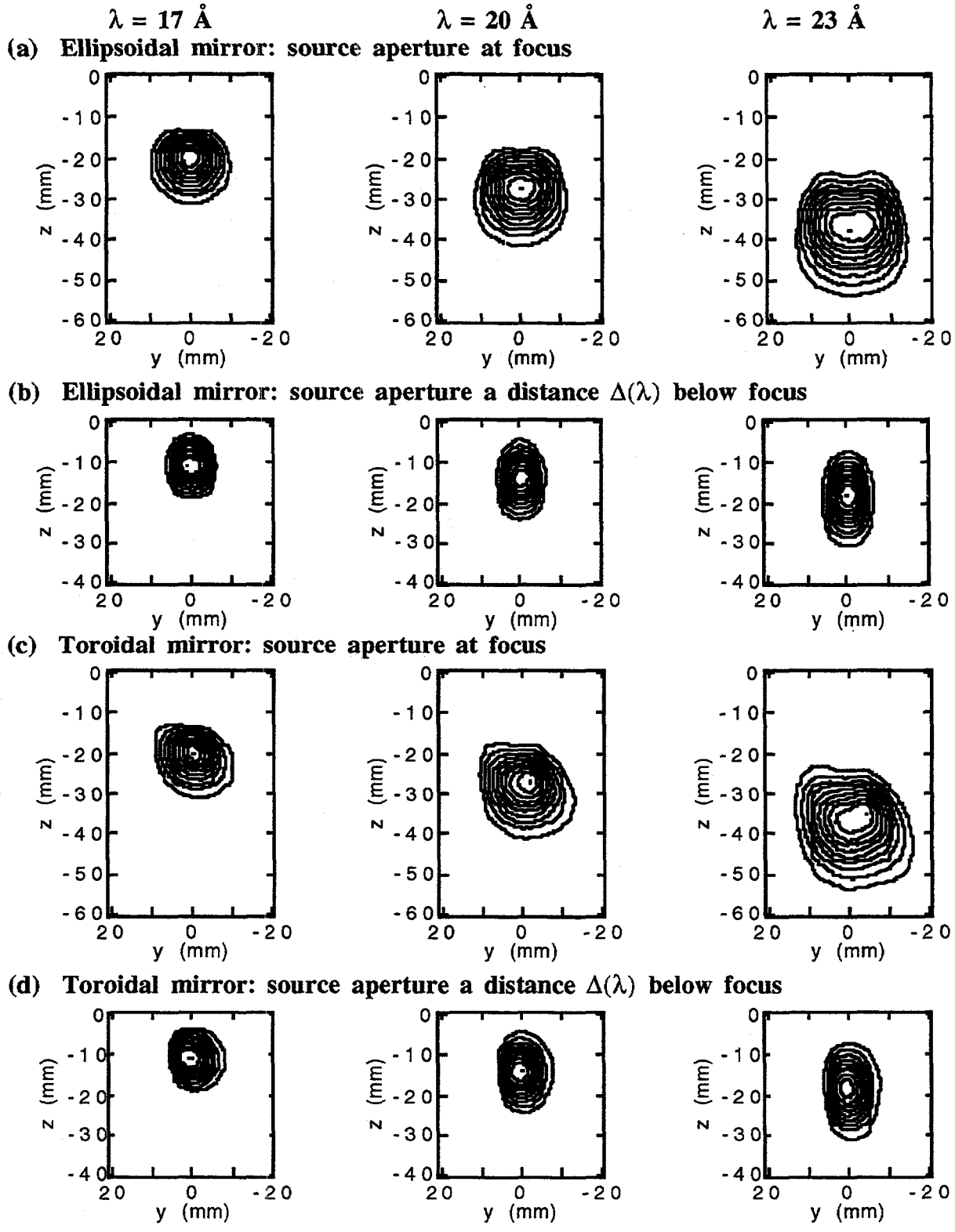

Fig. 3. Calculated images of a 10 mm-diameter source aperture for ellipsoidal and tordoidal mirrors and for three different wavelengths (17 Å, 20 Å and 23 Å reading from left to right across the page). The effect of the position of the source aperture on the quality of the image is shown for both types of mirror.

The calculations indicate that for typical neutron wavelengths and for $\Delta\lambda/\lambda$ = 15 %, there is little difference in the images formed by 4 m-long ellipsoidal and toroidal mirrors. The toroidal mirror image is asymmetric and slightly larger when the source aperture is positioned at the focus. However, on placing the source aperture a distance $\Delta(\lambda, L)$ below the focus, the image of the 10 mm-diameter aperture is vastly improved and the images formed by both mirror types are almost identical. This correction has already been discussed in refs. [3 - 5]. Essentially, the improvement, which is especially significant in the horizontal plane, occurs because lowering the source causes neutrons to strike the mirror at angles such that they appear to have come from points much closer to its focus. The remaining vertical distortion is due to the neutron wavelength distribution.

The results of calculations for two different wavelengths, $\lambda = 17$ Å and $\lambda = 23$ Å, and for three different wavelength distributions, $\Delta\lambda/\lambda = 10$, 15 and 25 %, are shown in Fig. 4. The image quality deteriorates rapidly with increasing wavelength and increasing wavelength distribution. The longer wavelength neutrons fall farther than the shorter wavelength neutrons, which spreads the beam. The only way to reduce this chromatic aberration is to use a mirror surface which is horizontal rather than vertical (ref. [6]).

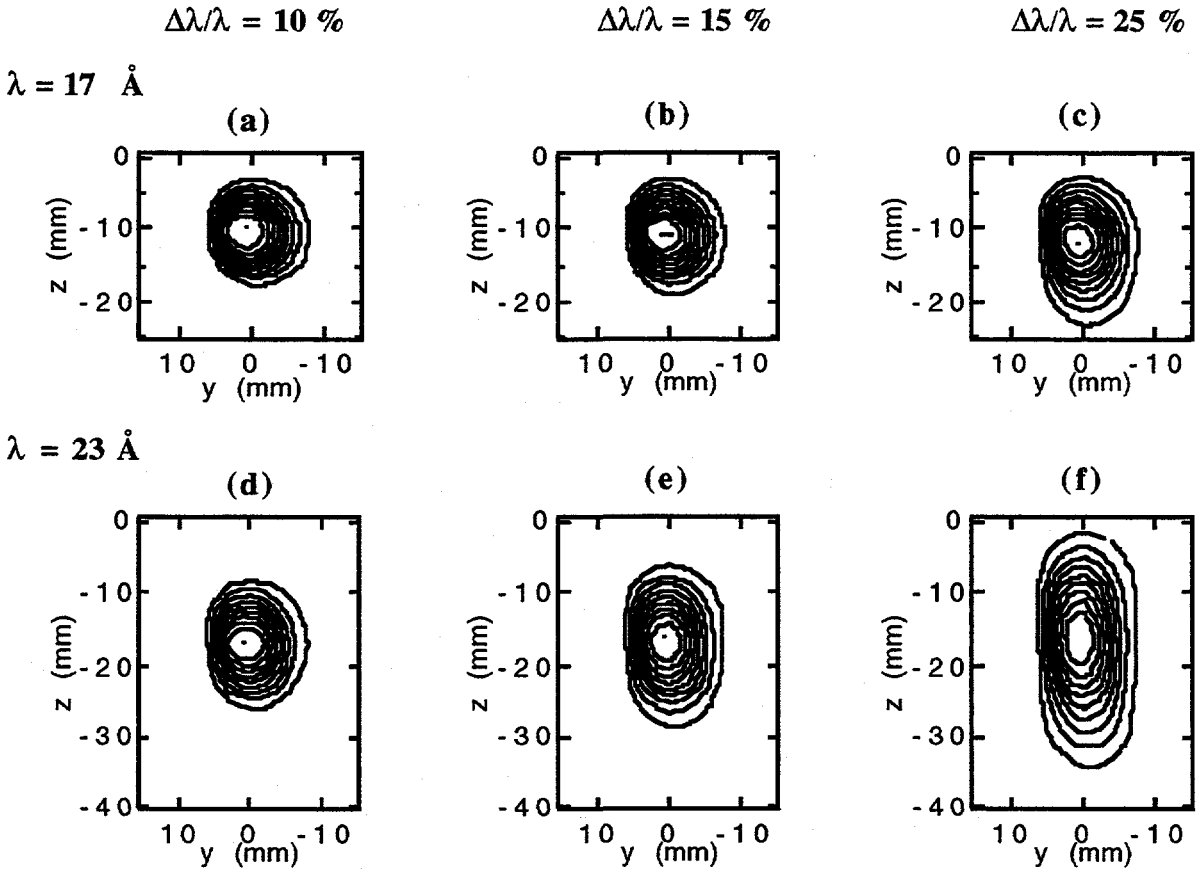

Fig. 4. Calculated contour plots of the images of a 10 mm-diameter source aperture positioned a distance $\Delta(\lambda,L)$ below the focus. (a-c) $\lambda = 17$ Å and $\Delta(\lambda,L) = 10.4$ mm, (d-f) $\lambda = 23$ Å and $\Delta(\lambda,L) = 19$ mm. The wavelength resolution is 10, 15 and 25 % reading from left to right across the page.

Flux gains

We have used the ray-tracing programme to estimate the flux gains that can be expected from the IN15 focusing mirror system compared with the standard instrument geometry. The relative

performance is analysed as a function of the q-resolution, δq. Given that the contribution of the wavelength spread to the overall instrumental resolution is identical for both configurations, we refer here only to the geometric contributions to the q-resolution.

For the standard IN15 instrument geometry the q-resolution is a function of both ϕ_e and ϕ_s, which are the source and sample aperture diameters, respectively. For $\phi_e = 2\phi_s$, we write the q-resolution as $\delta q = (\pi/\lambda)(2\phi_e/L)$ where L is the sample-to-detector distance. For the focusing geometry, ϕ_s is unimportant and we write the q-resolution as $\delta q = (\pi/\lambda)(f\phi_e/L)$ where the prefactor f accounts for the imperfect imaging properties of the toroidal mirror; it is a function of the source aperture size, the wavelength and the wavelength distribution. We estimated the values of f from the calculated images, defining δq as the value of q where the intensity has dropped to 10 % of its peak value. Typically f varied from 1.6 to 3.4, depending on the parameters of the simulation.

In order to cover a sufficiently large q-range, the calculations were performed for a range of source sizes, sample apertures and neutron wavelengths. For the standard configuration, the diameters of the source and sample apertures were in the range 10 - 30 mm and 5 - 15 mm respectively. The first ("source") aperture was placed a distance 4.67 m from the sample position. The neutron wavelength was varied between 9 and 25 Å. For the focusing mirror geometry, the source aperture was between 5 and 40 mm and the sample aperture diameter was fixed at 30 mm; the calculations were performed for λ = 16 to 25 Å. In order to make realistic estimates of the intensity gains, the number of rays "emitted" by the source at a given wavelength was proportional to the corresponding measured flux at the exit of the IN15 velocity selector; the source was assumed to be uniformly illuminated and the divergence was that of a neutron beam emerging from a Ni guide.

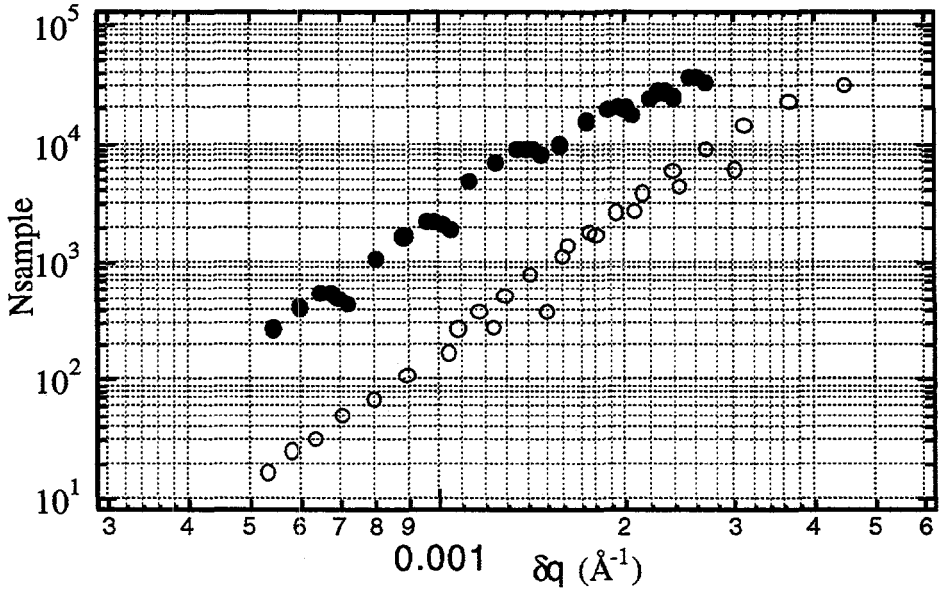

Fig. 5. Plot of the calculated intensity at the sample position as a function of the q-resolution for the
IN15 standard (open symbols) and focusing (filled symbols) instrument geometries.

Fig. 5. shows a plot of the intensity at the sample position as a function of the q-resolution for both IN15 instrument configurations. The intensity gain obtained with the focusing mirror increases the

lower the q-resolution. For $\delta q \approx 10^{-3}$ Å^{-1}, a tenfold gain in intensity is estimated. This could be increased further by using a larger sample aperture, though this is dependent on sample availability. It is obvious from the graph that the mirror is certainly of value in the low q-resolution range. However, these calculations do not take into account the surface microroughness of the reflecting surface, nor the small-angle scattering that can arise from the spin echo components (flippers, Fresnel coils). Both of these can influence the signal to noise ratio and hence, the minimum q value which will be experimentally accessible.

IN15 TOROIDAL MIRROR: ALIGNMENT AND PRELIMINARY TESTS

The eight mirrors were aligned using a 1 mm diameter halogen (diverging) light source placed at the focus (*i.e.* just after the velocity selector as shown in Fig. 2b). The image was observed on a screen placed at the other focus (*i.e.* at the position of the IN15 multidetector). Each mirror was individually aligned, starting with the central mirrors, and adjusted so that the images superposed. Individual images from the extreme mirrors are shown in Figs. 6a and 6b and the image obtained with all eight mirrors aligned is shown in Fig. 6c. The corresponding simulated images are shown in Figs. 6d-f, respectively. The images are viewed looking towards the mirror. The size of the image obtained with all eight mirrors is approximately 4 mm high, 8 mm wide. As can be seen, the calculated image is highly distorted and much wider than that obtained experimentally. This is because the mirrors were individually adjusted so as to achieve optimum focusing conditions.

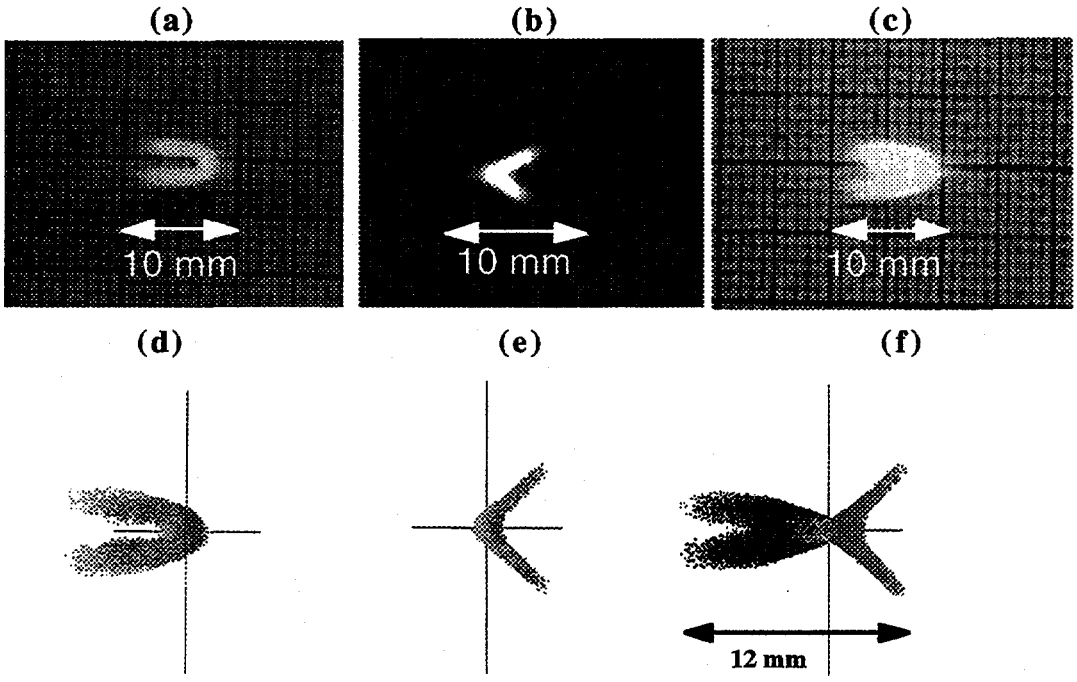

Fig. 6. Photographs of the focused images of a 1 mm-diameter light source: (a) extreme left mirror, closest to the light source, (b) extreme right mirror, (c) all eight mirrors. The images are observed looking towards the mirror and at a distance 10.7 m from the centre of the mirror. The corresponding calculated images are shown in figures d-f respectively.

IMAGING PROPERTIES OF THE TOROIDAL MIRROR SYSTEM

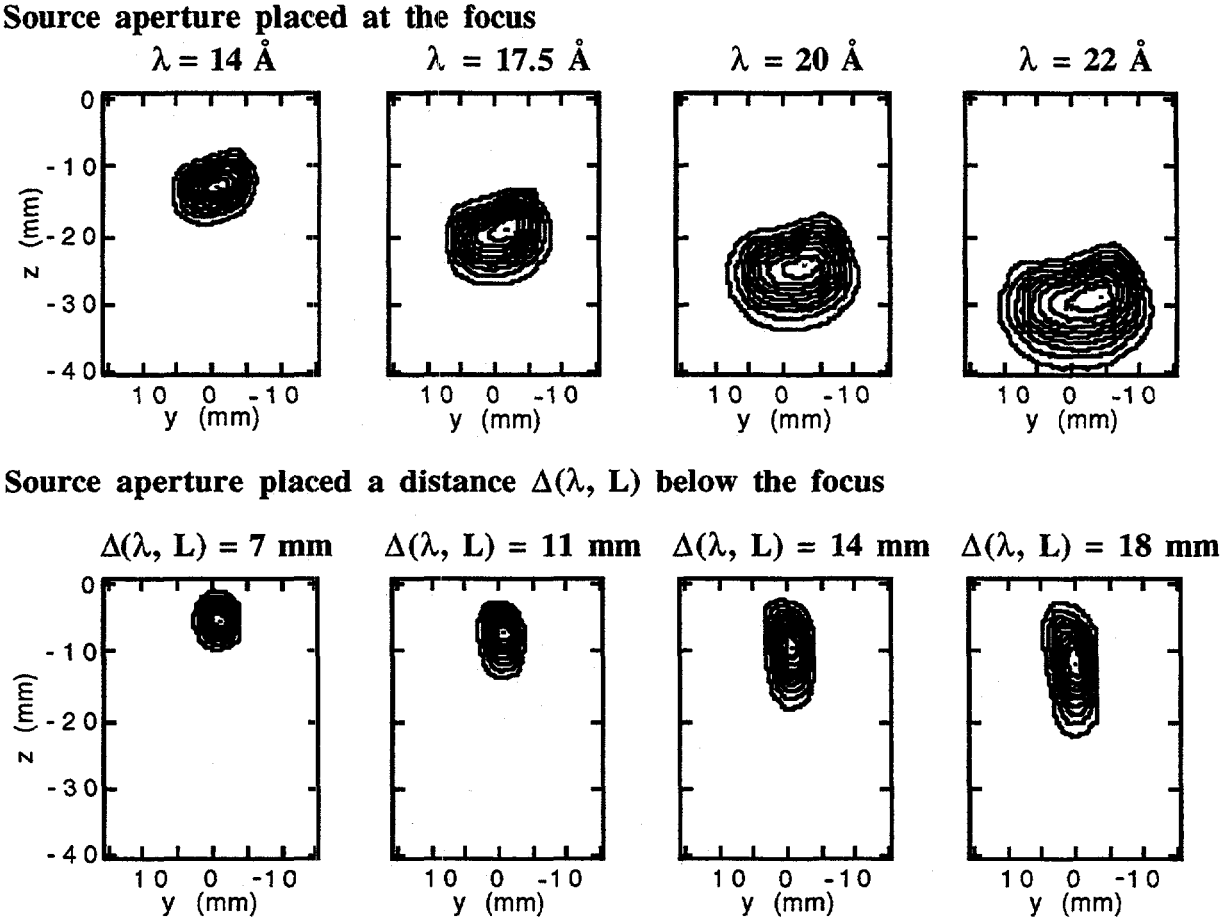

Fig 7. Measured contour plots (linear scale) of the focused neutron beam for a source aperture diameter of 2 mm. The wavelengths are 14, 17.5, 20 and 22 Å reading from left to right across the page. In the upper panel, the source aperture is positioned at the focus. In the lower panel, the source aperture is placed a distance Δ(λ,L) below the focus; the values of Δ(λ,L) are indicated in the figure for each of the wavelengths.

The imaging properties of the IN15 mirror were measured with a two-dimensional position-sensitive detector with a spatial resolution of 1.5 mm. The principal results of the initial tests may be found in ref. [5]. Fig. 7 shows the focused images of a 2mm-diameter source aperture for four different neutron wavelengths (14, 17.5, 20 and 22 Å). The measurements were made with a neutron wavelength distribution of 15 % (full-width at half-maximum). The images are viewed looking towards the detector. With the 2 mm diameter source aperture at the focus, the image rapidly enlarges with increasing wavelength and is located below the focus (which is at (y,z) = (0,0) in the figure). The shape of the image is asymmetric at all wavelengths. Such distortions may be attributed mainly to the gravitational fall of the neutrons and to the large wavelength distribution. Coma due to the great length of the mirror and aberrations due to the toroidal shape also contribute to the imperfect imaging. The lower panel of Fig. 7 shows what happens when the source aperture is located a distance Δ(λ,L) below the focus, where L = 10.7 m. We see an important improvement in the image quality for all wavelengths. This improvement is especially significant in the horizontal plane, the remaining vertical distortion is due to the neutron wavelength distribution.

Neutron intensity profiles of the focused neutron beam in the horizontal direction are shown in Fig. 8 for λ = 17.5 Å. The intensity profiles measured with and without a vertical shift of the source diaphragm are compared. The FWHM ($\Gamma_{1/2}$) of the image is substantially smaller when the source aperture is positioned below the focus (FWHM = 10.5 mm with source at focus, FWHM = 4.5 mm with source 11 mm below the focus). Furthermore, the contrast ratio (noise-to-peak ratio) is a factor of two times better at a distance $2\Gamma_{1/2}$ from the peak maximum when the source is vertically lowered and is of the order of 5×10^{-5} in both the horizontal and vertical directions for $q \approx 1.3 \times 10^{-3}$ Å^{-1}.

SUMMARY AND CONCLUSIONS

We have presented some results of ray-tracing calculations for the IN15 focusing mirror option. Our calculations indicate that the use of a toroidal mirror rather than an ideal ellipsoidal mirror is amply justified: the calculated images for both mirror types are almost identical for a range of typical values of the neutron wavlength and wavelength distribution. We have also used the ray-tracing programme to make realistic estimates of the overall gain in flux that can be expected from the completed mirror system. Including the effects of imaging errors, gains in beam intensity of the order of ten for $\delta q \approx 10^{-3}$ Å^{-1} should be attainable with the focusing mirror geometry. Finally, the preliminary tests of the 4-m long focusing mirror have shown that SANS optical focusing is feasible with a toroidal mirror and that with a high-quality reflecting surface, contrast ratios as low as 5×10^{-5} may be achieved for $q \approx 10^{-3}$ Å^{-1}.

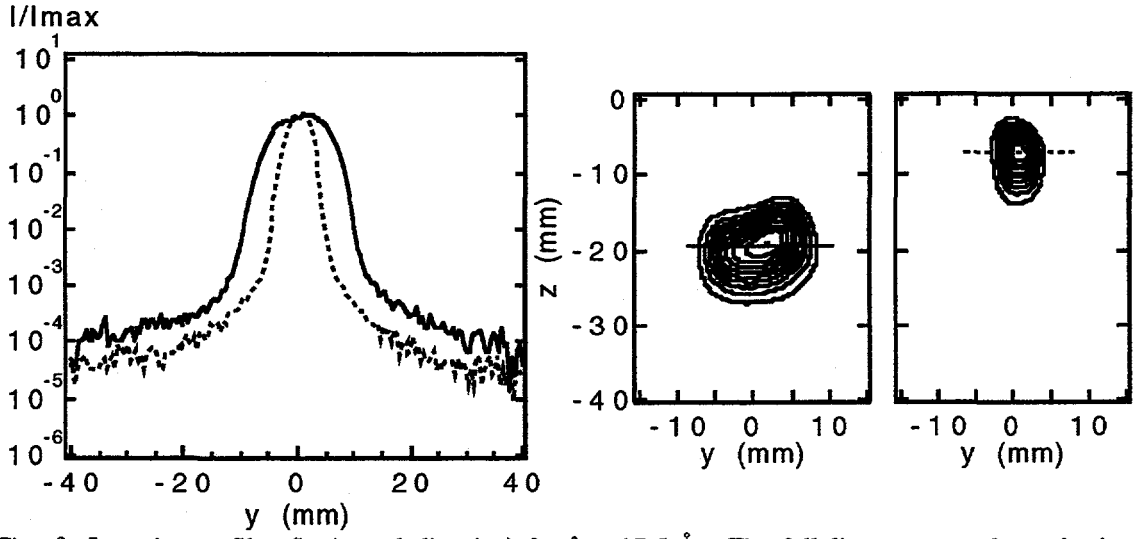

Fig. 8. Intensity profiles (horizontal direction) for λ = 17.5 Å. The full line corresponds to the image obtained with the 2 mm diameter source aperture at the focus, the dotted line corresponds to that obtained with the source aperture postioned $\Delta(\lambda,L)$ = 11 mm below the focus. The corresponding contour plots show the position and orientation of the intensity profiles.

REFERENCES

1. C. F. Majkrzak, C. J. Glinka and S. K. Satija, *Proc. SPIE* **983** 129 (1989); J.G. Barker and C. J. Glinka, *Proc. SPIE* **1738** 386 (1992).
2. B. Alefeld, D. Schwahn and T. Springer, *Nucl. Inst. and Meth. in Phys. Res.* **A274** 210 (1989); B. Alefeld, H. J. Fabian and T. Springer, *Proc. SPIE* **983** 120 (1989).

3. J.R.D. Copley, *Rev. Sci. Instrum.* **67**, 188 (1996).
4. C. Lartigue, J.R.D. Copley, F. Mezei, T, Springer, *J. Neut. Res.* **5**, 71 (1996).
5. C. Hayes, C. Lartigue, J.R.D. Copley, A. Kollmar, B. Alefeld, F. Mezei, D. Richter, T. Springer, *J. Phys. Soc. Jpn., Suppl. A* **65**, 312 (1996).
6. A. Kollmar, *private communication* .

TIME-OF-FLIGHT DIFFRACTOMETER WITH MULTIPLE PULSE OVERLAP - AN EXAMPLE FOR THE APPLICATION OF MODERN TOOLS FOR INSTRUMENT DESIGN

Uwe Stuhr, Günter S. Bauer and Werner Wagner
Paul Scherrer Institut
5232 Villigen PSI, Switzerland

Abstract

A Time-of-Flight Diffractometer with high pulse rates, allowing multiple frame overlap, is a completely novel design of an instrument dedicated for high resolution strain-field mapping. We elaborated a detailed concept of this instrument, applying analytical calculations and Monte Carlo computer simulations. Having established the instrument concept, the computer simulations will now be extended to optimize the total performance of the instrument. To illustrate the necessity and possibilities of applying modern tools for instrument design, we describe, as an example, the different steps towards the development of the detailed design of this instrument, which we intend to build at the Swiss spallation source SINQ in the near future.

INTRODUCTION

Neutron sources, as a matter of principle, do not possess high primary flux (as do nowadays the synchroton radiation facilities), and possibilities of flux improvements at the source or beamlines by implementing special devices are limited. Therefore, it is essential to optimize the instruments regarding neutron economy and best performance for a dedicated purpose. While a variety of special components are available or can be developed which allow substantial steps towards optimization, their combination can be complicated and very quickly develops to a multi-parameter problem. The design of a new instrument whose requirements touch the limits of feasibility can, therefore, often be optimized only by using modern, computer based tools and advanced methods for instrument design.

We experienced this situation during the design of a new instrument for the Swiss spallation neutron source SINQ: As one of the second generation instruments we envisage a dedicated instrument to map strain fields in bulk materials with high accuracy and spatial resolution, combined with the requirement to measure under extreme pressure and/or temperature, and in particular also highly radioactive materials.

For strain field measurements it is necessary that a samll gauge volume of the sample can be defined. This implies that only neutrons scattered in a small angular range near 90° can be used. Furthermore the instrument need not be optimized for structure analysis, but must allow determination of selected lattice constants with high accuracy. The combination of these requirements led to the concept of a multiple frame overlap time-of-flight diffractometer.

The present paper illustrates the different steps which were undertaken to reach a detailed design. Formulating the purpose of the instrument and goals, and even the principal concept did not require much more than the well-known "back-of-an-envelope" calculations. Working out details of the design and necessary properties of instrument components, computer-based analytical calculations became necessary. Finally, in order to simulate the performance of the overall concept and to optimize the spectrometer parameters, a Monte Carlo simulation program was written and adapted to the selected components and given boundary conditions.

THE INSTRUMENT CONCEPT - BASIC IDEAS

The condition of measuring at scattering angles near 90° and still covering a range of neutron wavelength can best be met by time of flight diffractometry. At present there exist two different types of time-of-flight-diffractometers:

The standard time-of-flight-diffractometer uses individual pulses. For each scattered neutron the wavelength is determined by the time between the source pulse or the opening of the chopper and the detection of the neutron. For an unambiguous determination of the neutron wavelength frame overlap must be avoided, i.e. the time between two pulses has to be chosen in a way that the fastest neutrons cannot catch up with the slowest ones of the previous pulse. Typical times between two pulses for those diffractometers are some 20ms.

The concept of a reverse time of flight- or Fourier-diffractometer follows a different philosophy. The chopper opening and closing times are the same. Therefore, the neutrons arriving at the sample (or detector) position at a given time can have originated from several hundreds of different pulses. Consequently, it is not possible to assign a detected neutron to a particular time of flight or wavelength. It is only possible to give a probability for each wavelength. Each recorded spectrum taken at a fixed chopper frequency is assigned to a spectrum of probabilities. Combining all the spectra measured with a variety of frequencies finally gives the desired wavelength-spectrum. The great advantage of a Fourier-diffractometer is the high gain in counting rate which exceeds that of the standard time of flight spectrometer by a factor of several hundreds. On the other hand the contrast of the spectra is poor. This is due to two facts: (i) The contrast of the chopper (defined below by Eq. (1)) is low and this contrast is even reduced by further time uncertainties on the flight path of the neutrons through the spectrometer and (ii) the difference in the arrival time of the neutrons of different Bragg-reflections (and pulses) is small compared to the time resolution.

The principal ideas of the spectrometer presented in the present study is (i) to optimise the conflicting quantities contrast and intensity of the measured spectra and (ii) to decouple them from the resolution of the instrument.

In the following we aim to explain an instrument concept which meets this conditions. The contrast of the spectra mainly consists of the contrast of the pulsed primary neutron flux and the contrast of the scattering function of the sample. A good contrast at the detector can therefore be achieved only by a high contrast K_C of the pulsed flux which we will define as

$$K_C = \frac{\int_0^{t_{cycle}} \left| \frac{I(t)}{\bar{I}} - 1 \right| dt}{2 \cdot t_{cycle}} \qquad (1)$$

where $\bar{I}$ is the average of the pulsed flux and t_{cycle} is the cycle time of the chopper. This contrast can be selected by the ratio of the opening time t_{open} to the cycle time, the so-called duty cycle η_C of the chopper. For a triangular shape of the intensity of the neutron pulse the contrast is given by:

$$K_C=(1-\eta_C)^2 \qquad (2)$$

whereas the average intensity $\bar{I}$ is proportional to η_C.

In order to assign the neutrons unambigously to the pulse they come from we will make use of the dependence of the arrival time t_{flight} of the neutrons on the scattering angle 2θ. For this, we need a 1-dimensional position sensitive detector with good spatial resolution.

For a given neutron momentum transfer Q at a Bragg-reflection the time of flight of a neutron between chopper and detector is:

$$t_{flight} = \frac{2 \cdot m_n}{\hbar \cdot Q} \cdot s_{tot}(\theta) \cdot \sin\theta \qquad (3)$$

where m_n is the neutron mass, $\hbar$ is Planck's constant and s_{tot} is the total length of the flight path of a neutron from the chopper to the detector which may vary with the scattering angle. In a contour plot of the neutron time of flight versus scattering angle (time-2θ-plot) each Bragg reflection is represented by a line. For a fixed geometry the slopes of these lines depend only on Q, or for a fixed θ only on the time of flight of the neutrons. Therefore we can use this slope to trace the slit of the chopper the neutrons come from and hence determine the neutron wavelength. This can be seen best if Eq. (3) is transformed to

$$\frac{dt}{d\theta} = t_{flight} \cdot \left(\cot\theta + \frac{1}{s_{tot}} \cdot \frac{ds_{tot}}{d\theta} \right) \qquad (4)$$

For an unambiguous determination of the slits through which the neutrons have passed we have to determine the slope $dt/d\theta$ with a relative accuracy of better than

$$\frac{\Delta(dt/d\theta)}{dt/d\theta} = \frac{t_{cycle}}{t_{flight}} \qquad (5)$$

To give an example, for neutrons with a velocity of 1500m/s, a pulse repetition rate of 10000/s and a total flight path of 15m we have to determine the slope with an accuracy of 1%. Consequently, we determine the Q-value only slightly better than 1% by the slope of the line in the time-2θ-plane. The final accuracy for the Q-value of the order of some 10^{-4} (or better: a FWHM of $\approx 2 \cdot 10^{-3}$) corresponding to the instrument resolution is obtained from the absolute value of the flight time given by the position of the line in the time-2θ-plane. This procedure allows us to work with a single chopper frequency.

The resolution of a time-of-flight instrument has a geometrical component and a component from uncertainty in the determination of the time of flight. The latter is mainly given by t_{open}/t_{flight} which depends, for a given length of the flight path, only on the width of the beam at the chopper and on the chopper speed. Therefore, the resolution of the instrument can be varied through the chopper speed. Since the average neutron flux does not depend on the chopper speed, the intensity at the detector as well as the contrast is independent on the resolution of the instrument. This is one major advantage compared to a standard time-of-flight-diffractometer.

A sketch of the proposed instrument is given in Fig. 1. Since the aim of this paper is to describe the procedure and the tools used to achieve a novel instrument design rather than to describe the instrument itself, the components are described only briefly. A detailed description of the instrument will be given elsewhere.

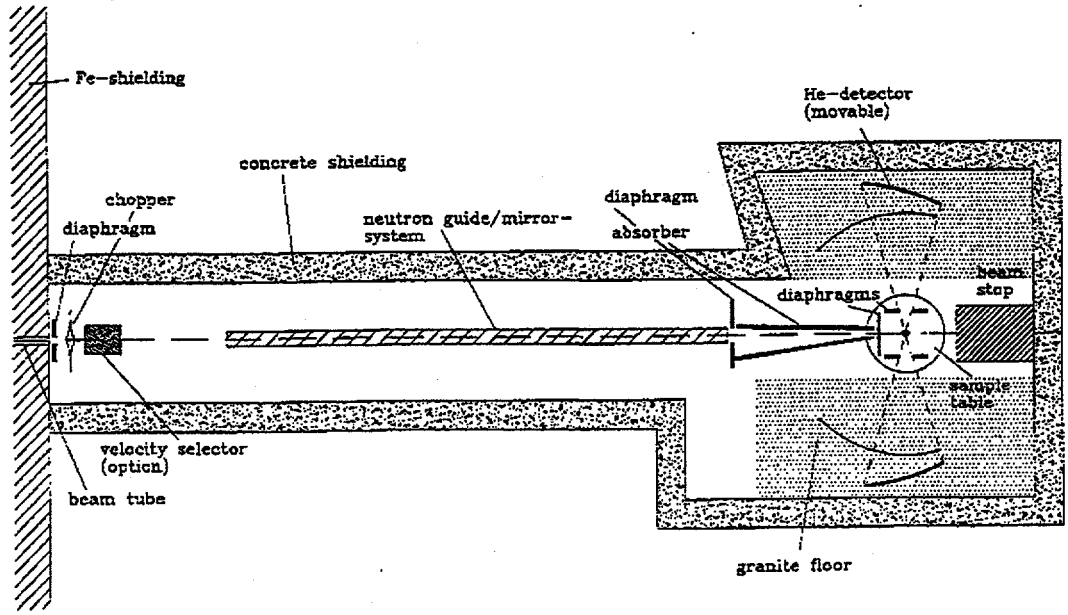

Fig. 1: Sketch of the instrument

Chopper

The envisaged disk-chopper with characteristics close to the limits of what is currently considered feasible yields a minimum pulse width of less than 8μs (FWHM) at a beam width at the chopper position of 4 mm. Since the total length of the flight path will be about 14 m, this pulse width contributes a relative uncertainty of ~ $8.6 \cdot 10^{-4}$ to the measured time of flight of neutrons with a velocity of 1500 m/s.

Neutron optics

In the following the expression 'neutron optics' is used for the entirety of elements between chopper and sample that interact with the neutron beam.
In order to obtain short chopper pulses the width of the beam at the chopper position has to be small. Therefore, the neutron optics between chopper and sample have to be optimised to have minimum losses of neutron density in phase space. The best way to transmit the neutrons with minimum losses in phase space density is to image the slit at the chopper onto the sample. This will be done by a neutron mirror with elliptical surface.
There are some further advantages of such a mirror: (i) It can transform a beam with a small width and a large divergence in to a broader beam with lower divergence without losses in phase space density (trumpet-effect). (ii) The mirror can be much shorter than the chopper-sample distance, therefore there is always enough space to insert sample equipment and beam manipulation devices like velocity selector, diaphragms etc.. (iii) All neutrons are reflected only once and within a narrow range of reflection angles, therefore the loss of neutrons is minimized, and, at the same time, neutrons with shorter wavelength than the critical one are suppressed very efficiently.
Detectors
To achieve well defined gauge volumes in the specimens the detectors are positioned at scattering angles between 90° and 120°. On each side of the sample a one-dimensional position-sensitive ^{3}He-detector, with an aperture of 30° will be used. The spatial resolution of each detector should be about 2mm. This is possible either with a microstrip-detector or with a high resolution wire-chamber detector. The thickness of a ^{3}He-detector for thermal neutrons is about 20-30 mm which corresponds to a time of flight of the neutrons of 10-40 μs. To avoid a time uncertainty of this magnitude which would spoil the time resolution of the instrument each detector element must be positioned in time focusing condition. According to Eq. (4) the time focusing condition is achieved if we chose $1/s \cdot ds_{tot}/d\theta = -\cot\theta$. Since the chopper-sample distance is constant $ds_{tot} = dr$ where r is the sample-detector distance and the above given condition reads $1/s \cdot dr/d\theta = -\cot\theta$.

SIMULATIONS AND OPTIMISATION OF THE NEUTRON OPTICS SYSTEM

So far, rather straight forward analytical considerations ("back-of-an-envelope" calculations) brought us to the point, where the principle ideas of contrast and intensity optimization, combined with a decoupling of resolution and intensity, could be realized by means of the above presented conceptual instrument design. For the optimization of single instrument components, we used computer-assisted analytical calculations. As an example, we present our computer simulations based on analytical equations which describe the neutron optics system. They describe the performance of a 7m neutron mirror of elliptical shape placed in 12m flight pass between chopper and sample. The simulations were restricted to the scattering plane, neglecting the influence of vertical divergence of the beam. The parameters kept fixed in the simulations are the following: the critical angle of the mirror chosen to be three times that of natural nickel, the reflectivity which is 1 up to this angle and 0 above, a width of 4 mm for the first diaphragm, 12 m length of flight path between the diaphragm and the sample. The direct flight path through the mirror device is obstructed by a second diaphragm. After having passed the neutron-optic system the simulated neutrons are monitored on a horizontal line perpendicular to the neutron beam. Fig. 2 shows the result for an ideally shaped mirror. If we replace this mirror by a polygon of 50 cm straight elements we get the phase space plot shown in Fig. 3. Both plots show the pear-shaped density distribution which is the result of the 'trumpet' effect of the mirror. The first part of the mirror transforms high divergences into a large beam width which is represented in the upper part of the pear. This shows that even when the diaphragm in the incoming beam is only 4 mm wide, the beam at the sample position has a width of about 8 mm at a divergence of about 0.1°. On the other hand the second part of the mirror produces a very narrow beam with a larger divergence which is very useful for small samples or gauge volumes. Thus, with the help of diaphragms at the end of the mirror and in front of the sample we can select either good collimation or small beam width.

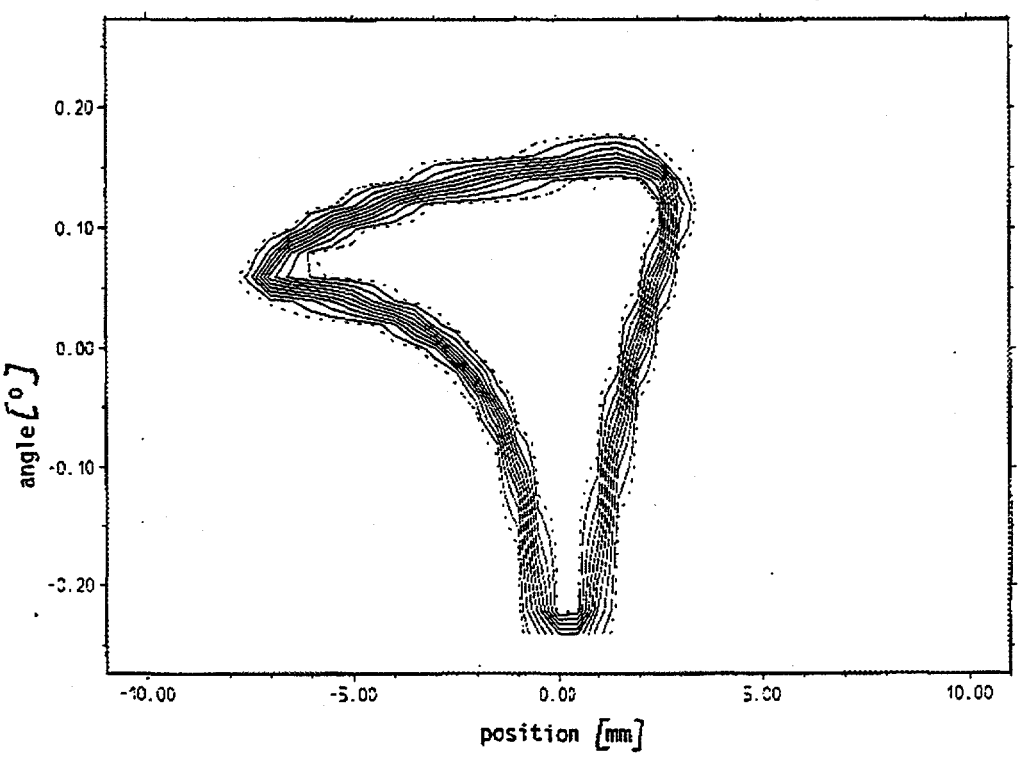

Fig. 2: Simulation result of the neutron optics system with ideally shaped mirror.

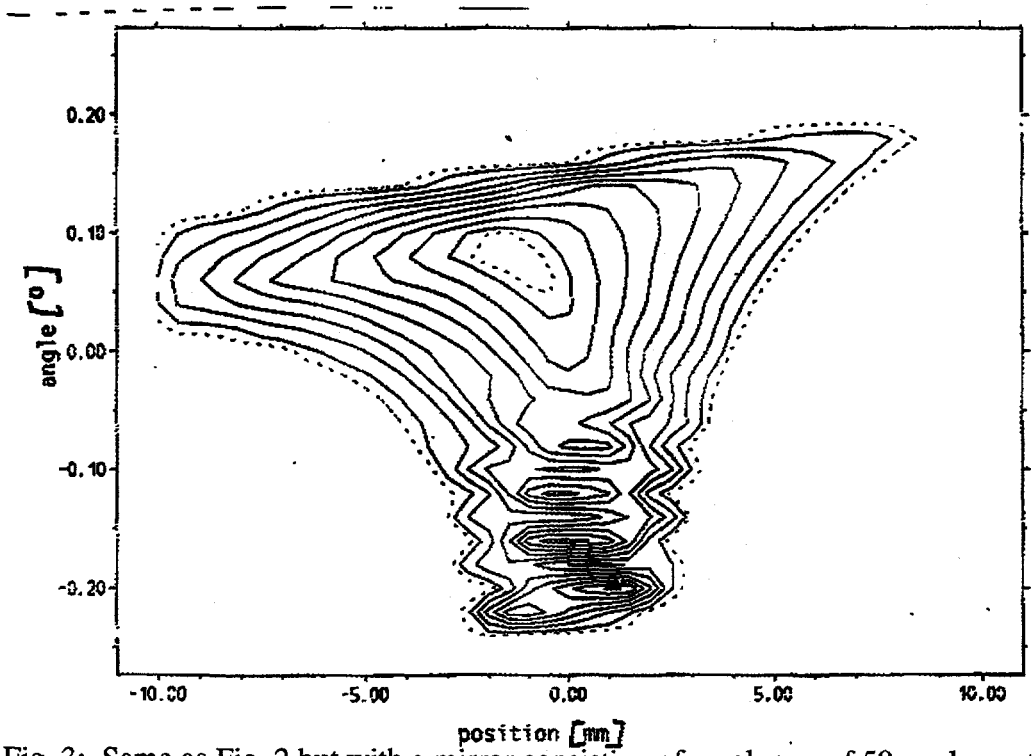

Fig. 3: Same as Fig. 2 but with a mirror consisting of a polygon of 50 cm long straight sections.

The suppression of the short wavelength by the mirror is demonstrated in Fig. 4 where the transmission of the neutron-optic system is plotted versus its wavelength. This figure also shows that we lose a factor of nearly two if we use a polygon of straight elements instead of an ideally curved mirror. A comparison of Figs. 2 and 3 shows why: The width of the beam at the sample is increased by nearly a factor of two by the straight elements compared to the ideal mirror, and consequently this factor is lost in phase space density.

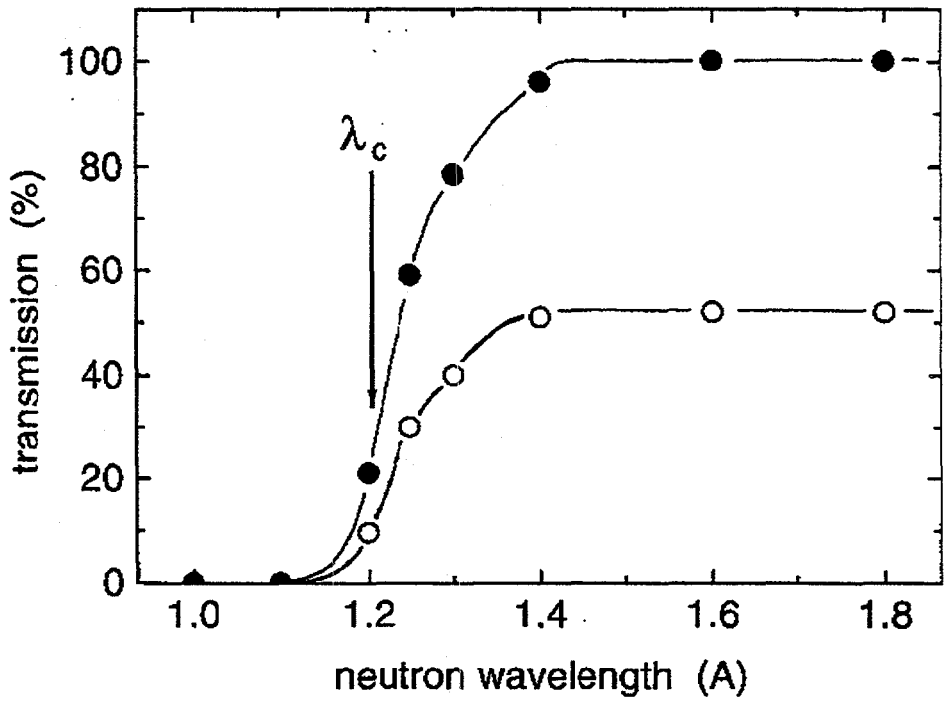

Fig. 4: Transmission of the n-optic system for a 2.5 mm wide sample as a function of the neutron wavelength. The closed symbols represent the data of the ideally shaped mirror, the open ones those of the polygon of straight elements.

MONTE-CARLO-SIMULATIONS - SCATTERING PERFORMANCE IN TIME-2θ-SPACE

The aim of this Monte Carlo program is mainly to demonstrate the function of the concept presented and to optimise the parameters of the secondary spectrometer. It is not (yet) a program which simulates the performance of the whole instrument.
The program, therefore, contains the following idealisations:

- no vertical divergence is considered (the simulation is performed only in the scattering plane),
- the primary beam and the sample have zero spatial extension
- the neutron flux is constant inside a given wavelength interval and zero outside
- the transmission function of the chopper has triangular shape
- the absorption probability in the detector is constant
- all neutrons are scattered in the half-circle where the linear detector is positioned (2π rather than 4π for better statistics)

The most important parameters concerning the detector, however, have been taken into account:

- the detector elements have a size of 2 x 20 mm^2

- they are arranged on a circle (whose center does not coincide with the sample position)
- the neutrons are allowed to pass several detector elements.

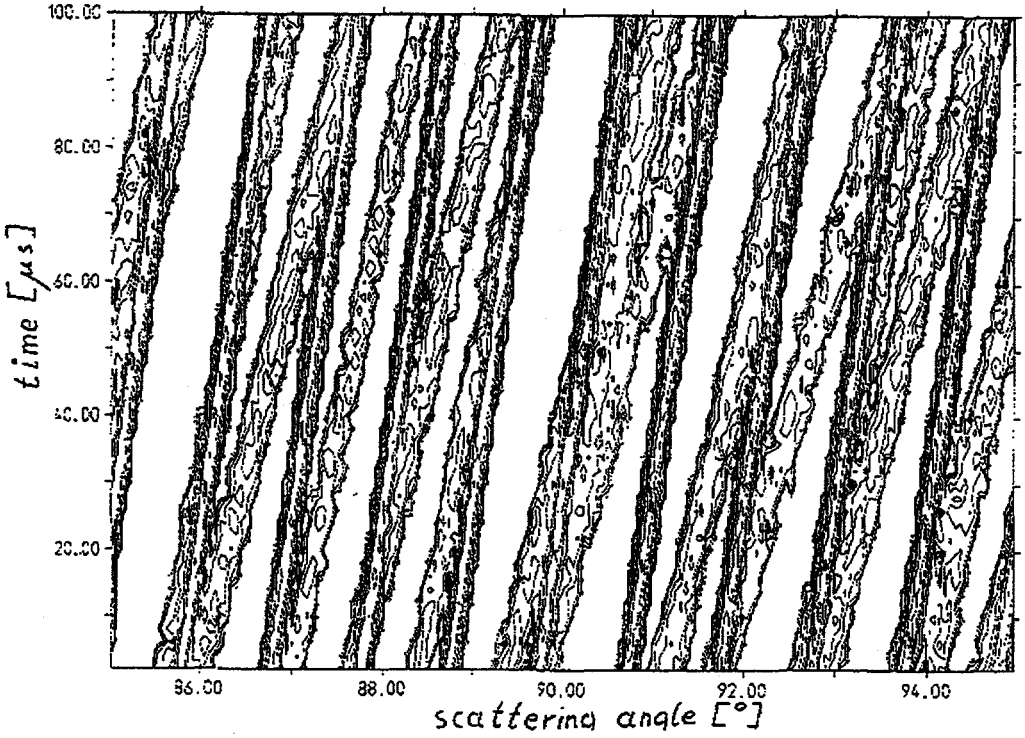

Fig. 5: Monte-Carlo simulation result in a time-2θ-contour-plot. For reasons of clarity only a 10°-region of the detector is shown.

Fig. 5 shows the simulation results by means of a contour plot in the time-2θ-plane. The contour lines represent 0.5% ,1% ,2% ,5%, 10%,20% 30% 50%, and 70% of the maximum intensity. The origin of the time scale is the opening of the chopper. For reasons of clarity only a 10° part of the 30° detector is shown. In this simulation 10^7 neutrons impinging on the chopper where used. The opening time of the chopper t_{open} was 10μs, and the ratio t_{cycle}/t_{open} was 10. The range of wavelengths was 1.5^{-5} Å, and the distance of the sample to the detector was 2m at 90° scattering angle. The plot shows the intersecting lines of different slope produced by the different Bragg-reflections.

These plots are stored in a histogram memory and the second part of the program evaluates these data. For the time being, the evaluation of the data is based on the following concept:
For every possible scattering vector and each detector element the time of flight is calculated. Than, for the given scattering vector, all detected neutrons in the corresponding time channel of each detector element are added (weighted with respect to their statistical errors). After finishing this procedure for every possible scattering vector the resulting spectrum is multiplied with a "damping" factor. This is necessary since in the procedure each element in the plot of Fig. 5 has been added several times to the spectrum. Now we can recalculate the angle-time contour plot expected for this first spectrum. The resulting contour plot is subtracted from the measured plot, and the calculation is repeated with this residual plot until no significant improvements are achieved. The result of this procedure for the data of Fig. 5 (but taking into account the whole 30°-range of the detector) is shown in Fig. 6.

One characteristic feature of such spectra is the occurrence of side peaks at each Bragg reflection. They correspond to wavelengths of neutrons attributed to an earlier or later pulse. These side peaks result from the way in which we evaluate the data. If we would actually fit the data, these peaks would vanish as long as the condition of Eq. (4) can be fulfilled. However, these side peaks have no influence on the determination of the Bragg peak position, which is the main purpose of

the instrument. Fig. 7 shows an enlargement of the region around the first Bragg reflection with the side peaks.

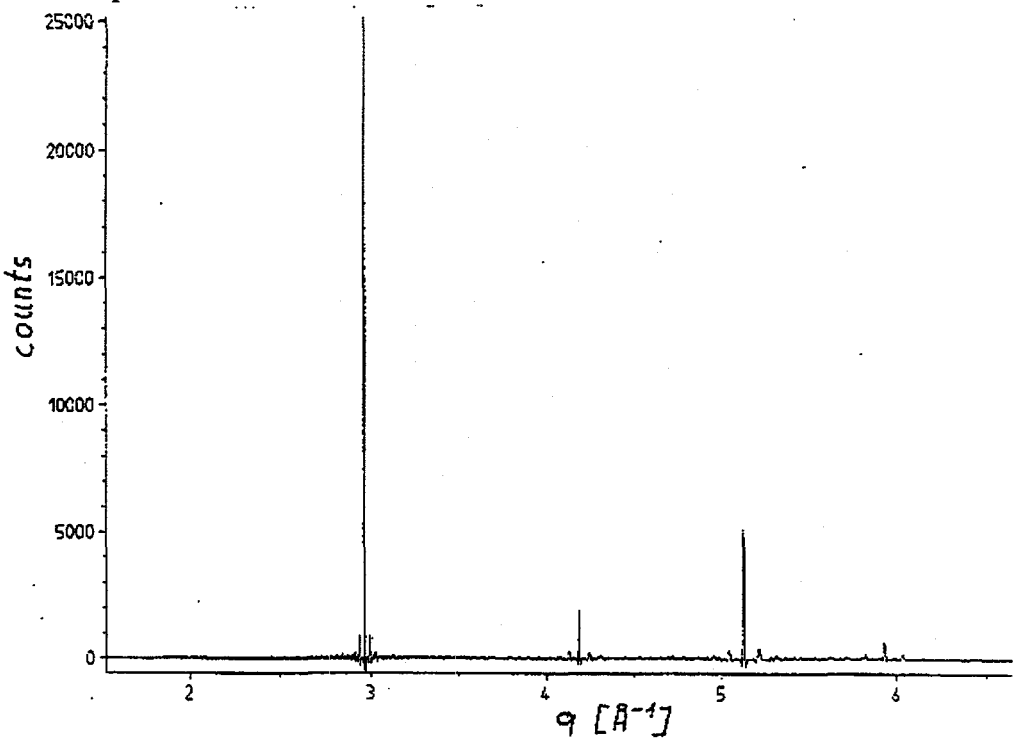

Fig. 6: Diffraction pattern calculated from the contour plot of Fig. 5.

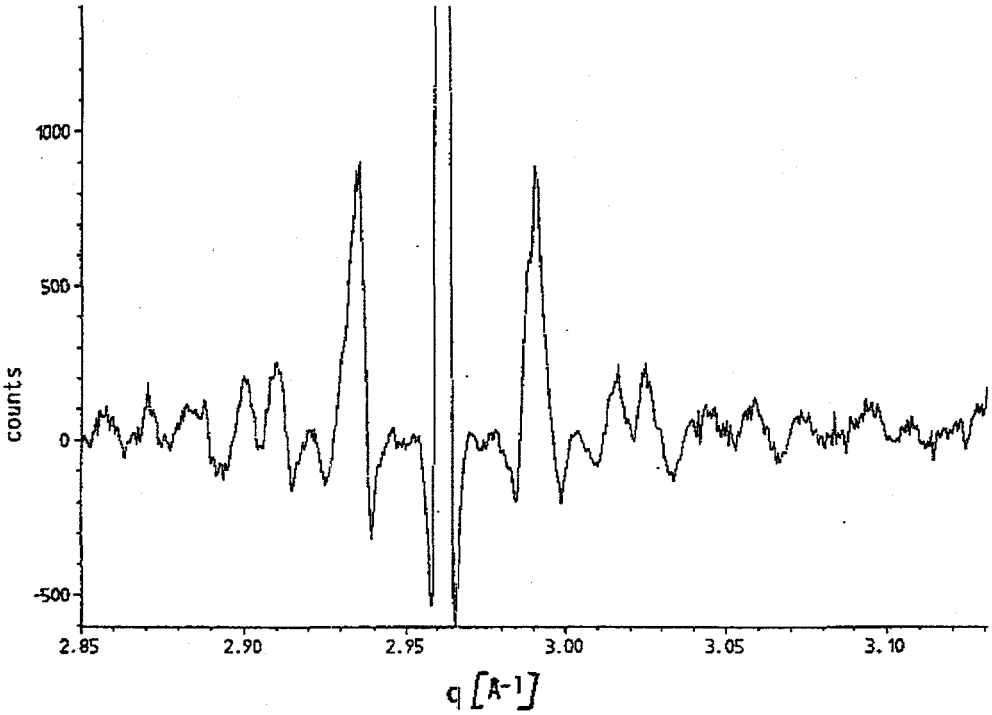

Fig. 7: Region of the first Bragg-peak in an enlarged scale which shows the side peaks.
In Fig 8 a simulation of the same sample but now with only 25% Bragg-scattering and 75% incoherent scattering is shown. It demonstrates that the quality does not suffer very much from high background levels.

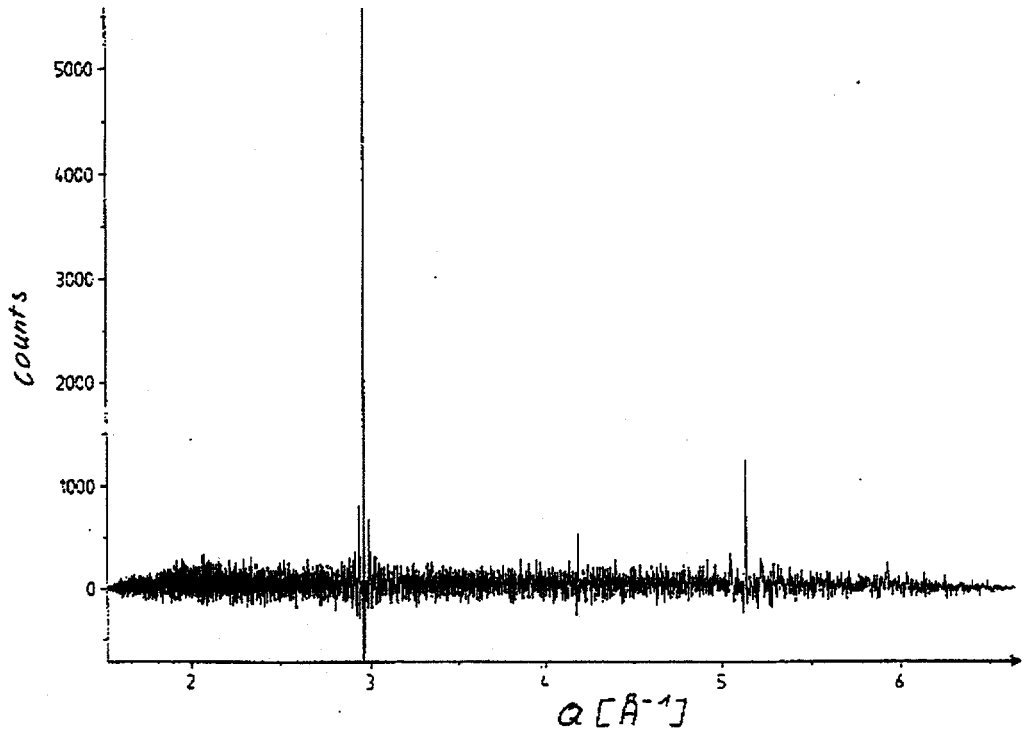

Fig. 8: Same as Fig. 7 but with a 'sample' with 75% incoherent scattering.

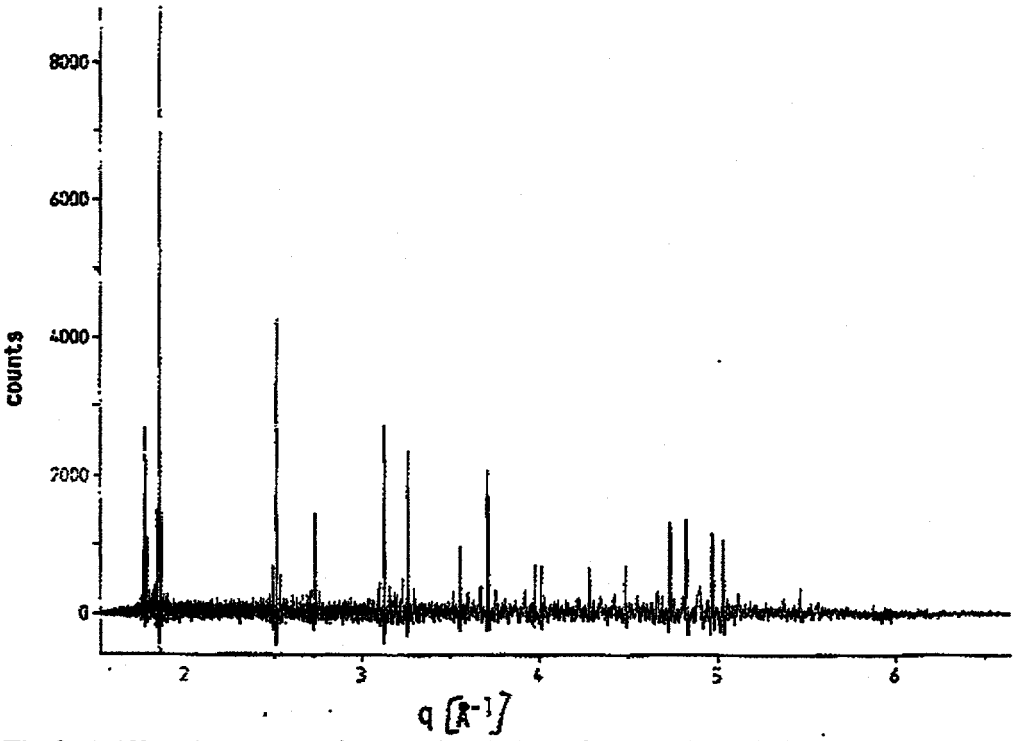

Fig 9: Diffraction pattern from a simulation of a sample with 17 Bragg reflections in the investigated Q-range. 10^8 neutrons at the chopper position were used for this simulation.

Increasing the number of Bragg reflections leads to a decrease in contrast in the time-2θ-pattern which reduces the statistics and makes the determination of weak Bragg reflections more difficult. In Fig. 9 a spectrum of a sample with 17 Bragg reflections in the investigated Q-range is shown. It demonstrates that such spectra are still measurable with this instrument. If the number of Bragg reflections increases further, the quality of the spectra decreases significantly. This may be considered as the penalty for the increased intensity of the instrument relative to the direct TOF technique. However, the purpose of this instrument is not primarily structure analysis; the main application will be the investigation of samples of simple materials with significantly less than 20 Bragg-reflections in the Q-range (which could, if necessary, be limited by a velocity selector in front of the mirror) .

CONCLUSION AND OUTLOOK

A novel concept of a time-of-flight diffractometer has been evaluated. The main advantage of this type of instrument is that it can be optimised to high flux and high resolution simultaneously, and that this optimisation can be adapted to the task the instrument is expected to perform. The high intensity is achieved by using many pulses of the chopper in short sequence and solving the frame overlap problem by evaluation of the time-2θ-pattern. A resolution of about 10^{-3} is expected for this diffractometer. Before starting the construction of the instrument we plan to carry out two more major tasks: Firstly, to run Monte-Carlo-simulations of the complete instrument involving all components with realistic characteristics. Secondly, and even more important, develop an improved procedure for the analysis of the time-2θ-plot.

AN OPTIMISED DESIGN OF A ROTAX-TYPE INSTRUMENT

H Tietze-Jaensch

ISIS Facility, Rutherford Appleton Laboratory, Chilton OX11 0QX, U.K.
Institut für Festkörperforschung, Forschungszentrum Jülich GmbH, D-52425 Jülich, FRG

Abstract

The rotating analyser (ROTAX) spectrometer has been devised and installed at ISIS. Practical scans in $(Q,\hbar\omega)$ space with a nearly arbitrary scan direction, i.e. polarisation of $\underline{\mathbf{q}}$ vs. $\underline{\mathbf{Q}}$, are possible and feasible with no compromises on the resolution. Valuable technological and methodological knowledge has been compiled for an improved version of such a type of instrument. At present, ROTAX lacks competitiveness with other spectrometers from an unexpectedly weak neutron flux of its particular beam-line and an unfavourable adaption of the analyser's drive power to the time frame or neutron source frequency

1. INTRODUCTION

The principle ideas of the rotating crystal analyser spectrometer ROTAX were first introduced in 1986 [1]. Meanwhile ROTAX has been devised and installed at ISIS. The method of inelastic neutron spectroscopy by using the rotating analyser principle has proved to provide feasible experimental scans in $(Q,\hbar\omega)$ space with a much enhanced scan versality. We emphasize the advantages of the rotating analyser technique compared with triple axis, direct geometry chopper and MAX-type inverted time-of-flight spectrometers. No compromises on the resolution with respect to the spinning analyser had to be made. The rotating analyser technique deserves a serious consideration for its use on a new intense short pulsed neutron source.

2. COMPARISON WITH OTHER SPECTROMETERS

On ROTAX various time-of-flight (tof) scans in $(Q,\hbar\omega)$ space can be performed [1,2]. Let's consider the "scattering paraboloid" for every type of neutron tof-spectrometer. All scattering takes place its surface and the more of it is covered simultaneously the better the efficiency of any particular instrument. The triple-axis spectrometer scans only one point at a time. It uses monochromatic incoming neutrons from a reactor source. On tof-machines the key-word is "multiplexing": numerous tof-channels are detected simultaneously. Parabolic tof-scans through an anticipated scattering point P in $(Q,\hbar\omega)$ space on the surface of the scattering paraboloid are obtained. The specific scan direction is fixed by the instrument's geometry and set-up, only on ROTAX this scan direction may well vary [1,2,3].

Fig 1 illustrates the scattering paraboloids and tof trajectories the various types of tof-spectrometers: a) A direct geometry chopper spectrometer (like HET/MARI/MAPS at ISIS [4]) operates at a fixed incident neutron energy Ei. With an array of detectors a range scattering angles ϕ_i at a surface section between the two k_f extremes is scanned. b) Inverted geometry scattering spectrometers (like PRISMA at ISIS [5]) run n scattering arms at constant final energies $E_f(n)$ and scattering angles $\phi_0 \pm n\Delta\phi$, the sample is bathed the white incident beam. Every arm defines its own and inverted scattering paraboloid culminating at their analyser's Bragg energies $-E_f(n)$. Geometric constraints to avoid detector clashes restrict the tof-trace along a line $d\underline{\mathbf{Q}}$ parallel to $\underline{\mathbf{k}}_i$. $Q_\perp$ is kept constant for all spectrometer arms and for times. A bunch of tof-parabolas through and around the considered point P is obtained to coarsely map its vicinity. No further adjustment of the scan direction can yet be made. For practical purposes of single-crystal spectroscopy $Q_\perp$ must be chosen in units modulo $2\pi/d_{hkl}$ which is, in practice, a considerable limitation of the feasibility of PRISMA as discussed in by Dorner [6].

This problem is overcome by the use of a non-uniformly rotating analyser crystal (ROTAX). There is only one analyser crystal that rotates and modifies the final energy $E_f(t)$ contineously. This instrument is characterised by a whole continuum of paraboloids rather than a discrete set (fig 1c). There are no clash conditions and no constraints of $Q_\perp$=const. The Q-trace of the tof-scan is parameterised by the Q-value of the centre-axis of the scattering paraboloids that moves in $(Q,\hbar\omega)$ space in accordance with the scan set out on ROTAX. So far we have introduced the const-$\hbar\omega$ and the const-$\underline{Q}/|Q|$ or const-Ψ scans [1,2] and there is a generalisation of the const-Ψ scans to the whole class of "linear-Q" scans [3].

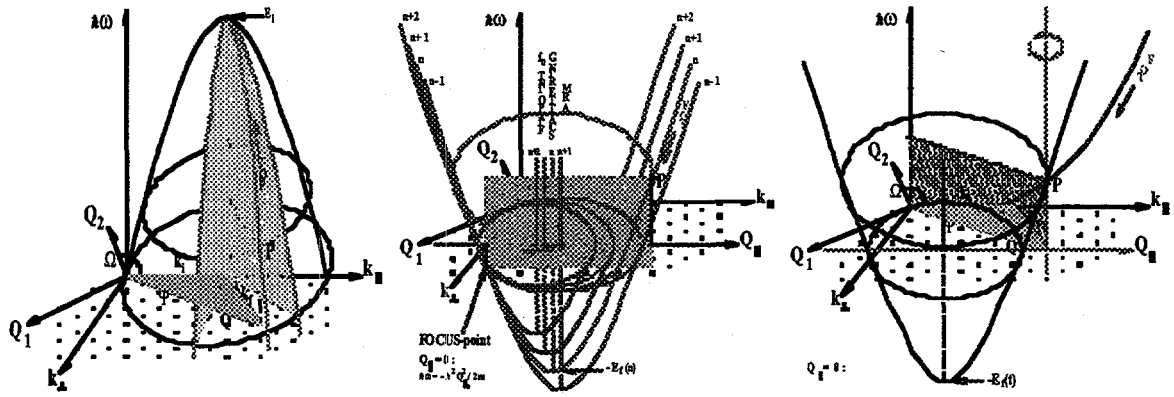

Fig. 1: scattering paraboiloids for a chopper (a), an invertedt geometry (b) and the ROTAX psectrometers, respectively. The same scattering triangle for a scan point P(Q, $\hbar\omega$) and an imaginative Q-lattice are shown for all 3 instrument types discussed in the text.

The technical performance of ROTAX scans is limited only by the time frame at an incident flight path L_i and the achievable angular acceleration on the analyser, i.e. the power resources of the analyser drive system. The analyser spin does not neccessarily have to follow an analytic curve, the analyser drive control works on an entirely digital basis. The vicinity of point P under consideration is observed with a high degree of pixeled density of scans when a linear detector array of high angular/spatial resolution is used. This is essential for evaluating the 2-dimensional multiplex advantage and it is the reason why ROTAX can acquire more usefull data simlutaneously with only one analyser than a PRISMA-type machine with n≈16 analyser-detector assemblies.

Experimental results of inelastic neutron scattering on ROTAX were published and described in detail, elswhere [7,8]. The results are satisfactorily, except of two facts that had lead to the decision to not further develop this instrument at ISIS:

1) The obtained intensities are too weak for inelastic applications because of defecient neutron flux on the particular ROTAX beam line at ISIS.
2) There is still insufficient power on the analyser drive system to make full use of all scan feasibilities on the rotating analyser system. This deficience, however, can be overcome with a revised geometric design of the machine (cf. below) and with today's technology.

3.) IMPROVED DESIGN OF A ROTAX TYPE INSTRUMENT

With respect to the resolution required a ROTAX type instrument would exploit its full features on a short pulsed neutron source. The ISIS instrument has proved the principal capability and feasility of such a set-up. Todays technology to run a digitally controlled gear-less direct drive of the non-uniformly spinning analyser crystal can be copied and easily installed. One needs an ordinary computer to design the anticipated (Q,ω) scan (e.g. with the software developed for ROTAX at ISIS) and then

- parameterise and store the values of the analyser's angular motion versus time.
- transfer the data to a high-performance standard signal processor that runs and controles a three-phase power inverter and inverted servo-motor of the analyser drive (the program establishes a dymanic control and feed-back of the actually achieved drive performance)
- start the scan, collect the data from a time-resolved linear position sensitive detector and
- combine the detector tof-data with the tof-dependend actually achieved analyser position data and neutron scan parameters for a proper interpretation of the results obtained.

All subsequent data treatment is standard-like.

The control and regulation hardware employed on ROTAX is sketched in fig. 2. Standard electronic hardware components and a commercially available servo-motor are used. The signal processor based control program manages the synchronisation with the pulsed source, scan and power generation, position verification and veto-handlung within 90 μs of time. The instantaneous position regulation itself takes typically 1 ms of time for 0.1° angular positioning accuracy to be achieved. These are limits to be required for ROTAX at ISIS.

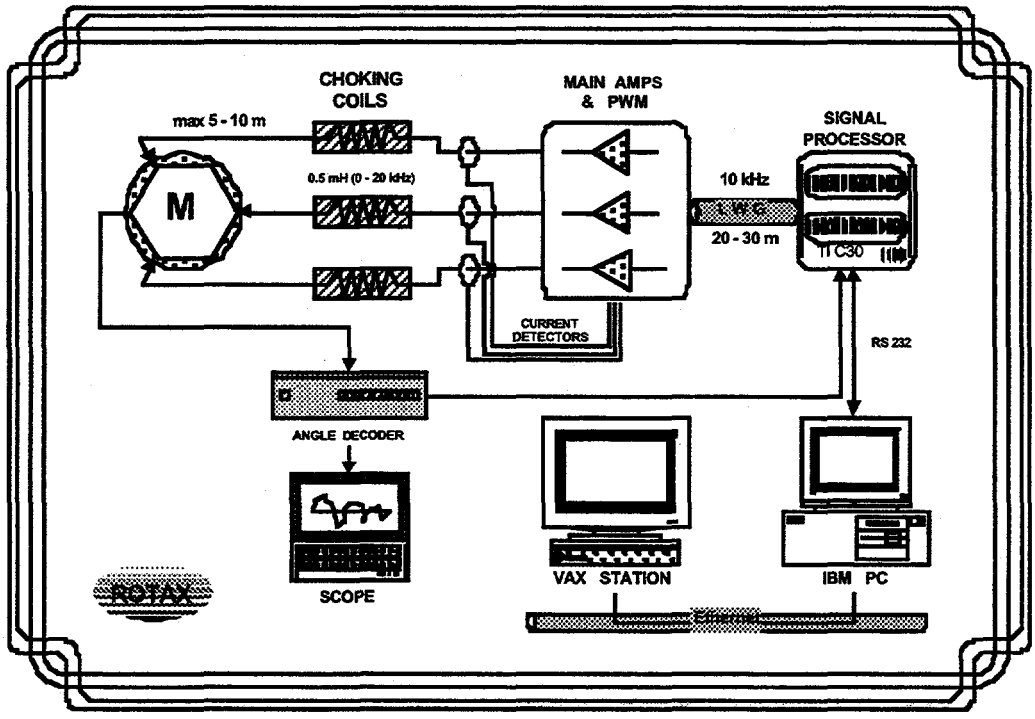

Fig. 2: Hardware of the ROTAX analyser drive after the 1995 technical impovements

With respect to the present technical power limitations a future instrument should stretch its time-of-flight length scale by approximately a factor of two, i.e. stretch its in-pile flight path to ca. 30 m. The result would be a twicely time-zoomed general motion and every scan would demand only 1/8 of the ROTAX analyser drive power. This would make many more scans to become technically feasible. However, such an instrument should view a pulsed (cold) moderator through a proper beam guide and not a simple beam tube on the grounds of neutron flux considerations. In principle, there could be more than only one secondary spectrometer, each arm possibly equipped with one or two multidetectors (cf. fig. 3).

With the experience gained on ROTAX at ISIS and with respect to the considerations explained above, a revised ROTAX type instrument would provide a real alternative to existing instrument designs but with a much enhanced scan flexibility and versality.

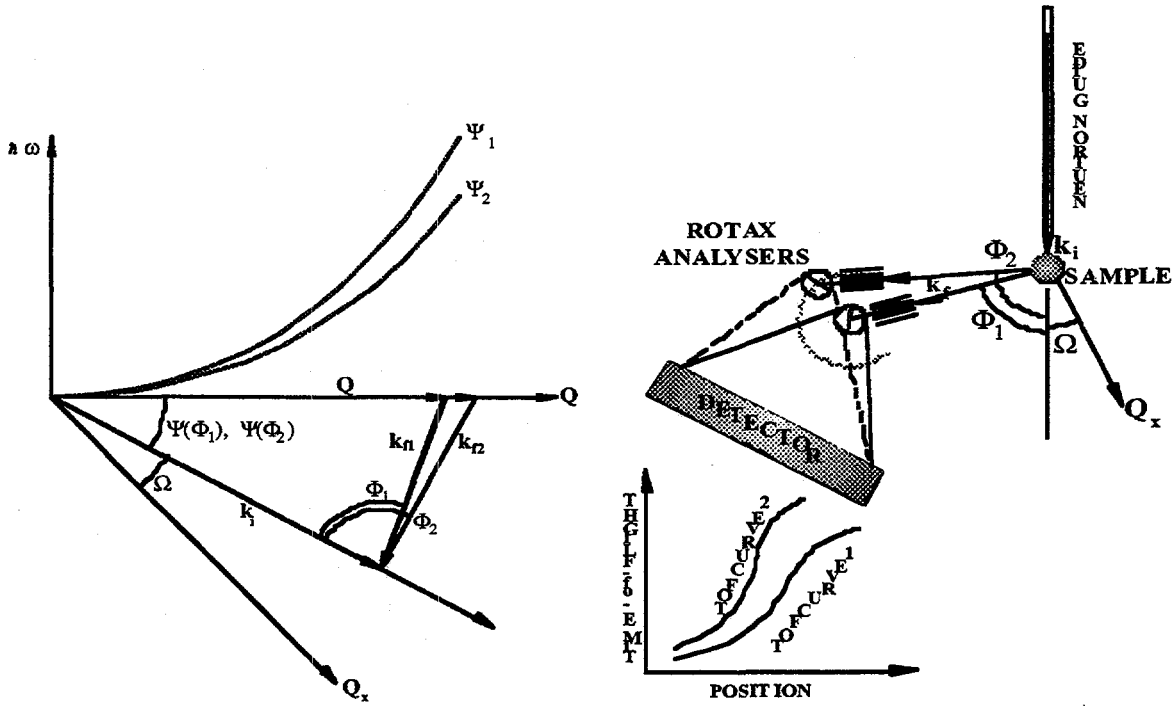

Fig. 3 Double-ROTAX set-up for two independent simultaneous scans in (Q,ħω) space.

ACKNOWLEDGEMENT

Numerous people had advised and helped us to get ROTAX off the ground; they can't be named explicitely here but their contributions have been very valuable. Financial support by the German Minister for Education and Research BMBF under contract no.s 03-ge3-wue and 04-wi3-bon is gratefully acknowledged.

REFERENCES

[1] R Geick and H Tietze, Nucl. Inst. & Meth. A 249 (1986) 325
[2] H Tietze and R Geick, Proc. ICANS IX, PSI 1986, SIN-rep. 40926 (1987) 389
[3] W Schmidt, H Tietze-Jaensch and R Geick, Proc. ICANS XII, Abingdon 1993, RAL rep. 94-025, p. I-293
[4] R S Eccleston and R Osborn, RAL rep. 94-117
S M Bennigton and R S Eccleston, RAL rep. 94-102
T G Perring, A D Taylor, R Osborn, D Mc Paul, A T Boothroyd and G Aeppli; Proc. ICANS XII, Abingdon 1993, RAL rep. 94-025, p. I-60
[5] U Steigenberger, M Hagen, R Caciuffo, C Petrillo, F Cilloco and F Sacchetti; Nucl. Instr. & Meth. B53 (1991) 87-96
[6] B Dorner, J Neutron Research 2.3 (1994) 115-127
[7] H Tietze-Jaensch, W Schmidt, R Geick and U Steigenberger; Physica B 213 & 214 (1995) 878-880
[8] H. Tietze-Jaensch, W. Schmidt, R. Geick and G. Will
Proc. ICANS XIII, PSI Switzerland 1995, PSI rep. 95-02 I-6 (1995) 130

MONTE-CARLO SIMULATION OF AN ULTRA SMALL-ANGLE NEUTRON SCATTERING INSTRUMENT BASED ON SOLLER SLITS.

Thomas Rieker
Center for Micro-Engineered Materials
Department of Chemical and Nuclear Engineering
University of New Mexico, Albuquerque, NM 87131

Paul Hubbard
Sandia National Laboratories
P.O. Box 5800
Albuquerque, NM 87185-1349

Abstract

Monte Carlo simulations are used to investigate an ultra small-angle neutron scattering instrument for use at a pulsed source based on a Soller slit collimator and analyzer. The simulations show that for a q_{min} of ~1e-4 $Å^{-1}$ (15 Å neutrons) a few tenths of a percent of the incident flux is transmitted through both collimators at q=0.

Introduction

A wide q-range is required to accurately determine the micro-structure of materials by small-angle scattering. Currently the widest q-ranges are available at reactor sources through a combination of variable geometry pinhole and Bonse-Hart instrumentation. Pulsed neutron sources, at present, provide pinhole instrumentation with a minimum q of ~0.003 $Å^{-1}$[1].

For a SANS instrument it is important to maintain high flux in the main beam, yet quickly suppress the tails of the main beam to obtain good signal-to-noise ratios in the scattering regime. We investigate here the possibility of extending the low-q limit at a pulsed source with a SANS instrument based on two Soller slit [2] packages - one as a collimator, the other as an analyzer, as shown in Figure 1. Soller slits are alternating sheets of transmitting and absorbing layers. They are insensitive to wavelength and therefore take advantage of the full spectrum available at pulsed sources. The angular resolution of this instrument is determined by the correlation of the two slit packages (just as in the Bonse-Hart spectrometer). Time of flight is used to gate the detector in order to determine the energy resolution and q value at a particular 2θ offset angle of the analyzer slit package.

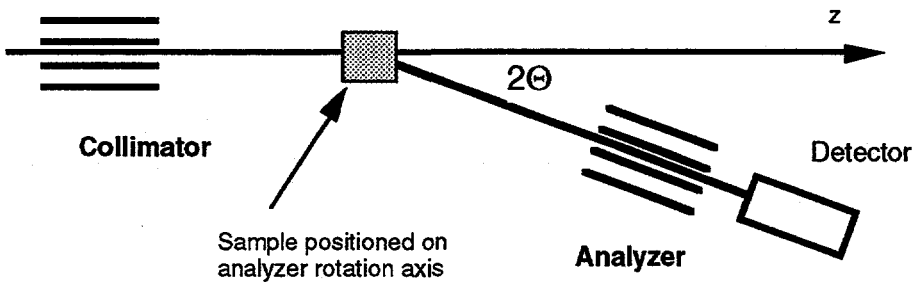

Figure 1. Schematic of an ultra small-angle neutron scattering instrument based on Soller slits.

Experiment

We performed Monte-Carlo simulations of the Soller slit ultra small-angle neutron scattering instrument on the IBM SP1 at the University of New Mexico. The geometry of our experiment is a circular source centered on the origin in the X, Y plane. The source is 5 cm in diameter as is a beam pipe of length 3m with long axis normal to the source and centered on the Z axis. The Soller slit packages are composed of alternating sheets of absorptive (thickness fixed in all calculations to 30 μm) and transmissive layers, both 3.5 cm in height and 15 cm in length. We chose an odd number of absorptive layers such that the central absorptive layer is centered on the Z-axis with its long direction along Z and the height along Y. The analyzer package is identical to the collimating package. For $2\theta = 0$ it has the same orientation as the collimator except that it is displaced along Z with a gap of 30 cm between the two packages. The analyzer package is rotated by an angle 2θ in the X, Z plane, about the sample position, midway between the two collimators.

The performance of a particular instrument geometry is tested as 2θ scans. At every 2θ point, 10^6 'neutrons' are created each with random r ($0 \le r \le 2.5$ cm) and ϕ ($0 \le \phi \le 2\pi$) in the plane of the source and random azimuthal angle θ ($0 \le \theta \le 2.5/300$). The X and Y coordinates of each neutron are calculated at the entrance and exit of each of the collimators (Z = 3.0 m, 3.15 m, 3.45 m, 3.60 m). Those that 'hit' an absorber or fall outside of the slit package are eliminated. Data is reported as number of neutrons passing through both collimators for each point in 2θ.

Results and Discussion

Figure 2 illustrates the trade-off of intensity with resolution. Each point represents a simulation with fixed Soller slit package dimension of 3.5 x 3.5 x 15 cm, but with varying thickness and therefore number of transmissive slits. Narrow transmissive slits yield high angular resolution and lead to low minimum q at a cost in overall transmission through both slit packages at $2\theta = 0$.

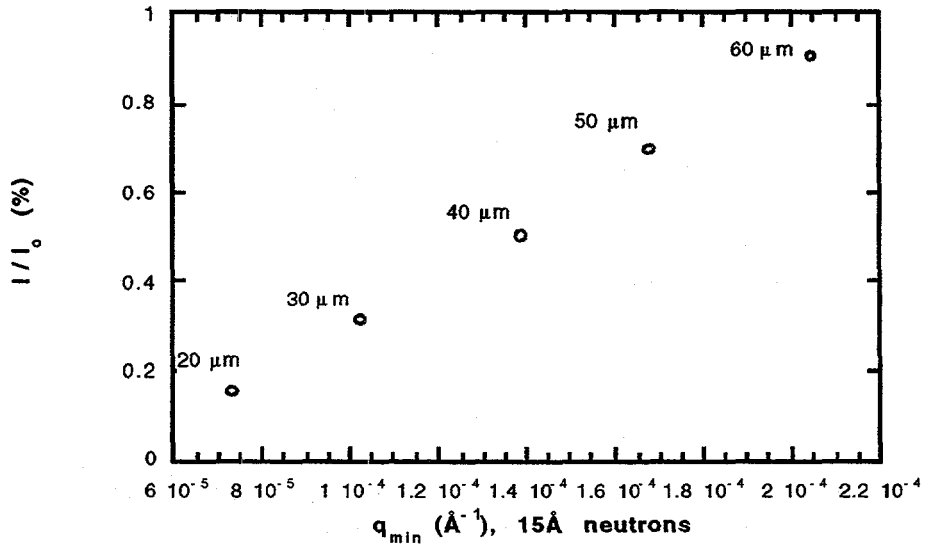

Figure 2. Percent transmission (I(2θ=0) at detector/10^6) vs. q_{min} (for 15Å neutrons and 2θ chosen as I(2θ=0)/10).

Figure 3 shows how the beam profile varies as the number of slits increases.

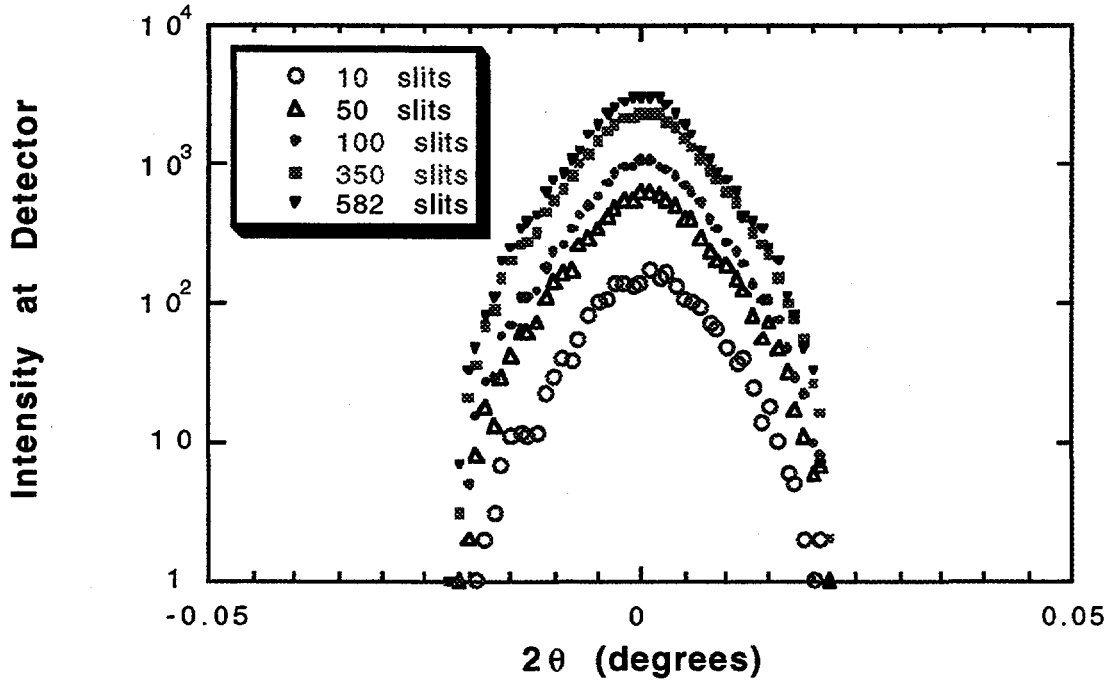

Figure 3. Beam Profiles. Intensity vs. 2θ for 10, 50, 100, 350, and 582 transmissive slits each 30 μm in width.

Practical considerations

Soller slits for neutron optics can be fabricated from Si sheets (transmissive layers) coated both sides with thin films of boron. Small angle scattering within the transmissive layers and reflectivity from the interfaces between absorptive and transmissive layers need to be suppressed. Single crystal silicon should yield no SANS. To avoid reflectivity, the boron needs to be index matched to the silicon. Fortunately, the coherent neutron scattering length of Si (b = 4.155 fm) lies between that for natural boron (b=5.3 fm) and B^{10} (b=-0.2 fm) making index matching possible.

Conclusions

To achieve low-q resolution on the order of 1e-4 $Å^{-1}$, the transmission through both collimators (2θ = 0) is a few tenths of a percent of the incident flux. While this is a substantial reduction, it is partially offset by the ability of the instrument to accept the entire neutron spectrum. Time of flight makes it possible to collect a range of q values at fixed 2θ.

Acknowledgments

The authors wish to thank Roger Pynn of the Los Alamos Neutron Science Center for suggesting the problem. And Ferenc Mezei of the Berlin Neutron Scattering Center, Berlin, Germany, for helpful discussions. This work supported by the United States Department of Energy under contract DE-AC04-94AL85000.

References

[1] See q-ranges quoted for LANSCE and IPNS; http://www.lansce.lanl.gov and http://pnsjph.pns.anl.gov, respectively

[2] See general scattering texts such as G.E. Bacon, Neutron Diffraction, Oxford University Press, NY, NY, 1975.

[3] W. Nistler and R. Scherm, Praktische Physik Vol. 3, ed. Kohlrausch, p 275, 1986.

Optical Polarizing Neutron Devices Designed for Pulsed Neutron Sources

M. Takeda, K. Kurahashi, Y. Endoh and S. Itoh*

Physics Department, Graduate School of Science, Tohoku University, Sendai 980-77, Japan
*Booster Synchrotron Utilization Facility, National Laboratory for High Energy Physics, Tsukuba 305, Japan

Abstract

We have designed two polarizing neutron devices for pulsed cold neutrons. The devices have been tested at the pulsed neutron source at the Booster Synchrotron Utilization Facility of the National Laboratory for High Energy Physics. These two devices proved to have a practical use for experiments to investigate condensed matter physics using pulsed cold polarized neutrons.

Introduction

Polarized neutrons are now widely used for condensed matter physics, especially in magnetism. However, compared with unpolarized neutrons, polarized neutrons have not been used extensively in experiments. This is mainly because more than a half of incident neutrons from sources are wasted by a polarizing device. Therefore, it is necessary to have more intense neutron sources and better polarizers for polarized neutron technique to be more popular for experiments. Plans to construct intense neutron sources have been proposed worldwide, and some have made progress. We have designed two polarizing devices using supermirrors for pulsed neutron sources based on e present configurations. One is a polarizing neutron guide (PNG) [1] and another is a polarizing beam-splitter (PBS) [2] by which polarized neutrons are introduced into two different beam lines from one beam line. Such devices have been used quite practically at the reactor based neutron sources, HMI, ILL and LLB, but never at pulsed neutron sources. We have already reported the performance of these devices [3-4]. This is a brief report on tests of PNG and PBS.

(a) Polarizing Neutron Guide (PNG)

The polarizing neutron guide was assembled by CILAS. It consists of a straight natural Ni guide tube with a beam cross section of 20 ×50 mm and 28 Fe/Si polarizing supermirrors. The mirrors form a V-shape in the guide tube from the top view, which cuts the total length of PNG in half compared with a straight alignment. The Fe/Si supermirror has a different critical momentum transfer value, Q_c^+ for + neutrons and Q_c^- for – neutrons, under which the total reflection of neutrons occurs according to each spin state. Here the "+" expresses neutron spin parallel to the magnetization of the supermirrors, and "–" opposite. The difference makes it possible to filter the + neutrons by the total reflection and produce polarized neutrons with – spin going through the supermirrors in the Q range between Q_c^+ and Q_c^- as shown in Fig. 1(a). In the case of Fe/Si supermirrors, Q_c^- is the same as Q_c of Si substrate, Q_c(Si), and cannot be artificially changed. On the other hand, Q_c^+ can be controlled by evaporation sequence to same extent. Therefore, as we have a larger Q_c^+, we have a wider wavelength band of polarized neutrons available. Mirrors of 1.6 Q_c(Ni) were used in PNG where Q_c(Ni) is the critical momentum transfer of natural Ni. The horizontal beam width of 20 mm and the Q_c^+ define the total length of PNG of 1200 mm and the incident angle of neutrons to the mirrors of 0.5 degrees. Under these conditions, polarized neutrons in the wavelength band of 3-10 Å are theoretically available.

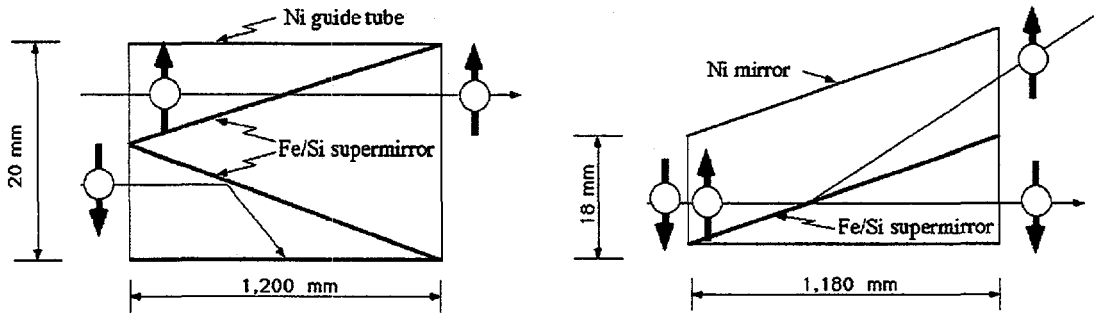

(a) Polarizing Neutron Guide (b) Polarizing Beam- Splitter

Fig. 1 Schematic representation of the Polarizing Neutron Guide (a) and Polarizing Beam-Splitter (b)

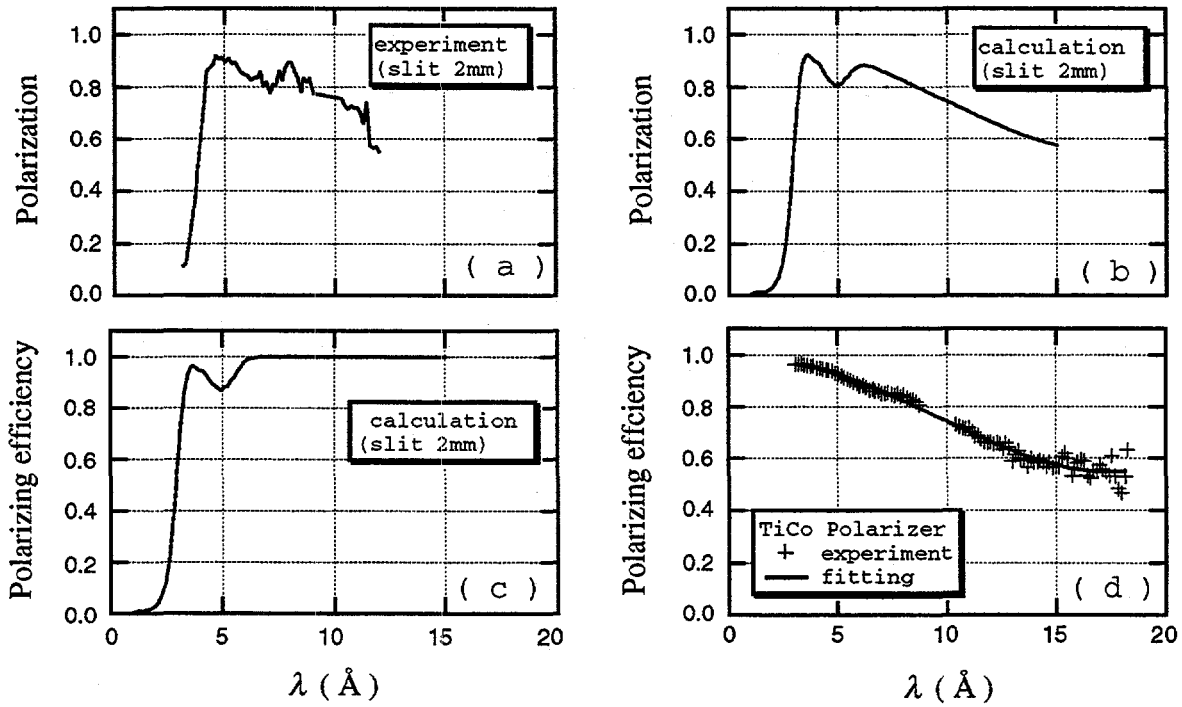

Fig. 2 (a) Observed and (b) calculated polarization of neutrons polarized by PNG. (c) and (d) are polarizing efficiencies of PNG and the Co/Ti spin analyzer, respectively.

PNG was mounted on the TOP spectrometer at the pulsed neutron source in the Booster Synchrotron Utilization Facility of the National Laboratory for High Energy Physics (KENS) by
replacing the end section of C3 cold neutron guide tube [5]. The C3 guide tube's beam cross section is 20 ×50 mm and curved has an actual cutoff wavelength of 3 Å. A polarizing The TOP Soller guide of Co/Ti supermirror was used as a spin analyzer, and a two-coil spin flipper was employed to determine polarizing efficiencies of PNG. A magnetic field of 200 Oe was applied to the supermirrors to saturate their magnetizations by ferrite magnets. Unpolarized neutrons, with the natural collimation of the C3 guide tube, were introduced to PNG, and transmitted neutrons were collimated by two pairs of horizontal slits between PNG and the analyzer. The intensities of outgoing neutrons were counted by a one dimensional position sensitive detector (PSD) system, however, intensities at all positional channels of PSD were summed up at each

TOF channel in these measurements. Polarizations of neutrons, $P(\lambda)$, were obtained by two intensities at each wavelength, $T^+(\lambda)$ and $T^-(\lambda)$, using the following expression,

$$P(\lambda) = \frac{T^-(\lambda) - T^+(\lambda)}{T^-(\lambda) + T^+(\lambda)} \qquad (1)$$

Here $T^+(\lambda)$ represents intensities when the spin flipper was activated and $T^-(\lambda)$ when it was not. Figure 2 (a) and (b) show the observed and calculated wavelength dependence of polarizations in the case of horizontal beam collimation of 0.06 degrees. The observed polarizations are the product of polarizing efficiencies of PNG itself by that of the Co/Ti analyzer. The calculated curve in Fig. 2 (b) was deduced by product of calculated PNG's efficiencies in Fig. 2 (c) by that of the analyzer measured in the other experiment as shown in Fig. 2 (d). In the calculation the standard matrix method was used to determine reflectivity and transmissivity of PNG [6], and experimental resolution was taken into account but absorption effect was ignored. Figure 2 indicates that the gradual decrease of polarization with increasing wavelength is not due to PNG but the analyzer. Therefore, it can be concluded that the polarizing efficiencies of PNG keep the values higher than 90% in the wavelength band of 3-9 Å. We have not directly measured the transmission of PNG. To compare with the Co/Ti analyzer, PNG provides twice as many polarized neutrons at the sample position of TOP (estimated by measurement of intensities of incoherent scattering of light water at the sample position).

(b) Polarizing Beam-Splitter (PBS)

In the case of PNG, neutrons with one spin state are used for experiments, and neutrons with the other were thrown away. PBS is intended to use both spin states of polarized neutrons. The + neutrons in the Q range between Q_c^+ and Q_c^- are totally reflected by the mirror, while the – neutrons are transmitted through the mirrors. In the case of PNG, the reflected polarized neutrons are absorbed by boron glasses under the Ni layer of guide tube. If there were no Ni layer and the boron glasses, the reflected polarized neutrons would be separated away from the transmitted ones with a separation angle of twice incident angle to the mirrors, as schematically shown in Fig. 1 (b). Therefore, the supermirror has a possibility of providing polarized neutrons to the two different beam lines from one beam line, without loss of intensity.

PBS was manufactured by OSMIC, Inc. From the top view, it is shaped as a trapezoid in order not to disturb the reflected polarized neutrons. The area of exit, 36 ×50 mm, is twice as large as that of the entrance, 18 ×50 mm. Fe/Si polarizing supermirrors of 3 Q_c(Ni) are mounted on the line between the apex of the shorter side of the trapezoid and the middle point of the longer side. The incident angle is set to be 0.9 degrees in order to polarize neutrons of wavelength longer than 3 Å by the 3 Q_c(Ni) polarizing supermirrors. The angle and the horizontal beam width at the entrance (18 mm) make the length of PBS total 1180 mm

PBS has been mounted on the TOP spectrometer by replacing the end section of the C3 guide tube in the same way as PNG. The Co/Ti analyzer and the spin flipper again were used to determine polarizing efficiencies of PBS. As the incident angle of PBS was set to be higher than that of PNG, polarized neutrons in a wider wavelength band of 3-18 Å were available by using PBS rather than PNG. A magnetic field of 300 Oe was applied to the mirrors by the permanent magnets.

Figure 3 shows the wavelength dependence of polarizations of transmitted neutrons (a) and that of reflected neutrons (b) after correcting polarizing efficiencies of the analyzer. In the figures the

experimental data are plotted by open circles. The line denoted as $P_T(\lambda)$, calculated by the same procedures as PNG, completely reproduces the observation. This indicates that the transmitted neutrons have an excellent polarization in the whole wavelength band of 3-18 Å. On the other hand, the deviation between the calculated curve, $P_R(\lambda)$, and the observation is very large for the reflected neutrons. This seems to be originated in the fact that the reflected beam is more divergent than transmitted one. Such a divergent beam effectively drops the polarizing efficiencies of the analyzer shown in Fig. 2 (d). The $P_R'(\lambda)$ is the calculated curve that takes into consideration the reduction of the efficiencies and contamination of unpolarized neutrons originated in geometrical configuration of experimental set-up. The correction greatly improved the simulation. The intensities of both transmitted and reflected beam were also well described by the calculation with the correction. These simulations show that the transmitted beam is well collimated and polarized but has less intensity, and that the reflected one is more divergent and less polarized but stronger than the transmitted one. The detailed procedures of these calculation appear in Reference 4.

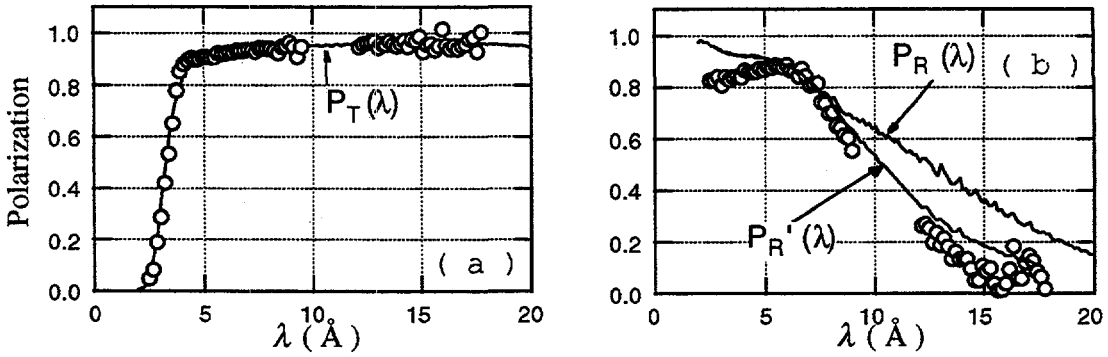

Fig. 3 Polarization of transmitted and reflected polarized neutrons produced by PBS.

Conclusions

We have made two polarizing neutron devices for the pulsed cold neutrons and investigated their performances. Comparison of experimental results of polarizing efficiencies of PNG with the simple calculation reveals that PNG has a good polarizing efficiencies, higher than 90% for the wavelength band of 3-10 Å. The polarizing efficiencies of transmitted polarized neutrons through PBS were also well reproduced by the simple calculation and keep excellent efficiencies higher than 95% in the whole wavelength band of 3-18 Å. That the reflected polarized neutrons have much less polarization can be well understood by the assumption that the reflected beam is more divergent than the transmitted ones. This indicates that the transmitted beam is suitable for experiments in which well-collimated polarized neutrons with high polarization are required. On the other hand, "reflected" neutrons are more intense than the "transmitted" one. Thus the reflected polarized neutron may be used for the experiments that require more intensity.

Acknowledgements

We would like to thank Professors H. Sugawara, M. Furusaka, H. Ikeda and N. Watanabe for illuminating discussions. One of authors (M.T.) extends thanks to Dr. K. Yamada for providing the opportunity to attend this workshop. This work was supported by Grant- in- Aid for Scientific Research (A) (No. 05402011) , (B) (No. 07554055) and (C) (No. 06640463) from the Ministry of Education, Science and Sports and Culture.

References

1. F. Mezei, *SPIE* **983**, 10 (1989).
2. Th. Krist et al., *Physica* **B213&214**, 939 (1995).
3. M. Takeda, K. Kurahashi, Y. Endoh and S. Itoh, *Proceedings of International Symposium on Neutron Optics and Related Research Facilities*, held in Research Reactor Institute, Kyoto University, 19-21 March, 1996, pp. 234-237.
4. S. Itoh and M. Takeda, *ibid*, pp. 199-202.
5. S. Itoh, T. Watanabe and Y. Endoh, *Proceedings of ICANS-XI*, held at National Institute for High Energy Physics, 22-26 October, 1991, pp. 797-780.
6. M. Born and E. Wolf: *Principles of Optics*, (Pergamon Press, Oxford, 1970).

A NEW CLASS OF NEUTRON DETECTORS

J. Bart Czirr
Photogenics Inc.

Abstract

An optimized neutron scattering instrument design must include all significant components, including the detector. For example, useful beam intensity is limited by detector dead time; detector pixel size determines the optimum beam diameter, sample size, and sample to detector distance; and detector efficiency vs. wavelength determines the available energy range. As an example of the next generation of detectors that could affect overall instrumentation design, we will describe a new scintillator material that is potentially superior to currently available scintillators. We have grown and tested several small, single crystal scintillators based upon the general class of cerium-activated lithium lanthanide borates. The outstanding characteristic of these materials is the high scintillation efficiency--as much as five times that of Li-glass scintillators. This increase in light output permits the practical use of the exothermic B (n, alpha) reaction for low energy neutron detection. This reaction provides a four-fold increase in capture cross section relative to the Li (n,alpha) reaction, and the intriguing possibility of demanding a charged-particle/ gamma ray coincidence to reduce background detection rates. These new materials will be useful in the thermal and epithermal energy ranges at reactors and pulsed neutron sources.

INTRODUCTION

Four exothermic neutron capture reactions dominate the low-energy neutron detector field: ^{3}He (n,p)T, ^{6}Li (n,α) T, ^{10}B (n,α) ^{7}Li, and Gd(n,gamma). The ^{3}He reaction utilized in gaseous proportional counters has been the most popular system for several decades, but Li based scintillators have begun to supplant these detectors at both reactors and pulsed sources. Aside from BF_3 proportional counters, no practical ^{10}B-based detectors have been available. This is unfortunate, because the ^{10}B (n,α) reaction possesses several advantages over the other reactions, namely the capture cross section of ^{10}B is 4.1 times that of ^{6}Li. The maximum range of the ^{10}B charged reaction products is 4 microns vs 40 microns for ^{6}Li. This permits the use of thinner detectors and could also result in superior spatial resolution in some situations. The 478 keV gamma ray that is emitted in 94% of the capture reactions in ^{10}B can be utilized as a coincidence signal to greatly reduce the effects of ambient gamma background. A condensed state ^{10}B detector will be much more efficient in thin layers than gaseous detectors.Edge effects are greatly reduced in solid detectors.In scintillator form, the ^{10}B detector recovery time can be much shorter than that of proportional counters.

The primary characteristic that has inhibited the use of ^{10}B-based scintillators is the low scintillation efficiency of B-loaded organic scintillators. The high energy-loss rate of the heavy charged reaction products is particularly detrimental to the efficient production of scintillation light in aromatic or aliphatic organic scintillator solvents. For example, in BC-454 (plastic) the light output per unit energy for the combined alpha, ^{7}Li signal from ^{10}B capture is only 4% that of electrons of the same energy. Another measure of the seriousness of

this problem is that the light output for the ^{10}B reaction (2.31 MeV) is only 10% of that for the ^{6}Li reaction (4.79MeV), both in liquid organic scintillators.

TECHNICAL RESULTS

In light of the significant advantages attached to the ^{10}B reaction, it seemed useful to search for a B- based scintillator with greatly improved scintillation efficiency. The lithium lanthanide borates have been reported in the literature as a class of stoichiometric laser materials which can incorporate three of the popular neutron absorbing nuclei: B, Li and Gd. When activated with Ce^{3+}, these materials achieve a remarkably high scintillation efficiency compared to organic scintillators. Table 1 lists the relative signal size of $Li_6Gd(BO_3)_3(Ce)$ compared to the three most efficient competing materials. In addition, the estimated absolute number of detected photoelectrons in a typical PM tube is shown for the three reactions of interest. These latter numbers are based upon the assumption that the number of detected photoelectrons from GS-20 glass scintillator is 960 per MeV of electron energy deposited. The observed factor of five improvement (over GS-20) in scintillation efficiency for the ^{6}Li reaction just compensates for the factor of five decrease in light output from ^{6}Li to ^{10}B in the borate scintillator. The result is that the signal size from the present sample of $Li_6Gd(BO_3)_3(Ce)$ upon ^{10}B capture equals that of GS-20 for ^{6}Li capture. This result should provide a practical, good-pulse-height-resolution signal for many applications.

Table I
SCINTILLATOR COMPARISON
RELATIVE PULSE HEIGHT

MATERIAL	$^{10}B(n,\ddot{a})$	$^{6}Li(n,\ddot{a})$	Gd(n,gamma)
$Li_6Gd(BO_3)_3$	1.0	1.0	1.0
BC-454 (plastic)	0.12	---	---
GS-20 (glass)	---	0.20	---
GSO (crystal)	---	---	0.67

	PE/ neutron	PE/ neutron	PE/ MeV gamma
$Li_6 Gd(BO_3)_3$	1450	7060	3390

PE = Detected photoelectrons in PM tube.

Table II
DETECTOR OVERVIEW

COLD 10meV	THERMAL 150meV	EPITHERMAL
	$^{7}Li\ Y\ ^{10}B$	$^{7}Li\ Gd\ ^{10}B$
^{3}He	$^{6}Li\ Y\ ^{11}B$	$^{6}Li\ Gd\ ^{11}B$
$Zn\ S\ (^{6}Li)$	^{3}He	$Zn\ S\ (^{6}Li)$
	$Zn\ S\ (^{6}Li)$	^{6}Li glass
	$^{7}Li\ Gd\ ^{11}B$	

Li Ln B = $Li_6\ Ln\ (BO_3)_3\ (Ce)$

An overview of present detectors and potential applications of the new materials is shown in Table II. The Li_6 Y $(BO_3)_3$(Ce) version of the detector is designed to increase the efficiency below 150 meV by replacing the competing high cross section Gd with Y. The various materials listed illustrated the versatility obtained by interchanging the various isotopes and chemical species.

The best Y based scintillator to-date is only 1.3 times that of GS-20, but as shown in Table III, the decay time is shorter than that of the Gd based material. Table IV lists the calculated efficiencies for three materials of interest. The efficiency for the two borates refers to the $^{10}B(n,\alpha)$ reaction. The effect of replacing gadolinium with low cross section yttrium is evident at low energy.

Table III

MATERIAL CHARACTERISTICS

^{6}Li-Glass	$Li_6Gd(BO_3)_3$	$Li_6Y(BO_3)_3$	
Relative Signal Amplitude ()	1.0	5.9	1.3(powder)
Atomic Density (X 10^{22} atoms cm^{-3})	1.72 (^{6}Li)	3.30 (^{6}Li)	3.30 (^{6}Li) 1.65 (^{10}B) 1.65 (^{10}B)
Macroscopic Cross-Section (cm^{-1}) (at thermal)	16.1 (^{6}Li)	63.3 (^{10}B)	63.3 (^{10}B)
Density (gm cm^{-3})	2.5	3.5	~2.8
Capture Peak, Electron Energy Equivalent (MeV)	1.47 (^{6}Li)	2.2 (^{6}Li) ------- 0.47 (^{10}B) -------	
Alpha-to-Beta Ratio 0.23	0.34	-------	
Signal Decay Time (ns)	70	200,700	100

Table IV

CALCULATED EFFICIENCIES* FOR NEUTRON CAPTURE

Neutron Energy (eV)	^{6}Li-Glass (GS-20) (%)	$Li_6Gd(^{10}BO_3)_3$ (%)	$Li_6Y(^{10}BO_3)_3$ (%)
0.0254	79	19	99.8
0.10	54	38	96
0.15	47	57	92
0.20	42	68	89
1.00	22	63	63

*All materials are 1.0 mm thick

Figure 1 shows the pulse height spectrum obtained from a thermal neutron irradiation of $Li_6Gd(BO_3)_3$(Ce). The peak near channel 400 is due to the ^{6}Li (n,α) reaction and that near channel 80 from $^{10}B(n,\alpha)$. The modest observed resolution is probably the result of imperfections in the small single crystal available.

Figure 2 shows the pulse height spectrum obtained from a NaI (Tl) well-type detector that surrounds a 6 cm^3 block of BC454 boron-loaded plastic scintillator. The system was irradiated with thermalized neutrons from a Cf source. The peak near channel 200 represents the full energy peak for the 478 keV gamma rays from ^{7}Li* de-excitation following the ^{10}B (n,α) reaction. No coincidence was required.

Figure 3 shows the result of requiring a coincidence with the ä +^{7}Li signal in the plastic scintillator. The large improvement in background suppression is seen. (The 100 channel shift in the peak position is due to electronics abnormalities).

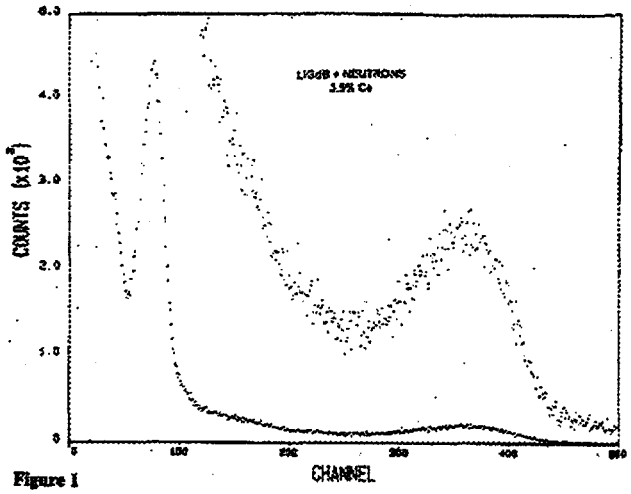

Figure 1

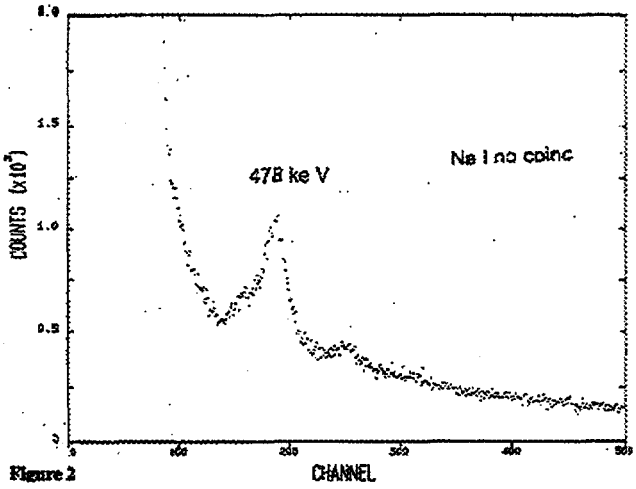

Figure 2

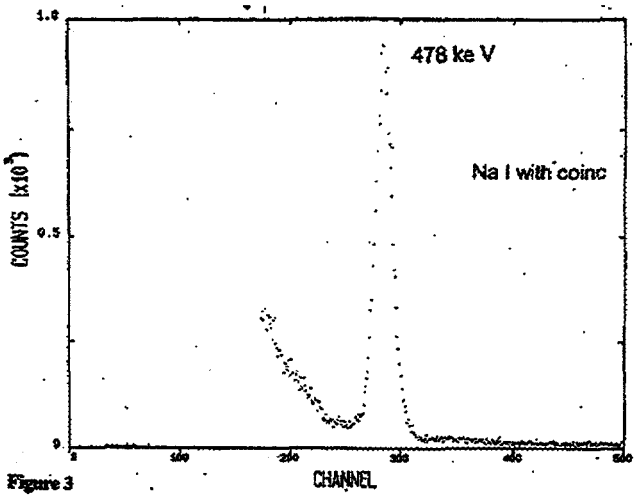

Figure 3

SUMMARIES

Roger Pynn:
Firstly, I would like to thank Rex Hjelm and the others on his team for organising this meeting. I think it was a good idea to assemble the community of designers of neutron spectrometers and discuss how we might make progress in a field which still seems to be need artisans to a much larger extent than many other fields of science.

As several speakers have stressed during this meeting, we design neutron spectrometers to learn something about condensed matter, and the adequacy of our design depends very strongly on what we are trying to learn. Because neutron sources are so feeble, a single type of neutron scattering spectrometer just will not serve all our needs, even though all we ever do is measure S(Q,E) over some appropriate dynamic range, with an appropriate resolution and statistical precision. As we all know, we are often forced to trade one "appropriate" variable against another to get data of the quality that we need.

Nevertheless, the world has changed in a way that makes some of the trade-offs we used to make redundant. In the early days of neutron scattering, Brockhouse invented the constant-Q scan as a way of collecting the data he needed in a serial fashion. Although he did not have some of the technology that he would have needed to collect data in parallel channels - such as position sensitive detectors and multi-crystal analysers - one of the most serious limitations Brockhouse faced was the complexity of interpreting parallel data channels. As a graduate student, I took inelastic scattering data with a cold-neutron time-of-flight spectrometer at Harwall using a large (150 cm^3) single crystal of magnesium. Like all TOF machines, the spectrometer recorded many channels of information in parallel. But because I didn't have sufficient computing power at my disposal, those parallel channels took a long time to process. I remember drawing scattering curves by hand on large pieces of graph paper and interpolating between phonon peaks. If I was lucky and waited until 2 am, I could get the entire Cambridge University computer to myself for an hour or so each night to analyse my data. 120 kilobytes of bulk store all to myself!

Modern computers have to a large extent made serial data accumulation a part of the history of neutron scattering. We can now think of neutron scattering as a technique for obtaining large quantities of information that we can mine with a PC to extract the data we need. Instead of spending 70% of an experiment looking for a window within which to observe a phenomenon of interest, we can now accumulate data, analyse and display it in real time, and plan our experimental strategy to maximise the information output. Unfortunately, in many cases our thinking about neutron scattering instrumentation has not kept pace with this computer revolution and we are still doing many things that are not optimal.

If you ask yourself how we design new neutron scattering spectrometers, I think you will find that we usually base them on what we have done in the past. We have rules of thumb which represent the wisdom distilled from our own mistakes and those of our predecessors. Dick Deslattes from NIST has pointed out that complex experiments never work until you have made all the mistakes that stand in the way of success. A corollary is that the only variable you have at your disposal to reach success is the speed with which you can make mistakes! That is why I am such a fan of computer simulations - they allow us to make mistakes quickly and without having to pay the price we used to have to pay for hardware that didn't quite work as we thought it should. I understand and accept all of the caveats that Kent Crawford and others have told us about - that we need to do analytical calculations to gain full understanding and that a simulation is only as good as the imagination of the scientist who defined the universe within which it operates. But, nonetheless, I believe that we are at the beginning of a new era of instrument design. One in which we will be able to simulate not only optics but also background sources. One in which we will be able to teach new graduate students to design instrumentation without forcing them to make the sort of expensive mistakes some of us have had to make in our time. And as the computer tools become more sophisticated, I am quite sure they will lead us to new ways of using neutrons for scattering experiments. We saw here, for example, in Roland's elegant talk, how to think about resolution in

real space and time instead of in the traditional reciprocal and energy space. This makes me wonder what one can learn by imposing more sophisticated spatial and angular correlations on neutron beams than we have done in the past. It is hard for me to think this through in any but the simplest circumstances, but it is trivial to simulate. Of course, all the simulation does for me is make me think about concrete results rather than generalities. It does not relieve me of the need to think. It just gives me something to think about. I claim this is a real advantage.

Of course, as John Copley and others have told us, we need to be careful how we develop and use simulation tools as a community. We will need to include all the right disclaimers. If we do not put in all of physics, we will not get complete answers. That is obvious to us now, but I would hate to have to explain to someone who relied on a simulation package that he or she should not have omitted neutronic shielding from their spectrometer even though the simulation did not indicate the need for such shielding!

As an example of the sophistication that is needed in simulations, let me come back to an issue that I briefly mentioned in a discussion period - surface roughness. If you want to use focusing mirrors as optical elements in a neutron spectrometer, you will need to consider carefully the effect of surface roughness. "Carefully" in this context means that you will need to consider not only the distribution of heights of the true surface with respect to an ideal flat surface, but also the length scales parallel to that ideal surface. The effects of "roughness", "waviness", and "misoriented facets" on the angular distribution of neutrons diffusely scattering from a focusing mirror are quite different and all need to be included in a simulation.

Another issue which I find quite confusing is the notion of "resolution". We are all used to thinking of this as a single number, basically because most of our calculations are done in the Gaussian approximation and it only takes one number to specify the width of such a function. We are all used to applying the Central Limit theorem to the "matching" of various contributions to the resolution, again because it clearly pertains when we are dealing with many contributions that are roughly Gaussian or triangular in shape. But what happens when transmission function of one of our spectrometer components is very asymmetric in some direction? Should we really be using the standard deviation to match various resolution elements of the spectrometer? I think Devinder Sivia clearly showed us examples where this is not the right thing to do. The intriguing thing is whether we can make improvements to our ability to retrieve information by deliberating using the asymmetry of some relevant functions, such as the time distribution of neutrons escaping from moderators at a pulsed spallation source.

Finally, I would like to stress my strong support for widespread collaboration on the design of new neutron scattering spectrometers. No facility has the opportunity to design and build many spectrometers per decade. They are just too complex and expensive. We just have to make sure that each time we build a new instrument it collects more information (measured as Mike Johnson told us, in "bits") than any neutron spectrometer that has been built previously to study similar science. I do not believe this is possible unless we pool our knowledge and collaborate to develop new tools - hardware and software. For this reason, I hope this conference will be the first of many that discuss ever more sophisticated approaches to the design of neutron scattering spectrometers.

Kent Crawford:

I would like to indicate my own ideas of what are some of the needs that have emerged from this workshop. This idea mentioned by Roger Pynn of perpetuating the knowledge base is very important and has various aspects. One of the most important of these is the rules-of-thumb that Roger mentioned frequently. Those are not written down anywhere. If we could get some mechanism for compiling those in an accessible form, I think that would be useful, not only to ourselves but to the people who follow along after us for designing instruments. Probably of lesser importance, but I think still useful, would be some sort of a centralized bibliography of relevant information.

One of the things that I feel fairly confident about is that it is going to be a long time before we are able to calculate everything that we need to know about instruments, so we are always going to have to have some places to do some testing. I urge strongly that we make every effort to preserve some beam lines in some various places to do these kinds of things.

A lot of the discussion has been associated with what might be done to improve Monte Carlo. I think it was quite clear that if we could incorporate some 3-D visualization it can make the Monte Carlo considerably more useful. The little bit that Frans Trouw showed us about how one might consider applying visualization capabilities was very intriguing.

We need a way of getting an easy definition of the geometry for the Monte Carlo codes. I am not quite sure what is the right way, but it has to be something that is user friendly and that doesn't take an expert in the program in order to use it. One thing that occurs to me is that there are a lot of solid modeling programs of one sort or another out there. Can one use those to define the geometry, say in something like a CAD program or other modeling program, and then output this geometry to the Monte Carlo program? Instruments are ultimately designed with a CAD program, so it would be nice to get the geometry from that.

Can the various code modules be defined to match more or less the physical modules that one would think of in an instrument. If you can do that, than it is an easy cut and paste operation to piece together the model for an instrument with different kinds of components.

The Monte Carlo code should be fast. I do not know whether the codes we have right now are fast enough. Maybe the computers will get fast enough to make that a non-issue.

It probably is important at some stage in this that we get some professional programming help. The neutron-scattering scientists are good at working out the physics that goes in these codes, but they are not, for the most part, particularly knowledgeable about how to make a good user interface for codes. For that I think it is important to get someone who is more in that line of work.

Finally, once these codes are working, it is important to benchmark them against some actual measurements. I think that would give everybody a lot more confidence that what we are calculating is correct.

New Challenges for Computational Evaluation of Neutron Scattering Instrument Performance.

F. Mezei, BENSC, Hahn-Meitner-Institut, Glienicker str. 100, 1409 Berlin, Germany

It has been slowly but generally recognized by now that, compared to fission reactors, spallation offers the superior method of neutron beam production for the whole of neutron scattering research. This change of technology, incidentally, also requires the complete redefinition of the ground rules for projecting neutron scattering facilities, namely the replacement of linear, step by step design by a *global system optimization*. Indeed, in the early days, neutron scattering activities were kind of "parasitic" on research reactors conceived, operated and financed for other use. The advent of a very few research reactors built for the primary purposes of neutron scattering work did not change much the process of project planning: The reactors could be fundamentally designed for providing the best thermal flux in the reflector region, i.e., optimized for a single parameter. All the rest was linearly added on, with little feedback on the fundamental design of the active zone of the reactor. For example, had the installation of a cold source cost a sum comparable to the construction costs of the reactor itself (in reality it is far from that), one would have to carefully weigh the advantages offered by cold neutrons against the necessary reduction of the reactor power and the thermal flux under boundary conditions, such as constant total costs or best cost- to-benefit ratio. Cold and hot sources could also be added to these reactors without detailed consideration of the instruments to be built, since the user requirements could simply be specified by "best flux at a given Maxwellian temperature." The linear adding-on approach has also been the rule when the current spallation sources were built. All of them have been based on recycled nuclear physics accelerator facilities, and this approach has determined many of the technical possibilities. However, the choice of the target station, and in particular that of the moderator, has involved an unprecedented amount of analysis of the variety of instrumental requirements. The current result is the definition of only a few canonical kinds of moderators, and the instruments are basically just added on to the predetermined best suited beam.

In contrast, let us project to one of the future, green field spallation sources dedicated to neutron scattering research. In trying to *fulfill the compulsory "best value for the money" requirement,* we are forced to reconcile items such as the choice of the ion source against fine details of instrumental response functions. The fundamental reasons for this are, of course, financial in all respects, and technical in some. For example, the variety of parameters characterizing the output of the proton accelerator system, (such as time averaged and peak beam power, beam energy per pulse, and pulse duration, (in contrast to the single crucial parameter, thermal flux in the reflector of a reactor) cannot be independently determined under the assumption of a given total budget. Thus, duration pulses of a given energy cost about twice as much to produce than ms long pulses of the same energy. So we end up, in this respect, with the choice between several-times-higher-energy long pulses, or more instruments that directly utilize short pulses. Making this choice requires weighting the merits for the whole scientific community of those instruments favored by higher energy pulses, against those favored by the short duration pulses. This has to be accomplished well before the accelerator goes to the final design stage. This means that now we are faced with early decisions which can only be accomplished with rather exact knowledge of the performance of the whole facility in experimental use; i.e., in contrast to past practice, we cannot proceed by linear adding-on in steps, building on the previous ones without fundamental feedback. The global system optimization we need to do requires a fairly exact *global "flight simulation"* to be available *well before any basic design choices* can properly be made. This is a new and most important challenge for the theoretical, "first principles" computational evaluation of neutron scattering instrument performance.

Before turning to the question of global optimization and an illustration that examines aspects of a specific example, let us consider a number of additional good reasons for trying to calculate the response of a neutron scattering instrument with high accuracy and reliability. The most important ones would include the following:

a) for optimizing the layout of an instrument,
b) for testing new ideas in instrument design,
c) for planning an experiment,
d) for evaluating an experiment.

The reason is quite obvious why, for all these purposes, a sufficiently exact knowledge of the behavior of a given instrumental setup is of crucial importance. On the other hand, a computational evaluation of a given instrumental configuration –analytical or via Monte Carlo simulation–played, up until now, a distant second role behind experiments performed using standard samples or a trial-and-error approach. The very well justified reason for this is the inferior precision and reliability of the calculations, compared, e.g., to a calibration run with a well known sample, such as Vanadium for incoherent elastic scattering. This lack of precision is due to two main factors: On the one hand, the complexity of the problem involving many dozens of parameters for the exact description of an instrumental configuration (such as monochromators, collimators, choppers, diaphragms, windows, detectors, shielding materials, air, etc., etc.). On the other hand, these parameters can only be known with a finite precision, and actually can vary with time, particularly in relation to detector efficiency. I would like to emphasize that, in any case, the calculation of the background neutron counting rate is to be excluded as a hopeless task, since in contrast to the incoming and scattered beams, we have no detailed knowledge of the trajectory of the neutrons counted in the background. (Note that this also applies to neutrons scattered both on the sample and on some structural components of the spectrometer, such as parts of the cryostat around the sample, while multiple scattering within the sample can be fairly well evaluated.)

The secondary role that instrument performance computation played in the past can be expected to change gradually. This is, without doubt, partially due to the evolution of the power of easily accessible computers, but there are other factors, too, which are related to neutron scattering techniques themselves. One such obvious aspect is the practical impossibility of doing more than a limited amount of "trial and error" experimental search on a large, expensive facility. In neutron scattering the most relevant trials only follow each other with several-year intervals, when a new instrument is built somewhere or an old instrument is refurbished. The spectacular progress of instrument performance in the past decades was as much due to learning from the shortcomings of the previous trial as to the introduction of materially improved components. With the increasing complexity of our instruments, (e.g., due to the simultaneous data collection in a large number of detectors), the feasibility of conventional trial and error instrument "tuning" rapidly decreases and we have to rely more and more on combinations of extensive calculations and limited, strategic experimental validations. This complexity also makes the planning and conducting of experiments more difficult without computational assistance, so we actually need to develop "*computer aided experiment conducting*" techniques, especially with the widespread availability of CAD tools. This amounts to nothing less than building up codes that provide the "*virtual instrument*" equivalents to the real spectrometers in order to facilitate two things: the finding of adequate data collection strategies for optimal use of the valuable and never sufficient beam time, as well as the evaluation of the collected data. In this approach the standard calibration runs will serve as validation anchors, allowing the validation and tuning of the virtual instrument code to he precision that is today only achieved by direct normalization of sample spectra to standard runs.

The theoretical basis of this kind of instrument model calculation– our understanding of neutron propagation in instrument components and samples– is fundamentally perfect. This can appear to be a paradox: For the description of the scattering processes the neutron is treated as perfect plane

wave, while for the evaluation of its trajectory through the various instrument parts, such as collimators, choppers, etc., the same neutron is considered a point- like particle with infinitely well defined velocity. It is also crucial for the evaluation of multiple scattering effects to be able to follow the classical neutron trajectories within the sample between two quantum mechanical scattering events. As Roland Gaehler [1] reported at the workshop, he and his collaborators tried to remove this paradox by also describing the neutron propagation through the whole instrument as a wave mechanical phenomenon. They borrowed this approach from light optics, where it is inevitable. Critically examined, their results confirm the validity of the above conventional dual approach in neutron scattering (precise classical trajectories of point-like particles scattered as waves when interacting with matter), since the optical coherence lengths calculated for neutrons, although much larger than the neutron wavelengths, remain negligible compared to the geometrical dimensions characterizing instrument components (such as collimator slits).In view of the large number of parameters defining an instrument, it is quite obvious that a precise calculation of the response cannot be practically performed in an analytical fashion, and we will have to work with Monte Carlo (or eventually numerical integration) codes. This is, of course, the standard approach to calculating the neutron transport and beam characteristics of fission reactors and also of spallation sources. It has, nevertheless, to be stressed that "[It is] a deplorable tendency to substitute a 'code' for a theory, to substitute a display of many curves for a detailed *physical* understanding of the system." [2]. This is particularly valid in an effort to optimize the performance of a whole facility or even just major parts of it. The Monte Carlo codes we are concerned with are much too complex and require so much CPU time even for just one part of the total system (say reflector-moderator layout, as an example), that no automatic search of an optimum can be built into the code. One has to resort to a trial and error approach, by which some phenomenological or more or less vague analytical understanding is used as a guide for Monte Carlo testing of various configurations, in the hope that the process converges. This is prominently valid for the optimization of the of the whole spallation source facility, including accelerator, target station and instruments. It also has also to be stressed that the boundary conditions play a determinant role in any optimization process. One *crucial boundary condition is a clear definition of the scientific goal* to be fulfilled, which curiously appears to be the most vague part of the discussion of projects. The definition of this goal implies an analysis of the of the spectrum of expected utilization of the facility , along with the assignment of relative weights to the various applications. For example, a facility optimized under the assumption that small angle scattering is of no future importance, while powder diffraction on small elementary cell samples is the overwhelming interest, would have hardly anything in common with the one which is optimized under the opposite assignment of priorities.

The results of a set of detailed Monte Carlo simulation calculations [3] presented in Figs. 1 and 2 provide specific examples of the issues we are confronted with and the kind of answers we can get. Small angle neutron scattering experiments have been simulated for three "equivalent" instruments operating on three different sources, viz., a 5 MW 50 Hz short pulse spallation source (SPSS), an equal average power 25 Hz long pulse spallation source (LPSS), and a continuous reactor source with the flux of ILL. By "equivalent" we mean equal angular resolution at equal sample cross section and by using identical x-y detectors. In the pin-hole geometry assumed, this practically means equal sample to detector distances (9 m in the examples) with matching incoming collimation paths. On the pulsed sources the whole instrument was supposed to be outside a 6 m-thick bulk shielding. On the pulsed sources the wavelength was determined by the time of flight, assuming a coupled cold moderator, a t_0 chopper and three wavelength band definition/frame overlap disc choppers (all choppers outside the bulk shielding). On the continuous source a 10 % FWHM velocity selector was assumed.

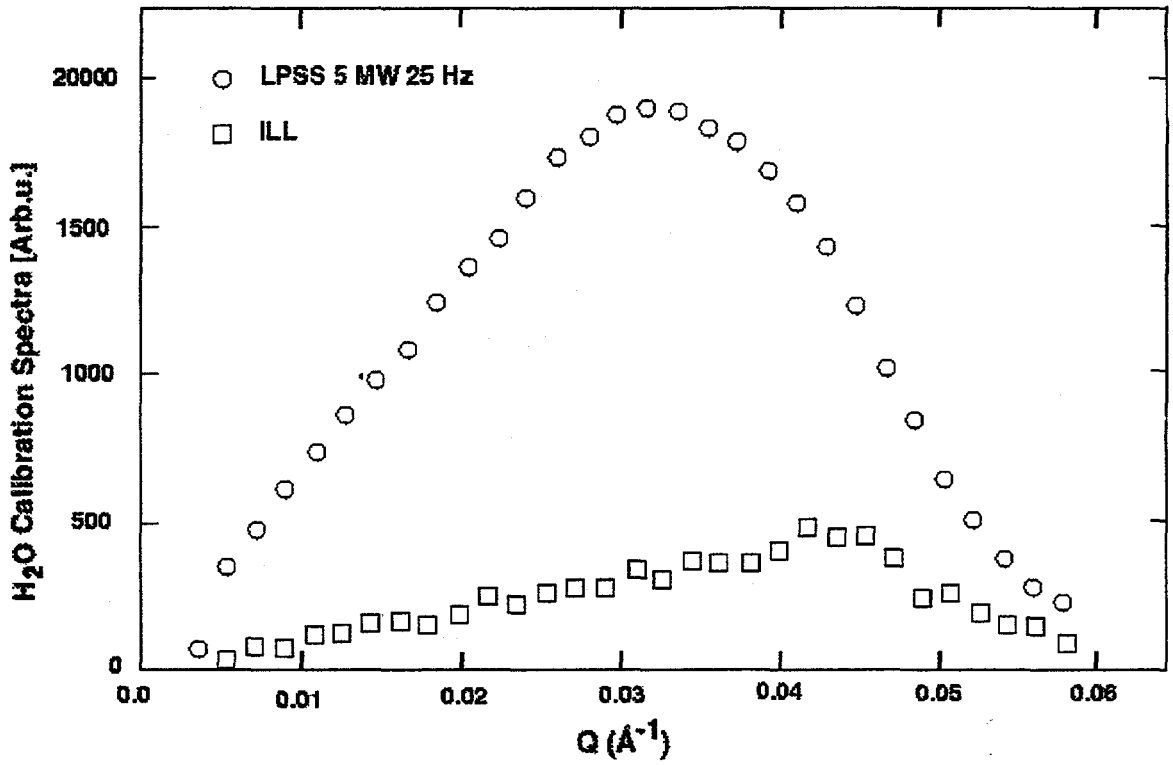

Fig. 1. Monte Carlo simulation results for measured calibration spectra for equal angular resolution and detector solid angle small angle neutron scattering experiments obtained on two neutron sources within equal data collection times.

Figure 1 shows the comparison of the as-measured isotropic scattering (H_2O sample) calibration spectra after bining into 30 momentum transfer Q channels (which for the continuous source means bining over detector pixels– - 1 by 1 cm in a 60 by 60 pixel detector, while for the pulsed sources the bining additionally involves the neutron wavelength). The ratio of the neutron data collection rate of the two sources is obviously Q dependent, and in addition the LPSS source covers a somewhat larger Q range in a single scan. Thus, the relative gain offered by the LPSS source cannot be fully characterized by a single number , e.g., by the ratio of the total number of neutrons collected in the spectra. Rather, it will somewhat depend on the Q range that is the most relevant in a given experiment. This illustrates one of the points to be made when comparing the same kind of instruments on different types of sources: The relative merits can generally be only roughly characterized by a global neutron intensity ratio, while a precise analysis reveals variations from one type of sample scattering function to another.

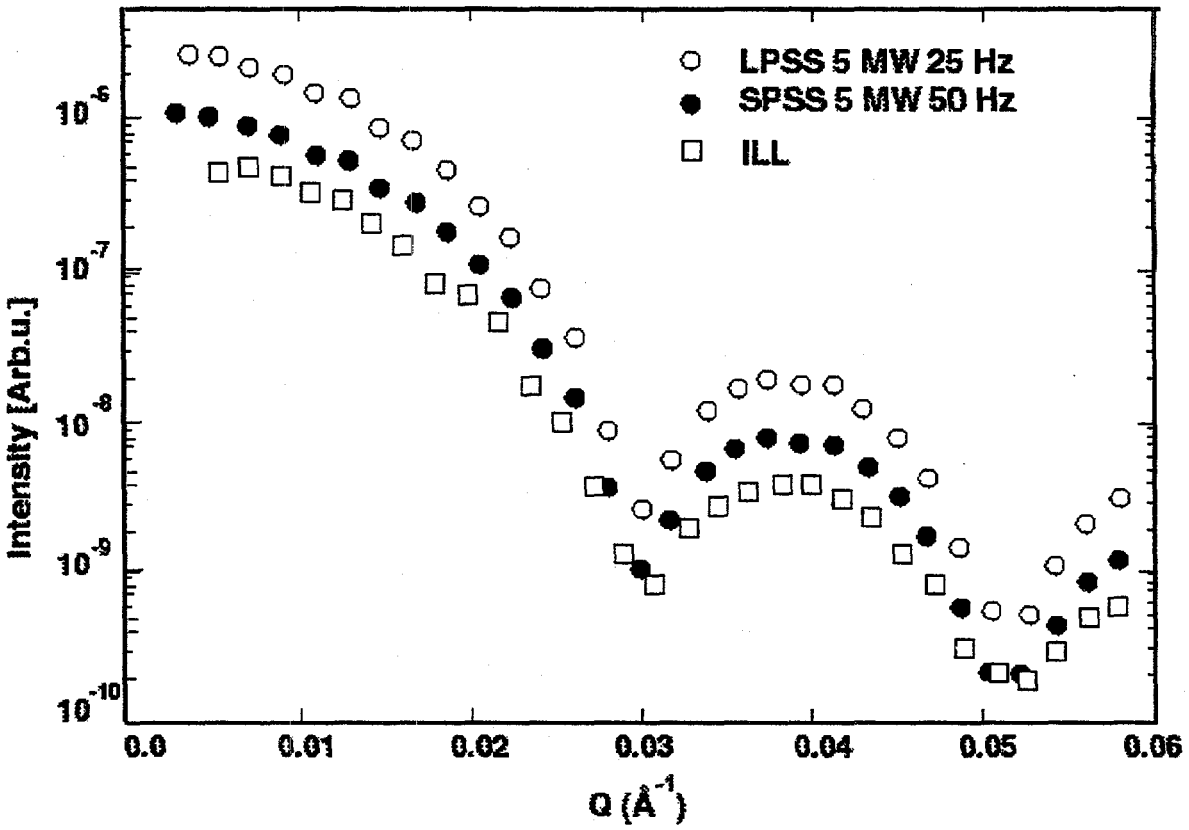

Fig. 2. Comparison of sample small-angle neutron scattering spectra for three neutron sources under conditions described in the caption of Fig. 1 and in the text.

In Figure 2 the normalized scattering spectra–the obtained I(Q) functions–from a sample of a dilute ensemble of hard spheres are shown for the three sources. In order to keep track of the intensity ratios, the I(Q) spectra as shown in the figure are multiplied by the total counting rate in the corresponding calibration run (cf. Fig 1). For the SPSS source it was assumed that the proton beam power was divided between two target stations, as usually envisaged, in a ratio 1:2. Using a 1:1 division ratio or a single 50 Hz target station would only have a minor effect on the final performance (well below a factor of 2). The superior performance of the LPSS variant is this case is due to its two-times-higher power per pulse, while the pulse length is fairly irrelevant, with the wavelength resolution already at least two times better than required by the comparison to the ILL-type instrument. The results in this figure illustrate features of the optimization of source performance in terms of cost-benefit ratio. Based on currently published cost estimates in various project studies, the construction costs of the three sources can be estimated to scale as 1:1.8:1 for the LPSS, SPSS and ILL, respectively. (If we assume an equal number of instruments on each source, the operational costs are rather close to each other, since they are dominated by the personal costs, and the rest is also not too much different, e.g., electric power vs. nuclear fuel.) Thus, in this application:

a) The LPSS approach provides a *neutron intensity 5 times higher)* than a continuous reactor source *at equal cost.*

b) The LPSS approach provides a *neutron intensity about 2 times* than the SPSS approach *at 55% of the cost.*

Both a) and b) demonstrate the absolute necessity of a serious cost-benefit optimization in new projects, because there are huge factors to be gained or lost. Of course, this optimization has to include the whole spectrum of instruments, and a proper synthesis of the relative merits for the

various instruments can only be accomplished in view of well defined scientific goals, which in turn determine the weights to be attributed to the various instruments and types of experiments. This inevitable task of optimization is a future challenge for all neutron source projects currently in discussion, and it is obvious that advanced instrument performance evaluation is a key input in the process.

References

[1] R. Gaehler et al, in this volume
[2] A. M. Weinberg and E.P. Wigner, The Physical Theory of Neutron Chain Reactions (Chicago University Press, Chicago, 1958) p. vi
[3] F. Mezei, Physica B. (in press)